International Review of
Physics
(IREPHY)

Contents

Dual Metal All Around Gate FinFET-3D Simulation 314
by H. Zolfaghari, S. E. Hosseini

The Improvement (G'/G) - Expansion Method to Construct the Exact Solutions of Nonlinear Differential Difference Equations 320
by Khaled A. Gepreel

Quantum Interference in a Four-Level EIT System and its Application to Photonic Logic Gates 333
by Peiyu Chen, Jian Qi Shen

Negative Matter, Dark Matter and Theoretical Test 340
by Yi-Fang Chang

Effect of Initial Stress on Wave Propagation in an Infinite Micropolar Elastic Solid Body 346
by E. Edfawy

Red Shift Band Gap Enhancement of the Nanostructure $ZnO_{100-x}Al_x$ Thin Films as a Function of Al Concentration for Optoelectronic Applications 352
by Nada M. Saeed, Manal M. Abdullah, Nathera A. Ali, Baha T. Chied

Electron Impact Collision Strengths for Fe XVI 358
by A. I. Refaie, A. A. Farrag

Structure and Properties of $YBa_2Cu_3O_{7-\delta}$ Superconductor Doped with MnO and NiO 365
by M. Kavosh, M. Arefian

Scrutiny of a Particle in Schwarzschild Black Hole and Tunneling Effect 368
by Amir Hassanfiroozi, Mohammadreza Maddah, Mahdi Massoumin

Modeling of Damage in the Behavior of Fiber-Matrix Interface of a Composite Material with a Genetic Algorithm 375
by Allel Mokaddem, Ahmed Boutaous

Effect of Initial Stress on Rayleigh Waves in a Thermoelastic Granular Medium 380
by G. A. Yahya

Magnetic Field and Relaxation Times Effects on the Propagation of Thermoelastic Waves from Isothermal or Insulated Boundaries of a Half Space 389
by S. M. Abo-Dahab, R. A. Mohamed, A. M. Abd-Alla

Influence of Initial Stress as a Convective Boundary Condition on Natural Frequencies of a Poroelastic Hollow Cylinder 402
by A. M. El-Naggar, Ibrahim A. Abbas, S. M. Abo-Dahab, M. Elsagheer

Praise Worthy Prize

International Review of Physics (I.R.E.PHY.), Vol. 5, N. 6
December 2011

Dual Metal All Around Gate FinFET-3D Simulation

H. Zolfaghari, S. E. Hosseini

Abstract – *In this paper, we present a dual metal all around gate structure for FinFET. This structure suppresses the short channel effects (SCEs) excellently due to increasing gate control on the channel and exhibit near ideal sub-threshold performance, evident by the very low drain-induced barrier- lowering (DIBL) and the inverse of the sub-threshold slope which is close to the theoretical limit (SS < 64 mV/dec). Moreover, the measured leakage currents are low and proper current saturation that transfers into large output resistances and makes these devices suitable for high-gain applications.* ***Copyright © 2011 Praise Worthy Prize S.r.l. - All rights reserved.***

Keywords*: Dual Metal, Three Metal, FinFET, DIBL, Subthreshold Slope, SCEs*

I. Introduction

FinFET is an attractive candidate to either succeed bulk CMOS technology at the end of scaling or to be integrated with bulk CMOS in various applications [1]. This structure is from multi-gate's family (MuGFET) devices, so that increasing gate control on channel [2] and, charge-sharing effects from source/drain region in the channel are decreased which results in suppressing short channel effects (SCEs) [3]. Fabrication of FinFETs is compatible with that of conventional CMOS [4].

Fully depleted channel FinFET solve threshold voltage (V_{th}) swing due to dopants density fluctuation and distribution, sub-threshold slope improved, thus exhibit low off-state (I_{off}) current, and cause on-state (I_{on}) current increased as well as enhances the device output resistance resulting in trans-conductance enhancement because of low channel dopants density [5],[6],[7].

While V_{th} tuning by implantation is difficult for narrow fin devices, work function tuning with metal gates is the preferred solution for FinFET devices [8].

This metal gates stack can be achieved by full silicidation of the poly gate [9], the combination of a metal (molybdenum) gate and a nitrogen implantation technique [10], or by metal deposition. In this paper we investigate dual metal and three metal FinFET performance by numerical 3-D simulation and compare dual metal with single-metal and three-metal FinFET structure.

II. Device Structure

A Schematic cross-sectional perspective of a fully depleted multi metal FinFET is illustrated in Figs. 1.

In this structure, the gate covers all around the Fin channel. Gate length is 30nm, compatible with future technology and adapted to CMOS scaling roadmap.

Fin width and height are 15 nm and gate oxide thickness is 1 nm. Channel doping concentration is 1×10^{16} /cm^3 to avoid dopant fluctuations and decrease sub-threshold swing.

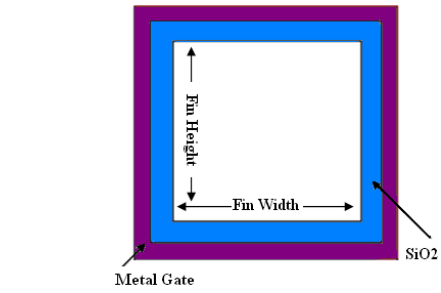

(a)

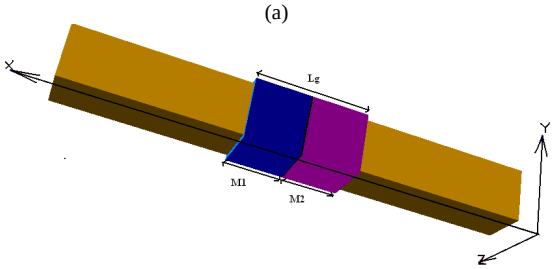

(b)

Figs. 1. (a) Schematic cross-sectional (b) 3D perspective of a fully depleted dual metal FinFET(M1and M2 are metal with φ_{M1} and φ_{M2})

For the single metal (SM) transistor the gate work function is assumed φ_{M1}=4.95 eV. For the dual metal (DM) case, the gate length is divided into L_1 and L_2 each of length 15 nm (L_1=L_2=L_g/2) with work functions φ_{M1}=4.95 eV and φ_{M2}=4.5 eV, respectively, and finally for the three metal (TM) transistor, the gate length is divided into L_1, L_2 and i each of length 10nm (L_1= L_2= L_3=L_g/3) with work functions φ_{M1}=4.95eV, φ_{M2}=4.8eV and φ_{M3}=4.5eV, respectively (with higher work function metal close to source). Fig. 2 shows the critical dimension and doping conditions used in the simulation.

Manuscript received and revised November 2011, accepted December 2011

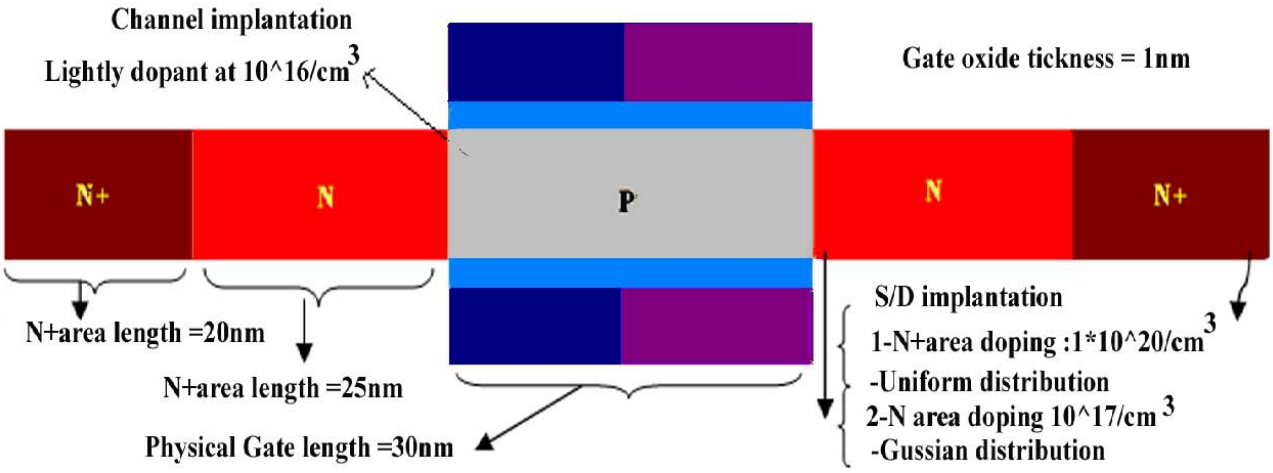

Fig. 2. Critical dimensions and implant conditions of FinFET structure used in the simulations

III. Simulation Results

In this section, simulation results are present for single metal (SM), dual metal (DM) and three metal (TM) gate FinFETs. Simulations are performed using the numerical simulator ATLAS Silvaco. The surface potential, electrical field, drain-induced barrier-lowering (DIBL), sub-threshold slope, threshold voltage, breakdown voltage and trans-conductance are investigated in this paper .

III.1. Surface Potential and Electrical Field

Fig. 3 shows the surface potential along the channel at *Vds*=0.5 V and *Vds*=1 V. As is shown in Fig. 3, the surface potential for SM FinFET is lower compared to the DM and the TM cases for all drain voltages. The surface potential of DM FinFET has a step near the middle of the channel which cause reduced short channel effects [11]. The surface potential of TM FinFET is very close to that of DM FinFET [12], with a small additional step in the potential due to small difference between φ_{M1} and φ_{M2}. For the DM FinFET the potential step is larger due to larger difference between work functions of the two metals. This causes more electrical field at $L_g/2$ and increases the carrier's energy moving toward the drain. Figure 4 shows the electrical field along the channel for the three transistors. The electrical field is increased with increasing the drain voltage (*Vds*=0.5 V, to *Vd*=1 V). For SM FinFET, the electrical field at drain side is very large, but for DM and TM FinFETs the peak electrical field is decreased considerably. DM FinFET has smallest peak electric field, which causes lower hot electron effects such as impact ionization and gate tunneling current. Moreover, for the DM and TM transistor, the electrical field is more uniform compared with SM finfet.

III.2. Output Characteristics

The transfer and output characteristics of the SM, DM and TM FinFETs are shown in Fig. 5 and Fig. 6 respectively, and extracted device parameters are summarized in Table I. As is evident from Fig. 5, Ion of SM FinFET is less than that of TM and DM FinFETs, but Ion of DM FinFET is close to that of TM case.

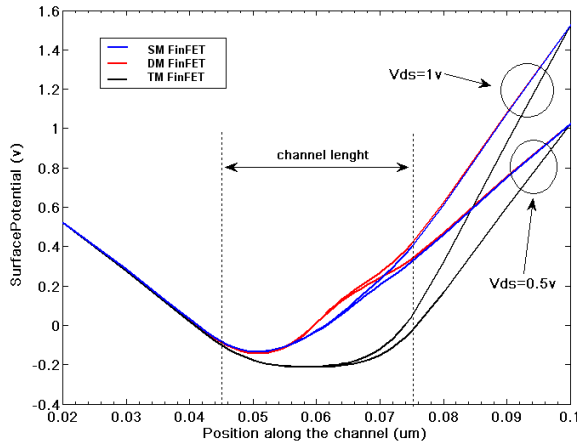

Fig. 3. Surface potential along the channel for TM FinFET φ_{M1}=4.95 eV, φ_{M2}=4.8 eV and φ_{M3} =4.5 eV, DM FinFET φ_{M1}=4.95 eV and =4.5 eV, and SM FinFET φ_M=4.95 eV

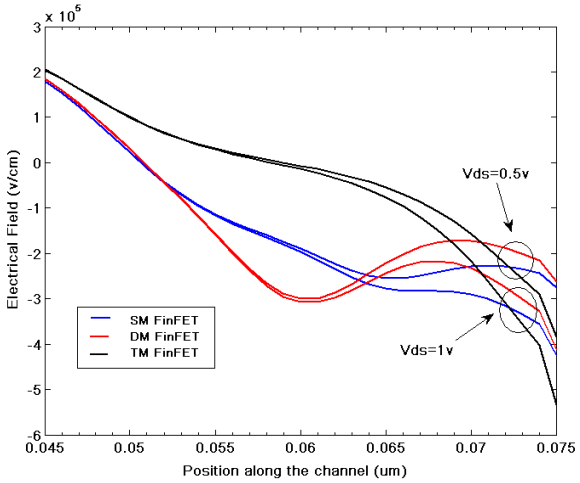

Fig. 4. Electrical field for SM, DM and TM FinFETs

Sub-threshold slopes (SS) are 61, 61.8 and 62 mV/dec for SM, DM and TM FinFETs respectively. For all of them DIBL is less than 2 mV/V which is excellent. Breakdown voltage (V_{BR}) of SM, DM and TM FinFETs are 1.15, 1.61 and 1.62 V respectively. The saturation current in DM FinFET is more than that of TM and SM ones.

TABLE I
DEVICE PARAMETERS FOR SM, DM AND TM FINFETS

Parameters	Sm finfet	Dm finfet	Tm finfet
Vth (V) *Vds*=1(V)	0.6911	0.6639	0.6588
DIBL(mV/V)	4.6	1	1.4
SS(mV/dec)	60.4	63	64.2
VBr (V)	1.15	1.61	1.62
Gm(uA/V)	10.9	10.28	10.28
I_{on}(uA)	3.33	3.61	3.45
I_{off} (A) (*vgs*=0V,Vd=1V)	$<6\times10^{-18}$	$<4\times10^{-17}$	$<6\times10^{-17}$

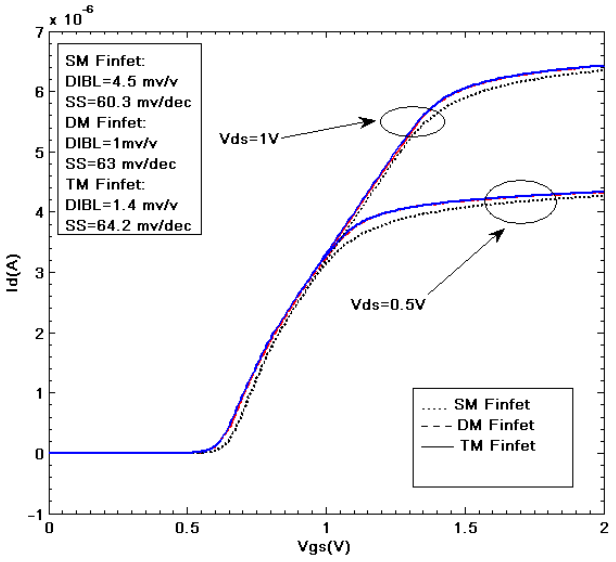

Fig. 5. Id –Vgs curve for the three FinFETs

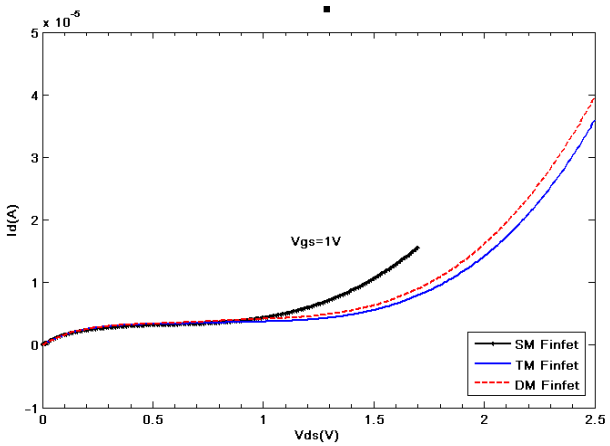

Fig. 6. Id –Vds curve for SM, DM and TM FinFETs at Vgs=1 V

Fig. 7 shows the output characteristic with gate-source voltage swept from 0.7V to 0.9V with 0.1 steps.

Fig. 8. shows the trans-conductance (g_m) for the three structures. The maximum g_m in SM, DM and TM FinFETs are 10.9, 10.28 and 10.28 uA/V respectively.

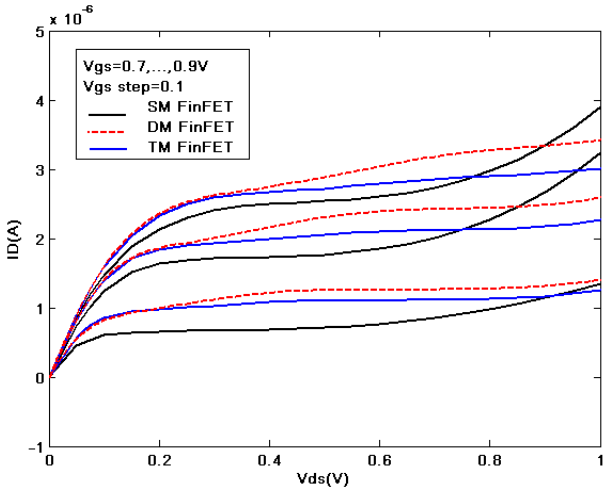

Fig. 7. Id –Vds curve for SM, DM and TM FinFETs for Vgs =0.7,...,1 V with 0.1 steps

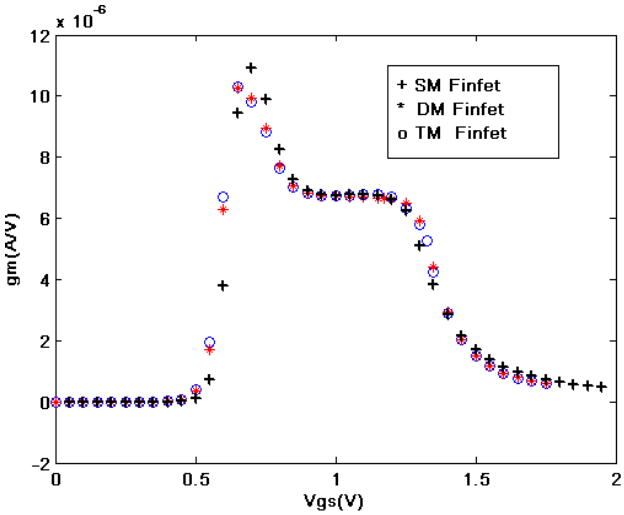

Fig. 8. Trans-conductance of SM, DM and TM FinFETs

For more analyses, we investigate doping concentration effects of N region, and gate-channel overlap effects on the device parameters. Increasing the doping density of N region from 10^{17}/cm^3 to 5×10^{18}/cm^3, and decreasing doping density of N+ region from 10^{20}/cm^3 to 5×10^{18}/cm^3 at the same time, increase the DIBL and sub-threshold slope, decrease the breakdown voltage and, as is seen from Fig. 9, the gm curve has a single hump, which indicates that premature corner inversion has been eliminated.

According to [13]-[14], the trans-conductance is increased as well. Table II summarizes the results.

We simulate the gate overlap with adding a 3 nm n-type region with doping concentration of 1×10^{17} /cm^3 in the channel at the drain and source sides as is shown in Fig. 10. Appending this region to the channel, results in

excellent device parameters for the three structures, which are summarized in Table III.

TABLE II
DEVICE PARAMETERS FOR SM, DM AND TM FINFETS

Parameters	Sm finfet	Dm finfet	Tm finfet
Vth (V) Vds=1(V)	0.6665	0.5915	0.5810
DIBL(mV/V)	11	6.2	9.8
SS(mV/dec)	60.4	64.4	64.4
VBr (V)	1.03	1.47	1.52
Gm(uA/V)	23.49	22.33	22.47
I_{on}(uA)	7.82	8.65	9.02
I_{off} (A) (vgs=0.05V, Vd=1V)	$<3\times10^{-16}$	$<2\times10^{-14}$	$<2\times10^{-14}$

TABLE III
SIMULATION RESULTS OF GATE OVERLAP FOR SM, DM AND TM FINFETS

Parameters	Sm finfet	Dm finfet	Tm finfet
Vth (V) Vds=1(V)	0.6909	0.6625	0.6578
DIBL(mV/V)	4.6	1.2	1.4
SS(mV/dec)	60.4	62.8	63.2
VBr (V)	1.151	1.61	1.62
Gm(uA/V)	10.97	10.37	10.97
I_{on}(uA)	3.33	3.61	3.45
I_{off} (A) (vgs=0.05V,Vd=1V)	$<2\times10^{-16}$	$<2.5\times10^{-16}$	$<3.5\times10^{-16}$

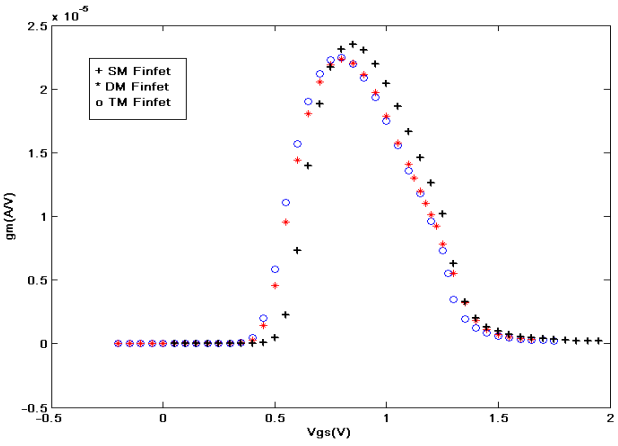

Fig. 9. Trans-conductance curve for SM, DM and TM FinFETs with increased N region doping

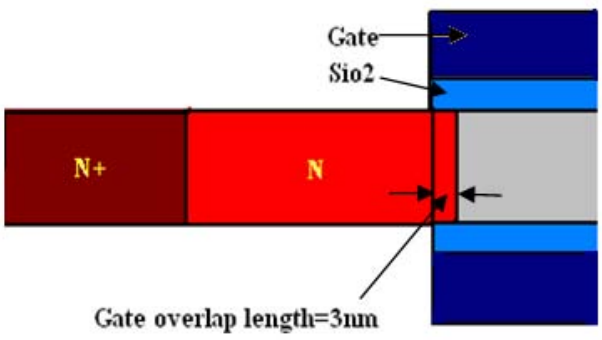

Fig. 10. Gate overlap length in the channel

III.3. Three Metal (TM) FinFET

In this section, we focus on TM FinFET and investigate the effect of variation of φ_{M2} on the characteristics of this structure. To do this, we change φ_{M2} from 4.55 eV that is close to φ_{M3}, to 4.9 eV which is close to φ_{M1} in steps 0.05 eV.

Fig. 11 shows the surface potential along the channel for *Vgs*=1 V and *Vds*=1 V. As can be seen, decreasing φ_{M2} increases the surface potential in the channel near the drain end, hence the major portion of the channel is shielded from the drain voltage variations. The electrical field along the channel for *Vgs*=1 V and *Vds*=1 V is shown in Fig. 12.

It is clearly visible that when the work functions φ_{M2} is close to φ_{M3} or φ_{M1}, the electrical field variation along the channel is large.

With φ_{M2} =4.7 eV the electrical field is more or less uniform along the channel. When φ_{M2} is close to φ_{M1} the maximum electrical field at the drain side is reduced, which causes reduced hot electron effects.

Up to φ_{M2} =4.7 eV the maximum electrical field at the drain side is not increased significantly, therefore, it seems that φ_{M2} =4.7 eV is the best value since causes both reduce hot electron effects and rather uniform electric field along the channel.

Fig. 13 shows the g_m versus φ_{M2}. This indicates that with increasing φ_{M2}, up to 4.8 eV, g_m decreases then increase again.

Figs. 14 (a), (b) and (c) show the DIBL, the sub-threshold slope and the breakdown voltage vs φ_{M2} for TM FinFET respectively.

These figures indicate that upon increasing φ_{M2} up to 4.8 eV, the DIBL, the sub-threshold slope and the breakdown voltage have regular variations, above φ_{M2}=4.8 eV these characteristics degrade.

According to Fig. 13, it seems that optimum value for φ_{M2} is 4.8 eV.

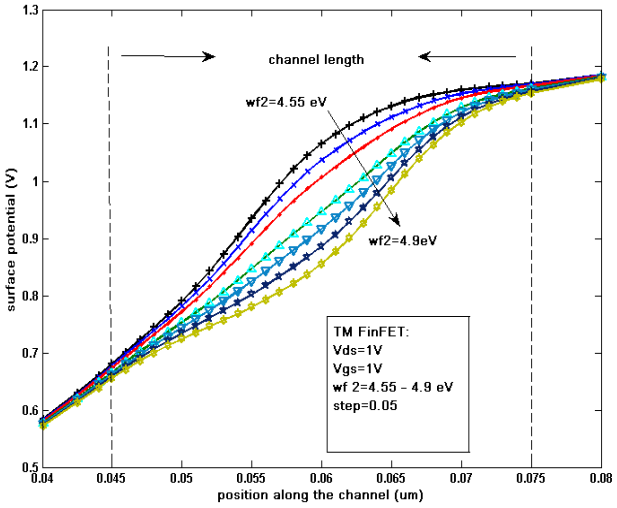

Fig. 11. Surface potential along the channel for TM FINFET with ΦM2=4.55,…,4.9 eV

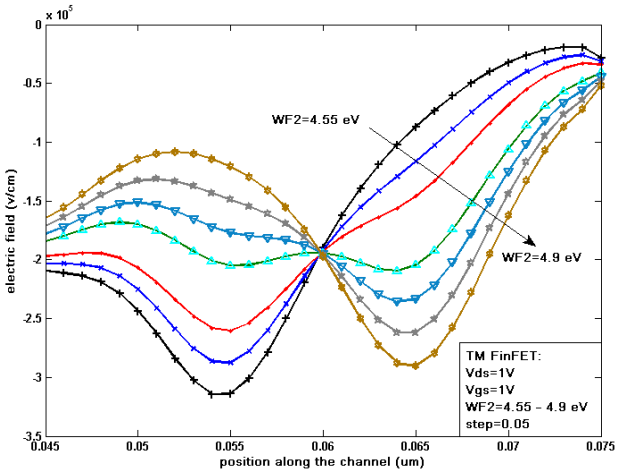

Fig. 12. Electrical field for TM FinFET with φM2=4.55,…,4.9 eV

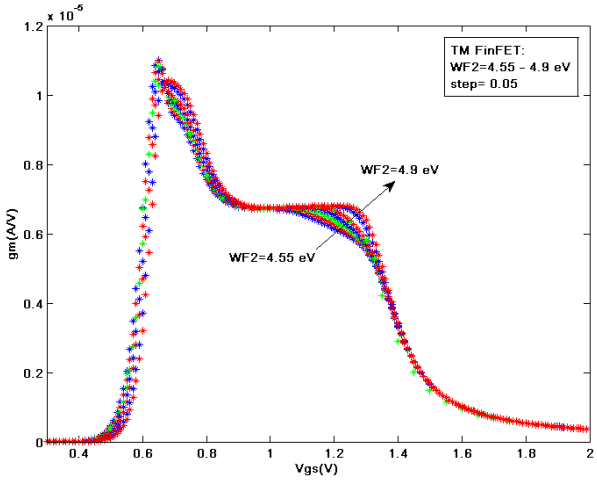

Fig. 13. Trans-conductance curve for TM FinFET with $\varphi M2$=4.55,…,4.9 eV

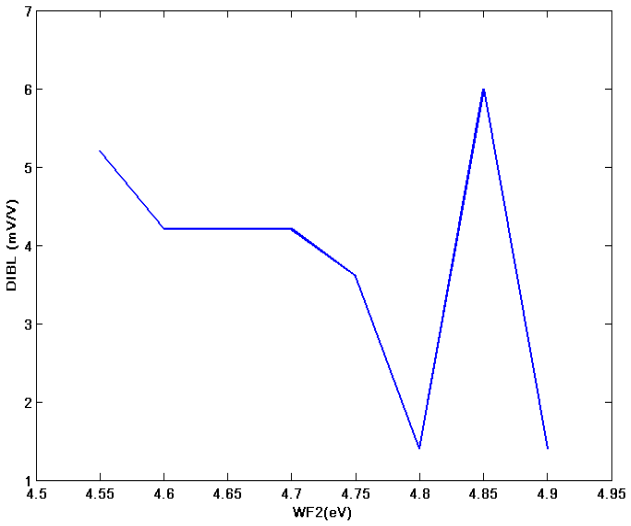

(a)

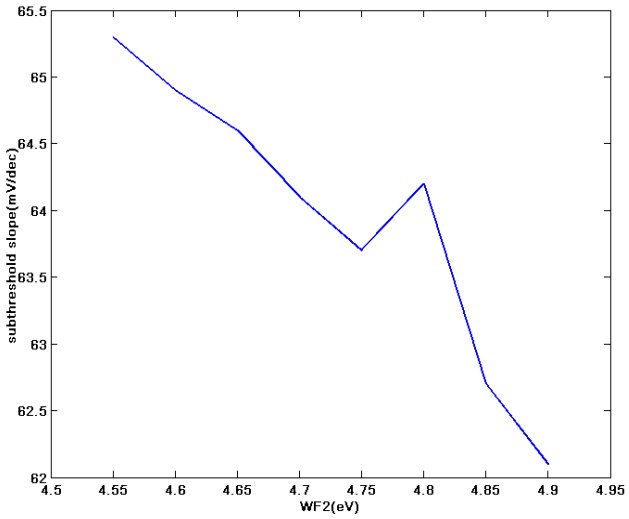

(b)

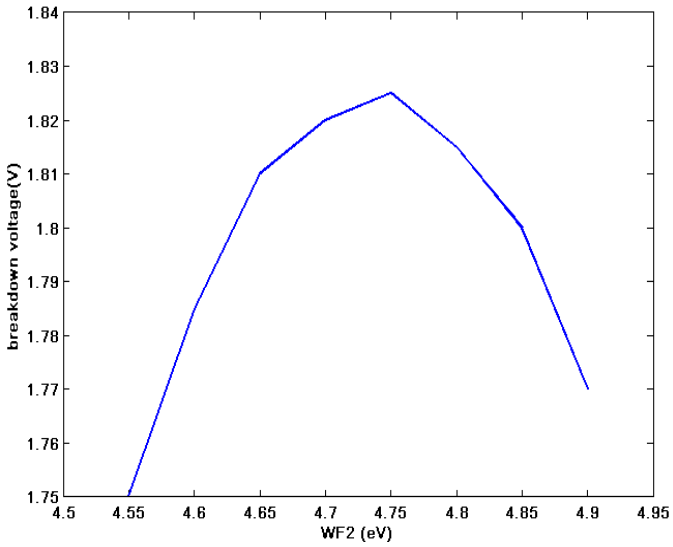

(c)

Figs. 14. (a) DIBL; (b) subthreshold slope; (c) breakdown voltage Vs work function for TM FinFET

IV. Conclusion

The fully depleted all around gate FinFET structures with single, dual and triple metal gates are investigated in this paper. It is shown that DM and TM FinFETs have improved short channel effects. Moreover, doping concentration effects at the source and the drain extensions on the device parameters are investigated. Simulations show that DM and TM transistors exhibit lower DIBL, excellent sub-threshold slope, higher breakdown voltage and on-state current. Also, decreasing electric field at the drain side results in lower hot carrier effects.

References

[1] S.-K. Sung, S.-H. Lee, B.-Y. Choi, J.J. Lee, J.-D. Choe, E.S. Cho, et al., SONOS-Type FinFET Device Using P+ Poly-Si Gate and High-k Blocking Dielectric Integrated on Cell Array and GSL/SSL for Multi-Gigabit NAND Flash Memory, *VLSI Technology Symposium 2006, Digest of Technical Papers*, 2006, pp. 86–87.

[2] J. Y. Song, W. Y. Choi, J. H. Park, J. D. Lee, and B. G. Park, "Design optimization of gate-all-around (GAA) MOSFETs," *IEEE Trans.Nanotechnol.*, vol. 5, no. 3, pp. 186–196, May 2006.

[3] X. Huang, W.-C. Lee, C. Kuo, D. Hisamoto, L. Chang,J. Kedzierski, E. Anderson, H. Takeuchi, Y.-K. Choi,K. Asano, V. Subramanian, T.-J. King, J. Boker, and C.Hu, "Sub 50nm FinFET: PMOS," *Int. Electron Devices Meeting Tech. Dig.*, Washington DC, 1999, pp. 67-70.

[4] Prateek Mishra, Anish Muttreja, and Niraj K. Jha, "FinFET Circuit Design" , *N.K. Jha and D. Chen (eds.), Nanoelectronic Circuit Design*, Springer Science+Business Media, LLC 2011.

[5] H.-S. P. Wong, "Beyond the conventional transistor," *IBM J. Res. Dev.*,vol. 46, no. 2/3, pp. 133–167, Mar.–May 2002.

[6] D. Hisamoto, W.-C. Lee, J. Kedzierski, H. Takeuchi, K. Asano, C. Kuo,E. Anderson, T.-J. Kingm, J. Boker, and C. Hu, "FinFET—A self-aligned double-gate MOSFET scalable to 20 nm," *IEEE Trans. Electron Devices*, vol. 47, no. 12, pp. 2320–2325, Dec. 2000.

[7] T. Sekigawa and Y. Hayashi, "Calculated threshold-voltage characterization of an XMOS transistor having an additional bottom gate," *Solid State Electron.*, vol. 27, no. 8/9, pp. 827–828, Aug./Sep. 1984.

[8] Takashi Matsukawa, Kazuhiko Endo, Yongxun Liu, Shinichi O'uchi, Yuki Ishikawa, Hiromi Yamauchi, Junichi Tsukada, Kenichi Ishii, Meishoku Masahara, Kunihiro Sakamoto, and Eiichi Suzuki, Threshold-Voltage Reduction of FinFETs by Ta/Mo Interdiffusion Dual Metal-Gate Technology for Low-Operating-Power Application, *Electron Devices, IEEE Transactions on* , vol.55, no.9, pp.2454-2461, Sept. 2008.

[9] J. Kedzierski, E. Nowak, T. Kanarsky, Y. Zhang, D. Boyd, R. Carruthers,C. Cabral, R. Amos, C. Lavoie, R. Roy, J. Newbury, E. Sullivan,J. Benedict, P. Saunders, K. Wong, D. Canaperi, M. Krishnan, K.-L. Lee,B. A. Rainey, D. Fried, P. Cottrell, H.-S. P. Wong, M. Ieong, andW. Haensch, "Metal-gate FinFet and fully-depleted SOI devices usingtotal gate silicidation," in *IEDM Tech. Dig.*, 2002, pp. 247–250.

[10] D. Ha, H. Takeuchi, Y.-K. Choi, T.-J. King, W. P. Bai, D.-L. Kwong,A. Agarwal, and M. Ameen, "Molybdenum-gate HFO CMOS FinFETs technology," in *IEDM Tech. Dig.*, 2004, pp. 643–646.

[11] M. Jagadesh Kumar,and Anurag Chaudhry, "Two-Dimensional Analytical Modeling of Fully depleted DMG SOI MOSFET and Evidence for Diminished SCEs" , *IEEE Transactions on Electron Devices*, Vol. 51, N° 4, April 2004.

[12] Pedram Razavi and Ali A. Orouji, "Nanoscale Triple Material Double Gate (TM-DG) MOSFET for Improving Short Channel Effects", *International Conference on Advances in Electronics and Micro- electronics*, pp. 11–14, 2008.

[13] H.S. Wong, M.H. White, T.J. Krutsck, R.V. Booth: Modeling of transconductance degradation and threshold voltage in thin oxide MOSFETs. *Solid-State Electronics*, 30-9,953(1987).

[14] E. Rauly, B. Iniguez, D. Flandre, C. Raynaud: Investigation of single and double gate SOI MOSFETs in accumulation mode for enhanced performances and reduced technological drawbacks. *Proceedings of ESSDERC*, 540 (2000).

Authors' information

Electronic and Computer Engineering Department,
Sabzevar Tarbiat Moallem University, Sabzevar, Iran.

Hamideh Zolfaghari was born in shirvan, Iran, 1982. She received the B.Sc. degree in electronic engineering from doctor shariati college, Tehran, Iran, in 2006. She is currently working toward the M.Sc. degree in electrical engineering at the SabzevarTarbiatMoallem University, Sabzevar, Iran . her current research interests include physical modeling, simulation and characterization of FINFET devices.

Seyed Ebrahim Hosseini received the B.Sc. degree in electrical engineering from Isfahan University of Technology, Isfahan, M.Sc. from TarbitModarres University, Tehran, Iran, and Ph.D. degree in electrical engineering from Sharif University of Technology, Tehran, Iran, in 2001. He is now associate professor of electronics engineering at the SabzevarTarbiatMoallem University. His research areas include microelectronicdevices, SOI transistors, anddevice modeling. He has authored or co-authored over 70 conference and journal papers.

Praise Worthy Prize

International Review of Physics (I.R.E.PHY.), Vol. 5, N. 6
December 2011

The Improvement (G'/G) - Expansion Method to Construct the Exact Solutions of Nonlinear Differential Difference Equations

Khaled A. Gepreel

Abstract – *In this article, we construct the traveling wave solutions involving parameters of the nonlinear differential difference equations via the lattice equation, the relativistic Toda lattice equations and the (1+1) – dimensional Toda equation in terms of the hyperbolic functions and trigonometric functions by using the improvement (G'/G)- expansion method, where G satisfies a discrete second order linear ordinary differential equation. When the parameters are taken special values, the solitary wave are derived from the traveling waves.* ***Copyright © 2011 Praise Worthy Prize S.r.l. - All rights reserved.***

Keywords: *The Improvement (G'/G) - Expansion Method, Traveling Wave Solutions, The Lattice Equation, The Relativistic Toda Lattice Equations , The (1+1) – Dimensional Toda Equation*

I. Introduction

It is well known that the investigation of differential-difference equations (DDEs) which describe many important phenomena and dynamical processes in many different fields, such as particle vibrations in lattices, currents in electrical networks, pulses in biological chains and so on, has played an important role in the study of modern physics.

Unlike difference equations which are fully discredited, DDEs are semi- discredited with some (or all) of their special variables discredited while time is usually kept continuous. DDEs also play an important role in numerical simulations of nonlinear partial differential equations (NLPDEs), queuing problems, and discretization in solid state and quantum physics.

Since the work of Fermi, Pasta, and Ulam in the 1960s [1], DDEs have been the focus of many nonlinear studies. On the other hand, many effective methods for obtaining the exact solutions of NPDEs have presented such as the inverse scattering method [2], Hirota's bilinear method [3], Backlund transformation [4], [5], Painlevé expansion [6], sine–cosine method [7], homogenous balance method [8], homotopy perturbation method [9]-[12], variation method [13], [14], Adomian decomposition method [15],[16], tanh - function method [17]-[19], Jacobi elliptic function expansion method [20]-[23], F-expansion method [24]-[26] and exp-function method [27]-[29].

Wang et al. [30] proposed a new method called the (G'/G) expansion method to look for the traveling wave solutions for nonlinear partial differential equations (NPDEs). By using the (G'/G) expansion method, Wang etal [30] and Zayed et al. [31], [32] has successfully obtained more traveling wave solutions for some important NPDEs. Recently Zhang et al. [33] had developed the (G'/G) expansion method for solving the NDDEs.

In this paper we use the improvement (G'/G) expansion method to find the traveling wave solutions for the lattice equation, the relativistic Toda lattice equations and the (1+1) – dimensional Toda equation in terms of hyperbolic functions, trigonometric functions.

II. Description of the Improvement (G'/G) Expansion Method for NDDEs

In this section, we would like to outline the algorithm for using the improved (G'/G) expansion method to solve NDDEs.

Consider a given system of M polynomial NDDEs:

$$\Delta\left(\begin{matrix} u_{n+p_1}(X),...,u_{n+p_k}(X),u'_{n+p_1}(X),..., \\ u'_{n+p_k}(X),...,u^{(r)}_{n+p_1}(X),...,u^{(r)}_{n+p_k}(X) \end{matrix}\right)=0 \quad (1)$$

where the dependent variable u has M components u_i , the continuous variable x has N components x_j , the discrete variable n has Q components n_i , the k shift vectors $p_s \in Z^Q$ and $u^{(r)}$ denotes the collection of mixed derivative terms of order *r*.

The main steps of the algorithm for using the improved (G'/G)- expansion method to solve NLDDEs are outlined as follows:

Step 1. When we seek traveling wave solutions of Eq. (1), the first step is to introduce the wave transformation:

Manuscript received and revised November 2011, accepted December 2011

$$u_{n+p_s}(X) = U_{n+p_s}(\xi_n)$$
$$\xi_n = \sum_{i=1}^{Q} d_i n_i + \sum_{j=1}^{Q} c_j x_j + \xi_0 \qquad (2)$$
$$s = 1,2,...,k$$

where the coefficients d_i, c_j and the phase ξ_0 are constants. The transformations (2) lead to write Eq. (1) into the following form:

$$\Delta\left(\begin{matrix} U_{n+p_1}(\xi_n),...,U_{n+p_k}(\xi_n), U'_{n+p_1}(\xi_n),..., \\ U'_{n+p_k}(\xi_n),...,U^{(r)}_{n+p_1}(\xi_n)),...,U^{(r)}_{n+p_k}(\xi_n) \end{matrix}\right) = 0 \quad (3)$$

Step 2. We suppose the following series expansion as a solution of Eq. (3):

$$U_n(\xi_n) = \sum_{i=0}^{m} \alpha_i \left(\frac{G'(\xi_n)}{G(\xi_n)}\right)^i + \sum_{j=1}^{m} \beta_j \left(\frac{G(\xi_n)}{G'(\xi_n)}\right)^j \qquad (4)$$

where α_i, β_j are constants to be determined later, $G(\xi_n)$ satisfies a discrete second order linear ordinary differential equation:

$$G''(\xi_n) + \lambda G'(\xi_n) + \mu G(\xi_n) = 0 \qquad (5)$$

where λ and μ are arbitrary constants. Using the general solutions of Eq. (5), we have:

$$\frac{G'(\xi_n)}{G(\xi_n)} = \begin{cases} \frac{\sqrt{\lambda^2-4\mu}}{2}\left(\frac{C_1 sinh\left(\frac{\sqrt{\lambda^2-4\mu}}{2}\xi_n\right) + C_2 cosh\left(\frac{\sqrt{\lambda^2-4\mu}}{2}\xi_n\right)}{C_1 cosh\left(\frac{\sqrt{\lambda^2-4\mu}}{2}\xi_n\right) + C_2 sinh\left(\frac{\sqrt{\lambda^2-4\mu}}{2}\xi_n\right)}\right) - \frac{\lambda}{2}, & \lambda^2 - 4\mu > 0 \\ \frac{\sqrt{4\mu-\lambda^2}}{2}\left(\frac{-C_1 sin\left(\frac{\sqrt{4\mu-\lambda^2}}{2}\xi_n\right) + C_2 cos\left(\frac{\sqrt{4\mu-\lambda^2}}{2}\xi_n\right)}{C_1 cos\left(\frac{\sqrt{4\mu-\lambda^2}}{2}\xi_n\right) + C_2 sin\left(\frac{\sqrt{4\mu-\lambda^2}}{2}\xi_n\right)}\right) - \frac{\lambda}{2}, & 4\mu - \lambda^2 > 0 \end{cases} \qquad (6)$$

Further. using the following identities:

$$\begin{aligned} sinh(x \pm y) &= sinh(x)cosh(y) \pm cosh(x)sinh(y), \\ cosh(x \pm y) &= cosh(x)cosh(y) \pm sinh(x)sinh(y) \end{aligned} \qquad (7)$$

and:

$$\begin{aligned} sin(x \pm y) &= sin(x)cos(y) \pm cos(x)sin(y) \\ cos(x \pm y) &= cos(x)cos(y) \mp sin(x)sin(y) \end{aligned} \qquad (8)$$

we can prove that (see [33]):

$$\frac{G'(\xi_{n\pm y})}{G(\xi_{n\pm y})} = \frac{\sqrt{\varepsilon(\lambda^2-4\mu)}}{2}\left(\frac{\frac{2}{\sqrt{\varepsilon(\lambda^2-4\mu)}}\left(\frac{G'(\xi_n)}{G(\xi_n)} + \frac{\lambda}{2}\right) \pm \varepsilon\, f\left(\frac{\sqrt{\varepsilon(\lambda^2-4\mu)}}{2}y\right)}{1 \pm \frac{2}{\sqrt{\varepsilon(\lambda^2-4\mu)}} f\left(\frac{\sqrt{\varepsilon(\lambda^2-4\mu)}}{2}y\right)\left(\frac{G'(\xi_n)}{G(\xi_n)} + \frac{\lambda}{2}\right)}\right) - \frac{\lambda}{2} \qquad (9)$$

where $\varepsilon = \pm 1$ and:

$$f\left(\frac{\sqrt{\varepsilon(\lambda^2-4\mu)}}{2}y\right) = \begin{cases} tanh\left(\frac{\sqrt{\lambda^2-4\mu}}{2}y\right), & \varepsilon = 1 \\ tan\left(\frac{\sqrt{4\mu-\lambda^2}}{2}y\right), & \varepsilon = -1 \end{cases} \qquad (10)$$

Thus the iterative relation can be written in the following form:

$$U_n\left(\xi_{n\pm p}\right)=\sum_{i=0}^{m}\alpha_i\left(\frac{\sqrt{\varepsilon\left(\lambda^2-4\mu\right)}}{2}\left(\frac{\frac{2}{\sqrt{\varepsilon\left(\lambda^2-4\mu\right)}}\left(\frac{G'\left(\xi_n\right)}{G\left(\xi_n\right)}+\frac{\lambda}{2}\right)\pm\varepsilon\, f\left(\frac{\sqrt{\varepsilon\left(\lambda^2-4\mu\right)}}{2}\varphi_s\right)}{1\pm\frac{2}{\sqrt{\varepsilon\left(\lambda^2-4\mu\right)}}\, f\left(\frac{\sqrt{\varepsilon\left(\lambda^2-4\mu\right)}}{2}\varphi_s\right)\left(\frac{G'\left(\xi_n\right)}{G\left(\xi_n\right)}+\frac{\lambda}{2}\right)}\right)-\frac{\lambda}{2}\right)^{i}+$$
$$+\sum_{j=1}^{m}\beta_j\left(\frac{\sqrt{\varepsilon\left(\lambda^2-4\mu\right)}}{2}\left(\frac{\frac{2}{\sqrt{\varepsilon\left(\lambda^2-4\mu\right)}}\left(\frac{G'\left(\xi_n\right)}{G\left(\xi_n\right)}+\frac{\lambda}{2}\right)\pm\varepsilon\, f\left(\frac{\sqrt{\varepsilon\left(\lambda^2-4\mu\right)}}{2}\varphi_s\right)}{1\pm\frac{2}{\sqrt{\varepsilon\left(\lambda^2-4\mu\right)}}\, f\left(\frac{\sqrt{\varepsilon\left(\lambda^2-4\mu\right)}}{2}\varphi_s\right)\left(\frac{G'\left(\xi_n\right)}{G\left(\xi_n\right)}+\frac{\lambda}{2}\right)}\right)-\frac{\lambda}{2}\right)^{-j} \tag{11}$$

where $\varphi_s = p_{s1}d_1 + p_{s2}d_2 + ...+ p_{sQ}d_Q$ and p_{sj} is the jth component of shift vector p_s.

Step 3. Determine the degree m of Eqs. (4) and (11) by balancing the highest order nonlinear term(s) and the highest order partial derivatives of U_n in Eq. (3).

Step 4. Substituting Eqs. (4) and (11) given the value of m determined in step 3 along with (5) into (3) and collecting all terms with the same order of $(G'(\xi_n)/G(\xi_n))$ together, the left-hand side of (3) is converted into polynomials in $(G'(\xi_n)/G(\xi_n))$. Then setting each coefficient of this polynomials to zero, we will derive a set of algebraic equations, from which the constants α_i, β_j, d_i and c_j can be explicitly determined by use of Mathematica or Maple.

Step 5. Using the results obtained in above steps, we can finally obtain exact solutions of Eq. (1).

III. Applications

In this section, we apply improvement (G'/G)-expansion method to construct the traveling wave solutions for some nonlinear DDEs vie the lattice equation, the relativistic Toda lattice equations and the (1+1) – dimensional Toda equation which are very important in the mathematical physics and have been paid attention by many researchers.

III.1. Example 1. The Lattice Equation

In this section, we study the lattice equation which takes the following form [33], [34], [35], [36]:

$$\frac{du_n(t)}{dt}=\left(\alpha+\beta u_n+\gamma u_n^2\right)\left(u_{n-1}-u_{n+1}\right) \tag{12}$$

where α,β and γ are nonzero constants. The equation contains Hybird lattice equation, mKdV lattice equation , modified Valterra lattice equation and Langmiuir chain equation:

(i) (1+1) dimensional Hybird lattice equation [35]:

$$\frac{du_n(t)}{dt}=\left(1+\beta u_n+\gamma u_n^2\right)\left(u_{n-1}-u_{n+1}\right)$$

(ii) mKdV lattice equation [35]:

$$\frac{du_n(t)}{dt}=\left(\alpha-u_n^2\right)\left(u_{n-1}-u_{n+1}\right)$$

(iii) Modified Valterra equation [35]:

$$\frac{du_n(t)}{dt}=u_n^2\left(u_{n-1}-u_{n+1}\right)$$

(iv) Langmiuir chain equation [36]:

$$\frac{du_n(t)}{dt}=u_n\left(u_{n+1}-u_{n-1}\right)$$

According to the above steps, to seek traveling wave solutions of Eq. (12), we construct the transformation:

$$u_n=U_n\left(\xi_n\right),\qquad \xi_n=d_1n+c_1t+\xi_0 \tag{13}$$

where d_1, c_1 and ξ_0 are constants. The transformation (13) permits us converting Eq. (12) into the following form:

$$c_1U_n'\left(\xi_n\right)=\left(\alpha+\beta U_n+\gamma U_n^2\right)\left(U_{n-1}-U_{n+1}\right) \tag{14}$$

where $' = \frac{d}{d\xi_n}$. Considering the homogeneous balance between the highest order derivative and the nonlinear term in (14), we get $m = 1$. Thus the solution of Eq. (14) has the following form:

$$U_n(\xi_n) = \alpha_0 + \alpha_1\left(\frac{G'(\xi_n)}{G(\xi_n)}\right) + \beta_1\left(\frac{G(\xi_n)}{G'(\xi_n)}\right), \qquad \alpha_1 \neq 0 \quad or \quad \beta_1 \neq 0 \tag{15}$$

$$U_{n+1} = \alpha_1\left(\frac{\sqrt{\varepsilon\left(\lambda^2-4\mu\right)}}{2}\left(\frac{\frac{2}{\sqrt{\varepsilon\left(\lambda^2-4\mu\right)}}\left(\frac{G'(\xi_n)}{G(\xi_n)}+\frac{\lambda}{2}\right)+\varepsilon\, f\left(\frac{\sqrt{\varepsilon\left(\lambda^2-4\mu\right)}}{2}d_1\right)}{1+\frac{2}{\sqrt{\varepsilon\left(\lambda^2-4\mu\right)}}\, f\left(\frac{\sqrt{\varepsilon\left(\lambda^2-4\mu\right)}}{2}d_1\right)\left(\frac{G'(\xi_n)}{G(\xi_n)}+\frac{\lambda}{2}\right)}\right)-\frac{\lambda}{2}\right)+$$

$$+\beta_1\left(\frac{\sqrt{\varepsilon\left(\lambda^2-4\mu\right)}}{2}\left(\frac{\frac{2}{\sqrt{\varepsilon\left(\lambda^2-4\mu\right)}}\left(\frac{G'(\xi_n)}{G(\xi_n)}+\frac{\lambda}{2}\right)+\varepsilon\, f\left(\frac{\sqrt{\varepsilon\left(\lambda^2-4\mu\right)}}{2}d_1\right)}{1+\frac{2}{\sqrt{\varepsilon\left(\lambda^2-4\mu\right)}}\, f\left(\frac{\sqrt{\varepsilon\left(\lambda^2-4\mu\right)}}{2}d_1\right)\left(\frac{G'(\xi_n)}{G(\xi_n)}+\frac{\lambda}{2}\right)}\right)-\frac{\lambda}{2}\right)^{-1} \tag{16}$$

$$U_{n-1} = \alpha_1\left(\frac{\sqrt{\varepsilon\left(\lambda^2-4\mu\right)}}{2}\left(\frac{\frac{2}{\sqrt{\varepsilon\left(\lambda^2-4\mu\right)}}\left(\frac{G'(\xi_n)}{G(\xi_n)}+\frac{\lambda}{2}\right)-\varepsilon\, f\left(\frac{\sqrt{\varepsilon\left(\lambda^2-4\mu\right)}}{2}d_1\right)}{1-\frac{2}{\sqrt{\varepsilon\left(\lambda^2-4\mu\right)}}\, f\left(\frac{\sqrt{\varepsilon\left(\lambda^2-4\mu\right)}}{2}d_1\right)\left(\frac{G'(\xi_n)}{G(\xi_n)}+\frac{\lambda}{2}\right)}\right)-\frac{\lambda}{2}\right)+$$

$$+\beta_1\left(\frac{\sqrt{\varepsilon\left(\lambda^2-4\mu\right)}}{2}\left(\frac{\frac{2}{\sqrt{\varepsilon\left(\lambda^2-4\mu\right)}}\left(\frac{G'(\xi_n)}{G(\xi_n)}+\frac{\lambda}{2}\right)-\varepsilon\, f\left(\frac{\sqrt{\varepsilon\left(\lambda^2-4\mu\right)}}{2}d_1\right)}{1-\frac{2}{\sqrt{\varepsilon\left(\lambda^2-4\mu\right)}}\, f\left(\frac{\sqrt{\varepsilon\left(\lambda^2-4\mu\right)}}{2}d_1\right)\left(\frac{G'(\xi_n)}{G(\xi_n)}+\frac{\lambda}{2}\right)}\right)-\frac{\lambda}{2}\right)^{-1} \tag{17}$$

Substituting Eqs. (15)-(17) along with (5) into Eq. (14) and cleaning the denominator and collecting all terms with the same order of $(G'(\xi_n)/G(\xi_n))$ together, the left hand side of Eq. (16) is converted into polynomial in $(G'(\xi_n)/G(\xi_n))$.

Setting each coefficient of this polynomial to zero , we derive a set of algebraic equations for $\alpha_0, \alpha_1, \beta_1, d_1$ and c_1. Solving the set of algebraic equations by using Maple or Mathematica , we have:

Case 1:

$$\alpha_1 = -\frac{\sqrt{\beta^2-4\alpha\gamma}}{\gamma\left(4\mu-\lambda^2\right)^{3/2}}\left[\lambda^2 \tan\left(\frac{\sqrt{4\mu-\lambda^2}}{2}d_1\right)-2\mu \sin\left(\sqrt{4\mu-\lambda^2}\,d_1\right)\right], \qquad \varepsilon = -1$$

$$c_1 = \frac{\beta^2-4\alpha\gamma}{\gamma\left(4\mu-\lambda^2\right)^{3/2}}\left[\lambda^2 \tan\left(\frac{\sqrt{4\mu-\lambda^2}}{2}d_1\right)-2\mu \sin\left(\sqrt{4\mu-\lambda^2}\,d_1\right)\right] \tag{18a}$$

$$\alpha_{-1}=-\frac{\mu\sqrt{\beta^2-4\alpha\gamma}}{\gamma\left(4\mu-\lambda^2\right)^{3/2}}\left[\lambda^2\tan\left(\frac{\sqrt{4\mu-\lambda^2}}{2}d_1\right)-2\mu\sin\left(\sqrt{4\mu-\lambda^2}d_1\right)\right]$$

$$\alpha_0=-\frac{1}{2\gamma\left(4\mu-\lambda^2\right)}\left[\begin{array}{l}\lambda\sqrt{\dfrac{\beta^2-4\alpha\gamma}{4\mu-\lambda^2}}\tan\left(\dfrac{\sqrt{4\mu-\lambda^2}}{2}d_1\right)\left(\lambda^2-4\mu\cos\sqrt{4\mu-\lambda^2}d_1\right)+\\ -\beta\lambda^2+4\mu\beta\end{array}\right] \tag{18b}$$

where $4\mu-\lambda^2>0$.

In this case, we obtain the trigonometric solution of Eq. (15):

$$\begin{aligned}u_n=&-\frac{2\lambda\mu\sqrt{\beta^2-4\alpha\gamma}}{\gamma\left(4\mu-\lambda^2\right)^{3/2}}\tan\left(\frac{\sqrt{4\mu-\lambda^2}}{2}d_1\right)\sin^2\left(\frac{\sqrt{4\mu-\lambda^2}}{2}d_1\right)-\frac{\beta}{2\gamma}+\\&-\frac{D_1}{2}\left(\frac{-c_1\sin\left(\dfrac{\sqrt{4\mu-\lambda^2}}{2}\xi_n\right)+c_2\cos\left(\dfrac{\sqrt{4\mu-\lambda^2}}{2}\xi_n\right)}{c_1\cos\left(\dfrac{\sqrt{4\mu-\lambda^2}}{2}\xi_n\right)+c_2\sin\left(\dfrac{\sqrt{4\mu-\lambda^2}}{2}\xi_n\right)}\right)+\\&-\frac{2\mu D_1}{\left(4\mu-\lambda^2\right)}\left[\left(\frac{-c_1\sin\left(\dfrac{\sqrt{4\mu-\lambda^2}}{2}\xi_n\right)+c_2\cos\left(\dfrac{\sqrt{4\mu-\lambda^2}}{2}\xi_n\right)}{c_1\cos\left(\dfrac{\sqrt{4\mu-\lambda^2}}{2}\xi_n\right)+c_2\sin\left(\dfrac{\sqrt{4\mu-\lambda^2}}{2}\xi_n\right)}\right)-\frac{\lambda}{\sqrt{4\mu-\lambda^2}}\right]^{-1}\end{aligned} \tag{19}$$

where: $D_1=\dfrac{\sqrt{\beta^2-4\alpha\gamma}}{\gamma\left(4\mu-\lambda^2\right)}\left[\begin{array}{l}\lambda^2\tan\left(\dfrac{\sqrt{4\mu-\lambda^2}}{2}d_1\right)+\\ -2\mu\sin\left(\sqrt{4\mu-\lambda^2}d_1\right)\end{array}\right]$ and: $\xi_n=d_1n-D_1t\sqrt{\dfrac{\beta^2-4\alpha\gamma}{\left(4\mu-\lambda^2\right)}}+\xi_0$.

Case 2:

$$\begin{aligned}\alpha_1&=-\frac{\sqrt{\beta^2-4\alpha\gamma}}{\gamma\left(\lambda^2-4\mu\right)^{3/2}}\left[\lambda^2\tanh\left(\frac{\sqrt{\lambda^2-4\mu}}{2}d_1\right)-2\mu\sinh\left(\sqrt{\lambda^2-4\mu}d_1\right)\right]\qquad \varepsilon=1,\\ c_1&=\frac{\beta^2-4\alpha\gamma}{\gamma\left(\lambda^2-4\mu\right)^{3/2}}\left[\lambda^2\tanh\left(\frac{\sqrt{\lambda^2-4\mu}}{2}d_1\right)-2\mu\sinh\left(\sqrt{\lambda^2-4\mu}d_1\right)\right]\\ \alpha_{-1}&=-\frac{\mu\sqrt{\beta^2-4\alpha\gamma}}{\gamma\left(\lambda^2-4\mu\right)^{3/2}}\left[\lambda^2\tanh\left(\frac{\sqrt{\lambda^2-4\mu}}{2}d_1\right)-2\mu\sinh\left(\sqrt{\lambda^2-4\mu}d_1\right)\right]\\ \alpha_0&=-\frac{1}{2\gamma\left(\lambda^2-4\mu\right)}\left[\lambda\sqrt{\frac{\beta^2-4\alpha\gamma}{\lambda^2-4\mu}}\tanh\left(\frac{\sqrt{4\mu-\lambda^2}}{2}d_1\right)\left(\lambda^2-4\mu\cosh\sqrt{\lambda^2-4\mu}d_1\right)-\beta\lambda^2+4\mu\beta\right]\end{aligned} \tag{20}$$

where $\lambda^2-4\mu>0$. In this case, we obtain the hyperbolic solution of Eq.(15):

$$u_n=\frac{2\lambda\mu\sqrt{\beta^2-4\alpha\gamma}}{\gamma\left(\lambda^2-4\mu\right)^{3/2}}tanh\left(\frac{\sqrt{\lambda^2-4\mu}}{2}d_1\right)sinh^2\left(\frac{\sqrt{\lambda^2-4\mu}}{2}d_1\right)+$$
$$-\frac{\beta}{2\gamma}-\frac{D_2}{2}\left(\frac{c_1\,sinh\left(\frac{\sqrt{\lambda^2-4\mu}}{2}\xi_n\right)+c_2\,cosh\left(\frac{\sqrt{\lambda^2-4\mu}}{2}\xi_n\right)}{c_1\,cosh\left(\frac{\sqrt{\lambda^2-4\mu}}{2}\xi_n\right)+c_2\,sinh\left(\frac{\sqrt{\lambda^2-4\mu}}{2}\xi_n\right)}\right)+ \tag{21}$$
$$-\frac{2\mu D_2}{\left(\lambda^2-4\mu\right)}\left[\left(\frac{c_1\,sinh\left(\frac{\sqrt{\lambda^2-4\mu}}{2}\xi_n\right)+c_2\,cosh\left(\frac{\sqrt{\lambda^2-4\mu}}{2}\xi_n\right)}{c_1\,cosh\left(\frac{\sqrt{\lambda^2-4\mu}}{2}\xi_n\right)+c_2\,sinh\left(\frac{\sqrt{\lambda^2-4\mu}}{2}\xi_n\right)}\right)-\frac{\lambda}{\sqrt{\lambda^2-4\mu}}\right]^{-1}$$

where:

$$D_2=\frac{\sqrt{\beta^2-4\alpha\gamma}}{\gamma\left(\lambda^2-4\mu\right)}\left[\begin{array}{l}\lambda^2\,tanh\left(\frac{\sqrt{\lambda^2-4\mu}}{2}d_1\right)+\\-2\mu\,sinh\left(\sqrt{\lambda^2-4\mu}d_1\right)\end{array}\right]$$

and:

$$\xi_n=d_1n-D_2\,t\sqrt{\frac{\beta^2-4\alpha\gamma}{\lambda^2-4\mu}}+\xi_0$$

Note that, there are other cases which are omitted here. We just list some exact solutions corresponding to case 1,2 to illustrate the effectiveness of the improved (G'/G) – expansion method.

III.2. Example 2. The Relativistic Toda Lattice Equations

In this subsection, we study Relativistic Toda lattice equations which take the following forms [36]:

$$\begin{aligned}\frac{du_n(t)}{dt}&=(1+\alpha u_n)(v_n-v_{n-1})\\ \frac{dv_n(t)}{dt}&=v_n\left(u_{n+1}-u_n+\alpha v_{n+1}-\alpha v_{n-1}\right)\end{aligned} \tag{22}$$

where α is a nonzero constant. Using the transformation $u_n=U_n(\xi_n)$, $v_n=V_n(\xi_n)$ and $\xi_n=d_1n+c_1t+\xi_0$ then Eq. (22) become:

$$\begin{aligned}c_1U_n'(\xi_n)&=(1+\alpha u_n)(v_n-v_{n-1})\\ c_1V_n'(\xi_n)&=v_n\left(u_{n+1}-u_n+\alpha v_{n+1}-\alpha v_{n-1}\right)\end{aligned} \tag{23}$$

where d_1, c_1, ξ_0 are constants and $'=d/d\xi_n$. Considering the homogeneous balance between the highest order derivatives and the nonlinear terms in (23), we have:

$$U_n(\xi_n)=\alpha_0+\alpha_1\left(\frac{G'(\xi_n)}{G(\xi_n)}\right)+\alpha_{-1}\left(\frac{G(\xi_n)}{G'(\xi_n)}\right), \tag{24}$$
$$\alpha_1\neq 0\ \ or\ \ \alpha_{-1}\neq 0$$

$$U_{n\pm1}=\alpha_1\left(\frac{\sqrt{\varepsilon\left(\lambda^2-4\mu\right)}}{2}\left(\frac{\frac{2}{\sqrt{\varepsilon\left(\lambda^2-4\mu\right)}}\left(\frac{G'(\xi_n)}{G(\xi_n)}+\frac{\lambda}{2}\right)\pm\varepsilon\,f\left(\frac{\sqrt{\varepsilon\left(\lambda^2-4\mu\right)}}{2}d_1\right)}{1\pm\frac{2}{\sqrt{\varepsilon\left(\lambda^2-4\mu\right)}}f\left(\frac{\sqrt{\varepsilon\left(\lambda^2-4\mu\right)}}{2}d_1\right)\left(\frac{G'(\xi_n)}{G(\xi_n)}+\frac{\lambda}{2}\right)}\right)-\frac{\lambda}{2}\right)+$$
$$+\alpha_{-1}\left(\frac{\sqrt{\varepsilon\left(\lambda^2-4\mu\right)}}{2}\left(\frac{\frac{2}{\sqrt{\varepsilon\left(\lambda^2-4\mu\right)}}\left(\frac{G'(\xi_n)}{G(\xi_n)}+\frac{\lambda}{2}\right)\pm\varepsilon\,f\left(\frac{\sqrt{\varepsilon\left(\lambda^2-4\mu\right)}}{2}d_1\right)}{1\pm\frac{2}{\sqrt{\varepsilon\left(\lambda^2-4\mu\right)}}f\left(\frac{\sqrt{\varepsilon\left(\lambda^2-4\mu\right)}}{2}d_1\right)\left(\frac{G'(\xi_n)}{G(\xi_n)}+\frac{\lambda}{2}\right)}\right)-\frac{\lambda}{2}\right)^{-1}+\alpha_0 \tag{25}$$

and:

$$V_n(\xi_n)=\beta_0+\beta_1\left(\frac{G'(\xi_n)}{G(\xi_n)}\right)+\beta_{-1}\left(\frac{G(\xi_n)}{G'(\xi_n)}\right), \qquad \beta_1\neq 0 \quad or \quad \beta_{-1}\neq 0 \tag{26}$$

$$V_{n\pm1}=\beta_1\left(\frac{\sqrt{\varepsilon\left(\lambda^2-4\mu\right)}}{2}\left(\frac{\frac{2}{\sqrt{\varepsilon\left(\lambda^2-4\mu\right)}}\left(\frac{G'(\xi_n)}{G(\xi)_n}+\frac{\lambda}{2}\right)\pm\varepsilon\, f\left(\frac{\sqrt{\varepsilon\left(\lambda^2-4\mu\right)}}{2}d_1\right)}{1\pm\frac{2}{\sqrt{\varepsilon\left(\lambda^2-4\mu\right)}}f\left(\frac{\sqrt{\varepsilon\left(\lambda^2-4\mu\right)}}{2}d_1\right)\left(\frac{G'(\xi_n)}{G(\xi_n)}+\frac{\lambda}{2}\right)}\right)-\frac{\lambda}{2}\right)+$$
$$+\beta_{-1}\left(\frac{\sqrt{\varepsilon\left(\lambda^2-4\mu\right)}}{2}\left(\frac{\frac{2}{\sqrt{\varepsilon\left(\lambda^2-4\mu\right)}}\left(\frac{G'(\xi_n)}{G(\xi_n)}+\frac{\lambda}{2}\right)\pm\varepsilon\, f\left(\frac{\sqrt{\varepsilon\left(\lambda^2-4\mu\right)}}{2}d_1\right)}{1\pm\frac{2}{\sqrt{\varepsilon\left(\lambda^2-4\mu\right)}}f\left(\frac{\sqrt{\varepsilon\left(\lambda^2-4\mu\right)}}{2}d_1\right)\left(\frac{G'(\xi_n)}{G(\xi_n)}+\frac{\lambda}{2}\right)}\right)-\frac{\lambda}{2}\right)^{-1}+\beta_0 \tag{27}$$

Substituting Eqs. (24)-(27) along with (5) into Eqs. (23) and cleaning the denominator and collecting all terms with the same order of $(G'(\xi_n)/G(\xi_n))$ together, the left hand sides of Eqs. (23) are converted into polynomials in $(G'(\xi_n)/G(\xi_n))$. Setting each coefficient of these polynomials to zero, we derive a set of algebraic equations for $\alpha_0,\alpha_1,\alpha_{-1},\beta_0,\beta_1,\ \beta_{-1},d_1$ and c_1. Solving the set of algebraic equations by using Maple or Mathematica , we get the following cases:

Case 1:

$$\varepsilon=1,\quad \alpha_{-1}=-\alpha\beta_{-1},\qquad c_1=\frac{\alpha\beta_{-1}}{\mu},$$
$$\alpha_0=-\frac{1}{2\mu\alpha}\left\{\alpha^2\beta_{-1}\sqrt{\lambda^2-4\mu}\,coth\left[\frac{d_1\sqrt{\lambda^2-4\mu}}{2}\right]+\left(2\mu+\alpha^2\beta_{-1}\lambda\right)\right\} \tag{28}$$
$$\beta_0=\frac{\beta_{-1}\sqrt{\lambda^2-4\mu}}{2\mu}coth\left[\frac{d_1\sqrt{\lambda^2-4\mu}}{2}\right]+\frac{\lambda\beta_{-1}}{2\mu}$$
$$\beta_1=\alpha_1=0$$

where d_1 and β_{-1} are arbitrary constants.

In this case, we obtain the hyperbolic solutions of Eqs. (22) in the following forms:

$$U_n=-\frac{1}{2\mu\alpha}\left\{\alpha^2\beta_{-1}\sqrt{\lambda^2-4\mu}\,coth\left[\frac{d_1\sqrt{\lambda^2-4\mu}}{2}\right]+\left(2\mu+\alpha^2\beta_{-1}\lambda\right)\right\}+$$
$$-\alpha\beta_{-1}\left[\frac{\sqrt{\lambda^2-4\mu}}{2}\left(\frac{C_1\,sinh\left(\frac{\sqrt{\lambda^2-4\mu}}{2}\xi_n\right)+C_2\,cosh\left(\frac{\sqrt{\lambda^2-4\mu}}{2}\xi_n\right)}{C_1\,cosh\left(\frac{\sqrt{\lambda^2-4\mu}}{2}\xi_n\right)+C_2\,sinh\left(\frac{\sqrt{\lambda^2-4\mu}}{2}\xi_n\right)}\right)-\frac{\lambda}{2}\right]^{-1} \tag{29}$$

and:

$$V_n = \frac{\beta_{-1}\sqrt{\lambda^2-4\mu}}{2\mu}\coth\left[\frac{d_1\sqrt{\lambda^2-4\mu}}{2}\right]+\frac{\lambda\beta_{-1}}{2\mu}+$$
$$+\beta_{-1}\left[\frac{\sqrt{\lambda^2-4\mu}}{2}\left(\frac{C_1\sinh\left(\frac{\sqrt{\lambda^2-4\mu}}{2}\xi_n\right)+C_2\cosh\left(\frac{\sqrt{\lambda^2-4\mu}}{2}\xi_n\right)}{C_1\cosh\left(\frac{\sqrt{\lambda^2-4\mu}}{2}\xi_n\right)+C_2\sinh\left(\frac{\sqrt{\lambda^2-4\mu}}{2}\xi_n\right)}\right)-\frac{\lambda}{2}\right]^{-1} \quad (30)$$

where:

$$\xi_n = d_1 n+\frac{\alpha\beta_{-1}}{\mu}t+\xi_0$$

Case 2:

$$\begin{aligned}&\varepsilon=1,\quad \alpha_1=-\alpha\beta_1,\quad c_1=-\alpha\beta_1,\\ &\alpha_0=\frac{1}{2}\beta_1\alpha\sqrt{\lambda^2-4\mu}\coth\left[\frac{d_1\sqrt{\lambda^2-4\mu}}{2}\right]+\\ &\quad-\frac{\left(2+\alpha^2\beta_1\lambda\right)}{2\alpha}\\ &\beta_0=-\frac{1}{2}\beta_1\sqrt{\lambda^2-4\mu}\ \coth\left[\frac{d_1\sqrt{\lambda^2-4\mu}}{2}\right]+\frac{\lambda\beta_1}{2}\\ &\beta_{-1}=\alpha_{-1}=0\end{aligned} \quad (31)$$

where d_1 and β_1 are arbitrary constants.

In this case, we obtain the hyperbolic solutions of Eqs. (22) in the following forms:

$$U_n=\frac{1}{2}\beta_1\alpha\sqrt{\lambda^2-4\mu}\coth\left[\frac{d_1\sqrt{\lambda^2-4\mu}}{2}\right]-\frac{1}{\alpha}+$$
$$-\frac{1}{2}\alpha\beta_1\sqrt{\lambda^2-4\mu}\left(\frac{C_1\sinh\left(\frac{\sqrt{\lambda^2-4\mu}}{2}\xi_n\right)+C_2\cosh\left(\frac{\sqrt{\lambda^2-4\mu}}{2}\xi_n\right)}{C_1\cosh\left(\frac{\sqrt{\lambda^2-4\mu}}{2}\xi_n\right)+C_2\sinh\left(\frac{\sqrt{\lambda^2-4\mu}}{2}\xi_n\right)}\right) \quad (32)$$

and:

$$V_n=-\frac{1}{2}\beta_1\sqrt{\lambda^2-4\mu}\coth\left[\frac{d_1\sqrt{\lambda^2-4\mu}}{2}\right]+$$
$$+\frac{1}{2}\beta_1\sqrt{\lambda^2-4\mu}\left(\frac{C_1\sinh\left(\frac{\sqrt{\lambda^2-4\mu}}{2}\xi_n\right)+C_2\cosh\left(\frac{\sqrt{\lambda^2-4\mu}}{2}\xi_n\right)}{C_1\cosh\left(\frac{\sqrt{\lambda^2-4\mu}}{2}\xi_n\right)+C_2\sinh\left(\frac{\sqrt{\lambda^2-4\mu}}{2}\xi_n\right)}\right) \quad (33)$$

where:

$$\xi_n = d_1 n - \alpha\beta_1 t + \xi_0$$

Case 3:

$$\begin{aligned}
&\varepsilon = -1, \quad \alpha_{-1} = -\alpha\beta_{-1}, \qquad c_1 = \frac{\alpha\beta_{-1}}{\mu}, \\
&\alpha_0 = -\frac{1}{2\mu\alpha}\left\{\alpha^2\beta_{-1}\sqrt{4\mu-\lambda^2}\,cot\left[\frac{1}{2}d_1\sqrt{4\mu-\lambda^2}\right]+\left(2\mu+\alpha^2\beta_{-1}\lambda\right)\right\} \\
&\beta_0 = \frac{\beta_{-1}\sqrt{4\mu-\lambda^2}}{2\mu}cot\left[\frac{1}{2}d_1\sqrt{4\mu-\lambda^2}\right]+\frac{\lambda\beta_{-1}}{2\mu} \\
&\beta_1 = \alpha_1 = 0
\end{aligned} \tag{34}$$

where d_1 and β_{-1} are arbitrary constants.

In this case, we obtain the trigonometric solutions of of Eqs. (22) in the following forms:

$$\begin{aligned}
U_n = &-\frac{1}{2\mu\alpha}\left\{\alpha^2\beta_{-1}\sqrt{4\mu-\lambda^2}\,cot\left[\frac{1}{2}d_1\sqrt{4\mu-\lambda^2}\right]+\left(2\mu+\alpha^2\beta_{-1}\lambda\right)\right\}+ \\
&-\alpha\beta_{-1}\left[\frac{\sqrt{4\mu-\lambda^2}}{2}\left(\frac{-C_1\,sin\left(\frac{\sqrt{4\mu-\lambda^2}}{2}\xi_n\right)+C_2\,cos\left(\frac{\sqrt{4\mu-\lambda^2}}{2}\xi_n\right)}{C_1\,cos\left(\frac{\sqrt{4\mu-\lambda^2}}{2}\xi_n\right)+C_2\,sin\left(\frac{\sqrt{4\mu-\lambda^2}}{2}\xi_n\right)}\right)-\frac{\lambda}{2}\right]^{-1}
\end{aligned} \tag{35}$$

and:

$$\begin{aligned}
V_n = &\frac{\beta_{-1}\sqrt{4\mu-\lambda^2}}{2\mu}cot\left[\frac{1}{2}d_1\sqrt{4\mu-\lambda^2}\right]+\frac{\lambda\beta_{-1}}{2\mu}+ \\
&+\beta_{-1}\left[\frac{\sqrt{4\mu-\lambda^2}}{2}\left(\frac{-C_1\,sin\left(\frac{\sqrt{4\mu-\lambda^2}}{2}\xi_n\right)+C_2\,cos\left(\frac{\sqrt{4\mu-\lambda^2}}{2}\xi_n\right)}{C_1\,cos\left(\frac{\sqrt{4\mu-\lambda^2}}{2}\xi_n\right)+C_2\,sin\left(\frac{\sqrt{4\mu-\lambda^2}}{2}\xi_n\right)}\right)-\frac{\lambda}{2}\right]^{-1}
\end{aligned} \tag{36}$$

where:

$$\xi_n = d_1 n + \frac{\alpha\beta_{-1}}{\mu}t + \xi_0$$

Case 4:

$$\begin{aligned}
&\varepsilon = -1, \quad \alpha_1 = -\alpha\beta_1, \qquad c_1 = -\alpha\beta_1, \\
&\alpha_0 = \frac{1}{2}\beta_1\alpha\sqrt{4\mu-\lambda^2}\,cot\left[\frac{1}{2}d_1\sqrt{4\mu-\lambda^2}\right]-\frac{\left(2+\alpha^2\beta_1\lambda\right)}{2\alpha} \\
&\beta_0 = -\frac{1}{2}\beta_1\sqrt{4\mu-\lambda^2}\;cot\left[\frac{1}{2}d_1\sqrt{4\mu-\lambda^2}\right]+\frac{\lambda\beta_1}{2} \\
&\beta_{-1} = \alpha_{-1} = 0
\end{aligned} \tag{37}$$

where d_1 and β_1 are arbitrary constants.

In this case, we obtain the trigonometric solutions of Eqs. (22) in the following forms:

$$U_n = \frac{1}{2}\beta_1\alpha\sqrt{4\mu-\lambda^2}\,cot\left[\frac{1}{2}d_1\sqrt{4\mu-\lambda^2}\right]-\frac{1}{\alpha}+ \\ -\frac{1}{2}\alpha\beta_1\sqrt{4\mu-\lambda^2}\left(\frac{-C_1\,sin\left(\frac{\sqrt{4\mu-\lambda^2}}{2}\xi_n\right)+C_2\,cos\left(\frac{\sqrt{4\mu-\lambda^2}}{2}\xi_n\right)}{C_1\,cos\left(\frac{\sqrt{4\mu-\lambda^2}}{2}\xi_n\right)+C_2\,sin\left(\frac{\sqrt{4\mu-\lambda^2}}{2}\xi_n\right)}\right) \tag{38}$$

and:

$$V_n = -\frac{1}{2}\beta_1\sqrt{4\mu-\lambda^2}\,cot\left[\frac{1}{2}d_1\sqrt{4\mu-\lambda^2}\right]+ \\ +\frac{1}{2}\beta_1\sqrt{4\mu-\lambda^2}\left(\frac{-C_1\,sin\left(\frac{\sqrt{4\mu-\lambda^2}}{2}\xi_n\right)+C_2\,cos\left(\frac{\sqrt{4\mu-\lambda^2}}{2}\xi_n\right)}{C_1\,cos\left(\frac{\sqrt{4\mu-\lambda^2}}{2}\xi_n\right)+C_2\,sin\left(\frac{\sqrt{4\mu-\lambda^2}}{2}\xi_n\right)}\right) \tag{39}$$

where $\xi_n = d_1 n - \alpha\beta_1 t + \xi_0$.

III.3. Example 3. The (1+1) – Dimensional Toda Equation

In this subsection, we study (1+1) – dimensional Toda equation which take the following form[37]:

$$\frac{d^2u_n(t)}{dt^2} = e^{u_{n-1}(t)-u_n(t)} - e^{u_n(t)-u_{n+1}(t)} \tag{40}$$

If, we take the transformation $\frac{dv_n(t)}{dt} = e^{u_{n-1}(t)-u_n(t)} - 1$, then (40) becomes:

$$\frac{d^2v_n(t)}{dt^2} = \left(\frac{dv_n(t)}{dt}+1\right)\left(v_{n-1}-2v_n+v_{n+1}\right) \tag{41}$$

Using the transformation $v_n = V_n(\xi_n)$ and $\xi_n = d_1 n + c_1 t + \xi_0$, then Eqs. (41) becomes:

$$c_1^2 V_n'' = \left(c_1 V_n' + 1\right)\left(V_{n-1} - 2V_n + V_{n+1}\right) \tag{42}$$

According the homogenous balance produce , we have:

$$V_n(\xi_n) = \alpha_0 + \alpha_1\left(\frac{G'(\xi_n)}{G(\xi_n)}\right) + \alpha_{-1}\left(\frac{G(\xi_n)}{G'(\xi_n)}\right), \tag{43}$$

$$\alpha_1 \neq 0 \quad or \quad \alpha_{-1} \neq 0,$$

$$V_{n\pm1} = \alpha_1\left(\frac{\sqrt{\varepsilon\left(\lambda^2-4\mu\right)}}{2}\left(\frac{\frac{2}{\sqrt{\varepsilon\left(\lambda^2-4\mu\right)}}\left(\frac{G'(\xi_n)}{G(\xi_n)}+\frac{\lambda}{2}\right)\pm\varepsilon\, f\left(\frac{\sqrt{\varepsilon\left(\lambda^2-4\mu\right)}}{2}d_1\right)}{1\pm\frac{2}{\sqrt{\varepsilon\left(\lambda^2-4\mu\right)}}f\left(\frac{\sqrt{\varepsilon\left(\lambda^2-4\mu\right)}}{2}d_1\right)\left(\frac{G'(\xi_n)}{G(\xi_n)}+\frac{\lambda}{2}\right)}\right)-\frac{\lambda}{2}\right)+ \\ +\alpha_{-1}\left(\frac{\sqrt{\varepsilon\left(\lambda^2-4\mu\right)}}{2}\left(\frac{\frac{2}{\sqrt{\varepsilon\left(\lambda^2-4\mu\right)}}\left(\frac{G'(\xi_n)}{G(\xi_n)}+\frac{\lambda}{2}\right)\pm\varepsilon\, f\left(\frac{\sqrt{\varepsilon\left(\lambda^2-4\mu\right)}}{2}d_1\right)}{1\pm\frac{2}{\sqrt{\varepsilon\left(\lambda^2-4\mu\right)}}f\left(\frac{\sqrt{\varepsilon\left(\lambda^2-4\mu\right)}}{2}d_1\right)\left(\frac{G'(\xi_n)}{G(\xi_n)}+\frac{\lambda}{2}\right)}\right)-\frac{\lambda}{2}\right)^{-1}+\alpha_0 \tag{44}$$

Substituting Eqs. (43) and (44) along with (5) into Eqs. (42) and cleaning the denominator and collecting all terms with the same order of $(G'(\xi_n)/G(\xi_n))$ together, the left hand sides of Eq. (42) are converted into polynomial in $(G'(\xi_n)/G(\xi_n))$. Setting each coefficient of these polynomial to zero , we derive a set of algebraic equations for $\alpha_0, \alpha_1, \alpha_{-1}, d_1$ and c_1. Solving the set of algebraic equations by using Maple or Mathematica, we get the following cases:

Case 1:

$$\begin{aligned} &\varepsilon = -1, \quad c_1 = \frac{2}{\sqrt{4\mu-\lambda^2}} sin\left(\frac{1}{2}\sqrt{4\mu-\lambda^2}\, d_1\right) \\ &\alpha_{-1} = -\frac{2\mu}{\sqrt{4\mu-\lambda^2}} sin\left(\frac{1}{2}\sqrt{4\mu-\lambda^2}\, d_1\right), \alpha_1 = 0 \end{aligned} \tag{45}$$

where α_0 is an arbitrary constant. In this case, we obtain the trigonometric solution of Eq. (42) in the following form:

$$V_n = \alpha_0 - \frac{2\mu\, sin\left(\frac{1}{2}\sqrt{4\mu-\lambda^2}\, d_1\right)}{\sqrt{4\mu-\lambda^2}} \left[\frac{\sqrt{4\mu-\lambda^2}}{2} \left(\frac{-C_1 sin\left(\frac{\sqrt{4\mu-\lambda^2}}{2}\xi_n\right) + C_2 cos\left(\frac{\sqrt{4\mu-\lambda^2}}{2}\xi_n\right)}{C_1 cos\left(\frac{\sqrt{4\mu-\lambda^2}}{2}\xi_n\right) + C_2 sin\left(\frac{\sqrt{4\mu-\lambda^2}}{2}\xi_n\right)} \right) - \frac{\lambda}{2} \right]^{-1} \tag{46}$$

where:

$$\xi_n = d_1 n + \frac{2}{\sqrt{4\mu-\lambda^2}} sin\left(\frac{1}{2}\sqrt{4\mu-\lambda^2}\, d_1\right) t + \xi_0$$

Case 2:

$$\varepsilon = 1, \quad c_1 = \frac{2}{\sqrt{\lambda^2-4\mu}} sinh\left(\frac{1}{2}\sqrt{\lambda^2-4\mu} d_1\right), \; \alpha_{-1} = -\frac{2\mu}{\sqrt{\lambda^2-4\mu}} sinh\left(\frac{1}{2}\sqrt{\lambda^2-4\mu} d_1\right), \alpha_1 = 0 \tag{47}$$

where α_0 is an arbitrary constant. In this case, we obtain the hyperbolic solution of Eq. (42) in the following form:

$$V_n = \alpha_0 - \frac{2\mu\, sinh\left(\frac{1}{2}\sqrt{\lambda^2-4\mu}\, d_1\right)}{\sqrt{\lambda^2-4\mu}} \left[\frac{\sqrt{\lambda^2-4\mu}}{2} \left(\frac{C_1 sinh\left(\frac{\sqrt{\lambda^2-4\mu}}{2}\xi_n\right) + C_2 cosh\left(\frac{\sqrt{\lambda^2-4\mu}}{2}\xi_n\right))}{C_1 cosh\left(\frac{\sqrt{\lambda^2-4\mu}}{2}\xi_n\right) + C_2 sinh\left(\frac{\sqrt{\lambda^2-4\mu}}{2}\xi_n\right)} \right) - \frac{\lambda}{2} \right]^{-1} \tag{48}$$

where:

$$\xi_n = d_1 n + \frac{2}{\sqrt{\lambda^2-4\mu}} sinh\left(\frac{1}{2}\sqrt{\lambda^2-4\mu} d_1\right) t + \xi_0$$

Case 3:

$$\begin{aligned} &\varepsilon = 1, \quad \alpha_1 = -\frac{1}{2\sqrt{-\mu}} sinh\left(2\sqrt{-\mu}\, d_1\right), \alpha_{-1} = \frac{\sqrt{-\mu}}{2} sinh\left(2\sqrt{-\mu}\, d_1\right), \\ &c_1 = -\frac{1}{2\sqrt{-\mu}} sinh\left(2\sqrt{-\mu}\, d_1\right), \quad \lambda = 0, \end{aligned} \tag{49}$$

where α_0 is an arbitrary constant. In this case, we obtain the hyperbolic solution of Eq. (42) in the following form:

$$V_n = \alpha_0 - \frac{1}{2}\sinh\left(2\sqrt{-\mu}\,d_1\right)\left(\frac{C_1\sinh\left(\sqrt{-\mu}\xi_n\right)+C_2\cosh\left(\sqrt{-\mu}\xi_n\right)}{C_1\cosh\left(\sqrt{-\mu}\xi_n\right)+C_2\sinh\left(\sqrt{-\mu}\xi_n\right)}\right)+$$
$$+\frac{1}{2}\sinh\left(2\sqrt{-\mu}\,d_1\right)\left(\frac{C_1\sinh\left(\sqrt{-\mu}\xi_n\right)+C_2\cosh\left(\sqrt{-\mu}\xi_n\right)}{C_1\cosh\left(\sqrt{-\mu}\xi_n\right)+C_2\sinh\left(\sqrt{-\mu}\xi_n\right)}\right)^{-1} \tag{50}$$

where:

$$\xi_n = d_1 n - \frac{t}{2\sqrt{-\mu}}\sinh\left(2\sqrt{-\mu}\,d_1\right)+\xi_0$$

Case 4:

$$\begin{aligned}
&\varepsilon = -1\\
&\alpha_1 = \frac{1}{2\sqrt{\mu}}\sin\left(2\sqrt{\mu}\,d_1\right)\\
&\alpha_{-1} = -\frac{\sqrt{\mu}}{2}\sin\left(2\sqrt{\mu}\,d_1\right)\\
&c_1 = \frac{1}{2\sqrt{\mu}}\sin\left(2\sqrt{\mu}\,d_1\right)\\
&\lambda = 0
\end{aligned} \tag{51}$$

where α_0 is an arbitrary constant. In this case, we obtain the trigonometric solution of Eq. (42) in the following form:

$$V_n = \alpha_0 + \frac{1}{2}\sin\left(2\sqrt{\mu}\,d_1\right)\left(\frac{-C_1\sin\left(\sqrt{\mu}\,\xi_n\right)+C_2\cos\left(\sqrt{\mu}\xi_n\right)}{C_1\cos\left(\sqrt{\mu}\xi_n\right)+C_2\sin\left(\sqrt{\mu}\xi_n\right)}\right)+$$
$$-\frac{1}{2}\sin\left(2\sqrt{\mu}\,d_1\right)\left(\frac{-C_1\sin\left(\sqrt{\mu}\,\xi_n\right)+C_2\cos\left(\sqrt{\mu}\xi_n\right)}{C_1\cos\left(\sqrt{\mu}\xi_n\right)+C_2\sin\left(\sqrt{\mu}\xi_n\right)}\right)^{-1} \tag{52}$$

where:

$$\xi_n = d_1 n + \frac{t}{2\sqrt{\mu}}\sin\left(2\sqrt{\mu}\,d_1\right)+\xi_0$$

References

[1] Fermi E, Pasta J, Ulam S. *Collected papers of Enrico Fermi II*. Chicago, IL: University of Chicago Press; 1965.

[2] M.J. Ablowitz and P.A. Clarkson, *Solitons, nonlinear Evolution Equations and Inverse Scattering Transform*, Cambridge Univ. Press, Cambridge, 1991.

[3] R.Hirota, Exact solution of the KdV equation for multiple collisions of solutions, *Phys. Rev. Letters* 27 (1971) 1192-1194.

[4] M.R.Miura, *Backlund Transformation*,Springer-Verlag, Berlin,1978.

[5] C.Rogers and W.F.Shadwick, *Backlund Transformations*, Academic Press, New York,1982.

[6] J.Weiss, M.Tabor and G.Garnevalle, The Paineleve property for partial differential equations, *J.Math.Phys*. 24 (1983) 522-526.

[7] D.S.Wang, Y.J.Ren and H.Q.Zhang, Further extended sinh-cosh and sin-cos methods and new non traveling wave solutions of the (2+1)-dimensional dispersive long wave equations, *Appl. Math.E-Notes*, 5 (2005) 157-163.

[8] M.L. Wang, *Phys. Lett*. A 213 (1996) 279.

[9] J.H. He, The homotopy perturbation method for nonlinear oscillators with discontinuities, *Appl. Math. Comput*., 151 (2004) 287-292.

[10] J.H. He,Comparison of homotopy perturbation method and homotopy analysis method, *Appl. Math. Comput*., 156 (2004) 527-539.

[11] J.H. He, Homotopy perturbation method for bifurcation of nonlinear wave equations, *Int. J. Nonlinear Sci. Numer. Simul*., 6 (2005) 207-208 .

[12] E.M.E.Zayed, T.A. Nofal and K.A.Gepreel, The homotopy perturbation method for solving nonlinear Burgers and new

coupled MKdV equations, *Zeitschrift fur Naturforschung* Vol. 63a (2008) 627 -633.
[13] H.M. Liu, Generalized variational principles for ion acoustic plasma waves by He's semi-inverse method, *Chaos, Solitons & Fractals*, 23 (2005) 573 -576.
[14] H.M. Liu, Variational approach to nonlinear Electrochemical system, *Int. J. Nonlinear Sci. Numer. Simul*.5, (2004), 95 -96.
[15] E. Babolian, J. Biazar and A.R.Vahidi, A new computational method for Laplace transforms by decomposition method, *Appl. Math. Comput.*, 150 (2004) 841-846.
[16] E.Babolian, J.Biazar and A.R.Vahidi, Solution of a system of nonlinear equations by Adomain decomposition method, *Appl. Math. Comput*., 150 (2004) 847-854.
[17] H.A. Abdusalam, On an improved complex tanh -function method, *Int. J. Nonlinear Sci.Numer. Simul*., 6 (2005) 99-106.
[18] E.M.E.Zayed ,Hassan A.Zedan and Khaled A. Gepreel, Group analysis and modified extended Tanh- function to find the invariant solutions and soliton solutions for nonlinear Euler equations , *Int. J. Nonlinear Sci. Numer. Simul*., 5 (2004) 221-234.
[19] L. De-Sheng, G. Feng and Z. Hong-Qing, Solving the (2+1) dimensional higher order Broer-Kaup system via a transformation and tanh- function method, *Chaos, Solitons & Fractals*, 20 (2004) 1021-1025.
[20] Y. Chen and Q. Wang, Extended Jacobi elliptic function rational expansion method and abundant families of Jacobi elliptic functions solutions to (1+1) dimensional dispersive long wave equation, *Chaos, Solitons and Fractals*, 24 (2005) 745-757.
[21] S.Liu, Z. Fu, S.D. Liu and Q. Zhao, Jacobi elliptic function expansion method and periodic wave solutions of nonlinear wave equations, *Phys. Letters A*, 289 (2001) 69-74.
[22] D. Lu, Jacobi elliptic function solutions for two variant Boussinesq equations, *Chaos, Solitons and Fractals*, 24 (2005) 1373-1385.
[23] E.M.E. Zayed, H.A. Zedan, and K.A. Gepreel, On the solitary wave solutions for nonlinear Hirota– Satsuma coupled KdV of equations, *Chaos Solitons Fractals*, 22 (2004) 285–303.
[24] M.A. Abdou, The extended F-expansion method and its applications for a class of nonlinear evolution equation, *Chaos, Solitons and Fractals* 31(2007) 95 -104.
[25] M .Wang and X. Li, Applications of F-expansion to periodic wave solutions for a new Hamiltonian amplitude equation, *Chaos, Solitons and Fractals* 24 (2005) 1257- 1268.
[26] S. Zhang and T.C. Xia, A generalized F-expansion method and new exact solutions of Konopelchenko-Dubrovsky equations, *Appl. Math. Comput*., 183 (2006) 1190-1200.
[27] J.H. He and X.H. Wu, Exp-function method for nonlinear wave equations, *Chaos, Solitons and Fractals*, 30 (2006) 700-708.
[28] S. Zhang, Application of Exp-function method to higher dimensional nonlinear evolution equation, *Chaos, Solitons and Fractals* 38 (2008) 270-276.
[29] S. Zhang, Application of Exp-function method to Riccati equation and new exact solutions with three arbitrary functions of Broer-Kaup- Kupershmidt equations, *Phys. Letters A*, 372 (2008)1873-1880.
[30] M.Wang, X.Li and J.Zhang, The $\left(G'/G\right)$- expansion method and traveling wave solutions of nonlinear evolution equations in mathematical physics, *Phys.Letters A*, 372 (2008) 417-423.
[31] E.M.E.Zayed and K.A.Gepreel, The $\left(G'/G\right)$- expansion method for finding traveling wave solutions of nonlinear PDEs in mathematical physics, *J. Math. Phys*., 50 (2009) 013502-013514.
[32] E.M.E.Zayed and Khaled A.Gepreel, Some applications of the $\left(G'/G\right)$ expansion method to non-linear partial differential equations, *Appl. Math. and Comput*., 212, 1-13.
[33] S. Zhang , L.Dong, J.Ba and Y.Sun, The $\left(G'/G\right)$- expansion method for nonlinear– difference equations, *Phys. Letters A*, 373 (2009) 905-910.
[34] G. Wu and T.Xia, A new method for constructing soliton solutions to differential- difference equation with symbolic computation, *Chaos, Solitons and Fractals*, 39 (2009) 2245-2248.
[35] F. Xie and J. Wang, A new method for solving nonlinear differential- difference equation, *Chaos, Solitons and Fractals*, 27 (2006) 1067-1071.
[36] C. Liu, Exponential function rational expansion method for nonlinear differential- difference equations, *Chaos, Solitons and Fractals*, 40 (2009) 708-716.
[37] Q. Wang and Y.Yu, New rational formal for (1+1)- dimensional Toda equation and another Toda equation, *Chaos, Solitons and Fractals*, 29 (2006) 904-915.

Authors' information

Mathematics Department,
Faculty of Science,
Zagazig University,
Egypt. Mathematics Department,
Faculty of Science,
Taif University,
El-Taif, El- Hawiyah, P.O.Box 888,
Kingdom of Saudi Arabia.
E-mail: kagepreel@yahoo.com

Praise Worthy Prize

International Review of Physics (I.R.E.PHY.), Vol. 5, N. 6
December 2011

Quantum Interference in a Four-Level EIT System and its Application to Photonic Logic Gates

Peiyu Chen[1], Jian Qi Shen[1,2*]

Abstract – *The intensity - and frequency - tunable probe transitions, where double-control destructive and constructive quantum interference is involved, in a four-level tripod-configuration atomic system is suggested for designing photonic logic gates. The influence of phase coherence between two transitions (driven by two control fields) on the probe transition is also studied. The real and imaginary parts of the relative electric permittivity and the relative impedance versus the normalized frequency detunings as well as the normalized Rabi frequencies of the two control fields are presented as illustrative examples to demonstrate the effects of double-control destructive and constructive quantum interference. The present scenario has potential applications in new photonic device design, e.g., logic gates and sensitive optical switches. Two photonic logic gates are designed by taking full advantage of the destructive and constructive quantum interference exhibited in the present four-level EIT (electromagnetically induced transparency) system.* ***Copyright © 2011 Praise Worthy Prize S.r.l. - All rights reserved.***

Keywords: *Electromagnetically Induced Transparency, Quantum Coherence, Quantum Interference, Photonic Logic Gates*

Nomenclature

Γ_3	Spontaneous emission decay rate
$\gamma_2, \gamma_{2'}$	Dephasing rates
$\Omega_c, \Omega_{c'}$	Rabi frequency of the control fields
Δ_p	Probe frequency detuning
$\Delta_c, \Delta_{c'}$	Frequency detunings of the control fields
β	Atomic electric polarizability
N	Atomic concentration of vapor
ε_r	Relative electric permittivity
α	Absorption index

I. Introduction

With the development of photonics and quantum optics, considerable attention was directed by scientists in many different areas at new techniques to manipulate light wave propagations by making use of artificial electromagnetic materials [1]. A particularly flexible and promising approach to manipulating light propagation has been that of quantum coherence. For example, the effects of quantum coherent control realized via atomic phase coherence, such as electromagnetically induced transparency (EIT), have captured intensive interest of many researchers over the last two decades [1]. Since a spectrally narrowband transmission (transparency) window within a quite broad absorption band can be established because of destructive quantum interference between atomic transition pathways [1], EIT is such a quantum optical phenomenon that if one resonant laser beam propagates in a medium (e.g., an atomic vapor or a semiconductor-quantum-dot material), the beam will get absorbed; but if two resonant laser beams instead propagate inside the same medium, neither would be absorbed. Thus the opaque medium becomes a transparent one. There are a number of phenomena that are relevant to EIT, including inversionless light amplification [2], cancellation of spontaneous emission [3], multi-photon population trapping [4], phase coherence control [5], [6] as well as EIT-induced negatively refracting materials [7]. Recently, EIT has attracted extensive attention of researchers in a variety of areas of atomic physics, optics, and condensed state physics [8]-[11]. These investigations include ultraslow light, superluminal propagation, and optical storage with atomic vapors [8]-[11]. As is well known, the probe light (and hence information) could be stored in a three-level system when turning off the control field (and would be read out when turning on the control field). This can be generalized to those cases of four-level systems, which can be used to realize light storage technique and device designs (such as logic gates, functional-operation devices and optical switches), so that it would open a good perspective of using EIT for new applications in technology of optical data storage and relevant information processing.

Since a four-level EIT system can exhibit more significant dispersion sensitive to the probe frequency than a conventional three-level system [1], [12], the

Manuscript received and revised November 2011, accepted December 2011

quantum optical properties of four-level EIT (such as double-control quantum interference [13], [14], transient turn-on and -off dynamics) as well as its application to photonic device design have focused intensive attention of some researchers [15]-[17].

In this paper we shall consider the double-control destructive and constructive quantum interference of a four-level tripod-configuration atomic system in more details, and then aim at designing some photonic logic gates by taking full advantage of the present quantum interference effects. As is known, the most remarkable feature of the present scheme is that the optical properties (absorption, transparency and dispersion) of an atomic system can be manipulated via the double-control multi-pathway interferences (multiple routes to excitation) [13], [14]. Such a four-level system will exhibit a two-level resonant absorption because the two control levels (driven by the two control fields) can form a dark state (and hence the destructive quantum interference occurs between the two transitions driven by the two control fields).

However, the present four-level system will also exhibit electromagnetically induced transparency to the probe field when the three lower levels (including the probe level and the two control levels) form a three-level dark state. Thus, the present scenario could find potential applications in designing a number of new devices (e.g., logic gates and sensitive optical switches) and would enable physicists to develop new techniques (e.g., quantum coherent information storage).

II. A Theoretical Model for a Four-Level EIT

Here we shall address the intriguing optical behavior of this four-level EIT atomic vapor. Consider a four-level atomic system with three ground levels |1>, |2>, |2'> and one excited level |3> (see Fig. 1 for its schematic diagram). This atomic system interacts with the electric fields of the probe wave and the two control light waves, which drive the |1>-|3>, |2>-|3> and |2'>-|3> transitions, respectively. As there are two control fields and one probe field interacting with the four-level system, the multilevel transitions, where the constructive and destructive interference among various transition pathways will arise, would give rise to novel optical behavior of the EIT medium [13], [14]. If, for example, the ratio of the intensities (characterized by the squares of the Rabi frequencies, i.e., $\Omega_c^*\Omega_c$ and $\Omega_{c'}^*\Omega_{c'}$) of the two control fields are taken to be certain proper values, the double-control destructive interference between |2>-|3> and |2'>-|3> transitions would occur. Then, it seems that the two levels |2> and |2'> as well as the two control fields (Ω_c, $\Omega_{c'}$) are absent, and hence the four-level system would be reduced to a simple two-level system {|1>, |3>} [14]. Thus, under this condition, the four-level EIT vapor is no longer transparent to the probe field.

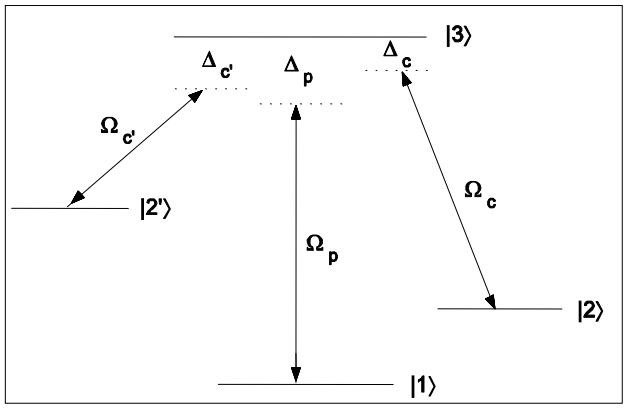

Fig. 1. The schematic diagram of a four-level tripod-configuration EIT atomic system. If one of the two control fields is switched off, the system will be reduced to a three-level one, and if both of the two control fields are switched off, it becomes a simple two-level system

The Schrödinger equation that governs the density matrix elements of the four- level atomic system is given by [13], [14]:

$$\begin{cases} \dot{\rho}_{21} = -\left[\dfrac{\gamma_2}{2} + i\left(\Delta_p - \Delta_c\right)\right]\rho_{21} + \dfrac{i}{2}\Omega_c^*\rho_{31} + \\ \qquad -\dfrac{i}{2}\Omega_p\rho_{23}, \\ \dot{\rho}_{2'1} = -\left[\dfrac{\gamma_{2'}}{2} + i\left(\Delta_p - \Delta_{c'}\right)\right]\rho_{2'1} + \dfrac{i}{2}\Omega_{c'}^*\rho_{31} + \\ \qquad -\dfrac{i}{2}\Omega_p\rho_{2'3}, \\ \dot{\rho}_{31} = \dfrac{i}{2}\left(\Omega_p\rho_{11} + \Omega_c\rho_{21} + \Omega_{c'}\rho_{2'1}\right) + \\ \qquad -\left(\dfrac{\Gamma_3}{2} + i\Delta_p\right)\rho_{31} - \dfrac{i}{2}\Omega_p\rho_{33} \end{cases} \tag{1}$$

Here, Γ_3 and $\gamma_2, \gamma_{2'}$ stand for the spontaneous emission decay rate and the collisional dephasing rates (nonradiative decay rates), respectively. $\Omega_c, \Omega_{c'}$ and Ω_p denote the Rabi frequencies of the two control fields and the probe field.

They are defined though $\Omega_c = \wp_{32}E_c/\hbar$, $\Omega_{c'} = \wp_{32'}E_{c'}/\hbar$ and $\Omega_p = \wp_{31}E_p/\hbar$ respectively, with E_c, $E_{c'}$ and E_p the slowly-varying amplitudes (envelopes) of the control fields and the probe field. The frequency detunings of the three applied optical fields are defined as $\Delta_p = \omega_{31} - \omega_p$, $\Delta_c = \omega_{32} - \omega_c$, and $\Delta_{c'} = \omega_{32'} - \omega_{c'}$ with ω_p and ω_c, $\omega_{c'}$ the mode frequencies of the probe and control fields, respectively. In general, the population (ρ_{11}) in the ground level $|1\rangle$ is almost unity (i.e., $\rho_{11} \to 1$).

t should be noted that the three-level EIT system is a special case of the four-level system. If, for example, one

of the control fields, say, $\Omega_{c'}$, is switched off (i.e., $\Omega_{c'}=0$), then the present four-level atomic system will be reduced to a three-level system.

In order to treat the optical response of the atomic system, we should have to solve the dynamical equation (1).

As the intensity of the probe field is sufficiently weak, the terms that contain $\Omega_p\rho_{i3}$ in Eq. (1) are negligibly small. Under this condition, one can obtain the steady solution to Eq. (1):

$$\begin{aligned}\rho_{21}&=-\frac{1}{4D}\Omega_p\Omega_c^*\left[\frac{\gamma_{2'}}{2}+i\left(\Delta_p-\Delta_{c'}\right)\right]\\ \rho_{2'1}&=-\frac{1}{4D}\Omega_p\Omega_{c'}^*\left[\frac{\gamma_2}{2}+i\left(\Delta_p-\Delta_c\right)\right]\\ \rho_{31}&=\frac{i}{2D}\Omega_p\left[\frac{\gamma_2}{2}+i\left(\Delta_p-\Delta_c\right)\right]\left[\frac{\gamma_{2'}}{2}+i\left(\Delta_p-\Delta_{c'}\right)\right]\end{aligned} \tag{2}$$

here the parameter D in the denominator is defined by:

$$\begin{aligned}D=&\left(\frac{\Gamma_3}{2}+i\Delta_p\right)\left[\frac{\gamma_2}{2}+i\left(\Delta_p-\Delta_c\right)\right]\cdot\\ &\cdot\left[\frac{\gamma_{2'}}{2}+i\left(\Delta_p-\Delta_{c'}\right)\right]+\\ &+\frac{1}{4}\Omega_{c'}^*\Omega_{c'}\left[\frac{\gamma_2}{2}+i\left(\Delta_p-\Delta_c\right)\right]+\\ &+\frac{1}{4}\Omega_c^*\Omega_c\left[\frac{\gamma_{2'}}{2}+i\left(\Delta_p-\Delta_{c'}\right)\right]\end{aligned} \tag{3}$$

By using the definition of the atomic electric polarizability, $\beta=2\wp_{13}\rho_{31}/\left(\varepsilon_0E_p\right)$, one can arrive at:

$$\begin{aligned}\beta\left(\Delta_p\right)=&\frac{|\wp_{13}|^2}{\varepsilon_0\hbar}\frac{i}{D}\left[\frac{\gamma_2}{2}+i\left(\Delta_p-\Delta_c\right)\right]\cdot\\ &\cdot\left[\frac{\gamma_{2'}}{2}+i\left(\Delta_p-\Delta_{c'}\right)\right]\end{aligned} \tag{4}$$

The relative electric permittivity, where the local field effect caused by the dipole-dipole interaction between neighboring atoms has been taken into account, is given by:

$$\varepsilon_{\mathrm{r}}=1+\frac{N\beta}{1-\frac{N\beta}{3}} \tag{5}$$

We shall also in this paper consider the absorption of the four-level atomic vapor to the probe light. The absorption index is defined by:

$$\alpha=2\pi\frac{Im\{n_{\mathrm{r}}\}}{Re\{n_{\mathrm{r}}\}} \tag{6}$$

It follows from the solutions (2) and (3) that the frequency detunings Δ_c, $\Delta_{c'}$ and the Rabi frequencies Ω_c, $\Omega_{c'}$ are the tunable parameters of the present four-level system. Whether it is the destructive or constructive quantum interference (among the transition pathways $|1\rangle$-$|3\rangle$, $|2\rangle$-$|3\rangle$ and $|2'\rangle$-$|3\rangle$ driven by the three optical fields) is determined by these tunable parameters, particularly by the two Rabi frequencies Ω_c, $\Omega_{c'}$.

III. Optical Properties of a Four-Level EIT via Quantum Interference Involved in Atomic Phase Coherence

We shall now consider the optical behavior induced by the destructive and constructive quantum interference. The atomic parameters of the present atomic vapor are given as follows: the spontaneous emission decay rate $\Gamma_3=2.0\times10^7\,\mathrm{s}^{-1}$, the dephasing rate $\gamma_2=1.0\times10^5\,\mathrm{s}^{-1}$, $\gamma_{2'}=2.0\times10^5\,\mathrm{s}^{-1}$, the electric-transition dipole moment $\wp_{13}=1.0\times10^{-29}\,\mathrm{C\cdot m}$, and the atomic concentration $N=1.0\times10^{20}\,\mathrm{m}^{-3}$. The general dispersive behavior (as well as its absorption index and relative impedance) of the four-level atomic vapor is presented in Figs. 2-4, respectively. Here the two frequency detunings of the two control fields and their Rabi frequencies are chosen as $\Delta_c=1.5\Gamma_3=3.0\times10^7\,\mathrm{s}^{-1}$, $\Delta_{c'}=4\Gamma_3=8.0\times10^7\,\mathrm{s}^{-1}$ and $\Omega_c=4.0\times10^7\,\mathrm{s}^{-1}$, $\Omega_{c'}=8.0\times10^7\,\mathrm{s}^{-1}$. From the imaginary part of ε_r in Fig. 2 (as well as the absorption index α in Fig. 3), one can see that there are three Autler-Townes absorption peaks (i.e., the Autler-Townes triplet), which are located at $\Delta_p=\Delta_c=1.5\Gamma_3$ and $\Delta_p=\Delta_{c'}=4\Gamma_3$. The imaginary part of ε_r and the absorption index α will take their minimums among the three Autler-Townes peaks. This corresponds to the fact that the transition pathways $|2\rangle$-$|3\rangle$ and $|2'\rangle$-$|3\rangle$ driven by the control fields destructively interference with the probe transition pathway $|1\rangle$-$|3\rangle$, and hence two spectrally narrowband transmission (transparency) windows opens up within the broadband absorption line [18]. It can also be seen that both the relative permittivity and the impedance would tend to 1 when the probe frequency detuning Δ_p approach Δ_c or $\Delta_{c'}$. This yields the double-control EIT effect.

We shall now concentrate our attention on the influence of the frequency-tunable control laser beams on the four-level atomic population. The real and imaginary parts of the relative electric permittivity and the impedance are plotted in Fig. 5 and the absorption index in Fig. 6, where the two Rabi frequencies of the two

control fields are chosen as $\Omega_c = 4.0\times10^7\,\mathrm{s}^{-1}$, $\Omega_{c'} = 8.0\times10^7\,\mathrm{s}^{-1}$ and the probe frequency is $\Delta_p = 1.0\times10^7\,\mathrm{s}^{-1}$.

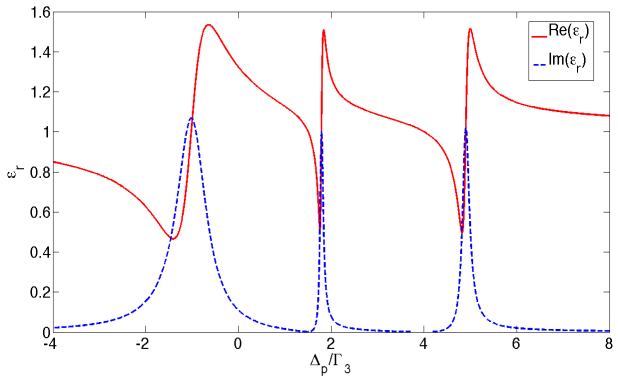

Fig. 2. The relative electric permittivity versus the normalized frequency detuning of the probe field. There are three peaks and three valleys in the dispersion curve of the real part of the four-level permittivity, and three peaks and two valleys in the dispersion curve of its imaginary part

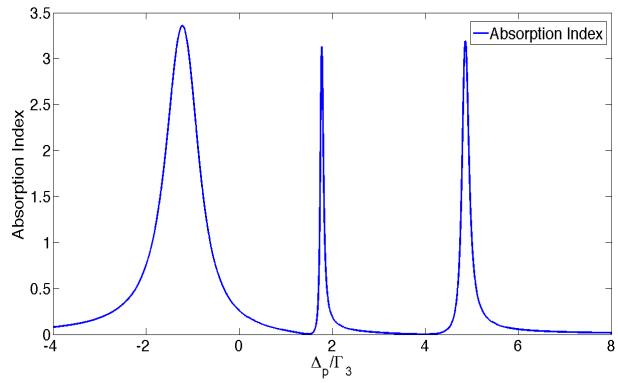

Fig. 3. The absorption index versus the normalized frequency detuning of the probe field

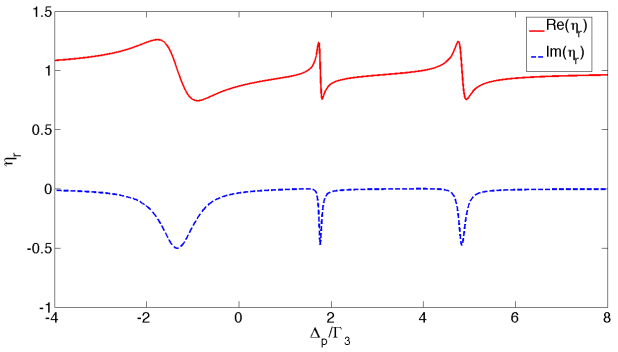

Fig. 4. The relative impedance versus the normalized frequency detuning of the probe field

It follows from Fig. 5 that the imaginary part of the electric permittivity vanishes and the real part would be unity when the frequency detunings Δ_c and $\Delta_{c'}$ of the control fields tend to the probe frequency Δ_p. The three-dimensional behavior of the absorption index plotted in Fig. 6 shows that the loss of the four-level atomic vapor would be quite large when the frequency detunings Δ_c and $\Delta_{c'}$ deviate from the probe frequency Δ_p. This would lead to the Autler-Townes peaks (Autler-Townes triplet).

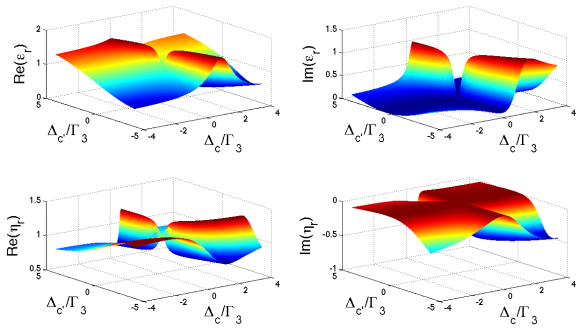

Fig. 5. The real and imaginary parts of the relative electric permittivity and the impedance versus the normalized frequency detuning of the two control fields

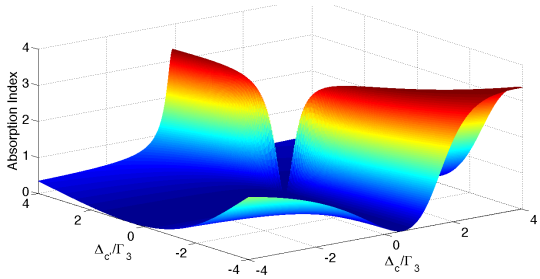

Fig. 6. The absorption index versus the normalized frequency detuning of the two control fields

We have studied the tunable optical response that is caused when one tunes the frequencies (and hence the frequency detunings) of the control fields. Now we are in a position to consider another controllable optical behavior that is induced by the tunable Rabi frequencies of the two control fields. In Fig. 7 and Fig. 8, the fixed parameters of frequency detunings are given by $\Delta_c = 3.0\times10^7\,\mathrm{s}^{-1}$, $\Delta_{c'} = 8.0\times10^7\,\mathrm{s}^{-1}$, and $\Delta_p = 1.0\times10^7\,\mathrm{s}^{-1}$. The real and imaginary parts of the relative electric permittivity and the impedance are presented as an illustrative example. From the imaginary part of the permittivity ε_r in Fig. 7 and the absorption index in Fig. 8, one can find that the absorption (loss) of the atomic vapor would decrease when one of the Rabi frequencies Ω_c, $\Omega_{c'}$ increases (this makes the ground level $|1\rangle$ become a dark state automatically). But it should be emphasized that when the ratio $\Omega_{c'}/\Omega_c$ are taken to be certain values, the absorption index would increase rapidly because there is destructive interference between the |2>-|3> and |2'>-|3> transitions, namely,

levels $|2\rangle$ and $|2'\rangle$ form a new dark state, which can be expressed by $N\left(\Omega_{c'}|2\rangle-\Omega_c|2'\rangle\right)$ with the normalized coefficient $N=1/\sqrt{\Omega_c^*\Omega_c+\Omega_{c'}^*\Omega_{c'}}$. Under this condition, it seems that the two control fields $\Omega_c,\Omega_{c'}$ as well as the two levels $|2\rangle$ and $|2'\rangle$ are not present, and hence the four-level system $\{|1\rangle,|2\rangle,|2'\rangle,|3\rangle\}$ is reduced to a two-level system $\{|1\rangle,|3\rangle\}$. Since now the steady density matrix element of the $|1\rangle$ - $|3\rangle$ transition driven by the probe field is $\rho_{31}=i\Omega_p\rho_{11}/\left[2\left(\Gamma_3+i\Delta_p\right)\right]$ (an expression for a typical response of two-level resonant absorption), an effect of significant absorption to the probe field will arise because of the double-control destructive quantum interference between the two transition pathways $|2\rangle\rightarrow|3\rangle$ and $|2'\rangle\rightarrow|3\rangle$.

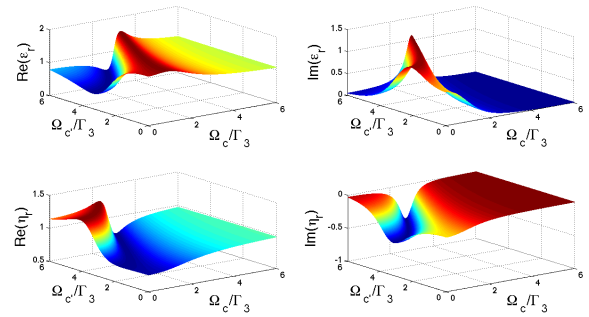

Fig. 7. The real and imaginary parts of the relative electric permittivity and the impedance versus the normalized Rabi frequencies of the two control fields

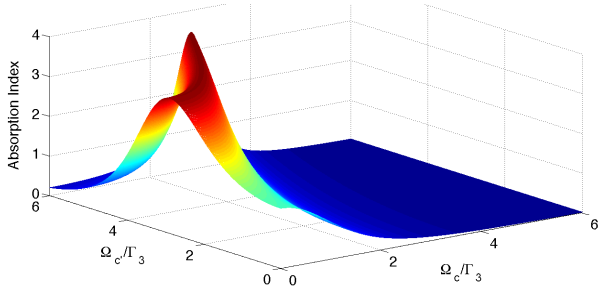

Fig. 8. The absorption index versus the normalized Rabi frequencies of the two control fields

In a word, the multilevel atomic coherence (various quantum interference effects) can be controllably manipulated by adjusting the intensities (or the Rabi frequencies) and the mode frequencies of the control fields.

In the section that follows, we shall design some typical photonic logic gates in order to show how the double-control quantum interference works in photonic devices.

IV. Design of Photonic Logic Gates

In the preceding section, we have shown the EIT phenomena depending on the frequency detunings and the Rabi frequencies, the latter of which indicate the light intensities of the control fields. According to the simulation results presented in the above, the four-level tripod-configuration atomic system becomes transparent or opaque to the probe beam when one tunes control beams' frequency detunings or control beams' light intensity.

With some appropriate definitions, these interesting EIT characteristics can be used to make basic logic operations, such as OR and EX-OR. Here, two photonic logic gates (OR Gate and EX-OR Gate) will be designed based on the EIT effect exhibited by the present four-level tripod-configuration atomic system.

First of all, two groups of definitions need to be clarified. One group is F (Frequency) EIT and I (Intensity) EIT. The other is DIM (Destructive quantum Interference Mechanism) and CIM (Constructive quantum Interference Mechanism). We shall interpret these two groups as follows:

i) FEIT means that the frequency detunings are used as inputs in the EIT-based logic gates. The logic function is operated by changing light's frequency detunings. The IEIT means that EIT photonic logic gates utilize light intensities as inputs and the logic gates work when the control light intensities change.

ii) DIM (Destructive quantum Interference Mechanism) means that the two control beams intensities are adjusted to meet $\Omega_1 a_1+\Omega_2 a_2\simeq 0$ (destructive quantum interference). Thus the four-level system is equivalent to a two-level system that can exhibit giant absorption. CIM (Constructive quantum Interference Mechanism) means that the two control beams intensities fulfill $\Omega_1 a_1-\Omega_2 a_2\simeq 0$ [14]. Under this condition, the probe field cannot be absorbed because of the constructive quantum interference between the |2>-|3> and |2'>-|3> transition pathways driven by the two control beams.

We are now in a position to present the working mechanisms of the EIT-based photonic logic gates (OR Gate and EX-OR Gate), which work by taking full advantage of the tunable optical responses of the four-level atomic system.

IV.1. OR Gate

This photonic logic gate is based on a four-level FEIT CIM tripod-configuration atomic system. According to the simulation result in Fig. 5 and Fig. 6, we shall design the OR logic gate. Rather than by changing the intensity of the two control beams, this OR logic gate operates the logical function by changing the frequency of control beams, which is available for some kinds of lasers (e.g. dye laser or $Ti_{:}^{3+}Al_2 0_3$ laser). When the frequency detuning (Δ_c or $\Delta_{c'}$) of the control beam is equal to

the frequency detuning (Δ_p) of the probe beam, we define that the logic operation INPUT1 or INPUT2 is 1. However, when the frequency detuning is much larger than the decay rate (Γ_3), such as $\Delta_c = \Delta_{c'} = -6\Gamma_3$, the logic operation INPUT1 or INPUT2 is defined as 0. Note that the probe beam is always present, and its frequency detuning is as small as possible (i.e., the probe field is almost resonant with the |1>-|3> transition). When the probe field is transmitted through the atomic medium without loss, the logic operation OUTPUT is 1. Otherwise, OUTPUT is 0. The schematic diagram of the OR gate is presented in Fig. 9, and the truth table is given in Table I.

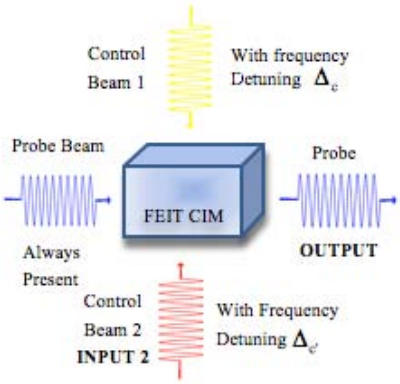

Fig. 9. The schematic diagram of the photonic OR gate designed based on the four-level tripod-configuration EIT atomic system. The probe beam and the two control beams, viewed as INPUT signals, are always present. The transmitted probe beam is viewed as an OUTPUT signal

TABLE I
THE TRUTH TABLE OF THE OR GATE BASED ON THE EIT PHENOMENON OF THE FOUR-LEVEL TRIPOD-CONFIGURATION ATOMIC SYSTEM

2 INPUT OR GATE		
A	B	Q
0	0	0
0	1	1
1	0	1
1	1	1

The working mechanism of the photonic OR logic gate is given as follows: when the frequency detuning (Δ_c or $\Delta_{c'}$) of any of the two control beams are equal to that of the probe beam (Δ_p), the four-level tripod-configuration atomic vapor is transparent to the probe beam and the probe beam is transmitted through the device without absorption, i.e. OUTPUT = 1.

However, if either of the control beams is far away from the resonant frequencies, i.e. $\Delta_c \to \Delta_p$ or $\Delta_{c'} \to \Delta_p$, the atomic vapor will present a sharp absorption of the probe beam, i.e. OUTPUT = 0.

IV.2. EX-OR Gate

This photonic logic gate is designed based on a four-level IEIT DIM tripod-configuration atomic system (e.g., the simulation result shown in Fig. 7 and Fig. 8). We suppose that both of the two control beams with Rabi frequency 1 and Rabi frequency 2 are at the resonant frequency for the atomic system to exhibit zero absorption, i.e., $\Delta_c \to \Delta_p$ and $\Delta_{c'} \to \Delta_p$. The input logic operation (INPUT1 or INPUT2) is equal to 1 when the input control beam is switched on, and is equal to 0 when the input control beam is switched off. Note that the probe beam is always present. We stipulate that the output logic operation is 1 when the probe beam is transmitted through the photonic device without absorption, and 0 when the probe beam loses its energy because of the giant absorption in the atomic medium. The schematic diagram of the EX-OR gate is presented in Fig. 10, and the truth table is given in Table II.

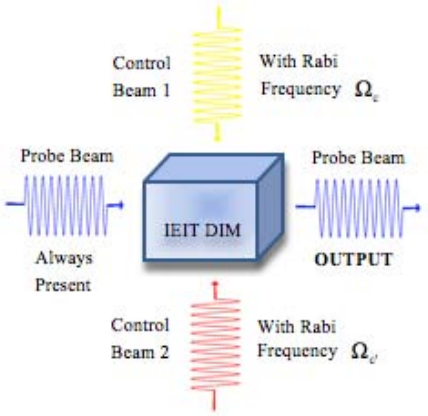

Fig. 10. The schematic diagram of an EX-OR gate (I-Form EIT logic gate) designed based on the four-level tripod-configuration atomic system

The working mechanism of the photonic EX-OR logic gate is given as follows: This EX-OR logic gate makes use of Destructive quantum Interference Mechanism (DIM). The two control beams (with its frequency close to the resonant frequency, i.e., $\Delta_c \to \Delta_p$ and $\Delta_{c'} \to \Delta_p$) play the role of inputs (i.e. INPUT1 & INPUT2).

Choose the proper intensity of the two control fields to fit the definition of DIM (i.e. $\Omega_c a_2 + \Omega_{c'} a_{2'} = 0$). When both of the two control beams are switched off (i.e. INPUT1 = 0 and INPUT2 = 0), the atomic vapor will become a two-level system and thus the resonant absorption will happen, and so the atomic vapor medium is opaque to the probe beam, i.e. OUTPUT = 0; If only one of the control beams is switched on (i.e. INPUT1 = 0, INPUT2 = 1 or INPUT1 = 1, INPUT2 = 0), the atomic vapor is a three-level system and then the single-control EIT to the probe beam will arise in this DIM vapor medium. The probe beam will propagate through the device without absorption, i.e. OUTPUT = 1; If both of the two control beams are switched on (i.e. INPUT1 = 1, INPUT2 = 1), the destructive quantum interference between the |2>-|3> and |2'>-|3> transition pathways (driven by the two control beams) will occur, and thus

the four-level system is equivalent to a two-level system, which can exhibit large resonant absorption, i.e. OUTPUT = 0.

TABLE II
THE TRUTH TABLE OF EX-OR LOGIC GATE BASED ON THE EIT PHENOMENON OF THE FOUR-LEVEL TRIPOD-CONFIGURATION ATOMIC SYSTEM

2 INPUT EX-OR GATE		
A	B	Q
0	0	0
0	1	1
1	0	1
1	1	0

V. Concluding Remarks

The optical property of a multilevel atomic vapor can be manipulated by controlling the quantum interference between the control transitions driven by the control fields.

A four-level system, where a three-level dark state is involved, shows more flexible optical responses than a conventional three-level EIT system [1]. EIT and the relevant quantum coherent effects would lead to many applications, e.g., designs of new photonic and quantum optical devices.

In this paper, we have investigated the tunable optical property that is induced by the double-control quantum interference.

The double-control quantum interference would be applicable to some new all-optical techniques, where one photon field can coherently control the other. Since all these new systems that would have promising applications in photonic technology (including designs of all-optical devices) have exhibited quantum coherent effects, we hope that the presented work of multilevel coherent control with a double-control four-level system may stimulate a new interest in this area, and that it would be experimentally realized in the near future.

Acknowledgments

This work is supported by the National Natural Science Foundation of China under Grant Nos. 11174250 and 60990320, Zhejiang Provincial Natural Science Foundation under Grant No.Y6100280, and the Fundamental Research Funds for the Central Universities of China.

References

[1] S. E. Harris: *Phys. Today* Vol. 50 (No.7) (1997), p. 36.
M. Fleischhauer, A. Imamoglu and J. Marangos: *Rev. Mod. Phys.* Vol. 77 (2005), p. 633.
[2] J. L. Cohen and P. R. Berman: *Phys. Rev.* A Vol. 55 (1997), p. 3900.
[3] S. Y. Zhu and M. O. Scully: *Phys. Rev. Lett.* Vol. 76 (1996), p. 388.
[4] C. Champenois, G. Morigi and J. Eschner: *Phys. Rev. A* Vol. 74 (2006), 053404.
[5] A. M. Zheltikov: *Phys. Rev. A* Vol. 74 (2006), 053403.
[6] A. Gandman, L. Chuntonov, L. Rybak and Z. Amitay: *Phys. Rev. A* Vol. 75 (2007), 031401.
[7] C. M. Krowne and J. Q. Shen: *Phys. Rev. A* Vol. 79 (2009), 023818.
[8] H. Schmidt and A. Imamoğlu: *Opt. Lett.* Vol. 21 (1996), p. 1936.
[9] L. J. Wang, A. Kuzmich and A. Dogariu: *Nature* Vol. 406 (2000), p. 277.
[10] P. Arve, P. Jänes and L. Thylén: *Phys. Rev. A* Vol. 69 (2004), 063809.
[11] J. Q. Shen, Z. C. Ruan and S. He: *Phys. Lett. A* Vol. 330 (2004), p. 487.
[12] M. O. Scully and M. S. Zubairy: *Quantum Optics*, Chapt. 7 (Cambridge Univ. Press, Cambridge, UK 1997).
[13] J. Q. Shen*: New J. Phys*. Vol. 15 (2007), p. 374.
[14] J. Q. Shen and P. Zhang: *Opt. Express* Vol. 15 (2007), p. 6484.
[15] E. Paspalakis and P. L. Knight: *J. Opt. B: Quantum Semiclass. Opt*. Vol. 4 (2002), p. S372.
[16] J. Q. Yao, H. B. Wu and H. Wang: *Acta Sin. Quantum Opt*. 9 (2003), p. 121.
[17] A. Gharibi, J. Q. Shen and J. Gu: *J. Phys. B: At. Mol. Opt. Phys*. Vol. 42 (2009), 055502.
[18] P. Weis, J. L. Garcia-Pomar, R. Beigang and M. Rahm: *arXiv*: 1108.5981 [physics.optics] (2011).

Authors' information

[1]Department of Optical Engineering, State Key Laboratory of Modern Optical Instrumentations, Yuquan Campus, Zhejiang University, Hangzhou 310027, China

[2]Centre for Optical and Electromagnetic Research, East Building No. 5, Zijingang Campus, Zhejiang University, Hangzhou 310058, China

[*]Corresponding author:
E-mail: jqshencn@yahoo.com.cn

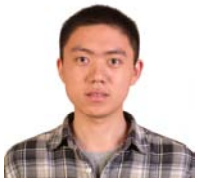

Peiyu Chen was born in Beijing, China in 1990. He was admitted to Zhejiang University in 2008. Now he is a senior undergraduate student in the Department of Optical Engineering at Zhejiang University. He would receive his Bachelor Degree of Engineering in June 2012. From March, 2010 to October, 2011, Peiyu Chen was an undergraduate researcher at the Center for Optical and Electromagnetic Research in Zhejiang University. Right now, he is doing research work on plasmonics at the Institute of Advanced Nanophotonics in Zhejiang University. In the summer of 2011, he worked in Department of Electrical Engineering at UCLA as a visiting researcher for ten weeks. Peiyu Chen's current research interest includes nano-plasmonics, silicon photonics and quantum coherence.

Jian Qi Shen was born in Hangzhou, China on November 30, 1974. He received the Bachelor Degree (Nanjing University, China in 1999) and Master Degree (Zhejiang University, China in 2002) in theoretical physics. He has been engaged in quantum optics and electromagnetism since 2002, and received the PhD in Optics from Zhejiang University and PhD in theoretical electromagnetism from the Royal Swedish Institute of Technology. In 2006-2008, he published a book entitled "Classical & Quantum Optical Properties of Artificial Electromagnetic Media" (Transworld Research Network, Kerala, India, 2008). Since 2008, he is an associate professor of Zhejiang University. Jian Qi Shen has published over 100 research papers and book chapters in the areas of optics, artificial electromagnetic materials, quantum theory and gravitation. His current research interest includes quantum coherence-based metamaterials, quantum vacuum and gravitational gauge theory.

Praise Worthy Prize

International Review of Physics (I.R.E.PHY.), Vol. 5, N. 6
December 2011

Negative Matter, Dark Matter and Theoretical Test

Yi-Fang Chang

Abstract – *The existence of the dark matter and the dark energy is a basic and complex problem. We discuss the Dirac's negative energy state. It should be a negative matter with some new characteristics, which are mainly the gravitation each other, but the repulsion with all positive matter. Such the positive and negative matters are two regions of topological separation in general case, and the negative matter is invisible. This is the simplest candidate of dark matter, and can explain some characteristics of the dark matter and dark energy. Recent phantom on dark energy is namely a type of negative matter. Based on a basic axiom and the two foundational principles of the negative matter, we research its predictions and possible tests. The negative matter should be a necessary development of Dirac theory. Finally, we propose the three basic laws of the negative matter. The existence of four matters on positive, opposite, and negative, negative-opposite particles will form the most perfect symmetrical world.*

Keywords*: Dark Matter, Negative Matter, Dark Energy, Repulsive Force, Test*

I. Introduction

The existence of the dark matter and the dark energy is a basic and complex problem. The dark matter in the solar neighborhood, in the Galaxy, in group of galaxies and cluster of galaxies, in the universe, is confirmed by the mass-to-light ratio and the galactic rotational curves, etc [1]. Now investigation of dark matter is a focus of fundamental interest to astronomers, astrophysicists, cosmologists, and nuclear and particle physicists [2].

Since 1981, the dark energy as a huge repulsive force is proposed in order to explain the acceleration of inflation in the universe [3], and may unify many different results of observations. Usually assume that the dark energy is a scalar field, which connects with the cosmological constant Λ [4], and it as the modified general relativity can explain many effects of the dark energy, but cannot explain the dark matter.

The Scientists proposed two different concepts: the dark matter and the dark energy, whose reason is both different exhibitions. The dark matter seems to have mass and may become huge conglomeration. Cosmologists compute that the gravitational conglomeration of these dark matters is a key function for the process formed galaxies from general matter. But the dark energy seems to be zero mass, and distributes uniformly in the whole space, and its interactions are repulsive. At present in the universe the dark matter has about 24% and the dark energy has about 72%, only 4% is visible matter. The dark matter is possibly the weakly interacting massive particle (WIMP), neutrino with mass, baryonic dark matter and nonbaryonic dark matter [5], [6], monopole, supersymmetric dark matter [7], axion [8], etc. Cosmologist divides the candidate of the dark matter into three types: hot, warm and cold dark matter. The dark energy seems to be the energy of vacuum.

Based on observations of a remarkable cosmic structure called the bullet cluster, Bradac, et al., discovered that this structure is actually two clusters of galaxies passing through one another [9]. Past observations have shown that only a very small percentage of mass in the universe can be explained by regular matter. The new research is the first to detect luminous matter and dark matter independent of one another, with the luminous matter clumped together in one region and the dark matter clumped together in another. These observations demonstrate that there are two types of matter: one visible and one invisible.

Scherrer proposed a new k-essence models in which the Lagrangian p is a function only of the derivatives of a scalar field. In the model the universe fills a kind of invisible fluid, and the models can serve as a unified model for dark matter and dark energy [10]. Soleng discussed dark matter and non-Newtonian gravity from general relativity coupled to a fluid of strings [11]. But, the tests of some known theories are very difficult.

II. Dirac's Negative Energy State

It is well-known that Dirac predicted anti-particles from its equation and the negative energy state, and he emphasized: we cannot ignore the negative energy states [12]. In order to prevent to jump continuously from positive energy state to negative energy state in the quantum theories, and keep the stability of world, Dirac proposed that as long as suppose that all the states of

Manuscript received and revised November 2011, accepted December 2011

negative energy are occupied except perhaps a few of small velocity. The vacuum of the realistic world has already been filling with all negative energy state, such the Pauli exclusion principle will come into play and prevent more than one electron going into any one state, and avoid this jumping difficulty. It is namely the well-known Dirac negative energy sea and whose vacancy or hole, which is an anti-particle (or opposite particle). From this the annihilation and creation between positive and opposite particles may be predicted. There is exact description in <The Principles of Quantum Mechanics> [13]. But, it prevent only jump of fermions, but cannot be applied to bosons. Therefore, the stability problem exists still. The negative energy state appears in all relativity theories, also in the classical theory [12].

The negative energy corresponds to the negative mass, so scientists consider that it will accelerate along a contrary direction under a force according to the Newton second law. Further, Bondi [14] considered three kinds of mass according to the measurement: inertial, passive gravitational, and active gravitational mass, and there are four cases. Here the negative matter responds perversely to nongravitational forces, responds like ordinary matter to gravitational forces, but produces repulsive gravitational fields. But, this is a question: Bondi believes that the positive body will attract the negative one (since all bodies are attracted by it), etc. According to the principle of equivalence in general relativity, inertial mass and gravitational mass should be equal always. Therefore, there are only three cases: positive and positive matters, positive and negative matters, negative and negative matters.

According to the mass-energy relation in Einstein's relativity, the Dirac's negative energy should correspond to the negative matter.

III. Negative Matter and its Main Characteristic

We think, first, the anti-(opposite) matter and the negative matter should be distinguished exactly. The anti-matter is that some properties of matter are opposite, for instance, charge, baryon number, lepton number, strangeness number and so on, but their masses and total energy are still positive. These particles include positron and various anti-particles. The existence of these particles is already verified. Both positive and opposite matters meet to annihilate to photons or mesons with conservation of energy and zero-charge. The negative matter has a negative mass and total energy. Its main characteristic should be the universal gravitation each other, but is the universal repulsion with all positive matter. Therefore, the creation of negative matter is difficult, but its existence should be also stable. In general case both of positive and negative matters are two regions of topological separation by different interactions. When the positive and negative matters with the same mass meet, they will become a real vacuum. But, so far their existence on the experiment is not final conclusion. Theoretically, in the negative matter there is also negative anti-matter with opposite charge and so on, but with negative mass [15]-[17].

We should extend the Dirac theory, and assume that Dirac sea is in fact a negative matter, and then the anti-particle is only a hole in Dirac sea. Because positive and negative matters are repulsive forces, these holes are stable. Such Dirac sea and its hole theory hold generally for various particles.

The Dirac equations of fermions can describe anti-matter. The cosmological constant Λ describes possibly the negative matter, which corresponds to the Λ term in the gravitational field equation. In the Klein-Gorden equation the m^2 term may correspond to $\pm m$, both describe bosons. In the Dirac equations $m \rightarrow -m$ may also describe the negative matter. A universal relation is:

$$E^2 = m^2c^4 + c^2p^2 \tag{1}$$

It may be generally applied for various positive, opposite and negative matters, and for all $\pm m$, $\pm E$ and $\pm p$. Only in the equations described negative matter the mass is negative, while in the equations described opposite matter the charge and so on are opposite. For a relation:

$$E^2 = m^2c^4 + c^2\left(p - \frac{q}{c}A\right)^2$$

i.e.:

$$p - \frac{q}{c}A = \pm\frac{1}{c}\sqrt{E^2 - m^2c^4} \tag{2}$$

$$\therefore q = \left(mv \mp \frac{1}{c}\sqrt{E^2 - m^2c^4}\right)\frac{c}{A} \tag{3}$$

Such the charge may be positive or negative, and is particular distinct for v=0. It corresponds to the opposite matter. The negative matter is possibly influence on the universal gravitational laws, classical mechanics, the motion laws of planet, electrodynamics, general relativity, quantum mechanics and so on. In this case the light ray is red shift at the neighborhood of a gravitational field (positive matter), and is violet shift at the neighborhood of a repulsive field (negative matter):

$$\Delta\lambda / \lambda = -MG / rc^2 \tag{4}$$

Of course, light emitted from the negative matter cannot be observed directly. The light ray should have repulsive deflection in a field of the negative matter:

$$\alpha = -4MG / c^2R \tag{5}$$

and a more general deflection should be:

$$\alpha = 4G\left(M_1 - M_2\right)/c^2 R \tag{6}$$

in which M_1 and M_2 are mass of the positive and negative matters, respectively.

For the Kepler laws of planet:

$$F\left(r\right) = -\frac{G}{r^2}\left(M_1 - M_2\right),\ \ u = \frac{1}{r} \tag{7}$$

So:

$$\frac{d^2 u}{d\vartheta^2} + u = \frac{G}{H}\left(M_1 - M_2\right) \tag{8}$$

Its solution is:

$$r = \frac{H/G\left(M_1 - M_2\right)}{1 + CH\cos\left(\vartheta - \vartheta_0\right)/G\left(M_1 - M_2\right)} \tag{9}$$

when $\vartheta_0 = 0$, it becomes a quadric curve:

$$r = \frac{p}{1 + e\cos\vartheta} \tag{10}$$

in which $e = Cp = CH/G\left(M_1 - M_2\right)$. It is ellipse for E<1 and $M_1 > M_2$; it is hyperbola for E>1 and $M_1 < M_2$; it is parabola for E=1 and $M_1 = M_2$. This is a modified Kepler first law. The Kepler second law should be invariable.

In the gravitational law:

$$F = -\frac{G}{r^2} m_1 m_2 \tag{11}$$

there are two masses, but in the Newton second law $F=ma$ there is only one mass. In order to keep the consistency of natural laws, and a repulsive force between positive and negative matters, we should suppose $-F=-ma$, i.e., $F=ma$ hold always for the negative matter, so that a is still an acceleration in the negative matter, while is always deceleration between the positive and negative matters.

In the special relativity the mass increases still. In the four-vector [18] change only is ($\pm mv$; $\pm E/c$), the time-like interval is $-v<-c$, i.e., $v>c$; the space-like interval is $-v>-c$, i.e., $v<c$, both are just opposite.

Therefore, the superluminal is in the time-like interval [18]. In the general relativity there is similarly curved time-space. In the quantum mechanics the negative matter may be still $E = h\nu$, in which $E\rightarrow -E$ and $-h\rightarrow h$. Such the de Broglie wave length is positive. The uncertainty principle:

$$\left(\Delta x\right)^2\left(\Delta p_x\right)^2 \geq \hbar^2/4 \tag{12}$$

is invariant, but another relation:

$$\left(\Delta x\right)\left(-\Delta p_x\right) \geq -\hbar/2 \tag{13}$$

will become probably to:

$$\left(\Delta x\right)\left(\Delta p_x\right) \leq \hbar/2 \tag{14}$$

The Heisenberg equation is also invariant, mass becomes an opposite sign in the Schrodinger equation, because the energy-momentum operators are invariant. Such:

$$-E = \frac{p^2}{\left(-2m\right)} + U\left(r\right) \tag{15}$$

whose corresponding equation in quantum mechanics is:

$$i\hbar\frac{\partial\psi}{\partial t} = \frac{\hbar^2}{2m}\nabla^2\psi - U\left(r\right)\psi \tag{16}$$

Here only $U\rightarrow -U$. The Klein-Gordon equation and the Dirac equations are invariant. But, an equation in an electromagnetic field is different:

$$\left[-E + e\varphi - \alpha\left(-cp + eA\right) + \beta\mu c^2\right]\psi = 0 \tag{17}$$

IV. Negative Matter is Possibly the Simplest Dark Matter

A unique dependable method determined all mass is to study their gravitation effect, for which the easiest method is the measurement of the circular speed curves in the galaxy [19]. These curves may be measured from the Doppler shift of spectrum [20].

The dark matter self does not emit light, and does also not interact with light. The negative matter is repulsive force for photon, and negative-photon with negative energy and negative mass is also repulsive force for general matter, both cannot be observed, and show the dark matter. The state equation of the dark energy is different with the equation of usual matter, and at present assume that it is repulsive force each other. So this may correspond to the negative matter [15]-[17]. According to the mass-energy relation in Einstein's relativity, the dark matter and dark energy should be unified.

Recently, Caldwell proposed phantom as cosmological consequences of a dark energy component with super-negative equation of state, whose cosmic energy density has negative pressure [21]. Then phantom becomes an important dark energy model [21]-[25]. Hong, et al., considered a higher dimensional gravity

theory with a negative kinetic energy phantom field and a cosmological constant [22]. Scherrer and Sen examined phantom dark energy models produced by a field with a negative kinetic term [23]. Chimento, et al., discussed the dark energy density derived from the 3-scalar phantom field, and its negative component plays the role of the negative part of a classical Dirac field [24]. Gonzalez, et al., presented the full nonlinear study of a phantom scalar field accreted into a black hole, which includes that the total energy of the space-time is positive or negative [25]. The total energy is negative, so it should be namely a negative matter.

The observations for luminous mass find that the velocity V is approximately constant, for example, in a range of radio 0.5 kpcs<*R*<20 kpcs for our Galaxy. This is an important proof of the existence of the dark matter, and which exists in the galactic halo. For a galaxy, if the movement of a star round the center of the galaxy obeys the Kepler law, and the negative matter is introduced, the equation of the star with mass m and distance *R* to the center will be:

$$\frac{Gm}{R^2}\left(M_1-M_2\right)=\frac{m}{R}V^2 \tag{18}$$

The total mass of this galaxy inside radius *R* is:

$$\begin{aligned} M\left(R\right)&=M_1+M_2= \\ &=\int_0^R\rho\left(r\right)dV=\int_0^R\rho\left(r\right)4\pi r^2dr \end{aligned} \tag{19}$$

such $\frac{dM\left(r\right)}{dr}=4\pi r^2\rho\left(r\right)$. The continuity equation is:

$$\frac{\partial\rho}{\partial t}+\nabla\left(\rho v\right)=0 \tag{20}$$

in which $\rho=\rho_1+\rho_2$ is a total density. The Euler equation is:

$$\begin{aligned} \left(\rho_1+\rho_2\right)\frac{dv}{dt}&=\left(\rho_1+\rho_2\right)\left[\frac{\partial v}{\partial t}+\left(v\cdot\nabla\right)v\right]= \\ &=-\nabla\left(p_1+p_2\right)-\left(\rho_1+\rho_2\right)\nabla\Phi \end{aligned} \tag{21}$$

The cosmological constant corresponds to a fictitious fluid introduced, whose density is $\rho_\Lambda=\Lambda/8\pi G$, and pressure is $p_\Lambda=-\Lambda c^2/8\pi G$. The mass-to-light ratio connects to $\left(\rho_1+\rho_2\right)/\rho_1=1+\rho_2/\rho_1$, such more is the negative matter, and bigger is the mass-to-light ratio.

From Eq.(18), we may obtain a radial velocity:

$$V=\sqrt{\frac{G\left(M_1-M_2\right)}{R}} \tag{22}$$

of the star, and an angle velocity:

$$\Omega=\sqrt{\frac{G\left(M_1-M_2\right)}{R^3}} \tag{23}$$

from the movement equation. Such this measurement determines only difference of positive mass and negative mass, i.e., a breaking part of symmetry between positive and negative matters.

We suppose an isolated particle system with the positive and negative matters under gravitational self interaction, whose kinetic energy:

$$T=T_1-T_2=\frac{1}{2}\left(\sum_i m_i\dot{r}_i^2-\sum_j m_j\dot{r}_j^2\right) \tag{24}$$

It is simplified to:

$$\begin{aligned} T&=\frac{1}{2}\left(M_1-M_2\right)<V^2>= \\ &=\frac{3}{2}\left(M_1-M_2\right)<V_{saw}^2> \end{aligned} \tag{25}$$

For an object of spherical symmetry the potential energy is:

$$\begin{aligned} U&=-\frac{G}{R}\left(M_1-M_2\right)^2= \\ &=-\frac{G}{R}\left(M_1^2+M_2^2-2M_1M_2\right) \end{aligned} \tag{26}$$

Applied the virial theorem determined the mass of cluster of galaxies, the sum of kinetic energy *T* and potential energy *U* for this system is:

$$2T+U=\frac{1}{2}\frac{d^2}{dt^2}\left(\sum_i m_i r_i^2-\sum_j m_j r_j^2\right)=0 \tag{27}$$

The kinetic energy of entire system in each particle as a galaxy is namely *T*. By above formula the mass of this galaxy becomes:

$$M_1-M_2=\frac{3R}{G}<V_{saw}^2> \tag{28}$$

Therefore, the existence of the negative matter will derive bigger decrease of mass by this way. For example, assume that the positive matter and negative matter are 55% and 45% of total mass, respectively. We observed mass that is only its 10%. Such the negative matter is possibly an important reason produced an effect of the dark matter.

The field equations of general relativity on the negative matter are:

$$G_{\mu\nu} = 8\pi k\left(T_{\mu\nu} - T'_{\mu\nu}\right) \tag{29}$$

i.e.:

$$G_{\mu\nu} + 8\pi kT'_{\mu\nu} = 8\pi kT_{\mu\nu} = G_{\mu\nu} + \Lambda g_{\mu\nu} \tag{30}$$

so Λ corresponds to the negative matter. And:

$$\begin{aligned}\Lambda &= 8\pi kT'_{\mu\nu} / g_{\mu\nu} = \\ &= \left[\rho' + \left(p'/c^2\right)\right]\left(u_\mu u_\nu / g_{\mu\nu}\right) - p'\end{aligned} \tag{31}$$

On the other hand, the gravitational field equation with the cosmological constant is extended to:

$$G_{\mu\nu} = 8\pi kT_{\mu\nu} \Rightarrow 8\pi k\left(T_{\mu\nu} + \Lambda g_{\mu\nu}\right) \tag{32}$$

Here $\Lambda g_{\mu\nu}$ corresponds to the negative energy state and vacuum energy, i.e., Dirac sea. The Friedmann equation is:

$$\ddot{R}(t) = -\frac{4}{3}\pi G\left[\left(\rho_1 - \rho_2\right) + 3\left(p_1 - p_2\right)/c^2\right]R(t) \tag{33}$$

in which $\left(\rho_1 - \rho_2\right) + 3\left(p_1 - p_2\right)/c^2$ is effective mass density:

$$\dot{R}^2 - \frac{8}{3}\pi G\left(\rho_1 - \rho_2\right)R^2 = 2C \tag{34}$$

in which $\dot{R}(t_0) = H_0$ is the Hubble constant. The density parameter is:

$$\Omega_0 = \frac{8\pi G\rho_0}{3H_0^2} = \frac{\rho_0}{\rho_c},\ \rho_0 = \rho_1 - \rho_2 \tag{35}$$

is an observed density. The accelerating expansion of the universe shows:

$$\left(\rho_1 - \rho_2\right) + 3\left(p_1 - p_2\right)/c^2 < 0$$

i.e.:

$$\rho_2 + \left(3p_2/c^2\right) > \rho_1 + \left(3p_1/c^2\right) \tag{36}$$

The negative matter is more than the positive matter.

For the negative matter there should also have the corresponding black hole, whose radius is:

$$r = -2Gm/c^2 \tag{37}$$

Various positive matter and black hole exhibit the gravitational lensing effect. While the negative matter and negative black hole will be the repulsive lensing phenomena. Both should be different in observations.

Moreover, we proposed that in quantum fluctuations the positive matter and negative matter are created at the same time, and derive an inflation cosmos. This corresponds to the cosmological mode created from nothing to all things. It may form the parallel worlds, or the many-worlds, or multiverse, etc. The Higgs mechanism is possibly a product of positive and negative matter [15].

V. Theoretical Test and the Basic Laws of Negative Matter

The existence of dark matter should affect some results of the Newtonian gravitation and the general relativity, for example, the cosmic average density will increase about 20 times. The dark matter is very complex, perhaps, the negative matter is only the simplest dark matter.

In the large-scale space, if there has a negative matter cluster in the positive matter, a part of positive matter will be screened, and another visible matter changes shape by the repulsive lens. Therefore, the visible matter looks much less. The negative matter and their screening positive matter will exhibit the invisible dark matter. According to this hypothesis, since the screening part and distorted part are different, the star-shape observed will be a little different from different positions of the Earth at the solar system. This season effect may be tested.

Further, the negative matter can predict: 1). There is repulsive force between positive and negative matters, and which obey the square inverse ratio law according to the Newtonian law. 2). General photons are reflected by negative matter, which exhibits a type of dark matter. 3).The dark matter includes the negative matter and the positive matter screened. 4). When the move speed between positive and negative matter is very big, and the kinetic energy is bigger than the potential energy, their colliding result will be a complete annihilation, whose leftover is only a mass-difference of positive and negative matters. 5). Usual light under interaction of negative matter is repulsive deflection, so it shows the repulsive lensing effect. 6). The negative matter is similar with invisible black hole, but is repulsive force for matter, and its mass is invariant. 7). The negative matter may represent the cosmic repulsion and the fast expansion. 8). The positive and negative matters under some exceeding conditions may be created from nothing at the same time. These will also be main tests of the existence of negative matter.

The negative matter as the simplest candidate of dark matter can explain some characteristics of a huge lack of mass on dark matter, and of a repulsive force of the dark energy. The negative matter determinates the cosmological constant, and changes possibly the gravitational lensing effect, and is consistent with the conformal gravity theory [26], and with the observation of the bullet galaxy cluster [9]. The latter shows

obviously a huge dissimilarity between the positive and negative matters. In this case two galaxies collide sharply and meet, but the negative and positive matters are repulsive each other, so the negative matter passes very quickly. Mortonson, et al., proposed the testable dark energy predictions from current data [27].

The above discussions are based on a basic axiom: the no-contradiction of natural laws, and on the two foundational principles:

1. The negative matter obeys the same natural laws of usual matter, including classical, relativistic and quantum physics.
2. There is universal repulsive force between the positive and negative matter. Of course, some concrete laws are possibly different, for example, the Kepler first law and so on.

Usually, one considers that Dirac predicted the opposite matter. In fact, the Dirac theory implied already the negative matter, which should be also a necessary development of this theory and the Dirac's negative energy state.

Finally, we propose particularly the three basic laws or principles of the negative matter:

I. The classical law. The negative matter is repulsive with the positive matter, and obeys the Lorentz transformation, etc.

II. The quantum law. For the fermions of the positive and negative matter, and corresponding Dirac equations and so on, both masses are opposite; while for the bosons of the positive and negative matter, and corresponding the Klein-Gordon equation and so on, both m^2 are the same.

III. The symmetry (completeness) law. Dirac pointed out: The physical laws are symmetrical between the positive and negative charge [13]. Further, the physical laws should be also symmetrical between the positive and negative matter. It will form the most perfect symmetrical world for four matters on positive, opposite, and negative, negative-opposite particles. If the negative matter is verified, a new and complete world will be exhibited.

References

[1] J.Binney and S.Tremaine, *Galactic Dynamics.* (Princeton University Press. 1987).

[2] K.Pretzl, Focus on dark matter. *New J. Phys*. 2(2000),1,001.

[3] P.J.E.Peebles and R.Bharat, The cosmological constant and dark energy. *Rev.Mod.Phys*. 75(2003),559-606.

[4] S.Weinberg, The cosmological constant problem. *Rev.Mod.Phys*. 61(1989),1-23.

[5] C.J.Copi, D.N.Schramm and M.S.Turner, Big-bang nucleosynthesis and the baryon density of the universe. *Science*. 267(1995),192-199.

[6] O.E.Gerhard and S.Silk, Baryonic dark halos: A cold gas component? *ApJ*. 472(1996),34-45.

[7] G.Jungman, M.Kamionkowski and K.Griest, Supersymmetric dark matter. *Phys.Reports*. 267(1996),195-373.

[8] E.P.S.Shellard and R.A.Battye, Origin of dark matter axions. *Phys.Reports*. 307(1998),227-234.

[9] M.Bradac, D.Clowe, A.H.Gonzalez, et al., A direct empirical proof of the existence of dark matter. *ApJ*. 652(2006),937-947.

[10] R.J.Scherrer, Purely kinetic k essence as unified dark matter. *Phys.Rev.Lett*. 93(2004), 011301.

[11] H.H.Soleng, Dark matter and non-newtonian gravity from general relativity coupled to a fluid of strings. *Gen.Rel.Grav*. 27(1995), 367-378.

[12] P.A.M.Dirac, The theory of electrons and protons. *Proc.Roy.Soc*. A126(1930),365-369.

[13] P.A.M.Dirac, *The Principles of Quantum Mechanics*.(Oxford. 1958).

[14] H.Bondi, Negative mass in general relativity. *Rev.Mod.Phys*. 29(1957),423-428.

[15] Yi-Fang Chang, Negative Matter, Repulsion Force, Dark Matter and Inflation Cosmos, Higgs Mechanism. 2007 *arXiv*:0705.2908.

[16] Yi-Fang Chang, Combination and incompatibility between quantum mechanics and relativity and their developments. *J.Yunnan University*. 30(2008),41-46.

[17] Yi-Fang Chang, Relations between Relativity and Quantum Mechanics, and Theoretical Developments. J.*Shangqiu Teachers College*. 24(2008),57-61.

[18] Yi-Fang Chang, *New Research of Particle Physics and Relativity*. (Yunnan Science and Technology Press.1989). Phys.Abst. 1990 V93, No1371.

[19] M.L.Kutner, *Astronomy: A Physical Perspective*. (Combridge Univ.Press. 2003).

[20] V.Rubin, The rotation of spiral galaxies. *Science*. 220(1983), 1339-1344.

[21] R.R.Caldwell, A phantom menace? Cosmological consequences of a dark energy component with super-negative equation of state. *Phys.Lett*. B545(2002),23-29.

[22] S.-T.Hong, J.Lee, T.H.Lee and P.Oh, Higher dimensional cosmological model with a phantom field. *Phys.Rev*. D78(2008), 047503.

[23] R.J.Scherrer and A.A.Sen, Phantom dark energy models with a nearly flat potential. *Phys.Rev*. D78(2008),067303.

[24] L.P.Chimento, M.Forte, R.Lazkoz and M.G.Richarte, Internal space structure generalization of the quintom cosmological scenario. *Phys.Rev*. D79(2009),043502.

[25] J.A.González and F.S.Guzmán, Accretion of phantom scalar field into a black hole. *Phys.Rev*. D79(2009),121501.

[26] P.D.Mannheim, Conformal gravity and the flatness problem. *ApJ*. 391(1992),429-432.

[27] M.J.Mortonson, W.Hu and D.Huterer, Testable dark energy predictions from current data. *Phys.Rev*. D81(2010):063007.

Authors' information

Yi-Fang Chang. A professor, Department of Physics, Yunnan University, Kunming, 650091, China. The research interests: Theoretical Physics, Particle Physics, Intersecting Science
Nationality: Chinese
E-mail: yifangchang1030@hotmail.com

Praise Worthy Prize

International Review of Physics (I.R.E.PHY.), Vol. 5, N. 6
December 2011

Effect of Initial Stress on Wave Propagation in an Infinite Micropolar Elastic Solid Body

E. Edfawy

Abstract – *In this paper we investigated generation waves in an infinite micropolar elastic medium under the influence of initial stress p and body forces $\vec{X}$. The equation of motion have been solved by applying the Fourier-Hankel transform. The components of displacement, the stress, the rotation and the couple stress have been obtained in analytical form as integrals involving Bessel function of first kind and of order zero.* ***Copyright © 2011 Praise Worthy Prize S.r.l. - All rights reserved.***

Keywords*: Wave Propagation, Elasticity, Initial Stress, Micropolar, Hankel's Transform*

I. Introduction

The analysis of vibrating cylinders has a very rich history in the field of solid mechanics. The dynamic problems of elastic bodies is an important and interesting research field for engineers and scientists. However, little attention has been given to the problem of the wave propagation in orthotropic circular cylinder. Abd-Alla and Mahmoud [1]-[2], investigated Magneto-thermoelastic problem in rotating non-homogeneous orthotropic hollow cylindrical under the hyperbolic heat conduction model and the effect of the rotation on propagation of thermoelastic waves in a non-homogeneous infinite cylinder of isotropic material. Abd-Alla, et al. [3]-[4], studied wave propagation modeling in cylindrical human longe wet bones with cavity and the effect of the rotation on the radial vibrations in a non-homogeneous orthotropic hollow cylinder.

Mahmoud [5]-[6], investigated wave propagation in cylindrical poroelastic dry bones and the effect of the non-homogeneity on wave propagation on orthotropic elastic media.

Abd-Alla, et al. [7], investigated the effect of the non-homogeneity on the composite infinite cylinder of isotropic and orthotropic materials. Some problems of the three-dimensional elastic theory for the axisymmetric free vibrations of hollow circular cylinders were studied and analyzed by Hutchinson and El-Azhary [8]. Abd-Alla and Farhan [9], investigated the effect of the non-homogeneity on the composite infinite cylinder of orthotropic materials. Wang and Shen [10], studied the two-dimensional problem of inclusions of arbitrary shape in magneto-electro-elastic composites. Cowin and Fraldi [11], investigated a dynamic problem of singularities associated with the curvilinear anisotropic elastic symmetries.

Ebenezer, et al. [12], investigated forced vibration of solid elastic cylinders.

Ding, et al. [13], Hou and Leung [14], obtained the analytical solution for the axisymmetric plane strain electro elastic dynamics of a non-homogeneous piezoelectric hollow cylinder. Hutchinson [15], investigated the free vibration problems of solid cylinder. Also, Markus and Mead, [16], presented an analytical method for investigating the dispersion behavior of axisymmetric and a symmetric wave motion in orthotropic cylinders. Chen, et al. [17]-[18], investigated the free vibration and general solution of nonhomogeneous transversely isotropic magneto-electro-elastic hollow cylinders. Sharma and Kumar [19], investigated asymptotic of wave motion in transversely isotropic plates. Toudeshky, et al. [20], studied sound transmission into a thick hollow cylinder with the fixed and boundary condition. Buchanan [21], investigated free vibration of an infinite magneto-elactro-elastic cylinder. Senitskii [22], studied stress state of a rotating inhomogeneous anisotropic cylinder of variable density.

The frequency equation for the plane vibration studied by Erguven [23]. Elnaggar and Abd-Alla [24] investigated thermoelastic problem in an infinite cylinder under initial stress, But they all considered initially stress free media. Besides the earth, many structural bodies are found to initially stressed. It is of practical importance to study the effect of the initial stresses on the waves propagated in these bodies.

The present investigation is concerned with the determination the displacement, the stress, the rotation and couple stress components in an infinite micropolar elastic medium under the effect of action of body forces and initial stress.

The problem is treated on the basis of the classical linear theory of micro elasticity throughout the analysis is supposed to be homogeneous, isotropic with respect to all physical properties. The wave equations of motion have been solved applying the Fourier-Hankel transform. The final results, the displacement, the stress, the

Manuscript received and revised November 2011, accepted December 2011

rotation, and the couple stress under the effect of action initial stress and body forces have been obtained in analytical form as integrals involving Bessel function of first kind and of order zero.

II. Formulation of the Problem

Let consider a homogeneous and isotropic micropolar elastic an infinite cylinder under initial stress p and body forces $\vec{X}$. The field of displacements $\vec{u}$ and rotations $\vec{w}$ is characterized by the symmetry with respect to z-axis.

The dynamic equations of motion under the effect of body forces and initial stress can be written as [1], [2]:

$$(\mu + \alpha + p)\nabla^2\vec{u} + (\lambda + \mu - \alpha)\nabla(\nabla\cdot\vec{u}) + +2\alpha\, curl\ \vec{w} - \rho\ curl\ \vec{w} + \vec{X} = \rho\,\frac{\partial^2 u}{\partial t^2} \tag{1}$$

$$(F + \varepsilon)\nabla^2\vec{u} + (F + \beta - \varepsilon)\nabla(\nabla\cdot\vec{w}) - 4\alpha\vec{w} + + 2\alpha\, curl\,\vec{u} = I\,\frac{\partial^2 u}{\partial t^2} \tag{2}$$

where $\vec{u}$ is the displacement vector, $\vec{w}$ is the rotation vector, $\vec{X}$ is the vector of body forces $\mu, \lambda, \alpha, \beta, F, \varepsilon$ are the natural constants.

If we refer the medium to cylindrical polar coordinates (r, Φ, z) and assume the independent of all causes and effects of the angle Φ, then equation (1) and (2) become:

$$(\mu + \alpha + p)(\nabla^2 u_r - \frac{u_r}{r^2}) + (\lambda + \mu + p - \alpha)\frac{\partial e}{\partial r} + - 2\alpha\ \frac{\partial \omega_\Phi}{\partial r} + p\,\frac{\partial \omega_\Phi}{\partial z} + X_r = \rho\,\frac{\partial^2 u_r}{\partial t^2}$$

$$(\mu + \alpha)\nabla^2 u_z + (\lambda + \mu - \alpha)\frac{\partial e}{\partial z} + \frac{2\alpha}{r}\frac{\partial}{\partial r}(r\omega_\Phi) + + \frac{p}{r}\frac{\partial}{\partial r}(r\omega_\Phi) + X_z = \rho\,\frac{\partial^2 u_z}{\partial t^2} \tag{3}$$

$$(F + \varepsilon)\left(\nabla^2\omega_\Phi - \frac{\omega_\Phi}{r^2}\right) - 4\alpha\omega_\Phi + +2\alpha\left(\frac{\partial u_r}{\partial z} + -\frac{\partial u_z}{\partial r}\right) = I\,\frac{\partial^2\omega_\Phi}{\partial t^2}$$

$$(F + \varepsilon)\left(\nabla^2\omega_r - \frac{\omega_r}{r^2}\right) - 4\alpha\omega_r + +(\beta + F - \varepsilon)\frac{\partial s}{\partial r} - 2\alpha\frac{\partial u_\Phi}{\partial z} = I\,\frac{\partial^2\omega_r}{\partial t^2} \tag{4}$$

$$(F + \varepsilon)\nabla^2\omega_z - 4\alpha\omega_z + +(\beta + F - \varepsilon)\frac{\partial s}{\partial z} + \frac{2\alpha}{r}\frac{\partial}{\partial r}(ru_\Phi) = I\,\frac{\partial^2\omega_z}{\partial t^2}$$

$$(\alpha + \mu)\left[\nabla^2 u_\Phi - \frac{u_\Phi}{r^2}\right] + 2\alpha\left(\frac{\partial\omega_r}{\partial z} - \frac{\partial\omega_z}{\partial r}\right) = = \rho\,\frac{\partial^2 u_z}{\partial t^2} - X_\Phi$$

where:

$$\vec{u} = (u_r, u_\Phi, u_z), \vec{\omega} = (\omega_r, \omega_\Phi, \omega_z), \quad \vec{X} = (X_r, X_\Phi, X_z)$$

$$e = \frac{1}{r}\frac{\partial}{\partial r}(ru_r) + \frac{\partial u_z}{\partial z} \qquad s = \frac{1}{r}\frac{\partial}{\partial r}(r\omega_r) + \frac{\partial\omega_z}{\partial z}$$

Using Helmholz's theorem [5] and introducting the potential $\Phi, \vec{\psi}$ and $\vec{\Gamma}$ by the equations:

$$u_r = \frac{\partial\Phi}{\partial r} + \frac{\partial^2\psi}{\partial r\partial z}$$
$$u_z = \frac{\partial\Phi}{\partial z} - \frac{1}{r}\frac{\partial}{\partial r}\left(r\frac{\partial\psi}{\partial r}\right) \tag{5}$$
$$\omega_\Phi = -\frac{\partial\Gamma}{\partial r}$$

while the body forces will be decomposed into the potential and solenoidal parts:

$$X_r = \rho\left(\frac{\partial\theta}{\partial r} - \frac{\partial\psi_\Phi}{\partial z}\right)$$
$$X_z = \rho\left(\frac{\partial\theta}{\partial z} + \frac{1}{r}\frac{\partial}{\partial r}(r\psi_\Phi)\right) \tag{6}$$

Substituting equations (5) and (6) into equations (3) we obtain the following system of wave equations:

$$\nabla^2\Phi - \frac{\rho}{(\lambda + 2\mu + \rho)}\frac{\partial^2\Phi}{\partial t^2} + \frac{\rho\theta}{(\lambda + 2\mu + \rho)} = 0 \tag{7}$$

$$\nabla^2\Phi - \frac{\rho}{(\lambda + 2\mu)}\frac{\partial^2\Phi}{\partial t^2} + \frac{\rho\theta}{(\lambda + 2\mu)} = 0 \tag{8}$$

$$-\frac{\partial}{\partial r}\left[\nabla^2\psi - \frac{\rho}{\left(\mu - \frac{\rho}{2}\right)}\frac{\partial^2\psi}{\partial t^2} + A\Gamma\right] + + \frac{\rho}{\left(\mu - \frac{\rho}{2}\right)}\psi_\Phi = 0 \tag{9}$$

$$-\frac{\partial}{\partial r}\left[\nabla^2\psi - \frac{\rho}{\left(\mu - \frac{\rho}{2}\right)}\frac{\partial^2\psi}{\partial t^2} + A\Gamma\right] + + \frac{\rho}{\left(\mu + \frac{\rho}{2}\right)}\psi_\Phi = 0 \tag{10}$$

$$-\frac{\partial}{\partial r}\left[\left(\nabla^2 - \frac{1}{c_4^2}\frac{\partial^2\psi}{\partial t^2} - \nu^2\right)\Gamma - B\nabla^2\psi\right] = 0 \tag{11}$$

where:

$$A = \frac{2\alpha}{\mu + \alpha} \qquad B = \frac{2\alpha}{F + \varepsilon}$$
$$\nu^2 = \frac{4\alpha}{F + \varepsilon} \qquad c_4 = \left(\frac{F + \varepsilon}{I}\right)^{\frac{1}{2}}$$

In the absence of initial stress equations (7)-(10) reduce to three equations only. We shall consider

compressional and distortional waves along the r-axis only. These waves are represented by equations (7), (9), and (11). Also, Using Helmholz's theorem [5] in equations (4) and introducing the potential $\Phi`$ , $\psi`$ and Ω , we obtain :

$$\omega_r = \frac{\partial \Phi`}{\partial r} + \frac{\partial^2 \psi`}{\partial r \partial z},\ \omega_z = \frac{\partial \Phi`}{\partial z} - \frac{1}{r}\frac{\partial}{\partial r}\left(r\frac{\partial \psi`}{\partial r}\right) \qquad u_\Phi = -\frac{\partial \Omega}{\partial r} \tag{12}$$

Substituting equations (12) into equations (4) we obtain the following system of wave equations:

$$\begin{gathered}\left(\nabla^2 - \nu_0^2 - \frac{1}{c_3^2}\frac{\partial^2}{\partial t^2}\right)\ \Phi` = 0 \\ -\frac{\partial}{\partial r}[\ (\nabla^2 - \nu_0^2 - \frac{1}{c_4^2}\frac{\partial^2}{\partial t^2})\,\psi` + B\Omega\ ] = 0 \\ -\frac{\partial}{\partial r}\left[(\nabla^2 + \frac{\rho}{\left(\mu - \frac{\rho}{2}\right)}\frac{\partial^2}{\partial t^2})\,\Omega - A\nabla^2\psi`\right] + \\ + \frac{1}{\left(\mu - \frac{\rho}{2}\right)}X_\Phi = 0\end{gathered} \tag{13}$$

where:

$$c_3 = (\frac{\beta + 2\mathrm{F}}{\mathrm{I}})^{\frac{1}{2}}\quad ,\nu_0^2 = \frac{4\alpha}{2\mathrm{F} + \beta}$$

We shall give the general solution of wave equations (7), (9) and (11) reccurring to Fourier-Hankel integral transformations.

III. Solution of Wave Equations

Applying the Fourier-Hankel integral transformation:

$$\begin{gathered}\widehat{\Phi}(\eta,\xi,\omega) = \\ = \frac{1}{2\pi}\iint_{-\infty}^{\infty} e^{i(\xi z + wt)}\ dzdt \int_0^\infty r\,J_0(\eta r)\Phi(r,z,t)dr \\ \Phi(r,z,t) = \\ = \frac{1}{2\pi}\iint_{-\infty}^{\infty} e^{-i(\xi z + wt)}\,dzdt \int_0^\infty r\,J_0(\eta r)\widehat{\Phi}(\eta,\xi,\omega)d\eta\end{gathered} \tag{14}$$

to equations (7), (9) and (11), we obtain a system of algebraic equations. The solution of this system gives the transforms $\widehat{\Phi}$, $\hat{\psi}$, $\hat{\Gamma}$:

$$\begin{gathered}\widehat{\Phi} = \frac{\rho\hat{\theta}}{(\lambda + 2\mu + \rho)(v^2 - \delta_1^2)} \\ \hat{\psi} = \frac{1}{\eta\Delta}\left[\frac{\rho((v^2 + v^2 - \delta_4^2)\hat{\psi}_\Phi}{\mu - \frac{\rho}{2}}\right] \\ \hat{\Gamma} = \frac{1}{\eta\Delta}\left[\frac{\rho v^2 s\psi_\Phi}{(\mu - \frac{\rho}{2})}\right]\end{gathered} \tag{15}$$

where:

$$\begin{gathered}v^2 = \xi^2 + \eta^2\ ,\ \Delta = (v^2 - \lambda_1^2)(v^2 - \lambda_2^2)\,, \\ \lambda_{1,2}^2 = \frac{1}{2}[\,(\delta_2^2 + \xi^2 - v^2) \mp \\ \mp[\,(\delta_2^2 + \xi^2 - v^2)^2 + 4\delta_2^2\xi^2]^{\frac{1}{2}}, \\ \xi^2 = \frac{4\alpha^2}{(\alpha + \mu)(F + \varepsilon)} \\ \delta_2 = w\,(\frac{\rho}{\left(\mu - \frac{\rho}{2}\right)})^{\frac{1}{2}}\ ,\delta_4 = \frac{w}{c_4}\end{gathered}$$

Let us perform the Fourier-Hankel integral transformation on the relations (5) and (6), we assume that:

$$\begin{gathered}\left(\hat{u}_r, \hat{X}_r, \hat{\psi}_\Phi\right) = \frac{1}{2\pi}\iint_{-\infty}^{\infty} e^{i(\xi z + wt)}\,dzdt \cdot \\ \cdot \int_0^\infty r\,J_0(\eta r)\cdot\ \widehat{\Phi}\,(\eta,\xi,\omega)d\eta\ \cdot \\ \cdot (u_r, X_r, \psi_\Phi)dr\left(\hat{\theta}, \hat{X}_z\right) = \\ = \frac{1}{2\pi}\iint_{-\infty}^{\infty} e^{i(\xi z + wt)}\ dzdt \cdot \\ \cdot \int_0^\infty r\,J_0(\eta r)\cdot(\theta, X_z)dr\end{gathered} \tag{16}$$

under these assumption we get:

$$\hat{u}_r = -\eta\widehat{\Phi} + i\xi\eta\hat{\psi}\ ,\hat{u}_z = -i\xi\widehat{\Phi} + \eta^2\hat{\psi}\ ,\quad \hat{\omega}_\Phi = \eta\hat{\Gamma} \tag{17}$$

$$X_r = -\rho\eta\hat{\theta} + i\rho\xi\hat{\psi}_\Phi\ ,\ X_z = -i\rho\xi\hat{\theta} + \rho\eta\hat{\psi}_\Phi \tag{18}$$

From the relation (18) we have:

$$\begin{gathered}\hat{\theta} = \frac{1}{\rho v^2}\left(i\xi\hat{X}_z - \eta\hat{X}_r\right), \\ \hat{\psi}_\Phi = \frac{1}{\rho v^2}\,(\eta X_z - i\xi X_r)\end{gathered} \tag{19}$$

Substituting from equations (15) and (19) into equations (17) we obtain the transforms of the quantities u_r , u_z expressed by the transforms X_r , X_z .

Performing the inverse Fourier - Hankel transformation we obtain finally:

$$\begin{gathered}u_r = \frac{1}{2\pi}\iint_{-\infty}^{\infty} e^{-i(\xi z + wt)}\ d\xi dw \cdot \\ \cdot \int_0^\infty J_1(\eta r)[\frac{\eta\left(i\xi\hat{X}_z - \eta\hat{X}_z\right)}{(\lambda + 2\mu + \rho)(v^2 - \delta_1^2)v^2} + \\ -\frac{i\xi}{\Delta}\left[\frac{(v^2 + v^2 - \delta_4^2)}{\left(\mu - \frac{\rho}{2}\right)v^2}\left(\eta\hat{X}_z - i\xi\hat{X}_r\right)\right]]\,d\eta\end{gathered} \tag{20}$$

$$u_z = -\frac{1}{2\pi}\iint_{-\infty}^{\infty} e^{-i(\xi z+wt)}\, d\xi dw \cdot \cdot \int_0^{\infty} rJ_0(\eta r)[\frac{i\xi\left(i\xi\hat{X}_z - \eta\hat{X}_z\right)}{(\lambda+2\mu+\rho)v^2(v^2-\delta_1^2)} + -\frac{\eta}{\Delta}\left[\frac{(v^2+v^2-\delta_4^2)\left(\eta\hat{X}_z - i\xi\hat{X}_r\right)}{\left(\mu-\frac{\rho}{2}\right)v^2}\right]] \quad (21)$$

$$\omega_\Phi = \frac{1}{2\pi}\iint_{-\infty}^{\infty} e^{-i(\xi z+wt)}\, d\xi dw \int_0^{\infty} \frac{\eta J_1(\eta r)}{\Delta}[\frac{s\left(\eta\hat{X}_z - i\xi\hat{X}_z\right)}{\left(\mu-\frac{\rho}{2}\right)}]\, d\eta \quad (22)$$

Knowing the displacement and rotations we are able to determine the components of the tensor of stresses τ_{ij} under initial stress p and the tensor of couple stresses μ_{ij} from the formula [2] as below:

$$\begin{aligned}
\tau_{rr} &= (\lambda+2\mu+p)\frac{\partial u_r}{\partial r} + (\lambda+p)\frac{u_r}{r} + \\
&\quad + (\lambda+p)\frac{\partial u_z}{\partial z} \\
\tau_{\Phi\Phi} &= (\lambda+2\mu+p)\frac{u_r}{r} + (\lambda+\rho)\frac{\partial u_z}{\partial r} + \\
&\quad + (\lambda+p)\frac{\partial \mu_z}{\partial z} + (\lambda+p)\frac{\partial u_z}{\partial z} \\
\tau_{zz} &= (\lambda+2\mu)\frac{\partial u_z}{\partial z} + \lambda\frac{u_r}{r} + \lambda\frac{\partial u_r}{\partial r} \\
\tau_{rz} &= \mu\left(\frac{\partial u_z}{\partial r} + \frac{\partial u_r}{\partial z}\right) - \alpha\left(\frac{\partial u_r}{\partial z} - \frac{\partial u_z}{\partial r}\right) + 2\alpha\omega_\Phi \\
\tau_{zr} &= \mu\left(\frac{\partial u_z}{\partial r} + \frac{\partial u_r}{\partial z}\right) + \alpha\left(\frac{\partial u_r}{\partial z} - \frac{\partial u_z}{\partial r}\right) + 2\alpha\omega_\Phi \\
\mu_{r\Phi} &= F\left(\frac{\partial \omega_\Phi}{\partial r} - \frac{\omega_\Phi}{r}\right) + \left(\frac{\partial \omega_\Phi}{\partial r} + \frac{\omega_\Phi}{r}\right) \\
\mu_{\Phi r} &= F\left(\frac{\partial \omega_\Phi}{\partial r} - \frac{\omega_\Phi}{r}\right) - \left(\frac{\partial \omega_\Phi}{\partial r} + \frac{\omega_\Phi}{r}\right) \\
\mu_{\Phi z} &= (F-\varepsilon)\frac{\partial \omega_\Phi}{\partial z} \\
\mu_{z\Phi} &= (F+\varepsilon)\frac{\partial \omega_\Phi}{\partial z}
\end{aligned} \quad (23)$$

Let us now consider a particular case ($\alpha = 0$) where the equations (1) and (2) become independent of each other and when there is no initial stress P, then from equations (20) – (22) we have :

$$u_r = \frac{1}{2\pi(\lambda+2\mu)}\iint_{-\infty}^{\infty} e^{-i(\xi z+\omega t)}\, d\omega d\xi \int_0^{\infty} \eta J_1(\eta r)\cdot \cdot \left[\frac{\left(\eta^2 + \delta^2\xi^2 - \frac{\rho\omega^2}{\mu}\right)\hat{X}_r + i\xi\eta(\delta^2-1)\hat{X}_z}{\left(v^2 - \frac{\rho\omega^2}{\lambda} + 2\mu\right)\left(v^2 - \frac{\rho\omega^2}{\mu}\right)}\right] d\eta \quad (24)$$

$$u_z = \frac{1}{2\pi(\lambda+2\mu)}\iint_{-\infty}^{\infty} e^{-i(\xi z+\omega t)}\, d\omega d\xi \int_0^{\infty} \eta J_0(\eta r)\cdot \cdot \left[\frac{\left(\xi^2 + \eta^2\delta^2 - \frac{\rho\omega^2}{\mu}\right)\hat{X}_z + i\xi\eta(\delta^2-1)\hat{X}_r}{\left(v^2 - \frac{\rho\omega^2}{\lambda} + 2\mu\right)\left(v^2 - \frac{\rho\omega^2}{\mu}\right)}\right] d\eta \quad (25)$$

$$\omega_\Phi = 0 \quad (26)$$

where:

$$\delta = \frac{\lambda+2\mu}{\mu}$$

The formula (24)-(25) which is similar to that which has been obtained by Elnaggar and Abd-Alla [6].

Let us now consider the system of wave equations (13).

Performing on these equations the integral transformation and taking into account that:

$$\begin{aligned}
\left(\hat{\Phi}`, \hat{\psi}`, \hat{\Omega}\right) &= \frac{1}{2\pi}\iint_{-\infty}^{\infty} e^{i(\xi z+wt)}\, dzdt \cdot \\
&\quad \cdot \int_0^{\infty} r\, J_0(\eta r)\ (\Phi`, \psi`, \Omega) d\eta, \\
\hat{X}_\Phi &= \frac{1}{2\pi}\iint_{-\infty}^{\infty} e^{i(\xi z+wt)}\, dzdt \int_0^{\infty} r\, J_1(\eta r)\, X_\Phi dr
\end{aligned} \quad (27)$$

we arrive at the following quantities:

$$\begin{aligned}
\hat{\Phi}` &= 0 \qquad , \hat{\psi}` = \frac{1}{\eta\Delta}\left(\frac{SX_\Phi}{\mu - \frac{\rho}{2}}\right) \\
\hat{\Omega} &= \frac{1}{\eta\Delta}\left(\frac{(v^2 + v^2 - \delta_4^2)\hat{X}_\Phi}{\mu - \frac{\rho}{2}}\right)
\end{aligned} \quad (28)$$

Let us perform also the Fourier-Hankel transformation on the relation (12) we get:

$$\begin{aligned}
\hat{\omega}_r &= -\eta\hat{\Phi}` + i\xi \mathrm{H}\hat{\psi}` \\
\omega_z &= i\xi\hat{\Phi}` + \mathrm{H}^2\hat{\psi}` \quad , u_\Phi = -\mathrm{H}\hat{\Omega}
\end{aligned} \quad (29)$$

Substituting equations (28) into equations (29), we obtain the transforms $\hat{\omega}_r$, $\hat{\omega}_z$, $\hat{u}_\Phi$ performing now the inverse Fourier-Hankel tranformation, we get:

$$\hat{\omega}_r = \frac{1}{2\pi}\iint_{-\infty}^{\infty} e^{-i(\xi z+\omega t)}\, d\omega d\xi \int_0^{\infty} \frac{\eta J_1(\eta r)\, i\xi}{\Delta}\left[\frac{s\hat{X}_\Phi}{\mu - \frac{p}{2}}\right] d\eta \quad (30)$$

$$\omega_z = \frac{1}{2\pi} \iint_{-\infty}^{\infty} e^{-i(\xi z + \omega t)}\, d\omega d\xi \int_0^{\infty} \frac{\eta^2 J_0(\eta r)}{\Delta} \left[\frac{s\hat{X}_\Phi}{\mu - \frac{p}{2}} \right] d\eta \tag{31}$$

$$u_\Phi = \frac{1}{2\pi} \iint_{-\infty}^{\infty} e^{-i(\xi z + \omega t)}\, d\omega d\xi \int_0^{\infty} \frac{\eta J_1(\eta r)}{\Delta} \left[\frac{(v^2 + v_0^2 - \delta_4^2) X_\Phi}{\mu - \frac{p}{2}} \right] d\eta \tag{32}$$

Now, the rotation ω_r, ω_z and the displacement u_Φ being known we can determine the stress τ_{ij} and the couple stresses μ_{ij} from the formula:

$$\mu_{rr} = 2F \frac{\partial \omega_r}{\partial r} + \beta s \;, \mu_{\Phi\Phi} = 2F \frac{\omega_r}{r} + \beta s$$
$$\mu_{zz} = 2F \frac{\partial \omega_z}{\partial z} + \beta s$$

$$\mu_{zr} = F \left(\frac{\partial \omega_z}{\partial r} + \frac{\partial \omega_r}{\partial z} \right) + - \left(\frac{\partial \omega_r}{\partial z} - \frac{\partial \omega_z}{\partial r} \right) \tag{33}$$

$$\tau_{r\Phi} = \mu \left(\frac{\partial u_\Phi}{\partial r} - \frac{u_\Phi}{r} \right) + \frac{\alpha}{r} \frac{\partial}{\partial r} (r u_\Phi) - 2\alpha\omega_z$$
$$\tau_{\Phi r} = \mu \left(\frac{\partial u_\Phi}{\partial r} - \frac{u_\Phi}{r} \right) - \frac{\alpha}{r} \frac{\partial}{\partial r} (r u_\Phi) + 2\alpha\omega_z$$
$$\tau_{\Phi z} = \mu \frac{\partial u_\Phi}{\partial r} - \frac{\alpha}{r} \frac{\partial}{\partial z} (r u_\Phi) - 2\alpha\omega_r$$
$$\tau_{z\Phi} = \mu \frac{\partial u_\Phi}{\partial z} + \frac{\alpha}{r} \frac{\partial}{\partial z} (r u_\Phi) + 2\alpha\omega_r$$

In the particular case, i.e. for $\to 0$, we obtain from equations (30 - 32):

$$\omega_r = 0 \quad , \omega_z = 0 \tag{34}$$

$$u_\Phi = \frac{1}{2\pi} \iint_{-\infty}^{\infty} e^{-i(\xi z + \omega t)}\, d\xi d\omega \int_0^{\infty} \eta J_1(\eta r) \frac{\hat{X}_\Phi}{\left(\mu - \frac{p}{2}\right)(v^2 - \delta_2^2)}\, d\eta \tag{35}$$

where :

$$\delta_2^2 = \frac{\mu}{\rho}$$

Equation (35) refers to the classical elastic medium under initial stress which is similar to that which has been obtained by Boiet [2], while the equations (34), where in , only the rotations cannot appear.

Similarly, One can derive the equations describing the displacements and rotations in the static problem as well as for vibrations changing harmonically in time.

References

[1] A.M. Abd-Alla and S. R. Mahmoud , Effect of the rotation on propagation of thermoelastic waves in a non-homogeneous infinite cylinder of isotropic material, *Int. J. of Mathematical Analysis*, Vol. 4,42, pp. 2051 – 2064, (2010).

[2] A.M. Abd-Alla and S. R. Mahmoud, Magneto-thermoelastic problem in rotating non-homogeneous orthotropic hollow cylindrical under the hyperbolic heat conduction model, *Meccanica*, Vol. 45, 4, pp. 451-462, (2010).

[3] A.M. Abd-Alla, A.N. Abd-Alla, and N.A. Zeidan, Transient thermal stresses in an isotropic infinite circular cylinder, *J. Applied Mathematics and Computation*, Vol. 121, pp. 93-122, (2001).

[4] A.M. Abd-Alla, S. R. Mahmoud and N.A. AL-Shehri, Effect of the rotation on the radial vibrations in a non-homogeneous orthotropic hollow cylinder , *Int. J. of Modern Physics B*, in press, 2010.

[5] S. R. Mahmoud , Wave propagation in cylindrical poroelastic dry bones, *J. of The Applied Mathematics & Information Sciences* , Vol. 4, No.2, pp. 209-226, (2010).

[6] S.R. Mahmoud, Effect of the non-homogeneity on wave propagation on orthotropic elastic media, *Int. J. of Contemporary Mathematical Sciences*, Vol. 5, 45, pp.2211 – 2224, (2010).

[7] A.M. Abd-Alla, T.A. Nofal, A.M. Farhan, Effect of the non-homogenity on the composite infinite cylinder of isotropic material, *Physics Letters A*, Vol. 372, pp. 4861-4864, (2008).

[8] J.R. Hutchinson and S.A. El-Azhary, Vibrations of free hollow circular cylinder, *J. Applied Mechanics*, Vol. 53, pp. 641-646, (1986).

[9] A.M.Abd-Alla and A.M. Farhan , Effect of the non-homogeneous on the compsite infinite cylinder of orthotropic material , *J. Physics Letters A*, Vol. 372, pp. 756-760, (2008).

[10] X. Wang and Y.P. Shen, Inclusions of arbitrary shape in magneto-electro-elastic composite materials, *Int. J. of Engineering Science*, Vol. 41, pp. 85–102, (2003).

[11] S.C Cowin and M. Fraldi, On singularities associated with the curvilinear anisotropic elastic symmetries, *Int. J. Non-Linear Mech*., Vol. 40, pp. 361-371, (2005).

[12] D.D. Ebenezer, K. K. Ravichandran, and P.Chandramouli, Forced vibrations of solid elastic cylinders, *J. Sound and Vibration*, Vol. 282, pp. 991-1007, (2005).

[13] H.J. Ding, H.M. Wang and P.F. Hou, The transient responses of piezoelectric hollow cylinders for axisymmetric plane strain problems, *Int. J. of Solids and Structures*, Vol. 40, pp. 105–123, (2003).

[14] P.F. Hou and A.Y.T. Leung, The transient response of magneto-electro-elastic hollow cylinders, *Smart Material Structure*, Vol. 13, pp. 762–776, (2004).

[15] J.R. Hutchinson, Vibrations of solid cylinders, *J. Appl. Mech*., Vol. 47, pp.901-907, (1980).

[16] S. Markus and D.J. Mead, Axisymmetric and asymmetric waves motion in orthotropic cylinders, *J. Sound and Vibration*, Vol.181, pp.127-147, (1995).

[17] W. Q. Chen, K. Y. Lee, and H. J. Ding, On free vibration of non-homogeneous transversely isotropic magneto-electro-elastic plates, *J. Sound and Vibration*, Vol. 279, pp.237- 251, (2005).

[18] W.Q. Chen, K.Y. Lee and H.J. Ding, General solution for transversely isotropic magneto-electro-thermo-elasticity and potential theory method, *I. J. Engineering Science*, Vol. 42, pp.1361-1379, (2004).

[19] J. N. Sharma, and R. Kumar, Asymptotics of wave motion in transversely isotropic plates, *J. Sound and Vibrations*, Vol. 274, pp.747-759, (2004).

[20] H.H. Toudeshky, M.R. Mofakhami and Sh.H. Hashemi, Sound transmission into a thick hollow cylinder with the fixed end boundary condition, *Applied Mathematical Modeling*, Vol. 33, pp. 1656-1673, (2009).

[21] G.R. Buchanan, Free vibration of an infinite magneto-electro-elastic cylinder, *J. Sound and Vibration*, Vol. 268, pp. 413-426, (2003).
[22] Y.E. Senitskii, Stress state of a rotating inhomogeneous anisotropic cylinder of variable density. *Int. J. Applied Mechanics*, Vol.28, pp.296-302, (1992).
[23] M.E. Erguven, A fundamental solution for transversely isotropic and non-homogeneous media, *Int. J. Engineering Science*, Vol. 25, pp.117-122, (1987).

Authors' information

Current address: Mathematics Department, Faculty of Science, Taif University, Taif 888, KSA
Permanent address: Mathematics Department, Faculty of Science, Assiut University, Assiut, Egypt

Praise Worthy Prize

International Review of Physics (I.R.E.PHY.), Vol. 5, N. 6
December 2011

Red Shift Band Gap Enhancement of the Nanostructure $ZnO_{100-x}Al_x$ Thin Films as a Function of Al Concentration for Optoelectronic Applications

Nada M. Saeed, Manal M. Abdullah, Nathera A. Ali, Baha T. Chied

Abstract – *Zinc Oxide doped Aluminum (ZnO:Al) is a promising material for electronic and optoelectronic applications. In this work, Aluminum doped zinc oxide materials was prepared as thin films onto hot substrate temperature at 420°C using chemical spray process technique. The precursor thin films ($ZnO_{100-x}Al_x$) are prepared by using aqueous zinc chloride solution and solution of $AlCl_3$,$6H_2O$ of molar concentration 0.10 M/L using x=3, 6, and 9.*

The crystallographic structures of the prepared films are analyzed using X-ray diffraction; the results show that the films are polycrystalline. The general morphology of ZnO:Al films are imaged by using Atomic Force Microscope (AFM), it constructed from nanostructure dimensions range between 81.7 nm-67.6 nm, it was reduced at increasing the ratio of doping. The photoluminescence (PL) spectrum of the prepared films was studied, the sharp peak can be referred to the direct energy gap, and there is a red shift in the PL peak at increasing the ratio of doping.

The optical properties of $ZnO_{100-x}Al_x$ films are studied using measurement from UV-VIS-NIR spectrophotometer at wavelength within the range (200-850) nm. The optical characterization shows that the transmittances of the doped films are reduced at increasing the ratio of doping.

The optical energy gap of $ZnO_{100-x}Al_x$ was calculated for direct allowed transition, the value of the energy gap also reduced to be 3.1 eV, 3.0.eV, 2.8 eV at x=3, 6, 9 respectively.

Keywords*: Zinc Oxide Doped Al, Thin Film Spray Pyrolysis, Nanostructure ZnO*

I. Introduction

Zinc Oxide (ZnO) is semiconductor material; Zinc and Oxygen belong to the 2nd and 6th groups of the periodic table, respectively.

This semiconductor is transparent conducting oxide (TCO) materials, which have the advantages of low cost, low toxicity, and high mechanical and thermal stabilities. Also it has several favorable properties such as good transparency, high electron mobility, wide band gap of 3.37 eV at room temperature, strong room-temperature luminescence.; those properties are already used in emerging applications as transparent electrodes in liquid crystal displays.

Thin films of undoped and doped ZnO are utilized for a wide variety of electronic applications, such as surface acoustic wave devices and transparent conducting electrodes.

Nanoscale porous structures of ZnO and ZnO:Al with high surface area find their application in chemical sensors and in energy-saving or heat-protecting windows and heat mirrors. Various techniques have been used to deposit undoped and doped ZnO films on different substrates, including, pulsed laser deposition, sputtering, sol-gel process and spray pyrolysis technique [1], [2].

M. De La L. Olvera *et al*, (2000), had studied the electrical, structural, morphological and optical characteristics of ZnO:Al thin films obtained by chemical spray are. They proved the dependence of the resistivity on the substrate temperature and the film thickness, the growth in the (002) direction was observed in all cases. The surface morphology was analyzed by using atomic force and scanning electron microscopy (AFM and SEM) techniques. High transmittance, 85%, was obtained in all cases; the band gap was of the order of 3.35 eV [3].

Other researchers, A. A. Ibrahim and A. Ashour, (2006), had prepared and studied ZnO/Si heterojunction by depositing n-ZnO films doped with aluminium on p-Si by spray pyrolysis method. Heterojunction solar cells were fabricated using the configuration Al/ZnO/Si/In. The electrical properties of the heterojunction were investigated by means of current– voltage measurements in the temperature range 295–375 K. The cells show the rectifying behavior characterized by the current–voltage (I–V) measurement under a dark condition, while photoelectric effects have been exhibited under the illumination. As a result, the conversion efficiency of the fabricated cell of about 6.6% was obtained [4].

In the University of Korea, Jae-Sung Hur et al, (2008), had studied the ability of improving solar cells by using

Manuscript received and revised November 2011, accepted December 2011

transparent conducting as window layers as a function of thickness. They used Al-doped ZnO thin as the top or the bottom transparent conducting window layer. This study examined the efficiency of solar cells as a function of the Al-doped ZnO film thickness. A 50-nm-thick intrinsic ZnO thin film was deposited by RF magnetron sputtering. The fill-factor and the conversion efficiency of a solar cell with a 310-nm-thick thin film were calculated to be 0.67 and 13.54 %, respectively, from the results of the J-V measurements [5].

Zinc Oxide doped Aluminum nanostructures are promising materials for optoelectronic applications, it can be used as window layer in photovoltaic devices especially for dye-sensitized solar cells and for electronic applications as thin-film transistors and light-emitting diodes[6].

ZnO is highly transparent, conductive when doped, and easily prepared by versatile methods, it has been researched as a barrier layer in inorganic thin film solar cells to improve device stability, so it has been demonstrated to be one of effective materials for fabricate the non-inverted polymer solar cells [7].

Polymer solar cells have seen remarkable progress in recent years and have developed from being a scientific curiosity to an emerging technology that can be manufactured industrially and demonstrated in real applications. Polymer solar cells have been heralded as the photovoltaic (PV) technology solving all the problems current PV technologies are faced with by providing convincing solutions to problems of cost and abundance of the materials that constitute them. The largest challenges to overcome this far have been the low performance and the short operational lifetime [8]-[13].

Today polymer solar cells are present power conversion efficiencies in excess of 8% and estimated operational lifetimes in the range of 2–5 years. The typical polymer solar cell is a multilayer structure with typically five layers stacked on top of each other. The active layer responsible for light absorption and generation of free charge carriers is typically the middle layer sandwiched between two charge selective layers. The two outer layers are highly conducting electrodes for extraction of the generated electrical current; one of those must be transparent. The electron selective layers have been combination with very thin wide band gap insulators such as LiF and MgF2. recently a new class of moderately conducting electron selective layers have been explored ;ZnO, TiO2, Nb2O5 [14].

The objective of the present work was to check whether Al could be incorporated by a simple low cost technique.

II. Experimental Details

ZnO:Al thin films are prepared onto hot glass substrates by using chemical spray pyrolysis technique using solution of Zinc Chloride ($ZnCl_2$) and $AlCl_3$,$6H_2O$, the molar concentration of the spray solution was 0.10 M/L, the flow rate of solution is 2 ml/Sec. $ZnO_{100-x}Al_x$ is deposited onto hot substrate temperature using x=3, 6 and 9, the substrate temperature is held constant at 420 °C.

Two experimental methods were used for thickness measurements; the "Weighting method" and the "Optical interference fringes method". The Weighting method gives an approximate value for the thickness of the thin films with an error 30 %. A digital balance with accuracy of ($\pm$ 0.1× 10^{-3} gm) was used for weighting the needed materials and for measured the thickness of the prepared films. He-Ne laser of wavelength 632.8 nm was used for measured the thickness of the films by optical interference fringes method, the thickness of all the prepared films were varied between 380-400 nm.

Fig. 1. The setup arrangement of the spray technique

X-ray diffraction technique was used to determine the crystalline structure of the films before and after doping. X-ray has the following information: source Cuk_α radiation of the wavelength $\mathring{A}\left(\lambda = 1.54060\, A^\circ\right)$, Current =30 m A, Voltage =40 kV, Scanning angle (20˚ to 60˚).

The surface morphology of the prepared films was tested by using Atomic Force Microscope (AFM).

The optical properties of ZnO:Al thin films are carried out from IR-VIS-UV spectrophotometer at wavelength within the range (200-850) nm.

III. Results and Discussions

III.1. Surface Morphology

The general morphology of $ZnO_{100-x}Al_x$ films are imaged by using Atomic Force Microscope (AFM), the image shows that the grain size of the prepared film is constructed from nanostructure of dimensions in order of 81.7nm, 75nm. 67.6nm at x 3, 6 and 9 respectively, the results is clearly indicate crystallites perpendicular to the substrate, agglomeration of small crystallites also seems to be present in the prepared films, as shown in Figs. 2(a), (b), (c).

Figures 2 (a), (b), (c) clearly indicate in small particle size, crystallite sizes were decreased due to increases of the Al concentration.

Although no cracks could be detected but some holes indicating, porosity is present.

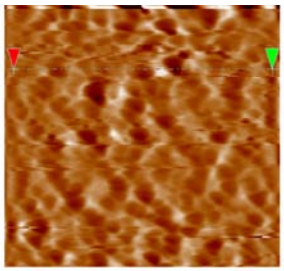

(a)

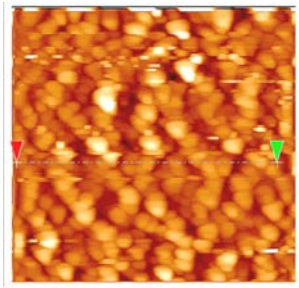

(b)

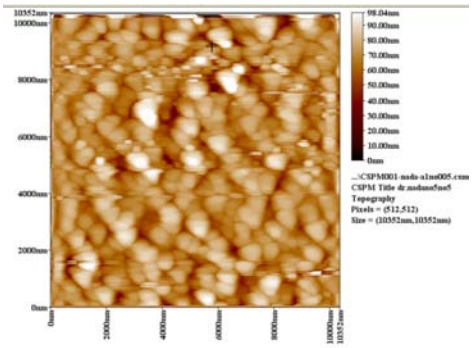

(c)

Figs. 2. The Surface Morphology of $ZnO_{100-x}Al_x$, thin film (at x 3, 6 and 9 respectively) takes from Atomic Force Microscope.(a)The grain size (average dimensions) =81.77 nm; (b)The grain size (average dimensions)=75 nm; (c)The grain size (average dimensions)= 67.65 nm

III.2. X-Ray Patterns

The X-ray diffraction patterns of the doped films of $ZnO_{100-x}Al_x$, at x= 3, 6 and 9 films deposited at 420 ^oC is obtained at 2θ from 20˚ to 60˚ glancing angle, there are only one sharp and three small peaks present, are shown in Figures 3, 4, 5 respectively. These figures show that the film is polycrystalline crystallized in the wurtzite phase and presents a preferential orientation along the c-axis, the highest peak observed at (002). The results are in agreement with the literature of American standard of testing materials (ASTM), as listed in Table I.

It is evident that aluminium doping decreasing the intensity of (002) peak, as listed in Table II. (102) peak becomes wide. No metallic Al characteristic peak was observed in the x-ray pattern, this may be due to Al replacing zinc substitutionally in the lattice or aluminum segregation to the non-crystalline regions in the grain boundary. Suchea et al. [15] reported for sputtered films, there is an optimum doping level (~4 at.%) after which Al atoms don't go the lattice.

The intensity of all peaks at (002) and the average grain size the nanostructure $ZnO_{100-x}Al_x$ (at x= 3, 6 and 9) films are listed in Table II.

TABLE I
THE VALUE OF D FOR ALL PEAKS OF $ZnO_{100-x}Al_X$ FILM TAKES FROM X-RAY PATTERN

FILMS	(hkl)	(2θ) Degree *(XRD)*	(2θ) Degree ASTM	d *(XRD)* (Å)	d ASTM (Å)
$ZnO_{97}:Al_3$	(100)	32.55	31.77	2.819	2.816
	(002)	34.35	34.42	2.608	2.602
	(101)	36.14	36.25	2.483	2.476
	(102)	47.45	47.54	1.912	1.911
$ZnO_{94}:Al_6$	(002)	34.35	34.42	2.608	2.602
	(101)	36.15	36.25	2.482	2.476
	(102)	47.43	47.54	1.915	1.911
$ZnO_{91}:Al_9$	(002)	34.45	34.42	2.601	2.602
	(101)	36.20	36.25	2.478	2.476
	(102)	47.52	47.54	1.911	1.911

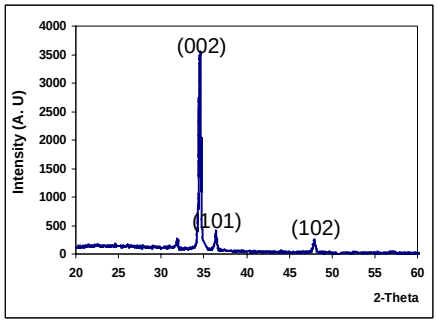

Fig. 3. X-ray diffraction (XRD) pattern of $ZnO_{97}Al_3$ film

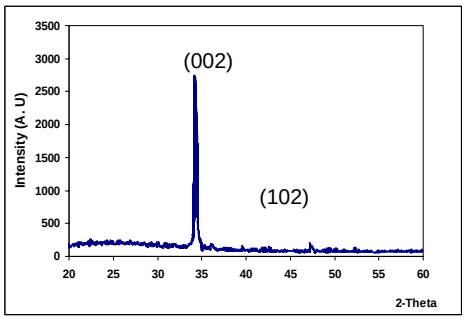

Fig. 4. X-ray diffraction (XRD) pattern of $ZnO_{94}Al_6$ films

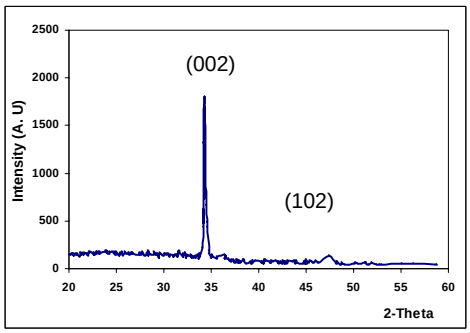

Fig. 5. X-ray diffraction (XRD) pattern $ZnO_{91}Al_9$ film

TABLE II
THE INTENSITY OF ALL PEAKS AT (002) AND THE AVERAGE GRAIN SIZE OF $ZnO_{100-X}Al_X$ FILMS (AT X= 3, 6 AND 9)

FILMS	Maximum Intensity at (002) peaks	Average grain size (nm)
$ZnO_{97}:Al_3$	3600	81.77
$ZnO_{94}:Al_6$	2700	75
$ZnO_{91}:Al_9$	1800	67.65

III.3. Photoluminescence Spectrum (Pl)

The photoluminescence spectra (PL) of the nanostructure $ZnO_{100-x}Al_x$ films are excited at 340 nm. The photoluminescence spectrum of the prepared films shows the sharp peak; it can be referred to the direct band transition between valance and conduction band, as show in Fig. 6, at these patterns there are small peaks which can be attributed to the formation of the surface states in the energy band gap [16].

The sharp peaks of the PL spectrum of $ZnO_{100-x}Al_x$ are recorded at 590 nm, 665, 678 nm at x= 3, 6 and 9 respectively. It can be observed that the PL peaks are created in the visible region, and there was shift in location of the sharp peaks at the PL spectrums of the all prepared films.

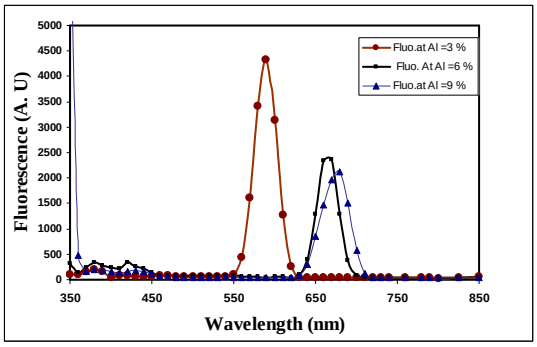

Fig. 6. Photoluminescence emission spectrum of the nanostructure $ZnO_{97}Al_3$, $ZnO_{94}Al_6$, and $ZnO_{91}Al_9$ films

III.4. The Transmission and the Absorption Spectrum

The transmission spectra of $ZnO_{100-x}Al_x$, thin films are estimated from UV- VIS-NIR spectrophotometer at wavelength within the range (200-850) nm.

Figure 7 represents the transmission spectrum of $ZnO_{100-x}Al_x$ films at x=3, 6, and 9, the average transmission was recorded within the visible region to be 52%, 45%, 37% for $ZnO_{97}Al_3$, $ZnO_{94}Al_6$ and $ZnO_{91}Al_9$ films respectively, as listed in Table III.

It was observed from these results that the average transmissions are found to decrease at higher Al doping concentrations; this might be attributed to an increase in the free-carrier concentration in the prepared films.

Therefore a lower resistivity and a higher transmission in the visible region are not entirely; this result was in good agreement with reference [2].

Figure 8 represents the absorption spectrum of $ZnO_{100-x}Al_x$ films at x=3, 6, and 9.

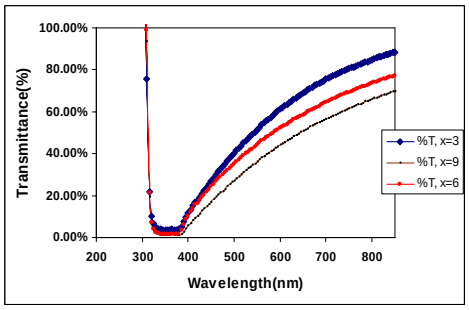

Fig. 7. The Transmission Spectrum of $ZnO_{100-x}Al_x$ films at x=3, 6, and 9

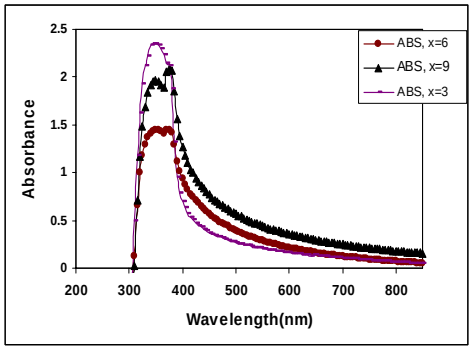

Fig. 8. The absorbance spectrum of $ZnO_{100-x}Al_x$ films at x=3, 6, and 9

III.5. The Optical Energy Gap

The optical band gap (E_g) is calculated by using plot $\alpha h\nu)^2$ vs. $h\nu$), the value of α is determined from transmittance spectra. The photon energy at the point where $(\alpha h\nu)^2$ is zero represents E_g.

The value of the energy gap of ZnO compound as a bulk is equal 3.31 eV but as thin film it is depend on the manufacturing techniques [17].

The energy gap is estimated by assuming a direct and indirect allowed transition between valence and conduction bands using the fallowing equation [18]:

$$(\alpha h\upsilon) = A^*\left(h\upsilon - E_g\right)^r \qquad (1)$$

where A^* is constant, α is the absorption coefficient, the absorption coefficient the film was calculated using the following relation:

$$\alpha = 2.303A/t \qquad (2)$$

where A is the absorbance, t is the thickness of the film. $h\upsilon$ is the incident photon energy, and r is constant which takes the values (1/2, 3/2, 2, and 3) depending on the material and the type of the optical transition whether it is direct or indirect.

The energy gap (E_g) is determined by extrapolating the straight line portion of the spectrum to $\alpha E = 0$.

The value of the optical energy gap is calculated for direct allowed transition, it is also reduced after the increasing of Al doping ratio, it was 3.1, 3.0.eV, 2.8 eV for $ZnO_{100-x}Al_x$ x=3, 6, and 9 respectively, as show in Figs. 9(a), (b), (c); these values are in good agreement with previously reported value [19], [20].

It can be mentioned from these figures that both the average transmittance and band gap are decrease at higher Al doping concentrations, as listed in Table III.

TABLE III
THE OPTICAL PROPERTIES OF $Zno_{100-x}al_x$ FILMS AT X =3, 6 AND 9

FILMS	Energy gap *(eV)*	Average transmissions % at 550 nm
$ZnO_{97}:Al_3$	3.1	52
$ZnO_{94}:Al_6$	3.0	47
$ZnO_{91}:Al_9$	2.8	35

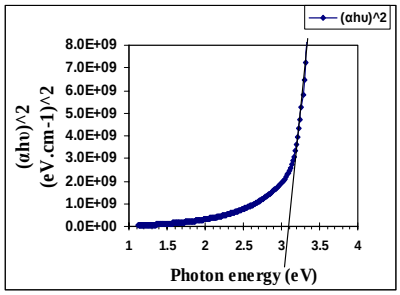

(a)

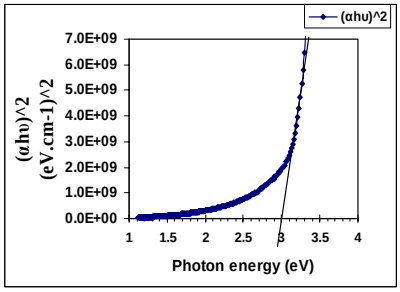

(b)

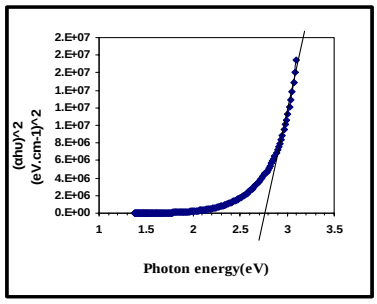

(c)

Figs. 9. The direct energy gap of $ZnO_{100-x}Al_x$ t films (at x =3, 6 and 9) (a) $ZnO_{97}:Al_3$ film; (b) $ZnO_{94}:Al_6$ film; (c) $ZnO_{91}:Al_9$ film

IV. Conclusion

Transparent $ZnO_{100-x}Al_x$ thin films are successfully prepared by using chemical spray pyrolysis technique at substrate temperature 420°C. The Aluminums particles could be successfully incorporated in ZnO thin films. The concentration of Al was intentionally chosen to be large (3, 6, and 9 at %) so that the effects of Al can be easily detected, it may be possible to try still lower concentrations.

The absorption of the films improved after doping; also it was found that the average transmittances of the prepared films are decrease at higher Al doping concentrations that because of the effect of the concentration of the free-carrier. The prepared films have wide direct band gap, the value of the direct energy gap is reduced after doping. Optimization of Al incorporation can give ZnO thin films with improved properties.

Acknowledgements

This work was supported by Physics Department-College of Science-University of Baghdad.

References

[1] A. Hernández Battez, R. González, J.L. Viesca, J.E. Fernández, J.M. Díaz Fernández, A. Machado, R. Chou, J. Riba, CuO, ZrO2 and ZnO nanoparticles as antiwear additive in oil lubricants, *Wear*, Volume 265, Issues 3–4, 31 July 2008, Pages 422-428.

[2] S. Hun Jeong, Bit Na Park, Dong-Geun Yoo and Jin-Hyo Boo. "Al-ZnO Thin Films as Transparent Conductive Oxides; Synthesis, Characterization, and Application Tests", *Journal of the Korean Physical Society*, March (2007), 50, 3 pp. 622-625.

[3] M. de la L. Olvera, A. Maldonado, R. Asomoza and M. Mele´ndez-Lira, "Chemical stability of doped ZnO thin films doped ZnO thin films" *Journal of Materials Science; Materials in Electronics*. (2000), 11, 1, pp. 1-5.

[4] A. A. Ibrahim and A. Ashour, " ZnO/Si solar cell fabricated by spray pyrolysis technique", *J. Mater Sci: Mater Electron*, 17, No. 10, (2006), pp. 835-839.

[5] J.S. Hur, J.-B. Song, J. Kim and D. ByunJae, "Efficiencies of CIGS Solar Cells Using Transparent Conducting Al-Doped ZnO Window Layers as a Function of Thickness", *Journal of the Korean Physical Society*, (2008), 53, 1, pp. 437-441.

[6] Sh. J Ikhmayies, N. M. Abu El-Haija, R. N. Ahmad-Bitar., "Electrical and optical properties of spray-deposited ZnO:Al thin films" GCREEDER Amman-Jordan, (2009), March 31.

[7] Z. Zhaoa, R. Teki, N. Koratkarc, H. Efstathiadisa, P. Haldara, " Metal oxide buffer layer for improving performance of polymer solar cells",*Applied Surface Science journal*, (2010), 256 ,pp. 6053–6056.

[8] T.D. Nielsen, C. Cruickshank, S. Foged, J. Thorsen, F.C. Krebs, "Business, market and intellectual property analysis of polymer solar cells". *Sol. Energy Mater. Sol. Cells* (2010), 94, 1553-1571.

[9] M. Helgesen, R. Søndergaard, F.C. Krebs, "Advanced materials and processes for polymer solar cell devices". *J. Mater. Chem.* (2010), 20, 36-60.

[10] F. C. Krebs, S. A. Gevorgyan, J. Alstrup, "A roll-to-roll process to flexible polymer solar cells: Model studies, manufacture and operational stability studies". *J. Mater. Chem.* (2009), 19, 5442-5451.

[11] F. C. Krebs, M. Jørgensen, K. Norrman, O. Hagemann, J. Alstrup,T. D. Nielsen, J. Fyenbo, K. Larsen, J. Kristensen, "A complete process for production of flexible large area polymer solar cells entirely using screen printing—First public demonstration", *Sol. Energy Mater. Sol. Cells*, (2009), 93, 422-441.

[12] F. C. Krebs, T. Tromholt, M. Jørgensen, "Upscaling of polymer solar cell fabrication using full roll-to-roll processing". *Nanoscale*, (2010), 2, 878-886.

[13] F.C. Krebs, T.D. Nielsen, J. Fyenbo, , M. Wadstrøm, M.S. Pedersen," Manufacture, integration and demonstration of

polymer solar cells in a lamp for the ―Lighting Africa initiative". *Energy. Environ. Sci*. (2010), 3, 512-525.
[14] N. Espinosa, H. Friis Dam, D. M. Tanenbaum, J. W. Andreasen, M. Jørgensen , and F. C. Krebs," Roll-to-Roll Processing of Inverted Polymer Solar Cells using Hydrated Vanadium(V)Oxide as a PEDOT:PSS Replacement", *Materials* 2011, 4, 169-182.
[15] M. Suchea, S. Christoulakis, N. Katsarakis, T. Kitsopoulos and G. Kiriakidis," Comparative study of zinc oxide and aluminium doped zinc oxide transparent thin films by direct current magnetron sputtering", *Thin Solid Films*, (2007), 515, 6562-6566.
[16] A. Nag. and D. D. Sarma."To Dope Mn^{2+} in a Semiconducting Nanocrystal", *J. Phys. Chem.C*, (2007), 111, 13641-13644.
[17] C. Gümü , O. M. Ozkendir, H. Kavak, Y. Ufuktepe. *Journal of Optoelectronics and Advanced Materials*, (2006), 8, 1, 299 - 303.
[18] S. Lindroos and G. Rusu, *J. Optoelectron. Adv. Materials*, (2005), 7, 2. p. 817.
[19] R. Asomoza, H. Malodonado, M. D. Olvera, T. Delgado, (1999). p .408.
[20] P. Sagar, M. Kumar, R.M. Mehra."Electrical and optical properties of sol-gel derived ZnO:Al thin films". *Materials Science-Poland*, (2005), 23, 3.

Authors' information

Department of Physics, College of Science, University of Baghdad

Nada M. Saeed (Corresponding author)
Place and/ date of birth: Iraq -Baghdad / 1962
Scientific Degree: B. Sc Physics, 1986, College of Science/ University of Baghdad-Iraq**.** M. Sc Optoelectronics, 2005, College of Science / University of Baghdad –Iraq.
Specialization: Optoelectronics.
Author's major field of study: Solar cells applications**.**
Carrier: Lecturer.
Work Address: Department of Physics / College of Science University of Baghdad.
E-Mail: nadaalkhanchi@yahoo.com

Praise Worthy Prize

International Review of Physics (I.R.E.PHY.), Vol. 5, N. 6
December 2011

Electron Impact Collision Strengths for Fe XVI

A. I. Refaie, A. A. Farrag

Abstract – *The energy levels and electron impact collision strengths have been calculated for Na- like iron. The MCDFGME package has been used in generating the relativistic wave functions and in calculating the energy levels and the plane wave Born (PWB) cross sections for the impact excitation.*

The energies of the lowest 21 levels of ($1s^2 2s^2 2p^6$) 3s, 3p, 3d, 4s, 4p, 4d, 4f, 5s, 5p, 5d, 5f, and 5g configurations are tabulated and the electron impact excitation collision strengths have been calculated among the considered 21 levels for electron energies K=50,100 and 200 Rydbergs. A comparison has been performed between the present calculations and the available data in literature showing a good agreement. ***Copyright © 2011 Praise Worthy Prize S.r.l. - All rights reserved.***

Keywords*: Electron Impact Excitation, Collision Strength*

I. Introduction

Iron is an abundant element in solar and fusion plasma, and its emission lines are observed in almost all the ionization stages, hence the need of theoretical atomic data for Fe ions since there is an insufficiency of required experimental results. Electron collisional excitations for Fe XVI ion have been the subject of interest due to their emission lines arising from transitions observed in laboratory [1] (Wang et al. (1988)), in solar ultraviolet, in extreme-ultraviolet (EUV) and in soft X-ray spectra[2]-[4] (Sandlin et al. (1986), Acton et al. (1985), Thomas et al. (1994)). The most recent examples include the work of Keenan et al. (2003) on EUV observations from the Solar Extreme-Ultraviolet Research Telescope and Spectrograph (SERTS) [5]. The most important calculations are those of Tayal (1994), the calculated collision strengths (Ω) and effective collision strengths (γ) for Fe XVI transitions among the $n \leq 4$ levels by using the standard R-matrix code for calculating the wavefunctions and collision strengths [6]. The atomic physics calculations of Eissner et al. (1999) and Cornille et al. (1997) for Fe XVI considered transitions between the $n \leq 4$ and $n \leq 5$ levels [7],[8], respectively. In their calculations they adopted the SuperStructure (SS) code of Eissner et al. (1974) for the generation of wavefunctions [9] and distorted-waves (DW) code of Eissner and Seaton (1972) for the scattering processes [10]. Recently, Aggarwal (2006) have used the General Purpose Relativistic Atomic Structure Package (GRASP) to calculate the energy levels and radiative rates [11], [17] and have generated excitation rates for Fe XVI using the fully relativistic Dirac atomic R-matrix code (DARC) with the inclusion of all levels with $n \leq 7$. Aggarwal (2007) has reported the results of transitions among 134 levels [12].

Then Aggarwal (2008) discussed the results for Ω and γ for the inner shell transitions of Fe XVI by using (DARC) [13], [18]. In the present work, the lowest 21 fine-structure levels among the ($1s^2 2s^2 2p^6$) 3s, 3p, 3d, 4s, 4p, 4d, 4f, 5s, 5p, 5d, 5f, and 5g configurations of Fe XVI have been calculated. The electron impact excitation collision strengths have also been calculated between the considered 21 levels at electron energies K=50, 100 and 200 Rydbergs. The Multi-configuration Dirac-Fock (MCDFGME) [14], [15] code has been used. The model and procedure are summarized in section 2. A comparison of the present data with the available observed values and also with the previous calculations are presented and discussed in section 3. A conclusion is given in section 4.

II. The MCDF Method

The general relativistic MCDF code developed by J.P. Desclaux and P. Indelicato [14], [15] has been used to calculate bound-state wave functions and energies. Details of the method, including the Hamiltonian and the processes used to build the wave functions can be found elsewhere [20], [21]. The total wave function is calculated with the help of the variational principle. The total energy of the atomic system is the eigenvalue of the equation:

$$H\,\Psi_{\prod,J,M}(\ldots, r_i \ldots.) = E_{\prod,J,M}\Psi_{\prod,J,M}(\ldots, r_i \ldots.) \qquad (1)$$

where $\prod$ is the parity, J is the total angular momentum eigen value, and M is its projection on the z axis J_z. In this equation, the hamiltonian is given by:

$$H = \sum_{i=1}^{N} H_D\,(r_i) + \sum_{i<j} V_{ij}\,(|r_{ij}|) \qquad (2)$$

Manuscript received and revised November 2011, accepted December 2011

where H_D is the one electron Dirac operator and V_{ij} is an operator representing the electron-electron interaction.

The expression of V_{ij} in Coulomb gauge and in atomic units, is:

$$V_{ij} = \frac{1}{r_{ij}} - \frac{\alpha_i \cdot \alpha_j}{r_{ij}} - \frac{\alpha_i \cdot \alpha_j}{r_{ij}}\left[cos\left(\frac{\omega_{ij} r_{ij}}{c}\right) - 1\right] + \\ + c^2(\alpha_i \cdot \nabla_i)(\alpha_j \cdot \nabla_j)\frac{cos\left(\frac{\omega_{ij} r_{ij}}{c}\right) - 1}{\omega_{ij}^2 r_{ij}} \quad (3)$$

where $r_{ij} = |r_i - r_j|$ is the inter-electronic distance, ω_{ij} is the energy of the exchanged photon between the two electrons, α_i are the Dirac matrices and c is the speed of light. The Coulomb gauge has been used as it was demonstrated to provide energies free from spurious contributions at the ladder approximation level and must be used in many-body atomic structure calculations [14], [15].

The term $\frac{1}{r_{ij}}$, represents the Coulomb interaction, the term $\frac{\alpha_i.\alpha_j}{r_{ij}}$ is the Gaunt (magnetic) interaction, and the last two terms of equation (3) stand for the retardation operator. In this expression the ∇ operators act only on r_{ij} and not on the following wave functions.

The MCDF method is defined by the particular choice of a trial function to solve the Dirac equation as a linear combination of configuration state functions (CSF):

$$|\Psi_{\prod,J,M,} >= \sum_{\nu=1}^{n} c_\nu \, |\nu, \prod, J, M > \quad (4)$$

The CSF are also eigenfunctions of the parity $\prod$, the total angular momentum J^2 and its projection J_z. The label ν stands for all other numbers (principal quantum number, etc.) necessary to define unambiguously the CSF.

The c_ν are the mixing coefficients and are obtained by the diagonalization of the Hamiltonian matrix coming from the minimization of the energy in Eq. (1) with respect to the c_ν.

The CSF are antisymmetric products of one-electron wave functions expressed as linear combinations of Slater determinants of Dirac 4-spinors:

$$|\nu, \prod, J, M > = \sum_{i=1}^{N\nu} di \begin{bmatrix} \Psi_1^i(r_1) & \cdots & \Psi_m^i(r_1) \\ \vdots & \ddots & \vdots \\ \Psi_1^i(r_m) & \cdots & \Psi_m^i(r_m) \end{bmatrix} \quad (5)$$

where the *Ψ-s* are the one-electron wave functions and the coefficients d_i are determined by requiring that the CSF is an eigenstate of J^2 and J_z. The d_i coefficients are obtained by requiring that the CSF are eigenstates of J^2 and J_z.The Multi-Configuration approach is characterized by the fact that a small number of configurations can account for a large amount of correlations.

Electron-impact excitation cross sections have been computed using the first Born approximation following the work of Kim et al. [22], [23].

In these calculations, the cross sections for the processes leading from each level *j* of the S^{q+} ion ground configuration, to the excited level *i* of the S^{q+} ion σ_{ji} have been obtained.

A Multi-Configuration Dirac-Fock (MCDF) wave function for the atom and a Dirac wave function for the free electron have been used. Only the Coulomb interaction between the free electron and the atomic electrons has been considered.

Then, the individual cross sections thus obtained were then weighted by the statistical weight *gj* of each j level of the configuration in order to obtain the excitation cross section σ_{ji}.

The relationship between the collision strengths Ω_{ij} for the electron impact excitation and the excitation cross sections σ_{ij} is given by:

$$\Omega_{ij} = \frac{\sigma_{ij} K_i^2 g_i}{\pi a_0^2} \quad (6)$$

have been used, where a_0 is the Bohr radius, g_i is the statistical weight of the initial target level, K_i^2 is the kinetic energy of the incident electron in Rydbergs (Ry).

III. Results and Discussion

III.1. Energy Levels

Since Fe XVI is a moderate heavy ion with (Z=26), the relativistic effects are expected to be important in the determination of the wave functions and subsequently in the calculation of the collision strengths Ω.

The present calculated energy levels for the 21 fine structure levels, the observed values of NIST [16], the theoretical calculations of Cornille et.al (1997) using the superstructure (SS) code of Eissner et al (1974) [8] , Aggarwal et.al. (2006), which used the GRASP code [17] with QED effects (GRASP1) and without QED effects (GRASP2) and the flexible atomic code FAC code of Gu [19] are presented in Table I.

In general, the present theoretical energies calculated using of MCDFGME code [14], [15] agree well in magnitude and ordering with the experimental ones (NIST)[16].

There is an excellent agreement between the present calculations and the other theoretical calculations of Grasp, FAC and the SS. The present calculated energy levels show accuracy up to 1%.

III.2. Collision Strengths

The present values for the collision strengths for Fe XVI based on the plane wave Born approximation PWB at energies at the incoming electron energies of 50, 100, 200 Rydbergs are given in Table II.

TABLE I
ENERGY LEVELS (in Ryd) FOR Fe XVI

Index	Configuration	Level	Nist	This work	Cornille	GRASP[a]	GRASP[b]	FAC
1	3s	$^2S_{1/2}$	0.000	0.000	0.000	0.000	0.000	0.000
2	3p	$^2P^o_{1/2}$	2.526	2.505	2.530	2.533	2.535	2.535
3	3p	$^2P^o_{3/2}$	2.717	2.720	2.716	2.728	2.725	2.725
4	3d	$^2D_{3/2}$	6.155	6.174	6.179	6.176	6.168	6.159
5	3d	$^2D_{5/2}$	6.182	6.200	6.209	6.205	6.194	6.184
6	4s	$^2S_{1/2}$	17.018	17.000	17.017	17.004	16.994	16.993
7	4p	$^2P^o_{1/2}$	18.025	18.004	18.021	18.008	18.000	17.999
8	4p	$^2P^o_{3/2}$	18.098	18.078	18.093	18.084	18.074	18.073
9	4d	$^2D_{3/2}$	19.357	19.342	19.364	19.349	19.337	19.328
10	4d	$^2D_{5/2}$	19.368	19.354	19.377	19.362	19.349	19.340
11	4f	$^2F^o_{5/2}$	19.908	19.882	19.914	19.894	19.880	19.887
12	4f	$^2F^o_{7/2}$	19.913	19.886	19.919	19.899	19.884	19.891
13	5s	$^2S_{1/2}$	24.500	24.240	24.266	24.248	24.236	24.233
14	5p	$^2P^o_{1/2}$	24.761	24.736	24.760	24.743	24.732	24.728
15	5p	$^2P^o_{3/2}$	24.797	24.772	24.796	24.781	24.768	24.765
16	5d	$^2D_{3/2}$	25.407	25.381	25.409	25.391	25.378	25.371
17	5d	$^2D_{5/2}$	25.412	25.387	25.416	25.398	25.384	25.377
18	5f	$^2F^o_{5/2}$	25.684	25.654	25.686	25.666	25.652	25.661
19	5f	$^2F^o_{7/2}$	25.687	25.656	25.689	25.668	25.654	25.663
20	5g	$^2G_{7/2}$	25.716	25.680		25.692	25.678	25.675
21	5g	$^2G_{9/2}$	25.716	25.682		25.694	25.679	25.676

TABLE II
COLLISION STRENGTHS (Ω_{ij}) FOR Fe XVI

Transition		Ω_{ij}			Transition		Ω_{ij}		
i	j	100 Ryd	200Ryd	50 Ryd	i	j	100 Ryd	200Ryd	50 Ryd
1	**2**	2.2095E+00	2.4840E+00	1.9303E+00	**3**	**13**	1.0229E-02	1.6436E-02	4.4267E-03
1	**3**	4.3324E+00	4.8857E+00	3.7731E+00	**3**	**14**	5.1629E-03	5.5938E-03	4.3014E-03
1	**4**	1.4088E-01	1.4158E-01	1.3947E-01	**3**	**15**	7.7039E-02	8.2320E-02	6.6481E-02
1	**5**	2.1181E-01	2.1288E-01	2.0967E-01	**3**	**16**	5.5123E-03	1.0135E-02	1.0595E-03
1	**6**	1.0193E-01	1.0994E-01	8.5909E-02	**3**	**17**	4.8861E-02	9.0272E-02	9.0153E-03
1	**7**	2.5042E-02	4.3491E-02	1.1233E-02	**3**	**18**	8.0420E-03	8.3452E-03	7.4360E-03
1	**8**	4.6358E-02	8.0309E-02	2.1434E-02	**3**	**19**	5.9600E-02	5.3868E-02	4.8382E-02
1	**9**	3.0245E-02	3.4937E-02	2.0862E-02	**3**	**20**	2.8368E-03	2.8368E-03	2.8368E-03
1	**10**	4.5025E-02	5.2038E-02	3.1001E-02	**3**	**21**	2.1451E-02	2.1451E-02	2.1451E-02
1	**11**	4.2047E-02	4.2047E-02	4.2047E-02	**4**	**5**	3.6262E-02	3.6262E-02	3.6262E-02
1	**12**	5.6065E-02	5.6065E-02	5.6065E-02	**4**	**6**	1.9352E-02	2.0235E-02	1.7584E-02
1	**13**	1.9669E-02	2.1220E-02	1.6566E-02	**4**	**7**	6.4770E-02	9.3635E-02	3.8716E-02
1	**14**	5.0253E-03	9.4519E-03	1.3032E-03	**4**	**8**	1.7227E-02	2.2632E-02	1.2377E-02
1	**15**	9.4698E-03	1.7786E-02	2.5756E-03	**4**	**9**	4.3649E-01	4.5708E-01	3.9535E-01
1	**16**	9.1593E-03	1.0295E-02	6.8885E-03	**4**	**10**	1.0486E-02	1.1204E-02	9.0499E-03
1	**17**	1.3677E-02	1.5382E-02	1.0268E-02	**4**	**11**	1.7283E+00	2.4595E+00	1.0076E+00
1	**18**	8.0064E-03	8.0064E-03	8.0064E-03	**4**	**12**	6.5624E-03	6.5624E-03	6.5624E-03
1	**19**	1.0688E-02	1.0688E-02	1.0688E-02	**4**	**13**	2.9009E-03	2.9961E-03	2.7106E-03
1	**20**	4.9633E-03	4.9633E-03	4.9633E-03	**4**	**14**	7.7671E-03	1.0890E-02	4.7356E-03
1	**21**	6.2039E-03	6.2039E-03	6.2039E-03	**4**	**15**	3.8067E-03	4.3992E-03	3.2361E-03
2	**3**	1.7269E-01	1.7269E-01	1.7269E-01	**4**	**16**	8.3917E-02	8.7047E-02	7.7658E-02
2	**4**	3.1633E+00	3.6143E+00	2.7068E+00	**4**	**17**	2.9914E-03	3.1012E-03	2.7718E-03
2	**5**	3.8284E-02	3.8284E-02	3.8284E-02	**4**	**18**	2.7526E-01	3.7963E-01	1.6291E-01
2	**6**	3.6621E-02	5.7319E-02	1.8892E-02	**4**	**19**	1.8913E-03	1.8913E-03	1.8913E-03
2	**7**	1.1970E-01	1.2698E-01	1.0514E-01	**4**	**20**	6.1452E-02	7.3209E-02	3.7945E-02
2	**8**	2.2081E-02	2.4359E-02	1.7527E-02	**4**	**21**	6.7321E-04	6.7321E-04	6.7321E-04
2	**9**	1.3157E-01	2.1802E-01	5.6817E-02	**5**	**6**	2.9270E-02	3.0601E-02	2.6609E-02
2	**10**	1.2788E-02	1.2788E-02	1.2788E-02	**5**	**7**	7.9980E-03	7.9980E-03	7.9980E-03
2	**11**	2.0978E-01	2.2445E-01	1.8045E-01	**5**	**8**	1.0639E-01	1.5570E-01	6.2113E-02
2	**12**	1.6357E-02	1.6357E-02	1.6357E-02	**5**	**9**	1.0592E-02	1.1316E-02	9.1468E-03
2	**13**	4.8000E-03	7.7059E-03	2.1114E-03	**5**	**10**	6.2080E-01	6.5295E-01	5.5652E-01

Transition		Ω_{ij}			Transition		Ω_{ij}		
i	j	100 Ryd	200Ryd	50 Ryd	i	j	100 Ryd	200Ryd	50 Ryd
2	14	2.3874E-02	2.5212E-02	2.1199E-02	5	11	9.9841E-02	1.5224E-01	4.8186E-02
2	15	4.8394E-03	5.2674E-03	3.9836E-03	5	12	2.4731E+00	3.5217E+00	1.4394E+00
2	16	3.1237E-02	5.3427E-02	9.9781E-03	5	13	4.3731E-03	4.5156E-03	4.0880E-03
2	17	3.5141E-03	3.5141E-03	3.5141E-03	5	14	1.7177E-03	1.7177E-03	1.7177E-03
2	18	3.5743E-02	3.6857E-02	3.3516E-02	5	15	1.5623E-02	2.1012E-02	1.0425E-02
2	19	3.2955E-03	3.2955E-03	3.2955E-03	5	16	3.0103E-03	3.1197E-03	2.7915E-03
2	20	1.7508E-02	1.7508E-02	1.7508E-02	5	17	1.2004E-01	1.2494E-01	1.1026E-01
2	21	2.4460E-03	2.4460E-03	2.4460E-03	5	18	1.6443E-02	2.3889E-02	8.4248E-03
3	4	5.6727E-01	6.5752E-01	4.7595E-01	5	19	3.8885E-01	5.3818E-01	2.2808E-01
3	5	5.5365E+00	6.3509E+00	4.7123E+00	5	20	5.5029E-03	6.8143E-03	2.8811E-03
3	6	8.0012E-02	1.2490E-01	4.1203E-02	5	21	8.6601E-02	1.0301E-01	5.3806E-02
3	7	2.4282E-02	2.6678E-02	1.9491E-02	6	7	8.9341E+00	9.9339E+00	7.9287E+00
3	8	3.8759E-01	4.1632E-01	3.3016E-01	6	8	1.7516E+01	1.9524E+01	1.5496E+01
3	9	1.8991E-02	3.7388E-02	2.9768E-03	6	9	6.1432E-01	6.1591E-01	6.1115E-01
3	10	2.0219E-01	3.6631E-01	5.9488E-02	6	10	9.2261E-01	9.2502E-01	9.1780E-01
3	11	3.5458E-02	3.9668E-02	2.7043E-02	6	11	1.1411E-01	1.1411E-01	1.1411E-01
3	12	2.9282E-01	3.1829E-01	2.4188E-01	6	12	1.5229E-01	1.5229E-01	1.5229E-01
6	13	3.4365E-01	3.5802E-01	3.1489E-01	10	11	1.6240E+00	1.7858E+00	1.4615E+00
6	14	1.0195E-01	1.5137E-01	6.0223E-02	10	12	3.3859E+01	3.7099E+01	3.0605E+01
6	15	1.8858E-01	2.7920E-01	1.1283E-01	10	13	1.5179E-01	1.5586E-01	1.4367E-01
6	16	6.8798E-02	7.4754E-02	5.6885E-02	10	14	3.5123E-02	3.5123E-02	3.5123E-02
6	17	1.0230E-01	1.1118E-01	8.4535E-02	10	15	6.6837E-01	9.2241E-01	4.3021E-01
6	18	6.6850E-02	6.6850E-02	6.6850E-02	10	16	4.1944E-02	4.3623E-02	3.8588E-02
6	19	8.9004E-02	8.9004E-02	8.9004E-02	10	17	2.0098E+00	2.0844E+00	1.8607E+00
6	20	7.1645E-02	7.1645E-02	7.1645E-02	10	18	1.8180E-01	2.6911E-01	9.7786E-02
6	21	8.9565E-02	8.9565E-02	8.9565E-02	10	19	4.3313E+00	6.0749E+00	2.6537E+00
7	8	6.5372E-01	6.5374E-01	6.5368E-01	10	20	1.2607E-01	1.3068E-01	1.1687E-01
7	9	1.5560E+01	1.7490E+01	1.3620E+01	10	21	1.8851E+00	1.9427E+00	1.7699E+00
7	10	1.6865E-01	1.6865E-01	1.6865E-01	11	12	9.7925E-02	9.7925E-02	9.7925E-02
7	11	6.0825E-01	6.0923E-01	6.0628E-01	11	13	1.6480E-02	1.6480E-02	1.6480E-02
7	12	4.7110E-02	4.7110E-02	4.7110E-02	11	14	4.7822E-02	4.8996E-02	4.5474E-02
7	13	2.1530E-01	3.0255E-01	1.3471E-01	11	15	2.0574E-02	2.0903E-02	1.9917E-02
7	14	3.7647E-01	3.9031E-01	3.4881E-01	11	16	1.9521E-01	2.4360E-01	1.5187E-01
7	15	7.9425E-02	8.3752E-02	7.0773E-02	11	17	1.4468E-02	1.7864E-02	1.1430E-02
7	16	3.5354E-01	5.2489E-01	2.0169E-01	11	18	1.6792E+00	1.7269E+00	1.5837E+00
7	17	3.4690E-02	3.4690E-02	3.4690E-02	11	19	1.4627E-02	1.5341E-02	1.3200E-02
7	18	3.5551E-01	3.7470E-01	3.1713E-01	11	20	1.6683E+01	1.8893E+01	1.2907E+01
7	19	3.1518E-02	3.1518E-02	3.1518E-02	11	21	2.4039E-02	2.4039E-02	2.4039E-02
7	20	2.4662E-01	2.4662E-01	2.4662E-01	12	13	2.2020E-02	2.2020E-02	2.2020E-02
7	21	3.6095E-02	3.6095E-02	3.6095E-02	12	14	8.4023E-03	8.4023E-03	8.4023E-03
7	9	2.8467E+00	3.2334E+00	2.4579E+00	12	15	7.9469E-02	8.1444E-02	7.5521E-02
7	10	2.7383E+01	3.0868E+01	2.3878E+01	12	16	9.7533E-03	9.7533E-03	9.7533E-03
7	11	1.2240E-01	1.2266E-01	1.2188E-01	12	17	2.4961E-01	3.1797E-01	1.8844E-01
7	12	8.6957E-01	8.7114E-01	8.6644E-01	12	18	1.4693E-02	1.5408E-02	1.3264E-02
7	13	4.6664E-01	6.5384E-01	2.9302E-01	12	19	2.2595E+00	2.3240E+00	2.1306E+00
7	14	8.6807E-02	9.1354E-02	7.7716E-02	12	20	5.5817E-01	6.4006E-01	4.1821E-01
7	15	1.2707E+00	1.3252E+00	1.1618E+00	12	21	2.1616E+01	2.4484E+01	1.6716E+01
7	16	7.8011E-02	1.1491E-01	4.5127E-02	13	14	2.5130E+01	2.7755E+01	2.2495E+01
7	17	6.0898E-01	9.3686E-01	3.1705E-01	13	15	4.9287E+01	5.4549E+01	4.4003E+01
7	18	7.3884E-02	7.9445E-02	6.2765E-02	13	16	1.6867E+00	1.6894E+00	1.6813E+00
7	19	5.2028E-01	5.5364E-01	4.5358E-01	13	17	2.5315E+00	2.5356E+00	2.5234E+00
7	20	4.4061E-02	4.4061E-02	4.4061E-02	13	18	4.0262E-01	4.0262E-01	4.0262E-01
7	21	3.0109E-01	3.0109E-01	3.0109E-01	13	19	5.3714E-01	5.3714E-01	5.3714E-01
9	10	1.7309E-01	1.7309E-01	1.7309E-01	13	20	8.7210E-02	8.7210E-02	8.7210E-02
9	11	2.3656E+01	2.5923E+01	2.1378E+01	13	21	1.0908E-01	1.0908E-01	1.0908E-01
9	12	2.8953E-02	2.8953E-02	2.8953E-02	14	15	1.7426E+00	1.7426E+00	1.7426E+00
9	13	1.0035E-01	1.0305E-01	9.4955E-02	14	16	4.6540E+01	5.1834E+01	4.1225E+01
9	14	4.1109E-01	5.5915E-01	2.7195E-01	14	17	4.6863E-01	4.6863E-01	4.6863E-01
9	15	9.3178E-02	1.2103E-01	6.7086E-02	14	18	2.1773E+00	2.1795E+00	2.1728E+00
9	16	1.4073E+00	1.4551E+00	1.3119E+00	14	19	1.6478E-01	1.6478E-01	1.6478E-01
9	17	4.1502E-02	4.3167E-02	3.8174E-02	14	20	2.6006E-01	2.6006E-01	2.6006E-01
9	18	3.0390E+00	4.2527E+00	1.8714E+00	14	21	4.3425E-02	4.3425E-02	4.3425E-02
9	19	2.1992E-02	2.1992E-02	2.1992E-02	15	16	8.6010E+00	9.6628E+00	7.5352E+00
9	20	1.3547E+00	1.3962E+00	1.2718E+00	15	17	8.2121E+01	9.1686E+01	7.2520E+01
9	21	1.4139E-02	1.4139E-02	1.4139E-02	15	18	4.3008E-01	4.3068E-01	4.2890E-01

Transition		Ω_{ij}			Transition		Ω_{ij}		
i	j	100 Ryd	200Ryd	50 Ryd	i	j	100 Ryd	200Ryd	50 Ryd
15	19	3.1094E+00	3.1130E+00	3.1023E+00	17	19	1.2526E+02	1.3665E+02	1.1383E+02
15	20	6.1587E-02	6.1587E-02	6.1587E-02	17	20	1.3278E-01	1.3280E-01	1.3274E-01
15	21	3.2894E-01	3.2894E-01	3.2894E-01	17	21	1.9697E+00	1.9699E+00	1.9692E+00
16	17	4.9637E-01	4.9637E-01	4.9637E-01	18	19	3.0825E-01	3.0825E-01	3.0825E-01
16	18	8.7467E+01	9.5438E+01	7.9466E+01	18	20	1.0573E+02	1.1199E+02	9.9446E+01
16	19	1.0163E-01	1.0163E-01	1.0163E-01	18	21	4.5098E-02	4.5098E-02	4.5098E-02
16	20	1.4488E+00	1.4490E+00	1.4485E+00	19	20	4.1329E+00	4.3647E+00	3.9004E+00
16	21	2.4630E-02	2.4630E-02	2.4630E-02	19	21	1.4652E+02	1.5464E+02	1.3838E+02
17	18	6.0313E+00	6.6003E+00	5.4602E+00	20	21	1.7566E-01	1.7566E-01	1.7566E-01

The present results are compared with those of Cornille et al (1997) [8] which used the distorted wave (DW) code of Eissner and Seaton (1972) for the scattering process and the generation of collision strengths, and with Aggarwal et al (2006, 2008) [11]-[13] where they employed the DARC program of Norrington and GRANT (2006) [18].

To have a quantitative understanding for the comparison, Figures 1, 2 and 3 shows the collision strengths of the three transition lines namely: $2p^6 3s\ ^2S_{1/2}$ -$2p^6 3p\ ^2P_{1/2}$, $2p^6 3s\ ^2S_{1/2}$ -$2p^6 3p\ ^2P_{3/2}$ and $2p^6 3p\ ^2P_{1/2}$ -$2p^6 3d\ ^2D_{3/2}$, which are dipole allowed transitions.

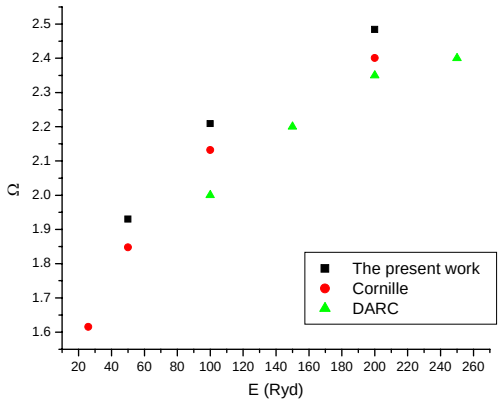

Fig. 1. Comparison of collision strengths for the transition: $2p^6 3s\ ^2S_{1/2}$ -$2p^6 3p\ ^2P_{1/2}$

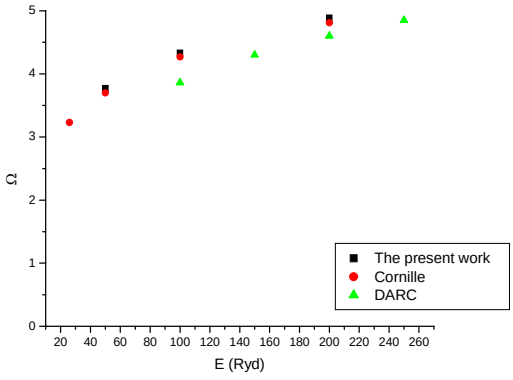

Fig. 2. Comparison of collision strengths for the transition: $2p^6 3s\ ^2S_{1/2}$ -$2p^6 3p\ ^2P_{3/2}$

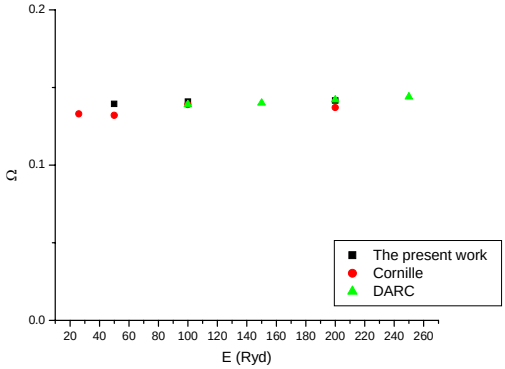

Fig. 3. Comparison of collision strengths for the transition: $2p^6 3p\ ^2P_{1/2}$ -$2p^6 3d\ ^2D_{3/2}$

It is clear from Figures 1, 2 and 3 that there is an agreement between the different calculations and they all present the same trends, the discrepancy is up to 3.8 % with Aggarwal et al. and 4.1% with Cornille et al. The values of the collision strengths Ω for any of these calculations can be safely used for the determination of the excitation rates for these transitions.

Similar comparisons for other transitions are presented in Figures 4, 5 and 6 where the present calculations have been compared for the three dipole forbidden transitions namely: $2p^6 3s\ ^2S_{1/2}$ - $2p^6 3d\ ^2D_{3/2}$, $2p^6 3s\ ^2S_{1/2}$ - $2p^6 3d\ ^2D_{5/2}$, $2p^6 3p\ ^2P_{1/2}$ - $2p^6 3p\ ^2P_{3/2}$, with those of Cornille et al. and Aggarwal et al.

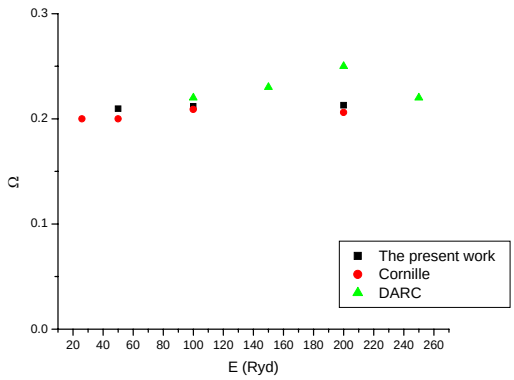

Fig. 4. Comparison of collision strengths for the transition: $2p^6 3s\ ^2S_{1/2}$ - $2p^6 3d\ ^2D_{3/2}$

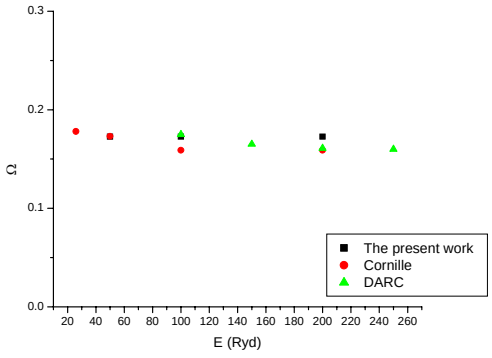

Fig. 5. Comparison of collision strengths for the transition: $2p^6 3s\ ^2S_{1/2} - 2p^6 3d\ ^2D_{5/2}$

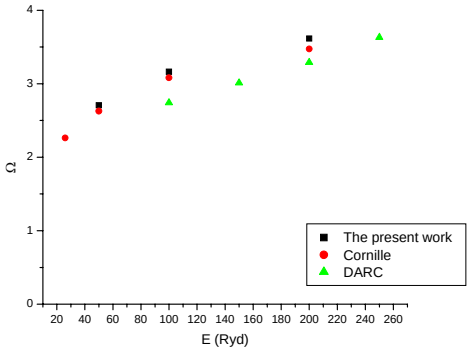

Fig. 6. Comparison of collision strengths for the transition: $2p^6 3p\ ^2P_{1/2} - 2p^6 3p\ ^2P_{3/2}$

It is clear from the Figures that there is an agreement between the different calculations the discrepancy is up to 1.9 % with Aggarwal et al. and 8.6 % with Cornille et al. Since there is no selection rules in the electron – atom collision through the dipole forbidden transitions, thus the collision strength for the allowed transition, Figures 1, 2 and 3 are one order of magnitude larger than that of the forbidden transitions Figures 4, 5 and 6. Figures 7, 8 and 9 present the dipole forbidden transitions namely: $2p^6 4s\ ^2S_{1/2} - 2p^6 5d\ ^2D_{3/2}$, $2p^6 4s\ ^2S_{1/2} - 2p^6 5d\ ^2D_{5/2}$, $2p^6 4p\ ^2P_{1/2} - 2p^6 5p\ ^2P_{3/2}$.

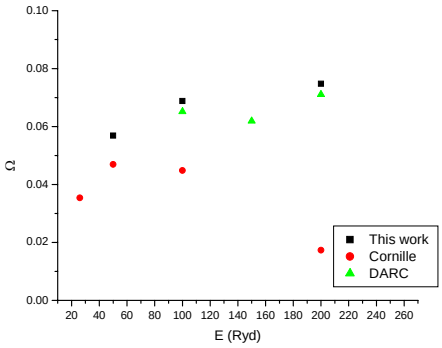

Fig. 7. Comparison of collision strengths for the transition: $2p^6 4s\ ^2S_{1/2} - 2p^6 5d\ ^2D_{3/2}$

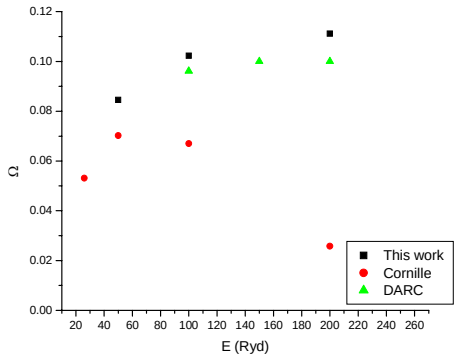

Fig. 8. Comparison of collision strengths for the transition: $2p^6 4s\ ^2S_{1/2} - 2p^6 5d\ ^2D_{5/2}$

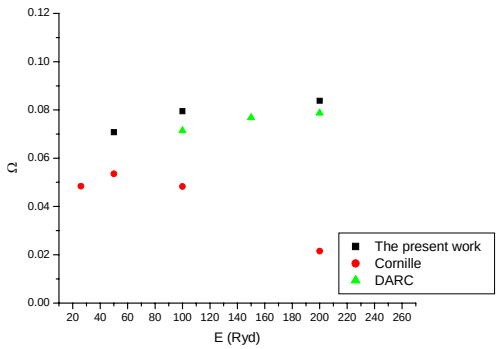

Fig. 9. Comparison of collision strengths for the transition: $2p^6 4p\ ^2P_{1/2} - 2p^6 5p^2P_{3/2}$

As it is clear from the figures, the present data are in good agreement with DARC values but a large discrepancy up to a factor of four exists with the values of Cornille et al., the differences with the values of Cornille et al could be attributed to the inclusion of a limited range of partial waves in their DW calculations as mentioned by Aggarwal et al.[11]-[13].

The present calculations of the electron impact excitation collision strengths based on the plane wave born cross sections give reliable results especially for high impact energies. The present calculated values agree with those of the more sophisticated existing calculations (Aggarwal et. al.) within 1% up to 15% for most of the transitions.

IV. Conclusion

The primary goal of this paper is to compute systematically reliable ab-initio electron impact excitation cross-sections and collision strengths for astrophysical applications and for plasma modeling. Therefore, the MCDFGME code used for performing the calculations add a different reliable procedure to the existing ones to compute the electron excitation cross-sections and collision strengths. In the present work, the results for energy levels, collision strengths for

transitions among the 21 lowest levels of Fe XVI have been presented for all transitions at 50, 100, 200 Rydbergs. The present calculations have been performed in the plane wave Born approximation and relativistic effects have been included in the generation of the wave functions. The MCDFGME code has been used in performing the calculations.

References

[1] J.-S. Wang, H. R.Griem, R. Hess and W. L. Rowan, Measurement of ionization and recombination rates for FeXVI–Fe XXII from time-resolved spectroscopy of tokamak plasmas, *Phys. Rev*. A 38 (1988) 4761-4765.

[2] G. D. Sandlin, j.-D. F. Bartoe, R.Tousey and M. E.Van Hoosier, The high- resolution solar spectrum, 1175-1710 A, *Astrophys. J. Suppl*. 61 (1986) 801-898.

[3] L. W. Acton, M. E. Bruner, W. A. Brown, B. C. Fawcett, W. Schweizer and R.J. Speer, Rocket spectrogram of a solar flare in the 10-100 A region, *APJ*, 291(1985) 865-878.

[4] R. J. Thomas, W. M. Neupert, Ultraviolet spectrum of a solar active region from SERTS, *APJS*, 91 (1994) 461-482.

[5] F. P. Keenan, A. C. Katsiyannis, J. W. Brosius, J. M. Davila and R. J. Thomas, Emission lines of Na-like ions in spectra obtained with the solar EUV research telescope and spectrograph (SERTS), *MNRAS*, 342 (2003) 513-518.

[6] S. S. Tayal, Electron collisional excitation strengths for Fe XVI, *APJ*, 426 (1994) 449-453.

[7] W. Eissner, M. E. Galavs, C. Mendoza , Zeippen, C. J., Atomic data from the IRON Project. XXXIV. Electron impact excitation of Fe XVI, *A&AS*, 136 (1999) 385-394.

[8] M. Cornille, J. Dubau, H.E. Mason, C. Blancard, W.A. Brown, UV and soft X-ray lines from Fe XVI observed in solar and stellar spectra. A&A, 320 (1997) 333-341.

[9] C. P. Bhalla and K. R. Karim, Theoretical dielectric satellite lines of the neon X resonance line, *Rev. Sci. Instrum*. 57, 2055 (1986).

[10] Eissner, W., Seaton, M. J., Computer programs for the calculation of electron-atom collision cross sections. I. General formulation, *J. Phys. Mol. Phys*., 5 (1972) 2187.

[11] K. M. Aggarwal, F. P. Keenan, Electron impact excitation of Fe XVI: radiative and excitation rates. *A&A*, 450 (2006) 1249-1257.

[12] K. M. Aggarwal, F. P. Keenan, Energy levels and Radiative rates for inner shell transitions of Fe XVI, *A&A*, 463 (2007) 399-404.

[13] K. M. Aggarwal, F. P. Keenan, Effective collision strengths for inner shell transitions of Fe XVI, *J. Phys. B At. Mol. Phys*., 41 (2008) 15701-157010.

[14] Desclaux, J. P., A multiconfiguration relativistic Dirac-Fock program. *Comput. Phys. Commun*., 9 (1975) 31-45.

[15] Indelicato, P., Desclaux, J. P., MCDFGME, a multicofiguration Dirac-Fock and general matrix elements program (release 2005), http://dirac.spectro.jussieu.fr/mcdf(2005).

[16] NIST atomic spectra database: http:// www. nist.gov/asd.

[17] K. G. Dyall, I. P. Grant, C. T. Johnson, F. A. Parpia and E. P. Plummer, GRASP: a general-purpose relativistic atomic structure program, *Computer Phys. Commun*. (1989) 55, 424.

[18] P. H. Norrington and I. P. Grant, The grasp2K relativistic atomic structure package *Comput. Phys. Commun*. 177 (2007) 597-622.

[19] M. F. Gu, Indirect X-Ray Line-Formation Processes in Iron L-Shell Ions, *ApJ*, 582 (2003) 1241-1250.

[20] I. P. Grant and H. M. Quiney, New trends in quantum systems in chemistry and physics, *Adv. At. Mol. Phys*. 23 (1988) 37-86.

[21] P. Indelicato, Projection operators in multiconfiguration Dirac-Fock calculations: Application to the ground state of heliumlike ions, *Phys. Rev*. A 51 (1995) 1132-1145.

[22] Y.-K. Kim and K.-T. Cheng, Fubini Sum Rule and Analyticity in Angular Momentum Plane,*Phys. Rev*. A 18 (1978) 36-39.

[23] Y.-K. Kim and M. Inokuti, Total Cross Sections for Inelastic Scattering of Charged Particles by Atoms and Molecules. V. Evaluation to the Next Order beyond the Bethe Asymptote, *Phys. Rev*. A 3 (1971) 665-678.

Authors' information

Department of Physics, Faculty of Science, Cairo University, Egypt
E-mail: Amal1_ibrahim1@yahoo.com

Praise Worthy Prize

International Review of Physics (I.R.E.PHY.), Vol. 5, N. 6
December 2011

Structure and Properties of $YBa_2Cu_3O_{7-\delta}$ Superconductor Doped with MnO and NiO

M. Kavosh, M. Arefian

Abstract – *In this paper, the $YBa_2Cu_3O_7$ superconductor is prepared by using the solid state method and the effect of doping bulk MnO and NiO on the structure, lattice parameter and oxygen coefficient changing. The results show that these doping doses make a phase transition from orthorhombic to tetragonal in MnO. But in NiO the composition remains orthorhombic in all ranges of doping, not affect so much on the structure and lattice parameters. The electrical resistance of samples increased with doping.*

Keywords*: Superconductor, Structure, Substitutions, Critical Temperature*

I. Introduction

The importance of substitution issue in superconductors is so important that many of superconductor compositions of copper oxide are the outcomes of studies and surveys on substitution of different elements in this group of substances. Doping of some substances such as medium metals of zinc and cobalt in $YBa_2Cu_3O_{7-\lambda}$ instead of copper makes some changing on substance structure and transition temperature. In this paper, by using different amounts of zinc oxide instead of copper, we survey changing due to it. In this research we dope (*M=Ni, Mn*) by *x* equals to 0, 0.1, 0.2, 0.3 by $YBa_2Cu_3O_{7-\lambda}$ and also study that substitution of M for Cu makes what effect on lattice constant structure and critical temperature [1], [2].

II. Description of Experiment and Conclusions

In order to structuring these samples we used solid state method. In this method, in order to providing substances with general formula of $YBa_2Cu_{3-x}Ni_xO_{7-\lambda}$ from CuO, Y_2O_3, BaO_2 and NiO and in order to providing $YBa_2Cu_{3-x}Mn_xO_{7-\lambda}$ from CuO, Y_2O_3, BaO_2 and MnO. [3]These substances with appropriate stocumetry were mixed together and then were milled. The resultant powder by helping of cylindrical steel frame and hydraulic smashing converted to pellet.

Then samples by the rate of 3°C/min were raised in the forge to achieve to 930°C and it have been maintaining in that temperature for 24 h, then by the rate of 0.1° C/min and stilly decreases and thus, it allows oxygen absorption to products After the end of structuring gangue step the experiment of meissner effect carried out in liquid nitrogen temperature on samples, none of the samples show this effect, that it represent that this substitutions has lowered transition temperature severely. [4] By using radiation diffraction diagrams of *x* samples, standard card and computer software, lattice constants and extensive biont volume were attained according to Table I and II [5], [6].

TABLE I
LATTICE PARAMETERS AND UNIVALENT CELL VOLUME OF $YBa_2Cu_{3-x}Mn_xO_y$ COMPOSITIONS

Impurity Mn	Parameter a ^{0} A	Parameter b ^{0} A	parameter c ^{0} A	univalent cell $^{0\,3}$ A
X=0/1	3/84	3/86	11/70	173/79
X=0/2	3/85	3/85	11/65	172/61
X=0/3	3/85	3/85	11/55	171/19

TABLE II
LATTICE PARAMETERS AND UNIVALENT CELL VOLUME OF $YBa_2Cu_{3-x}Ni_xO_y$ COMPOSITIONS

Impurity *Ni*	Parameter a ^{0} A	Parameter b ^{0} A	Parameter c ^{0} A	Univalent cell $^{0\,3}$ A
X=0/1	3/80	3/85	11/65	171/33
X=0/2	3/82	3/847	11/642	171/08
X=0/3	3/83	3/84	11/60	170/60

In according to above tables, lattice parameters and biont cell volume changing unto increasing of doping percent has been drawn. In according to lattice parameters and drawen diagrams we understood that in duped samples with *Mn*, by *x* increasing structural changing from ourtorombic to tetragonal has been done. But in samples containing *Ni*, occurs no structural changing and compositions containing *Ni* remained in all the ranges of ourtorombic, meanwhile *x* includes special range that is called dissolution limit. This limit for *Ni* places between 0 and 0.3 [7].

Manuscript received and revised November 2011, accepted December 2011

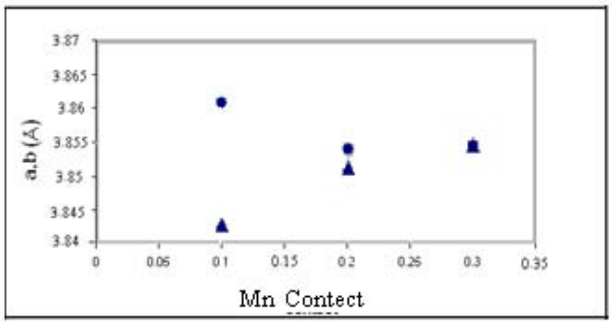

Fig. 1. Changing of lattice parameters of (a) and (b) unto changing of Mn coefficient in $YBa_2Cu_{3-x}Mn_xO_y$ compositions

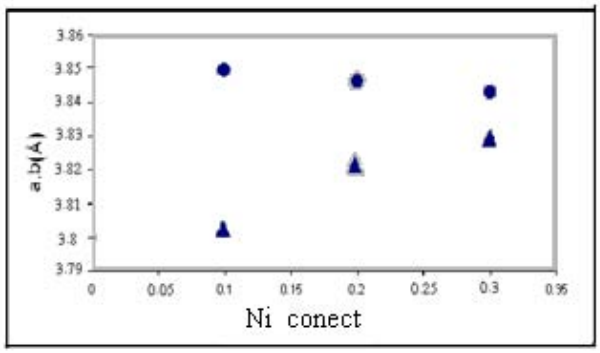

Fig. 2. Changing of lattice parameters of (a) and (b) unto changing of Zn coefficient in $YBa_2Cu_{3-x}Ni_xO_y$ compositions

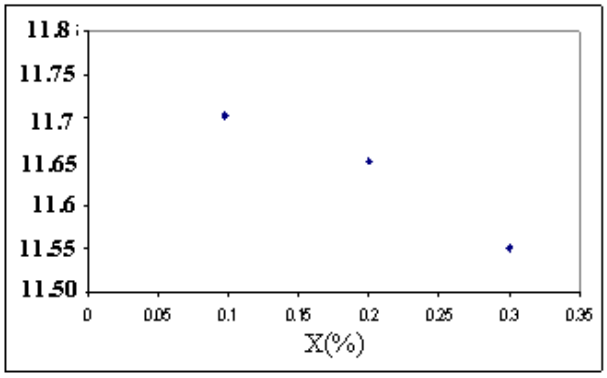

Fig. 3. Changing of lattice parameter (c) interchanging *f Mn* coefficient in $YBa_2Cu_{3-x}Mn_xO_y$

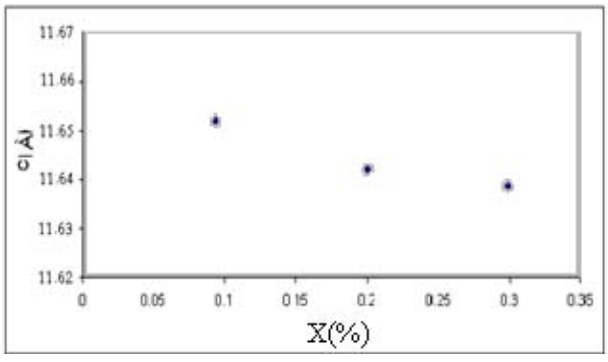

Fig. 4. Changing of lattice parameter (c) unto changing *f Ni* coefficient in $YBa_2Cu_{3-x}Ni_xO_y$

Changing of parameter (*c*) in above figures show similar manner for *Ni* and *Mn*, so that by increasing x, parameter (*c*) decreases.

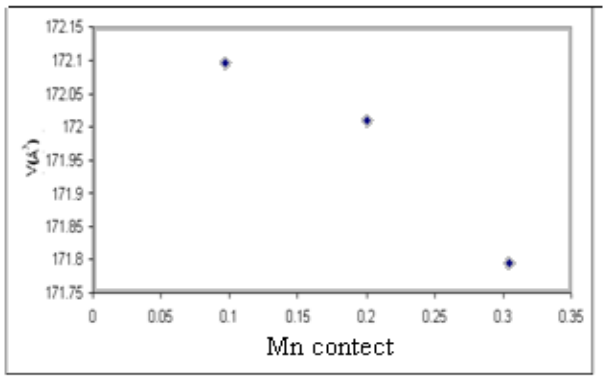

Fig. 5. Changing of univalent cell volume unto changing of Mn coefficient, $YBa_2Cu_{3-x}Mn_xO_y$

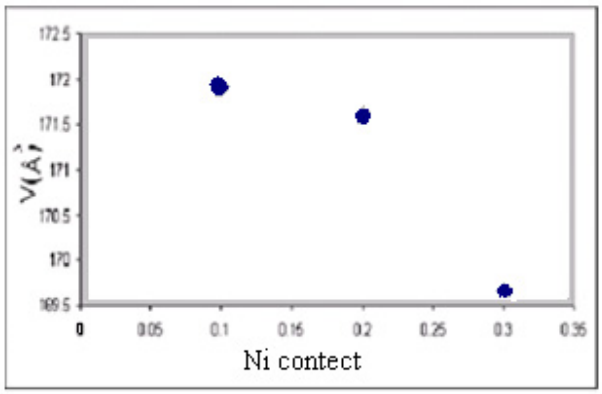

Fig. 6. Changing of univalent cell volume unto changing of *Ni* coefficient

In according to Figures 5 to 6 it can be said that samples containing *Ni* and *MN* represent expectable changing, because ionic radius of copper is more than Ni and Mn ,volume in compositions containing *Ni* and *Mn* by *x* increasing have to be reduced, since replaces by a similar ion. After the end of gangue structuring step, experiment of meisser on the samples carried out in the liquid nitrogen temperature. The samples show this effect only in *x*=0.1. But in the other substitutions do not show this effect. In order to measuring critical temperature, in 4 places, wire was curled around the bars and in order to make better connection silver glue was used. By using standard method, 4 TC bars wee measured as it was expected substitution of copper has complicated effect on superconductor properties and critical temperature and causes severe decreasing of TC. Finally oxygen coefficient of samples or duped as one of the most important determining parameters of superconductor properties was determined by iodometric titration method.In according to Table III, changing of lattice parameters (a) and (b) unto changing of oxygen coefficient was drawen [8].

TABLE III
MEASURING OXYGEN COEFFICIENTS OF SAMPLES BY IODOMETRIC TITRATION METHOD

Measured sample	Oxygencofficient	Percent being ourtormbic
Pure sample Y	6/9	0/77
doped sample with 0/1 Ni	6/89	0/65
doped sample with 0/2 Ni	6/87	0/35
doped sample with 0/3 Ni	6/75	0/17
doped sample with 0/1 Mn	6/93	0/25
doped sample with 0/2 Mn	6/91	0
doped sample with 0/3 Mn	6/81	0

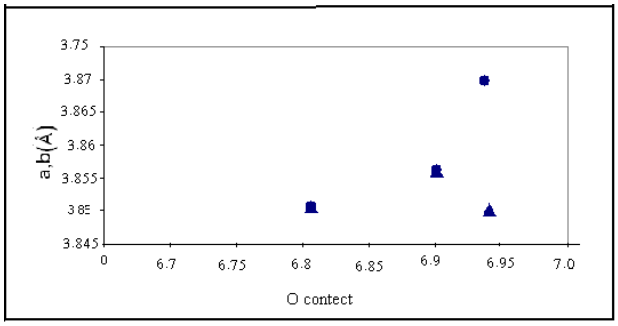

Fig. 7. Changing of lattice parameters a(▲) and b(●) unto changing oxygen coefficients in $YBa_2Cu_{3-x}Mn_xO_y$

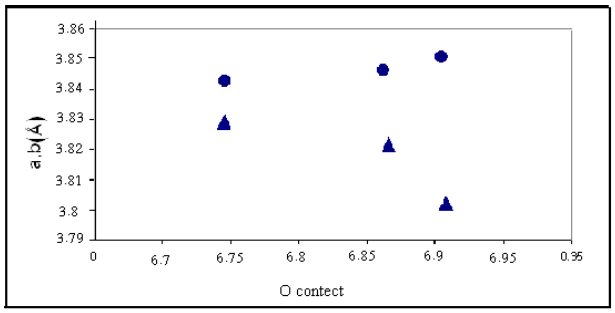

Fig. 8. Changing of lattice parameters a(▲) and b(●) unto changing oxygen coefficients in $YBa_2Cu_{3-x}Ni_xO_y$

In the case of *NI* ,yet it is not completely significant that which of the Cu(1) and Cu(2) places are preferable .of course , with due attention to lack of structured transition temperature probably *Ni* ions substitute in the Cu(2) place [9], [10].

III. Conclusion

In this paper, $YBa_2Cu_3O_{7-\delta}$ superconductor where *M=Ni*, Mn and was structured by contents equal to 0, 0.1, 0.2, 0.3.the resultant conclusion of duping effect of NiO, *MnO* on structure, lattice constant critical temperature and oxygen coefficient amounts have been surveyed . Study on changing of parameters (*a*) and (*b*) unto doping for *NiO* showed that $YBa_2Cu_{3-x}Ni_xO_y$ composition remained in all the ranges of ourtorombic duping and its biont cell volume and parameter (*c*) decreases. oxygen coefficient amounts also are compatible to lattice parameter diagrams of (*a*) and (*b*). in duping *MnO*, by increasing of *x*, transition phase has been done from ourtorombic to tetragonal and biont cell volume and also parameter (*c*) decreas.

References

[1] B. Raveau, et al,, *Crystal* chemistry of high-T_c superconducting oxides, *Springer Series in Materials Science (Springer, Berlin, 1991).*
[2] K. S. Hass, *Solid state physics, 42(Academic press, New York, (1989).*
[3] E. Dagatto, *Rev. Mod.Phys.(1994*).
[4] M . Murakami, Supercond.Sci. Tecol.(1992).
[5] F. S. Galasso, *Structure and preparation of perovskite type Compounds (pergamon, N. Y., 1969*).
[6] B. Raveau, C. Michel, M. Herview and D. Groult, *Crystal chemistry of high-T_c superconducting oxides, Springer* Series in Materials Science (1991).
[7] V. Daadmeher, et al, *Mod. Phys. Lett.B 16 (2002*).
[8] J. M. Tarascon, et al, *Phys. Rev.(1988).*
[9] A . Manthiram, et al, *Soc.109, 6667(1987).*
[10] J . d .Jorgensen, et al, *Phys. Rev. B 36, 3608(1987).*

Authors' information

Department of Physics, Masjed Soleyman Branch, Islamic Azad University, Masjed Soleyman, Iran.

Mehrdad Kavosh now is a faculty member in department of Physics in Masjed Soleyman Brnach, Islamic Azad University, Masjed Soleyman, Iran as a lecturer and researcher.

Praise Worthy Prize

International Review of Physics (I.R.E.PHY.), Vol. 5, N. 6
December 2011

Scrutiny of a Particle in Schwarzschild Black Hole and Tunneling Effect

Amir Hassanfiroozi[1], Mohammadreza Maddah[2], Mahdi Massoumin[3]

Abstract – *By solving Klein-Gordon equation in Schwarzschild metric, we can attain some convergent equations in different black hole points. that give us some information about particles in these intervals and also shift of energy level in this particle, inspection of equation of motion and interpretation of black hole potential and also we can calculate coefficient of particle transmission in consequence of quantum tunneling, in this paper we proceed to investigate most of mentioned subjects.* ***Copyright © 2011 Praise Worthy Prize S.r.l. - All rights reserved.***

Keywords*: Schwarzschild Metric, Black Hole, Tunneling, WKB Approximation*

Nomenclature

M	Black hole mass
μ	Particle mass
$r*$	The tortoise radial coordinate
Y_{lm}	Spherical Harmonics

I. Introduction

Black holes are one of the most fascinating parts of theoretical, astrophysical and cosmological physics ever since Einstein's discovery of the theory of general relativity of gravitation. They are very important members of the universe. Because of their huge gravitational force no objects, not even light, can escape from them. There exists a region called "event horizon" beyond which all objects are strongly attracted towards the center of a black hole leaving absolutely no chance for them to crossover the event horizon to the outer region.

The simplest solution of Einstein's equations is the Schwarzschild solution. Its metric describes the deformation of space-time produced be a static object with a spherical symmetry. The idea is that the energy of the particle changes sign as it crosses the horizon, so that a pair created. Just inside or outside the horizon can materialize with zero total energy, after one member of the pair has tunneled to the opposite side. In this method, particles are allowed to follow classically forbidden trajectories, by starting just behind the horizon onward to infinity.

The particles then travel back in time, since the horizon is locally to the future of the external region. Thus the classical one particle action becomes complex and so the tunneling amplitude is governed by the imaginary part of this action for the outgoing particle. However, the action for the ingoing particle must be real. Since classically a particle can fall behind the horizon. This present has the purpose to find mentioned [1].

II. The Equation

A massless particle in a black hole background is described by the Klein-Gordon equation [2]. We write Klein-Gordon equation $\left(\frac{\partial^2}{c^2\partial t^2} - V^2\right) = 0$ in Schwarzschild metric. We can find its function by separation of variables method as follows:

$$\psi_{lm}(t,r,\theta,\phi) = \frac{R_{l\omega}(r)}{r} Y_{lm}(\theta,\phi)\, e^{-i\omega t} \qquad (1)$$

The $R_{l\omega}(r)$ differential equation shown below:

$$\frac{d^2R_{l\omega}}{dr*^2} + \left(\omega^2 - \frac{l(l+1)}{r^2} + \frac{2M}{r^3}\right)\left(1 - \frac{2M}{r}\right)R_{l\omega} = 0 \qquad (2)$$

Regge and Wheleer (RW) [1], [3] proved the vacuum stability of the Schwarzschild black hole, which source is a freely falling test mass m towards black hole of large mass *M*. The RW partialdifferential equation, derived from the Einstein field equations, represents the first order perturbations of the Schwarzschild metric. The tortoise radial coordinate $r*$ defined by:

$$r* = r + 2M\, ln\left|\frac{r}{2M} - 1\right| \qquad (3)$$

Also $Y_{lm}(\theta,\phi)$ is spherical Harmonics and ω is separating constant.

Now, we rewrite this equation on the basis of$r$ and use transformation of below variable:

$$\frac{d^2}{dr*^2} = \frac{dr}{dr*}\frac{d}{dr}\frac{dr}{dr*}\frac{d}{dr} = \\ = \left(\frac{dr}{dr*}\right)^2\frac{d^2}{dr^2} + \frac{d}{dr}\left(\frac{dr}{dr*}\right)\frac{d}{dr}\ , \\ \frac{d^2}{dr*^2} = \left(1 - \frac{2M}{r}\right)^2\frac{d^2}{dr^2} + \frac{2M}{r^2}\frac{d}{dr} \qquad (4)$$

Manuscript received and revised November 2011, accepted December 2011

with the position $r* = r + 2M\ ln|\frac{r}{2M} - 1|$ is finally recast as [4]:

$$\left(1-\frac{2M}{r}\right)^2\frac{d^2R_{l\omega}}{dr^2}+\frac{2M}{r^2}\frac{dR_{l\omega}}{dr}+ \\ +\left(\omega^2-\frac{l(l+1)}{r^2}+\frac{2M}{r^3}\right)\left(1-\frac{2M}{r}\right)R_{l\omega}=0 \quad (5)$$

By using follow change variable:

$$1-\frac{2M}{r}=z \quad (6)$$

$$\frac{d^2}{dr^2}=\left(\frac{dz}{dr}\right)^2\frac{d^2}{dz^2}+\frac{d}{dz}\left(\frac{dz}{dr}\right)\frac{d}{dz}=\left(\frac{4M^2}{r^4}\right)\frac{d^2}{dz^2} \quad (7)$$

$$\frac{d}{dr}=\frac{2M}{r^2}\frac{d}{dz} \quad (8)$$

We replacing in corrected equations:

$$z^2(1-z)^4R''+(1-z)^4R'+ \\ +\left[4M^2w^2-\begin{pmatrix}z(1-z)^2l(l+1)+\\+z(1-z)^3\end{pmatrix}\right]R=0 \quad (9)$$

Now, we engage to investigate asymptotical behavior in 0 and 1 point. Where $z \to 0$ by:

$$z^2R''+R'+\left(4M^2w^2-(1+l(l+1)z)\right)R=0 \quad (10)$$

$$R\sim A\,e^{\frac{z\left(-1-\sqrt{(1}-4\left(-1-l-l^2+4M^2w^2\right)z^2\right)\right)}{2z^2}}+ \\ +B\,e^{\frac{z\left(-1+\sqrt{(1}-4\left(-1-l-l^2+4M^2w^2\right)z^2\right)\right)}{2z^2}} \quad (11)$$

and z tends to 1, by dividing $(1-z)^4$ on total equation, we have second equation (2) it is obtained that:

$$R''+R'+ \\ +\left[\frac{4M^2w^2}{(1-z)^4}-\left(\frac{l(l+1)}{(1-z)^2}+\frac{1}{1-z}\right)\right]R=0 \quad (12)$$

III. Analytical Solution

An analytic solution of the Regge-Wheeler (RW) equation has been found via the Frobenius methodat the regular singularity of the horizon 2*M* (z tends to zero). Let us consider above equation.

We start with define follow constants:

$$A=l\,(l+1) \quad (13)$$

$$B=4\,M^2w^2 \quad (14)$$

$$z^2R''+R'+(B-(1+A)z)R=0 \quad (15)$$

By some calculations that are shown in appendix we achieve to explicit equation as follows:

$$R= \\ =c_0\left[\begin{matrix}1-4\,M^2w^2z+\left(\frac{(1+l\,(l+1))}{2}+\frac{16M^4w^4}{2}\right)z^2+\\-\left(\begin{matrix}\frac{2(1+l\,(l+1))4\,M^2w^2+(2+4\,M^2w^2)}{6}\times\\\times\frac{\left((1+l\,(l+1))+16M^4w^4\right)}{6}\end{matrix}\right)z^3+\cdots\end{matrix}\right] \quad (16)$$

In the second state that z tends to one, equations are given by:

$$R''+R'+\left(\frac{B}{(1-z)^4}-\frac{A}{(1-z)^2}-\frac{1}{1-z}\right)R=0 \quad (17)$$

Hence:

$$R''+R'+\left(\frac{B}{(z-1)^4}-\frac{A}{(z-1)^2}+\frac{1}{z-1}\right)R=0 \quad (18)$$

By some calculations that are shown in appendix we achieve to explicit equation as follows:

$$R=c_5\left[\begin{matrix}\left(\frac{4\,M^2w^2}{l\,(l+1)-6}\right)x^3+x^5+\\+\left(\frac{4}{4\,M^2w^2(l\,(l+1)-6)}\right)x^6+\\+\frac{(l\,(l+1)-20)}{4\,M^2w^2}x^7+\cdots\end{matrix}\right] \quad (19)$$

IV. Equations of Motion in Orbit

We solve problem by supposing such potentials [7]:

$$V(r)=\left(\frac{l(l+1)}{r^2}+\frac{2M}{r^3}\right)\left(1-\frac{2M}{r}\right)= \\ =\frac{l(l+1)}{r^2}+-\frac{2M(l(l+1)-1)}{r^3}-\frac{4M^2}{r^4} \quad (20)$$

Equation of motion in the direction of "*r*" and "*θ*" are as follows:

$$m\,\ddot{r}-m\,r\,\dot{\theta}=F(r) \quad (21)$$

$$m\,r\,\ddot{\theta}+2m\,\dot{r}\dot{\theta}=0 \quad (22)$$

That we have form second equation:

$$\frac{d}{dt}\left(mr^2\dot{\theta}\right)=\frac{dL}{dt}=0 \quad (23)$$

$$L=mr^2\dot{\theta}=0 \quad (24)$$

$$\theta=\theta_0+\int\left(\frac{L}{mr^2}\right)dt \quad (25)$$

But for first equation, by changing below variable, this equation becomes simpler to same extent:

$$u=\frac{1}{r} \quad (26)$$

$$r = \frac{1}{u} \tag{27}$$

$$\frac{d^2u}{d\theta^2} = -u - \frac{m}{L^2u^2} F\left(\frac{1}{u}\right) \tag{28}$$

Now it is adequate to have potential equation and to obtain force for it is first derivative as follows:

$$V(r) = \frac{l(l+1)}{r^2} - \frac{2M(l(l+1)-1)}{r^3} - \frac{4M^2}{r^4} \tag{29}$$

$$a = l(l+1) \tag{30}$$

$$b = 2M(l(l+1)-1) \tag{31}$$

$$c = 4M^2 \tag{32}$$

$$V(r) = \frac{a}{r^2} - \frac{b}{r^3} - \frac{c}{r^4} \tag{33}$$

$$F(r) = \frac{dV}{dr} = \frac{-2a}{r^3} + \frac{3b}{r^4} + \frac{4c}{r^5} \tag{34}$$

$$F\left(\frac{1}{u}\right) = -2a\,u^3 + 3b\,u^4 + 4c\,u^5 \tag{35}$$

$$\frac{d^2u}{d\theta^2} = -u - \frac{m}{L^2u^2}(-2a\,u^3 + 3b\,u^4 + 4c\,u^5) \tag{36}$$

$$\frac{d^2u}{d\theta^2} = -u - \frac{m}{L^2}(-2a\,u + 3b\,u^2 + 4c\,u^3) = \\ = -u\left(1 + \frac{2am}{L^2}\right) - \frac{3bm}{L^2}\mathrm{U}^2 - \frac{4mc}{L^2}u^3 \tag{37}$$

$$\frac{d^2u}{d\theta^2} + u\left(1 + \frac{2am}{L^2}\right) - \frac{3bm}{L^2}u^2 + \frac{4mc}{L^2}u^3 = 0 \tag{38}$$

That contrary to investigate equation in analytical mechanics, it consists of second and third power of u [5].

V. The Equation of a Point Mass in Schwarzschild Black Hole

The metric for such a black hole is of the form:

$$ds^2 = c^2(1+f)dt^2 - (1+h)dr^2 + \\ -r^2d\theta^2 - r^2Sin^2\theta\,d\varphi \tag{39}$$

Other equation becomes:

$$\ddot{t} + \frac{f'}{1+f}\dot{r}\dot{t} = 0 \tag{40}$$

$$\ddot{r} + \frac{c^2}{2}f'(1+f)\dot{t} - \frac{f'}{2(1+f)}\dot{r}^2 + \\ -r(1+f)\left(\dot{\theta}^2 + Sin^2\theta\,\dot{\varphi}^2\right) = 0 \tag{41}$$

$$\ddot{\theta} + \frac{2}{r}\dot{r}\dot{\theta} - Sin\theta Cos\theta\,\dot{\varphi} = 0 \tag{42}$$

$$\ddot{\varphi} + \frac{2}{r}\dot{r}\dot{\varphi} + 2\,Cot\theta\dot{\theta}\dot{\varphi} = 0 \tag{43}$$

We used a variation equation on $\frac{d}{dk}$ coordinate:

$$\dot{t} = \frac{dt}{dk} = \frac{a}{1+f} \tag{44}$$

$$r^2\dot{\varphi}\,Sin^2\theta = b \tag{45}$$

In which a and b are integral constants [6].

VI. Motion in the Planar Orbit

We want to consider the motion in planar orbit in $\theta = \frac{\pi}{2}$. Equation (42) shows that if primary condition is $\theta = \frac{\pi}{2}$ and $\dot{\theta} = 0$ so always we will have $\ddot{\theta} = 0$ and particle continues to orbitmovement in this page and particle stays in the plane $\theta = \frac{\pi}{2}$. Now we write Schwarzschild metric for movement in $\theta = \frac{\pi}{2}$, and we take development of geodesic length of dsas dk path parameters. Hence by choice $dk = ds$, equation (46) becomes equation (47):

$$ds^2 = c^2\left[1 - \frac{2MG}{c^2r}\right]dt^2 - dr^2\left[1 - \frac{2MG}{c^2r}\right]^{-1} + \\ -r^2\left(d\theta^2 + Sin^2\theta\,d\varphi^2\right) \tag{46}$$

$$1 = c^2\left[1 - \frac{2MG}{c^2r}\right]\dot{t}^2 - \frac{\dot{\mathrm{R}}^2}{\left[1 - \frac{2MG}{c^2r}\right]} - r^2\dot{\varphi}^2 \tag{47}$$

By invoking equation (44) in equation (47), remove $\dot{t}$ and use of equation (45) we write:

$$\left(\frac{dr}{ds}\right) = \left(\frac{r^2}{b}\right)\left(\frac{dr}{d\varphi}\right) \tag{48}$$

By using this relation we remove $\dot{r}$ from equation (45):

$$\frac{b^2}{r^4}\left(\frac{dr}{d\varphi}\right)^2 = c^2a^2 - \left(1 - \frac{2MG}{c^2r}\right)\left(1 + \frac{b^2}{r^2}\right) \tag{49}$$

By replace $= \frac{1}{r}$, equation (49) can be written as follows:

$$\left(\frac{dr}{d\varphi}\right)^2 = \frac{c^2a^2}{b^2} - \frac{1}{b^2}\left(1 - \frac{2MG}{c^2}u\right)(1 + b^2u^2) \tag{50}$$

$$\left(\frac{dr}{d\varphi}\right)^2 = \frac{c^2a^2}{b^2} - \left(\frac{1}{b^2} + u^2 - \frac{2MG}{c^2b^2}u - \frac{2MG}{c^2}u^3\right) \tag{51}$$

The above equation can be simplified by deriving on φ:

$$\frac{d^2u}{d\varphi^2}\frac{du}{d\varphi} = -\left(u - \frac{MG}{c^2b^2} - \frac{3MG}{c^2}u^2\right)\frac{du}{d\varphi} \qquad (52)$$

The state of $\frac{du}{d\varphi}$ is related to the solution for a circular orbit. We want consider elliptically orbit.
So $\frac{du}{d\varphi} \neq 0$ and hence we divide above equation on $\frac{du}{d\varphi}$ to attain below relation:

$$\frac{d^2u}{d\varphi^2} + u = \frac{MG}{c^2b^2} + \frac{3MG}{c^2}u^2 \qquad (53)$$

The above equation will be changed to Newton equation for an elliptically orbit without term $\frac{3MG}{c^2}u^2$.

The answer of Newton equation is as follows:

$$u = \frac{MG}{c^2b^2}\left[1 + e\,Cos\left(\varphi - \varphi_0\right)\right] \qquad (54)$$

That is e exit from the center of orbit ($e = \frac{f}{2a}$ and f is the distance between two focuses and a is the half of big diameter length in ellipse). By using this approximation in which u^2 is replacing by disordered solution in right side and we can solve equation (53):

$$\frac{d^2u}{d\varphi^2} + u = \frac{MG}{c^2b^2} + \frac{3M^3G^3}{c^6b^4}\left[1 + e\,Cos\left(\varphi - \varphi_0\right)\right]^2 \qquad (55)$$

An approximate solution for above equation is as follows:

$$u = \frac{MG}{c^2b^2}\left[1 + e\,Cos\left(\varphi - \varphi_0 - \Delta\varphi\right)\right] \qquad (56)$$

Circle if e = 0, ellipse if 0 ≤ e < 1 (as for planets orbiting the Sun). Perihelion (closest approach to Sun) occurs when $\varphi = \varphi_0 + \Delta\varphi$:

$$\Delta\varphi = \left(\frac{2M^2G^2}{c^4b^2}\right)\varphi \qquad (57)$$

And we disregarded from sentences larger than second power of $\frac{MG}{b^2c^2}$, actually we can suppose it the correction.

VII. Potential Form

By finding derivation roots and placing it on second derivative we can find concavity direction:

$$\frac{dV}{dr} = \frac{-2a}{r^3} + \frac{3b}{r^4} + \frac{4c}{r^5} \qquad (58)$$

$$r_1 = -\frac{-3b - \sqrt{9b^2 + 32\,ac}}{4a} \qquad (59)$$

$$r_2 = -\frac{-3b + \sqrt{9b^2 + 32\,ac}}{4a} \qquad (60)$$

$$\frac{d^2V}{dr^2} = \frac{6a}{r^4} - \frac{12b}{r^5} - \frac{20c}{r^6} \qquad (61)$$

By setting $r_1$and r_2 in above equation it is conclude that we have two concaves in two directions.

1. For the first quantum state having $l = 0$, $a = 0$ hence $9b^2 + 32ac = 9b^2$, so for lowest angular momentum, potential curve $V(r)$ decrease towards origin. There is a not minimum radial distances and all orbits pass through origin ($r = -\frac{6b}{0}$) .
2. For follow region :

$$9b^2 + 32\,ac = 1 + \frac{3.5ac}{b^2} \quad , \quad 3.5ac = b^2\,, x = l(l+1) \qquad (62)$$

$$x = l(l+1) < \frac{3.5c - 8m^2 \pm \sqrt{56\,m^2c + \frac{49}{4}c^2}}{8m^2} = Ъ \qquad (63)$$

For this region of angular momentum, always potential $V(r)$ is negative and in similar $r_1$and r_2 by selecting positive and negative sign in their equations have two minimum and maximum. Particles that their E energy are between $V(r_1)$ and $V(r_2)$ are located in closed elliptical orbit.

3. If $x > Ъ$, as is shown in Figure 1, the picture potential curve have $V(r)$ positive maximum.Particles having this angular momentum and positive energy -$E > 0$ – lower than maximum $V(r)$ will not reach to origin.
4. Also particle in r_1 situation is in unstable condition and in situation r_2 it has stable condition.

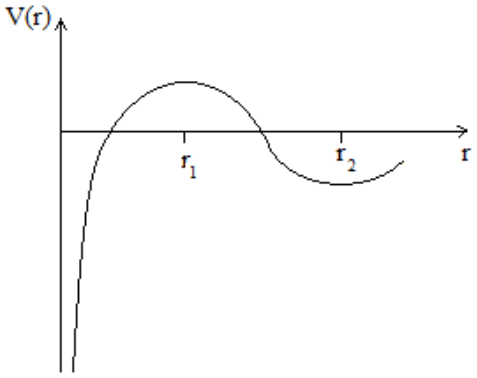

Fig. 1. HypotheticalPotential shape and their extremum

VIII. WKB Approximation

This technique, originally in the form suggested by Schutz and Will, based on elementary quantum mechanical arguments, was later developed into apowerful technique with which accurate results have been derived [8].

We want inspect the transmittance probability of

particle by using WKB approximation, it was given by:

$$|T|^2 \simeq exp\left[-2\int_{r_0}^{r} dr \sqrt{\frac{2\mu}{\hbar^2}(V(r)-E)}\right] \quad (64)$$

By substituting potential equation in above equation, we have:

$$|T|^2 \simeq exp\left[-2\int_{r_0}^{r} dr \sqrt{\frac{2\mu}{\hbar^2}\left(\left(\frac{a}{r^2}-\frac{b}{r^3}\right)\left(1-\frac{2M}{r}\right)+\right)}\right] \quad (65)$$
$$-E$$

$$a = l(l+1), \;\; b = 2M$$

μ is mass of particle in relations.

We can compute above mentioned integral asshown, but weknew, it is not a surprise because, at the present do not guess a general form for WKB. Do you attain to a physical agreement between classical and quantum answers? Yes, according to Heisenberg uncertainty principle, this the relation attained in the field of discussion about wave packet. In quantum mechanics, in a state in which the momentum is certainly p the probability $|< r \mid p >|^2$ of finding the particle at point r is independent of r, the position is then completely uncertain.

Similarly if the position of the particle is certainly at r the probability $|< p \mid r >|^2$ of finding the particle to have momentum p isindependent of p , as so momentum is uncertain. Since quantum functions are none-localized thus deal to probability. But, manner of the wave packet is more controllable and it has set in special a limit that is localized. As that we have carried out in the Klein-Gordon equation answers and we considered them as a series of answers, series as discrete integral pointing to wave packet in relations. Also the relation of the transmission coefficient is the word that is not acceptable with classical model. In the limit relation that the angular momentum is very big (quantum number l is great) this relation equal zero:

$$|T|^2 \simeq \lim_{l\to\infty} exp\left[-\sqrt{\frac{\mu}{2\hbar^2}}[\, f(r)]\right] = \frac{1}{exp[\infty]} = 0 \quad (66)$$

IX. Conclusion

Let us now summarize the findings in the present paper. In this paper we consider the equation related to Klein-Gordon and it is get after separation of variables method. In fact I will reveals for r tends to $2M$ and ∞. Thus, we can consider the motions in these regions, which are useful. Also, by used method wereach to convergent equations that removed some of ambiguities appear in prior equations. In continuance we calculated equations of motion in orbit and finally we reach to a nonlinear equation that is not closed and it has two asymptotic curves. Also, we find equations of motion in planar orbit mentioned equation is an additive correction to constant rate in φ or it is spin motion in Perihelion orbit situation, as we observed it is correct for a planet. It was shown that transmittance coefficient was related the quantum concepts. But, it is most important for Hawking radiation and entropy, absorption and so on. We do not mention them. Hawking has argued that while black holes may be created by classical collapse, their disintegration is a quantum phenomenon. We provided simple expressions for the WKB approximation for tunneling.

Appendix

i. Calculations for Equation

We consider answer as below square series:

$$R = c_0 + c_1 z + c_2 z^2 + \cdots + c_n z^n + \cdots$$

In the state that z tends to zero, equations are given by:

$$R' = c_1 + 2\,c_2 z + 3\,c_3 z^2 + \cdots + n c_n z^{n-1} + \cdots$$
$$R'' = 2\,c_2 + 3*2\;c_3 z + \cdots + n(n-1)c_n z^{n-2} + \cdots$$

By substituting above:

$$\begin{aligned} 2\,c_2 z^2 + 3*2\;c_3 z^3 + \cdots + n(n-1)c_n z^n + \cdots & c_1 \\ + 2\,c_2 z + 3\,c_3 z^2 + \cdots + n c_n z^{n-1} + \cdots & \\ + Bc_0 + Bc_1 z + Bc_2 z^2 + \cdots + Bc_n z^n & \\ + \cdots - (1+A)c_0 z - (1+A)c_1 z^2 & \\ - (1+A)c_2 z^3 - \cdots - (1+A)c_n z^{n+1} & \\ - \cdots = 0 & \end{aligned}$$

$$\begin{aligned} 2\,c_2 z^2 + 3*2\;c_3 z^3 + \cdots + n(n-1)c_n z^n + \cdots & c_1 \\ + 2\,c_2 z + 3\,c_3 z^2 + \cdots + (n & \\ + 1)c_{n+1} z^n + \cdots + Bc_0 + Bc_1 z & \\ + Bc_2 z^2 + \cdots + Bc_n z^n + \cdots & \\ - (1+A)c_0 z - (1+A)c_1 z^2 & \\ - (1+A)c_2 z^3 - \cdots - (1+A)c_{n-1} z^n & \\ - \cdots = 0 & \end{aligned}$$

Coefficient of z^0 : $c_1 = -Bc_0$

Coefficient of z^1 : $c_2 = \frac{(1+A)c_0 - Bc_1}{2}$

Coefficient of z^2 : $c_3 = \frac{(1+A)c_1 - (2+B)c_2}{3}$

Coefficient of z^3 : $c_4 = \frac{(1+A)c_2 - (2*3-B)c_3}{4}$

Coefficient of z^n : $c_{n+1} = \frac{(1+A)C_{n-1} - (n*(n-1)-B)C_n}{n+1}$

Thus:

$$c_{n+1} = \frac{(1+A)C_{n-1} - (n*(n-1)-B)C_n}{n+1}$$

Eventually we achieve to explicit equation, as shown below:

$$R = c_0 + c_1 z + c_2 z^2 + \cdots + c_n z^n + \cdots \quad , \quad z = 1 - \frac{2M}{r}$$

$$R = c_0 \left[1 - Bz + \left(\frac{(1+A) + B^2}{2} \right) z^2 - \left(\frac{2(1+A)B + (2+B)}{6} \times \frac{\left((1+A) + B^2\right)}{6} \right) z^3 + \cdots \right]$$

ii. Calculation for Equation

We defined series:

$$R = \sum c_m x^m$$

We change variable as below:

$$z - 1 = x \quad , \frac{dR}{dz} = \frac{dR}{dx} \quad , \frac{d^2R}{dz^2} = \frac{d^2R}{dx^2}$$

$$R'' + R' + \left(\frac{B}{x^4} - \frac{A}{x^2} + \frac{1}{x} \right) R = 0$$

$$R = c_0 + c_1 x + c_2 x^2 + \cdots + c_m x^m + \cdots$$

$$R'' + R' + (Bx^{-4} - Ax^{-2} + x^{-1}) R = 0$$

$$R' = m \sum c_m x^{m-1} \ ,$$

$$R'' = m\,(m-1) \sum c_m x^{m-2}$$

By substituting above:

$$2\,c_2 + 3 * 2\;c_3 x + \cdots + m(m+1) c_{m+1} x^{m-1} + \cdots c_1 + 2\,c_2 x + 3\,c_3 x^2 + \cdots + m c_m x^{m-1} + \cdots + \frac{c_0 B}{x^4} + \frac{B c_1}{x^3} + \frac{c_2 B}{x^2} + \cdots + B c_{m+3} x^{m-1} + \cdots \frac{-A c_0}{x^2} - \frac{A c_1}{x} - A c_2 - \cdots - A c_{m+1} x^{m-1} - \cdots + \frac{c_0}{x} + c_1 + c_2 x + \cdots + c_m x^{m-1} + \cdots = 0$$

Coefficient of $\frac{1}{x^4}$:

$$c_0 B = 0 \ , B \neq 0 \ , c_0 = 0$$

Coefficient of $\frac{1}{x^3}$:

$$B c_1 = 0, c_1 = 0$$

Coefficient of $\frac{1}{x^2}$:

$$c_2 B - A c_0 = 0, c_2 = 0$$

Coefficient of $\frac{1}{x}$:

$$-A c_0 = c_0, A \neq 0, c_0 = 0$$

Coefficient of x^0:

$$2\,c_2 + c_1 + B c_4 - A c_2 + c_1 = 0, c_4 = 0$$

Coefficient of :

$$3 * 2\;\; c_3 + 2\,c_2 + B c_5 - A c_3 + c_2 = 0 \quad , c_3 = \frac{B c_5}{A - 6}$$

Coefficient of x^2:

$$12 c_4 + 3\,c_3 + B c_6 - A c_4 + c_3 = 0 \ , \qquad c_6 = \frac{4 c_5}{B(A-6)}$$

Coefficient of x^3:

$$20 c_5 + 4 c_4 + B c_7 - A c_5 + c_4 = 0 \ , \ \ c_7 = \frac{(A-20) c_5}{B}$$

$$\sum (m\,(m-1) c_m x^{m-2} + m c_m x^{m-1} + B c_m x^{m-4} - A c_m x^{m-2} + c_m x^{m-1}) = 0$$

$$\sum (m(m+1)\,c_{m+1} + m c_m + B c_{m+3} - A c_{m+1} + c_m x^{m-1}) x^{m-1} = 0$$

$$m(m+1) c_{m+1} + m c_m + B c_{m+3} - A c_{m+1} + c_m = 0$$

Now, we have reversion relation:

$$c_{m+3} = \frac{(m(m+1) - A) c_{m+1} + (m+1) c_m)}{B}$$

We achieve to explicit equation for second equation, as shown below:

$$R = c_0 + c_1 x + c_2 x^2 + \cdots + c_m x^m + \cdots = 0 + 0 + 0 + \left(\frac{B c_5}{A-6} \right) x^3 + 0 + c_5 x^5 + \left(\frac{4 c_5}{B(A-6)} \right) x^6 + \frac{(A-20) c_5}{B} x^7 + \cdots$$

$$R = c_5 [\left(\frac{B}{A-6} \right) x^3 + x^5 + \left(\frac{4}{B(A-6)} \right) x^6 + \frac{(A-20)}{B} x^7 + \cdots]$$

Acknowledgements

The authors are grateful to Dr. Hossein Ghafarnejhad for the suggestions and discussions on this issue. Also this research was supported by a grant of University of Semnanand brilliant talent office in this University, Semnan, Iran.

Reference

[1] Regge T. and Wheeler J.A., 1957. *Phys. Rev*., 108, 1063.
[2] Asymptotic completeness for the Klein-Gordon equation on the Schwarzschild metric, alien bachelor, http:// www.numdam.org/item?id=AIHPA-1994-61-4-411-0
[3] MathewsJ., *J. Soc. Ind. Appl. Math.*, **10** (1962) 768.
[4] Gravitational lensing by galaxy quantization states. Franklin potter & Howard G.preston, http:// www.arxiv.org /gr-qc/0405025v1
[5] Mechanics, Keith R.Symon, translated by AzamNiroomand Rad and Gholam Hossein Hamedani, published by Sharif University, Tehran,Iran.
[6] Introduction to general relativity, by Atwater. Harry Albert, Oxford Pergamon Press 1974, translated by Seied Kamal AldinSeiedYaghobi and Hossein Fakhri, published by Foorozesh, Tabriz,Iran.
[7] Kostas D. Kokkotas and Bernd Schmidt, "Quasi-Normal Modes of Stars and Black Holes", *Living Rev. Relativity* 2, (1999), 2.
[8] Quantum Mechanics, Stephen gasiorowicz, third edition,

translated by Dr.Hooshang Sepehri and Iraj Jalal Pour, published by Noor Pardazan, Tehran, Iran.

Authors' information

Amir Hassanfiroozi received B.S degree in Solid State Physics and the M.S degree in Photonic-Communication from University of Semnan, Iran, in 2009 and 2011, respectively; he is currently working toward the Ph.D. Program. His current research focuses on Optoelectronics applicationsand medical diagnosis using microscopy techniques.

Mohammadreza Maddah received B.Sc. degree in applied physics on Solid State and dual M.Sc. in Gravitation Physics and Photonics-Communication from University of Tehran and University of Semnan, Iran, respectively, in 2011. His current research focused on Image Processing in biomedical applications.

Mahdi Massoumin received B.S degree in Nuclear Physics, Mashhad, Iran in 2005 to 2009 and the M.S degree in Photonic-Communication from University of Semnan, Iran, in 2009 and 2011, respectively; he is currently working toward the Ph.D. Program. His current research focuses on Antenna design and Photonics Crystal applications.

Praise Worthy Prize

International Review of Physics (I.R.E.PHY.), Vol. 5, N. 6
December 2011

Modeling of Damage in the Behavior of Fiber-Matrix Interface of a Composite Material with a Genetic Algorithm

Allel Mokaddem, Ahmed Boutaous

Abstract – *The objective of this work is to develop an analytical model to evaluate the influence of thermal stress on the damage of the fiber-matrix interface composite material T300/914; from the properties of the fiber, matrix and interfacial bonding characteristics. The model takes into account the effects of temperature that result in the gradual deterioration of the fiber-matrix interface. This study developed a genetic algorithm has shown the influence of heat stress beyond a critical threshold of damage to the interface, and also showed that the gradual deterioration of the matrix has a greater influence on the damage of the interface compared to that of the fiber.*

Keywords*: Composite, Interface, Fiber, Matrix, Shear, Thermal Stress, Damage*

I. Introduction

The number and complexity of the mechanical tests required for the development of an industrial project related to the verification of the mechanical properties of materials used to obtain reliable results by numerical simulation. Indeed, the objective of this contribution is to highlight the evolution of the influence of thermal stress on the damage of the fiber matrix interface of a composite (T300/914) by genetic algorithm. In a composite material, damage to the matrix and the fibers break the following characteristics Lissart [3]:

- Cracks in the matrix generated by unidirectional tensile stresses are distributed in a completely random, according to the distribution of microstructural defects;
- During the rupture of a fiber within the yarn, the stress borne by the broken fiber is distributed equally on all surviving fibers;
- The ruin of the composite is reached for a critical rate of broken fibers.

In this work, we developed an analytical model using a genetic algorithm. The static model described below, shows the gradual degradation of the matrix and fiber damage to the fiber-matrix interface is based on the Cox [1].

II. Development

II.1. Definitions

Damage to the matrix, when the stress is uniform, is given by formula (1) Weibull [4]:

$$D_m = 1 - exp\left\{-V_m\left[\frac{\sigma + \sigma_m^T}{\sigma_{0m}}\right]^{m_m}\right\} \qquad (1)$$

with:

- (σ): applied stress;
- $\left(\sigma_m^T\right)$: heat stress;
- (V_m): the volume of the matrix;
- $\left(m_m et \sigma_{0m}\right)$: Weibull parameters.

After creation of a crack, a fragment of length L will give rise to two fragments of size $L = L_1$ and $L_2 = X \cdot L \cdot (1\text{-}X)$ (X being a random number between 0 and 1). At each crack up a fiber, a fiber-matrix debonding length 2l will occur with a corollary decrease of creating a new crack in part because the matrix unloaded. At each increment of stress, the break is calculated. All blocks which break reaches 0.5 give rise to new cracks. A broken fiber is discharged along its entire length Lissart [3]. That is to say it cannot break once. The rupture follows a law similar to that described for the matrix:

$$D_f = 1 - exp\left\{-A_f \cdot L_{equi} \cdot \left[\frac{\sigma_{max}^f}{\sigma_{0f}}\right]^{m_f}\right\} \qquad (2)$$

with:

- (σ_{max}^f): The maximum stress applied
- (L^{equi}): is the length of the fibers would have the same break in a consistent manner.

II.2. Interface Behavior

Interfacial shear stress τ reflects the transfer of forces through the fiber-matrix debonding. The corresponding stress field in a composite is depicted in Figure 1. The applied load is fully supported by the fibers at the cracks over a length 2l0 gradient linear constraint exercised in

Manuscript received and revised November 2011, accepted December 2011

adjacent regions of the decohesion length 2*l*.

II.3. Thermal Stresses

The field of thermal stresses resulting from differential expansion of the fiber and matrix during cooling after preparation of the composite at high temperature. It is given by the following equations Lebrun [2]:

$$\sigma_f^T = E_f \frac{a}{1+a}\left(M_2 - M_0\right) \tag{3}$$

$$\begin{aligned} M_0(T) &= \int_{T_0}^{T_e} \left(\alpha_m - \alpha_f\right) dT \\ M_2(T) &= \int_{T_0}^{T} \left(\alpha_m - \alpha_f\right) dT \end{aligned} \tag{4}$$

T_0 room temperature, the temperature T_e of development, T the test temperature and finally α_f α_m and expansion coefficients of the fiber and matrix.

So it would be interesting to see the influence of thermal stress on the damage of the interface based on the Cox [1]:

$$\beta_1^2 = \frac{2G_m}{E_f r_f^2 \, ln\left(\frac{R}{r_f}\right)} \tag{5}$$

$$\tau = \frac{E_f a \varepsilon}{2} \beta_1 th\left(\beta_1 \, l/2\right) \tag{6}$$

with:

- (G_m) : shear modulus of the matrix;
- (E_f) : Young's modulus of the fiber;
- (ε) : déformation ;
- (a) : radius of the fiber;
- (R) : half the distance;
- (τ) : shear stress of the interface.

III. Numerical Simulation by a Genetic Algorithm

III.1. Development

Our job is to maximize the damage of fiber-matrix interface of composite carbon / epoxy (T300/914) by a genetic algorithm using an analytical model based on the theory of Cox.

The principle of this algorithm relies on the use of genetic operators to evolve a population of individuals randomly generated number 100 with a maximum generation equal to 50 as stopping criterion.

The genes of the chromosome represent the following variables: the mechanical stress which is between 0 and defined as the maximum stress tests stress, the temperature varies between T_o = 30°C and the temperature of preparing the epoxy matrix T_e = 150°C, the thermal stress generated is calculated using the formula (3) taking into account the expansion coefficients of carbon fibers and epoxy matrix. Then a selection operator (linearly by dividing the odds by rank individuals in the population, these individuals are ranked and positioned to make the best of them is inserted in the front row and one whose quality is lower in rank or $k = N$). This allows parents to select who will then be crossed via a crossover operator.

The 'children' are modified resulting in a random probability defined at the outset (probMut = 0.5) and thus form a new generation, the process is repeated until convergence.

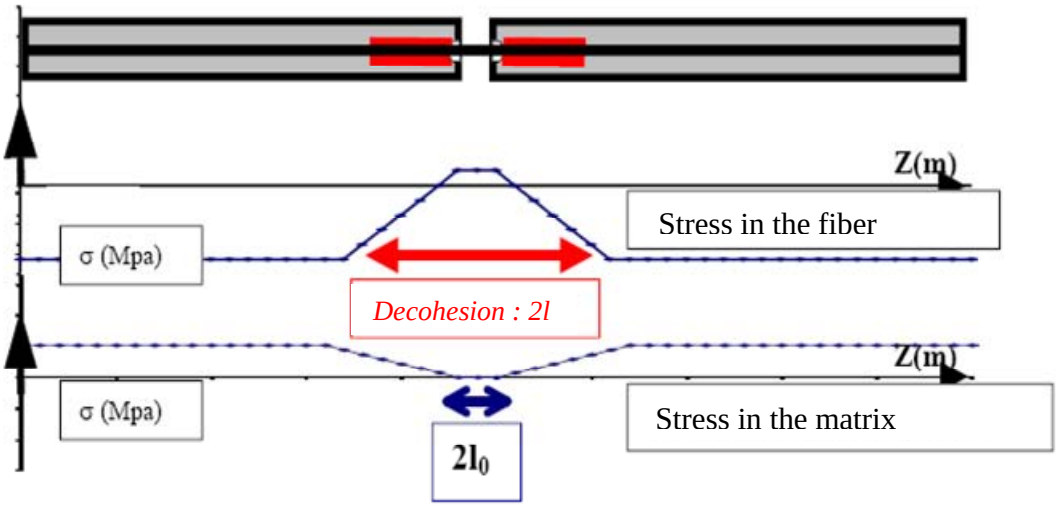

Fig. 1. Profile of a constraint in the vicinity of a fiber

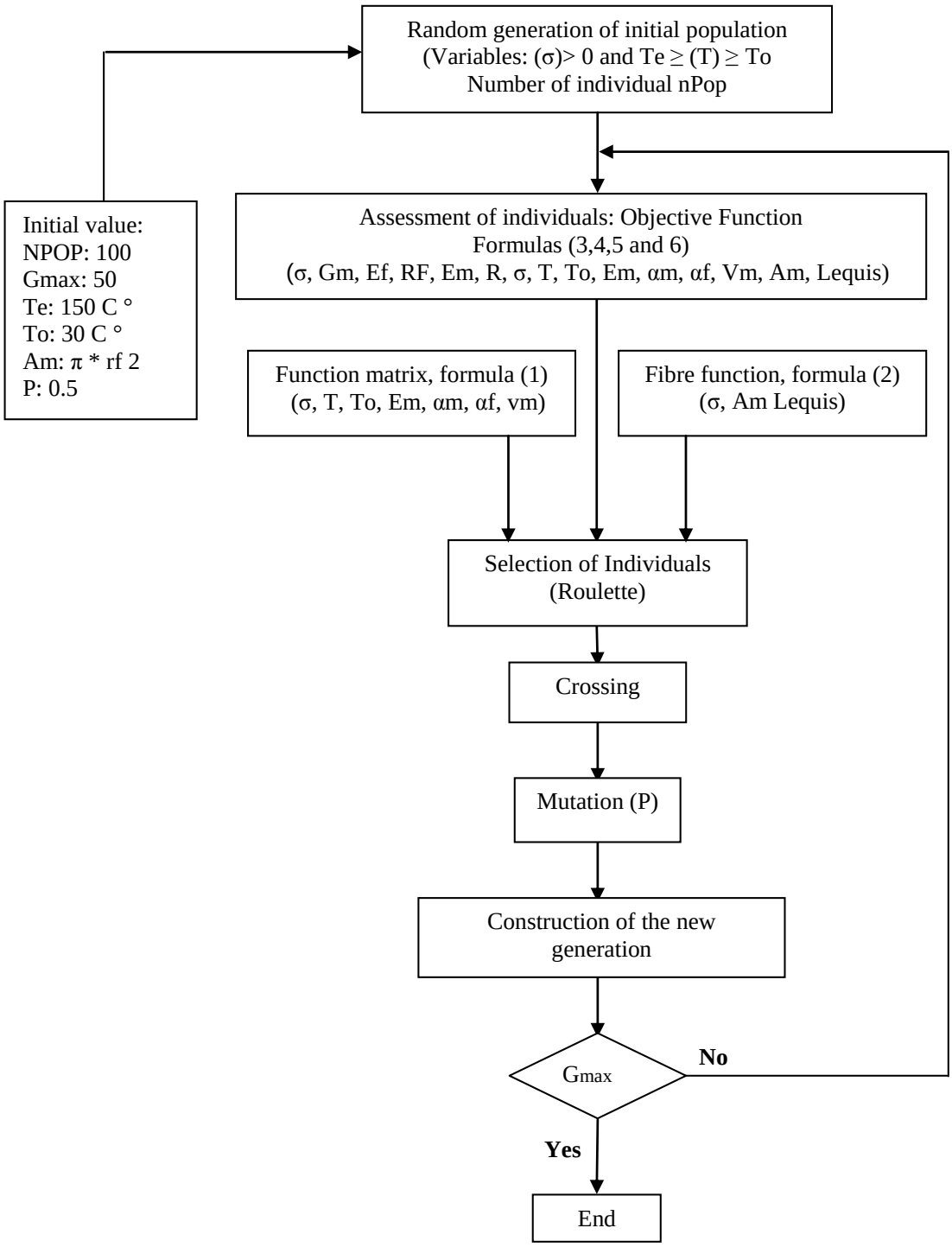

Fig. 2. The flowchart of genetic algorithm

IV. Simulation Results

The data used in the simulation by a genetic algorithm (GA) are Young's modulus of the fiber, the shear modulus of the matrix, the fiber length, the radius of the fiber, the coefficients of thermal expansion, thermal stress and mechanical stress.

It was noted the influence of mechanical stress on the damage of the matrix T300/914 (Fig. 3), and found the same way that heat stress at a great influence on the progressive degradation of the matrix (Figure 4).

Figure 5 shows the influence of mechanical stress on the damage of the fiber, we found that damage to the matrix is more important compared to the damage of the fiber.

We conclude that thermal stress beyond a critical threshold to a great influence on the damage of the interface, and it is perfectly linked to damage of the matrix and less important compared to the damage to the fiber (Fig. 6).

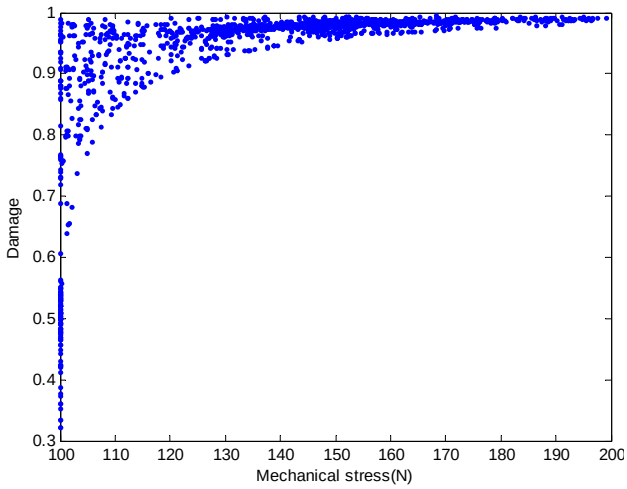

Fig. 3. Influence of mechanical stress on the damage of the matrix

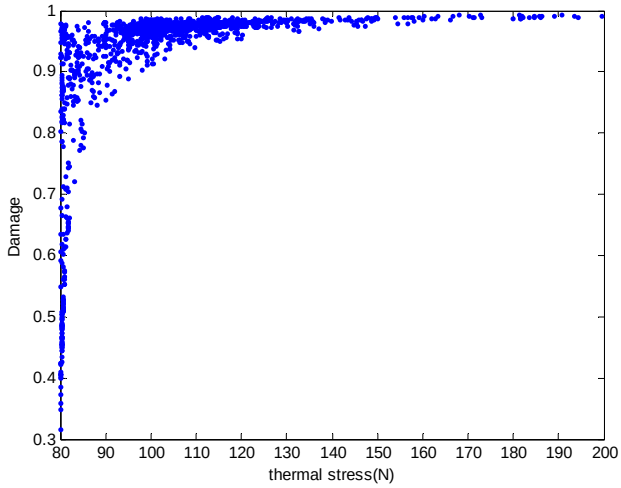

Fig. 4. Influence of heat stress on the damage of the matrix

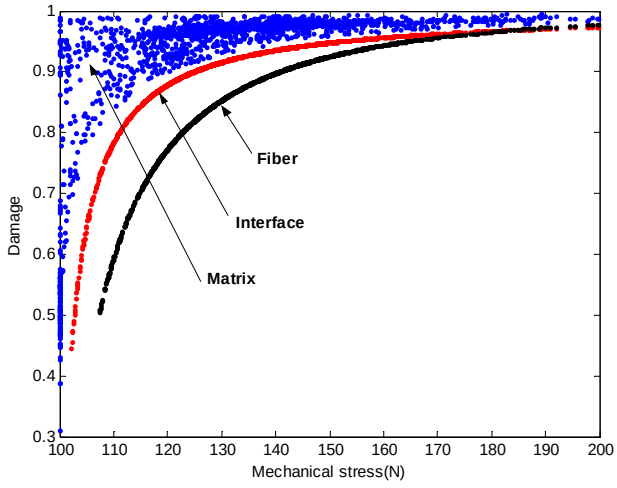

Fig. 5. Influence of heat stress on the damage of the fiber

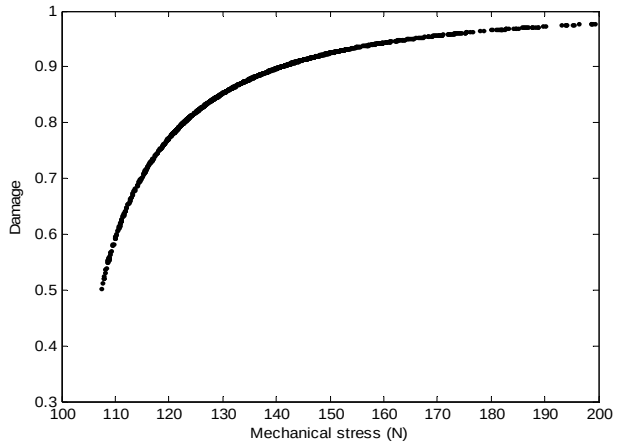

Fig. 6. Influence of thermal stress on the damage of the fiber-matrix interface

V. Conclusion

Our simulation model by a genetic algorithm has shown that thermal stress beyond a critical threshold induces a rapid and severe damage of the interface, and that damage to the interface is much more linked to the progressive degradation matrix to damage the fiber. We plan to validate this model by experimental measurements on materials more sensitive to high temperature.

References

[1] COX H.L,«The elasticity and strength of paper and other fibrous materials(Elasticité et résistance du papier et autres matériaux fibreux). *British Journal of Applied Physics*. (1952), P:72-79».

[2] Lebrun G-A., *Comportement thermomécanique et durée de vie de composites à matrice céramique : théorie et expérience*, Thèse de Doctorat n° 1606, Université de Bordeaux I,1996.

[3] Lissart N., « Domage and failure in ceramic matrix minicomposites :experimental study and model. », *acta mater*., Vol.45,n°3,pp. 1025-1044,1997.

[4] Weibull W., "A statistical Eng.Sci.Proc.,151, 1939.,pp.1-45. theory of the strength of materials", *Royal Swedish Academy of Eng. Sci. Proc*., 151, (1939) pp.1-45.

Authors' information

Allel Mokaddem
Date and place of birth: 09.14.1975 in Saida (Algeria)
Occupation: Professor first year teaching at the University of Science and Technology of Oran (Algeria)
District Director Saida GPL / Naftal Sonatrach Group (Western Region)
Address: City In Nahada No. 118 Rebahia Saida
E-mail: mokaddem.allel@Gmail.fr
Fax: +21348520482
Secondary education: Bachelor of Science in 1994
Educational qualifications:
• Engineering degree status (U. Es Senia / Oran)
• Magister degree in physics of materials (USTO / Oran)
• Joined PhD Doctor of Science (4th year)
Professional experience:

2000-2001: Framework for studies at the company Naftal (Saida)
2001-2009: Head of Centre barreling (Saida District GPL / Naftal)
2009-2011: Head of Technical Department and Maintenance (GPL Saida District / Naftal)
2009-present: Teaching first year Magister at the University of Science and Technology of Oran (Algeria)
: Member of the research team of Professor A. Boutaous "Characterization and behavior of materials in biomedical" University of Oran USTO Physics Department.
2011-present: Director Saida District GPL / Naftal Sonatrach Group (Western Region)
Areas of interest: Physics mechanics, Renewable energy, Theory of damage, Laminated Composites, Biomaterials

Ahmed Boutaous
Born 20/04/1961
USTO BP1505 EL-M' NAO UAR ORAN ALGERIA.
E-mail: aboutaous@yahoo.fr
Formation:
April 2006 Diploma of doctorate of state at the university of sciences and technology of Oran USTO, November 1993 Diploma of material Magister, university of be Sénia Oran, June 1987 Diploma for the occupation of engineer of state in mechanical engineering, university of sciences and technology of Oran USTO, June 1981 Baccalaureat technical series, college the Palm trees Oran Algeria.
Teaching activities (graduation and post-graduation.)
1994-1997 Teacher of technology, USTO ORAN,
1997-1999 National service,
1999 - to date Main of the conferences, USTO ORAN.
2009/2010/2011 persons in charge of Magister "Characterization and behavior of materials for the biomedical one."
Fields of competence

1. Digital simulation: modeling and simulation of physical and mechanical phenomena FORTRAN, Matlab, castem 2000
2. Physics of materials: characterization of materials, composite and polymeric materials.
3. Experimental: mechanical tests in traction, tiredness, hardness.
4. Control equips data-processing.

Praise Worthy Prize

International Review of Physics (I.R.E.PHY.), Vol. 5, N. 6
December 2011

Effect of Initial Stress on Rayleigh Waves in a Thermoelastic Granular Medium

G. A. Yahya[1,2]

Abstract – *In this paper, we study the effect of initial stress and coupled thermoelastic parameter ε on the propagation of Rayleigh waves in a granular medium under incremental thermal stresses. We also obtain the frequency equation, in the form of a twelfth-order determinantal expression. The numerical solution of the frequency equation has been obtained. The results represented graphically. The results indicate that the effect of initial stress and coupled parameter are very pronounced.*

Keywords*: Rayleigh Waves, Thermoelastic Waves, Granular Medium, Frequency Equation, Initial Stress*

I. Introduction

The dynamical problem in granular media of generalized magneto-thermoelastic waves has been studied in recent times, necessitated by its possible applications in soil mechanics, earthquake science, geophysics, mining engineering and plasma physics, etc. The granular medium under consideration is a discontinuous one and is composed of numerous large or small grains. Unlike a continuous body each element or grain cannot only translate but also rotate about its center of gravity. This motion is the characteristic of the medium and has an important effect upon the equations of motion to produce internal friction It was assumed that the medium contains so many grains that it will never be separated from each other during the deformation and that each grain has perfect thermo-elasticity. The effect of the granular media on dynamics was pointed out by Oshima [1]. The dynamical problem of a generalized thermo-elastic granular infinite cylinder under initial stress has been illustrated by El-Naggar [2]. Rayleigh wave propagation of thermo-elasticity or generalized thermo-elasticity was pointed out by Dawan and Chakraporty [3]. Rayleigh waves in a magneto-elastic material under the influence of initial stress and a gravity field were discussed by Abd-Alla et al. [4] and El-Naggar et al. [5]. Rayleigh waves in a thermo-elastic granular medium under initial and influence of gravity on the propagation of waves in granular medium are analytically discussed by Ahmed [6] respectively. Abd-Alla and Ahmed [7] discussed the problem of Rayleigh wave propagation in an orthotropic medium under gravity and initial stress. Magneto-thermoelastic problem in rotating non-homogeneous orthotropic hollow cylinder under the hyperbolic heat conduction model is discussed by Abd-Alla and Mahmoud [8]. Wave propagation in a generalized thermo-elastic solid cylinder of arbitrary cross-section is discussed by Venkatesan and Ponnusamy [9]. Some problems discussed the effect of rotating of different material.

Thermoelastic wave propagation in a rotating elastic medium without energy dissipation studied by Roychoudhuri and Bandyopadhyay [10]. Sharma and Grover [11] are studied the body wave propagation in rotating thermoelastic media. Thermal stresses in a rotating non-homogeneous orthotropic hollow cylinder were discussed by El-Naggar et al. [12]. Abd-Alla, et al. [13] investigated the numerical solution of magneto-thermoelastic problem non-homogeneous isotropic material. Propagation of Rayleigh waves in an elastic half-space of orthotropic material was studied by Abd-Alla [14].

On generalized magneto-thermoelastic Rayleigh waves in a granular medium under the influence of agravity field and initial stress were investigated by Abd-Alla, et al. [15].

The aim of this paper is to investigate, the effect of initial stress and coupled thermoelastic parameter on propagation of Rayleigh waves in a thermo-elastic granular medium.

General solution is obtained by using Lame' potential. The frequency equation of Rayleigh waves is obtained in the form of a determinant. Dispersion curves are computed numerically for a specific model and presented graphically. The results indicate that the effect of initial stress and coupled parameter are very pronounced

II. Formation of the Problem

Consider a system of orthogonal Cartesian axes x_1, x_2, x_3 such that the interface and the free surface of the granular layer resting on the granular half-space of different material are the planes $x_3 = H$ and $x_3 = 0$, respectively, the origin O is any point on the free surface, x_3- axis is positive in the direction towards the exterior of

Manuscript received and revised November 2011, accepted December 2011

the half-space, and the x_1-axis is positive along the direction of Rayleigh waves propagation.

The state of deformation in the granular medium is described by the displacement vector $\underline{U}(u_1,0,u_3)$ of the centre of gravity of a grain and the rotation vector $\underline{\xi}(\xi, \eta, \zeta)$ of the grain about its centre of gravity.

There exist a stress tensor and stress couple and are non-symmetric, that is:

$$\tau_{ij} \neq \tau_{ji} \ , \qquad M_{ij} \neq M_{ji} \quad i = 1,2,3 \tag{1}$$

The stress tensor τ_{ij} can be expressed as the sum of symmetric and ant-symmetric tensors:

$$\tau_{ij} = \sigma_{ij} + \sigma_{ij}^{'} \tag{2}$$

where:

$$\sigma_{ij} = \frac{1}{2}\left(\tau_{ij} + \tau_{ji}\right) \ , \qquad \sigma_{ij}^{'} = \frac{1}{2}\left(\tau_{ij} - \tau_{ji}\right) \tag{3}$$

The symmetric tensor $\sigma_{ij} = \sigma_{ji}$ is related to the symmetric strain tensor:

$$e_{ij} = e_{ji} = \frac{1}{2}\left(\frac{\partial u_i}{\partial x_j} + \frac{\partial u_j}{\partial x_i}\right) \tag{4}$$

by the Hook's law.

The anti-symmetric stress $\sigma_{ij}^{'}$ are given by:

$$\begin{gathered}\sigma_{23}^{'} = -F\frac{\partial \xi}{\partial t} \ , \ \sigma_{31}^{'} = -F\frac{\partial \eta}{\partial t} \ , \\ \sigma_{12}^{'} = -F\frac{\partial \zeta}{\partial t} \ , \sigma_{11}^{'} = \sigma_{22}^{'} = \sigma_{33}^{'} = 0\end{gathered} \tag{5}$$

where F is the coefficient of fraction:

The stress couple M_{ij} is given by:

$$M_{ij} = M\nu_{ij} \tag{6}$$

where M is the third elastic constant:

$$\begin{gathered}\nu_{11} = \frac{\partial \xi}{\partial x_1} \ , \nu_{22} = 0 \ , \nu_{33} = \frac{\partial \zeta}{\partial x_1} \ , \nu_{23} = 0 \ , \\ \nu_{31} = \frac{\partial \xi}{\partial x_3} \ , \nu_{12} = \frac{\partial}{\partial x_1}(\eta + \omega_2) \ , \\ \nu_{32} = \frac{\partial}{\partial x_3}(\eta + \omega_2) \ , \\ \nu_{13} = \frac{\partial \zeta}{\partial x_1} \ , \nu_{21} = 0\end{gathered} \tag{7}$$

where $\omega_2 = \frac{1}{2}\left(\frac{\partial u_1}{\partial x_3} - \frac{\partial u_3}{\partial x_1}\right)$ is the component of rotation.

The heat conduction equation is given by [16]:

$$K\nabla^2 T = \rho C_e \frac{\partial T}{\partial t} + \gamma T_0 \nabla \cdot \frac{\partial \underline{U}}{\partial t} \tag{8}$$

where K is the thermal conductivity, T is the temperature change about the initial temperature T_0, ρ is the density, C_e is the specific heat per unit mass at constant strain, γ is equal to $\alpha(3\lambda+2\mu)$, α is the thermal expansion coefficient, and λ and μ are Lame's constants and t is the time.

The components of incremental stress in terms of the displacement are given by:

$$\begin{gathered}\sigma_{11} = (\lambda + 2\mu + p)\frac{\partial u_1}{\partial x_1} + (\lambda + p)\frac{\partial u_3}{\partial x_3} - \gamma T \\ \sigma_{33} = \lambda\frac{\partial u_1}{\partial x_1} + (\lambda + 2\mu)\frac{\partial u_3}{\partial x_3} - \gamma T \\ \sigma_{11} = \mu\left(\frac{\partial u_1}{\partial x_3} + \frac{\partial u_3}{\partial x_1}\right)\end{gathered} \tag{9}$$

The dynamical equations of motion are [20], [21]:

$$\begin{gathered}\frac{\partial \tau_{11}}{\partial x_1} + \frac{\partial \tau_{13}}{\partial x_3} + p\frac{\partial \omega_2}{\partial x_3} = \rho\frac{\partial^2 u_1}{\partial t^2} \\ \frac{\partial \tau_{12}}{\partial x_1} + \frac{\partial \tau_{32}}{\partial x_3} = 0 \\ \frac{\partial \tau_{13}}{\partial x_1} + \frac{\partial \tau_{33}}{\partial x_3} + p\frac{\partial \omega_2}{\partial x_1} = \rho\frac{\partial^2 u_3}{\partial t^2}\end{gathered} \tag{10}$$

$$\begin{gathered}\tau_{23} - \tau_{32} + \frac{\partial M_{11}}{\partial x_1} + \frac{\partial M_{31}}{\partial x_3} = 0 \\ \tau_{31} - \tau_{13} + \frac{\partial M_{12}}{\partial x_1} + \frac{\partial M_{32}}{\partial x_3} = 0 \\ \tau_{12} - \tau_{21} + \frac{\partial M_{13}}{\partial x_1} + \frac{\partial M_{33}}{\partial x_3} = 0\end{gathered} \tag{11}$$

These equations, when the stresses are substituted, take the forms:

$$\begin{gathered}(\lambda + 2\mu + p)\frac{\partial^2 u_1}{\partial x_1^2} + \left(\mu + \frac{p}{2}\right)\frac{\partial^2 u_1}{\partial x_3^2} + \\ + \left(\lambda + \mu + \frac{p}{2}\right)\frac{\partial^2 u_3}{\partial x_1 \partial x_3} - \gamma\frac{\partial T}{\partial x_1} + \\ -F\frac{\partial}{\partial t}\left(\frac{\partial \eta}{\partial x_3}\right) = \rho\frac{\partial^2 u_1}{\partial t^2}\end{gathered} \tag{12}$$

$$\frac{\partial}{\partial t}\left(\frac{\partial \xi}{\partial x_3} - \frac{\partial \zeta}{\partial x_1}\right) = 0 \tag{13}$$

$$\begin{gathered}\left(\lambda + \mu + \frac{p}{2}\right)\frac{\partial^2 u_1}{\partial x_1 \partial x_3} + \left(\mu - \frac{p}{2}\right)\frac{\partial^2 u_3}{\partial x_1^2} + \\ +(\lambda + 2\mu)\frac{\partial^2 u_3}{\partial x_3^2} - \gamma\frac{\partial T}{\partial x_3} + F\frac{\partial}{\partial t}\left(\frac{\partial \eta}{\partial x_1}\right) = \rho\frac{\partial^2 u_3}{\partial t^2}\end{gathered} \tag{14}$$

$$-F\frac{\partial \xi}{\partial t} + M\,\nabla^2 \xi = 0 \tag{15}$$

$$-F\frac{\partial \eta}{\partial t} + \mathrm{M}\nabla^2(\eta + \omega_2) = 0 \tag{16}$$

$$-F\frac{\partial \zeta}{\partial t} + M\nabla^2 \zeta = 0 \tag{17}$$

III. Solution of the Problem

Let the constants $\lambda, \mu, \rho, F, M, \gamma$ and $\overline{\lambda}, \overline{\mu}, \overline{\rho}, \overline{F}, \overline{M}, \overline{\gamma}$ be characteristics of the layer and the half-space, respectively. Let us introduce the displacement potentials $\phi(x_1, x_3, t)$ and $\psi(x_1, x_3, t)$ which are related to the displacement components u_1 and u_3 by the relations:

$$u_1 = \frac{\partial \phi}{\partial x_1} - \frac{\partial \psi}{\partial x_3}, \qquad u_3 = \frac{\partial \phi}{\partial x_3} + \frac{\partial \psi}{\partial x_1} \tag{18}$$

Substituting from (18) into (12), (14), and (16), we see that ϕ and ψ satisfy the wave equations:

$$\propto^2 \nabla^2 \phi - \frac{\partial^2 \phi}{\partial x^2} - \frac{\gamma}{\rho} T = 0 \tag{19}$$

$$\beta^2 \nabla^2 \psi - \frac{\partial^2 \psi}{\partial x^2} + s \frac{\partial \eta}{\partial t} = 0 \tag{20}$$

$$-s' \frac{\partial \eta}{\partial t} + \nabla^2 \eta - \nabla^4 \psi = 0 \tag{21}$$

where:

$$\propto^2 = \frac{\lambda + 2\mu + p}{\rho}, \qquad \beta^2 = \frac{\mu + (p/2)}{\rho}, \qquad s = \frac{F}{\rho}, \qquad s' = \frac{F}{M} \tag{22}$$

From (18), the heat conduction Equation (8) becomes:

$$K \nabla^2 T = \rho C_e \frac{\partial T}{\partial t} + \gamma T_0 \nabla^2 \cdot \frac{\partial \phi}{\partial t} = 0 \tag{23}$$

Elimination of T from (19) and (23), gives:

$$\left(\nabla^2 - \frac{1}{\chi} \frac{\partial}{\partial t}\right)\left(\propto^2 \nabla^2 \phi - \frac{\partial^2 \phi}{\partial t^2}\right) - \varepsilon \nabla^2 \frac{\partial \phi}{\partial t} = 0 \tag{24}$$

where:

$$\chi = \frac{K}{\rho C_e}, \qquad \varepsilon = \frac{\gamma^2 T_0}{\rho K} \tag{25}$$

Also, η can be eliminated by the use of (20) and (21) as follows:

$$\left(\nabla^2 - s' \frac{\partial}{\partial t}\right)\left(\beta^2 \nabla^2 \psi - \frac{\partial^2 \psi}{\partial t^2}\right) - \varepsilon \nabla^4 \frac{\partial \psi}{\partial t} = 0 \tag{26}$$

$$\phi = \phi_1(x_3) exp\{i(Lx_1 - bt)\} \tag{27}$$

$$\psi = \psi_1(x_3) exp\{i(Lx_1 - bt)\} \tag{28}$$

$$(\xi, \eta, \zeta) = \{\xi_1(x_3), \eta_1(x_3), \zeta_1(x_3)\} \cdot \cdot exp\{i(Lx_1 - bt)\} \tag{29}$$

where b is real positive and L in general complex.

Substituting from (29) into (13), (15), and (17), gives:

$$D\xi_1 - iL\zeta_1 = 0 \tag{30}$$

$$D^2 \xi_1 + h^2 \xi_1 = 0 \tag{31}$$

$$D^2 \zeta_1 + h^2 \zeta_1 = 0 \tag{32}$$

where:

$$h^2 = ibs' - L^2, \qquad D \equiv d/dx_3$$

Solutions of (31) and (32), are:

$$\xi_1 = A_1 e^{ihx_3} + A_2 e^{-ihx_3}, \quad \zeta_1 = B_1 e^{ihx_3} + B_2 e^{-ihx_3} \tag{33}$$

respectively.

From (30) and (33), we obtain:

$$h(A_1 e^{ihx_3} - A_2 e^{-ihx_3}) + -L(B_1 e^{ihx_3} - B_2 e^{-ihx_3}) = 0 \tag{34}$$

Equating the coefficient of e^{ihx_3} and e^{-ihx_3} to zero in (34), gives:

$$A_1 = \frac{L}{h} B_1, \qquad A_2 = -\frac{L}{h} B_2 \tag{35}$$

Also, substituting from (27) and (28) into (24) and (26), we obtain:

$$\left[\propto^2 D^4 + \left(b^2 - 2L^2 \propto^2 + ib\varepsilon + \frac{ib \propto^2}{\chi}\right) + + \propto^2 L^4 - b^2 L^2 - ibL^2 \varepsilon - \frac{ibL^2 \propto^2}{\chi} + \frac{ib^3}{\chi}\right] \phi_1 = 0 \tag{36}$$

$$\left[\begin{array}{c}(\beta^2 - ibs) D^4 + \\ + (b^2 - 2L^2 \beta^2 + ibs' \beta^2 + 2ibsL^2) D^2 + \\ + (\beta^2 - ibs) L^4 - (b - is' \beta^2) bL^2 + ib^3 s'\end{array}\right] \psi_1 = 0 \tag{37}$$

The solution of (36) and (37) has the form:

$$\phi_1 = A_3 e^{m_3 x_3} + B_3 e^{-m_3 x_3} + + A_4 e^{m_4 x_3} + B_4 e^{-m_4 x_3} \tag{38}$$

$$\phi_1 = E_3 e^{n_3 x_3} + F_3 e^{-n_3 x_3} + + E_4 e^{n_4 x_3} + F_4 e^{-n_4 x_3} \tag{39}$$

where:

$$(m_3^2, m_4^2) = L^2 - \frac{b(b + i\varepsilon)}{2\alpha^2} + - \frac{ib}{2\chi} \pm \frac{b}{2\alpha^2}\left[(b + i\varepsilon)^2 - 2i\alpha^2 (b + i\varepsilon) - \frac{\alpha^4}{\chi}\right]^{1/2} \tag{40a}$$

$$(n_3^2, n_4^2) = \\ = \frac{\begin{bmatrix} 2L^2\beta^2 - b^2 - ib\beta^2 s' + \\ -2ibL^2 s \pm b[(b - i\beta^2 s')^2 - 4b^2 ss']^{1/2} \end{bmatrix}}{2(\beta^2 - ibs)} \quad (40b)$$

Using (20), (28), (29), and (39), we get:

$$\eta_1 = \Omega_3(E_3 e^{n_3 x_3} + F_3 e^{-n_3 x_3}) + \\ +\Omega_4(E_4 e^{n_4 x_3} + F_4 e^{-n_4 x_3}) \quad (41)$$

where:

$$\Omega_3 = \frac{-i\beta^2}{bs}\left(n_3^2 - L^2 + \frac{b^2}{\beta^2}\right)$$

$$\Omega_4 = \frac{-i\beta^2}{bs}\left(n_4^2 - L^2 + \frac{b^2}{\beta^2}\right) \quad (42)$$

from (19), (27), and (38), we have:

$$T = \begin{bmatrix} \Omega_3'(A_3 e^{m_3 x_3} + B_3 e^{-m_3 x_3}) + \\ +\Omega_4'(A_4 e^{m_4 x_3} + B_4 e^{-m_4 x_3}) \end{bmatrix} \cdot \\ \cdot exp[i(Lx_1 - bt)] \quad (43)$$

where:

$$\Omega_3' = \frac{\rho\alpha^2}{\gamma}\left(m_3^2 - L^2 + \frac{b^2}{\alpha^2}\right)$$

$$\Omega_4' = \frac{\rho\alpha^2}{\gamma}\left(m_4^2 - L^2 + \frac{b^2}{\alpha^2}\right) \quad (44)$$

The functions ξ_1, ζ_1, η_1, φ_1, and ψ_1 in the state of the lower medium must vanish as $x_3 \to \infty$ and using the symbols with a bar for the quantities in the lower medium (except x_3 , L, b, p). Assuming the real parts of m_3, m_4, n_3 , n_4 are positive while the imaginary part of h is negative, we obtain, for $x_3 > H$:

$$\overline{\xi}_1 = -\frac{L}{h}\overline{B}_2 e^{-i\overline{h}x_3}$$

$$\overline{\zeta}_1 = \overline{B}_2 e^{-i\overline{h}x_3}$$

$$\overline{\eta}_1 = \overline{\Omega}_3\overline{F}_3 e^{-\overline{n}_3 x_3} + \overline{\Omega}_4\overline{F}_4 e^{-\overline{n}_4 x_3}$$

$$\overline{\phi}_1 = \overline{B}_3 e^{-\overline{m}_3 x_3} + \overline{B}_4 e^{-\overline{m}_4 x_3} \quad (45)$$

$$\overline{\psi}_1 = \overline{F}_3 e^{-\overline{n}_3 x_3} + \overline{F}_4 e^{-\overline{n}_4 x_3}$$

$$\overline{T} = \overline{\Omega}_3'\overline{B}_3 e^{-\overline{m}_3 x_3} + \overline{\Omega}_4'\overline{B}_4 e^{-\overline{m}_4 x_3}$$

IV. Boundary Conditions and Frequency Equation

The boundary conditions on the interface $x_3 = H$ are:

$$(i)\ u_1 = \overline{u}_1\ , (ii)\ u_3 = \overline{u}_3\ , (iii)\ \xi = \overline{\xi}$$

$$(iv)\ \eta = \overline{\eta}\ , \quad (v)\ \zeta = \overline{\zeta}, \quad (vi)\ M_{33} = \overline{M}_{33}$$

$$(vii)\ M_{31} = \overline{M}_{31}, (viii)\ M_{32} = \overline{M}_{32}\ , (ix)\ \tau_{33} = \overline{\tau}_{33} \quad (46)$$

$$(x)\ \tau_{31} = \overline{\tau}_{31}\ , (xi)\ \tau_{32} = \overline{\tau}_{32}\ , \ (xii)\ T = \overline{T}$$

$$(xiii)\ \frac{\partial T}{\partial x_3} + \theta T = \frac{\partial \overline{T}}{\partial x_3} + \overline{\theta}\,\overline{T}$$

The boundary conditions on the free surface $x_3 = 0$ are:

$$(xiv)\ M_{33} = 0\ , \quad (xv)\ M_{31} = 0\ ,$$

$$(xvi)\ M_{32} = 0\ \ (xvii)\ \tau_{33} = 0\ \ (xviii)\ \tau_{31} = 0 \quad (47)$$

$$(xix)\ \tau_{32} = 0\ , \quad (xx)\ \frac{\partial T}{\partial x_3} + \theta T = 0$$

where:

$$M_{33} = M\frac{\partial \zeta}{\partial x_3}\ , M_{32} = M\frac{\partial}{\partial x_3}(\eta - \nabla^2\psi)\ , M_{31} = M\frac{\partial \xi}{\partial x_3}$$

$$\tau_{33} = \lambda\nabla^2\phi + 2\mu\left(\frac{\partial^2\phi}{\partial x_3^2} - \frac{\partial^2\psi}{\partial x_1 \partial x_3}\right) - \gamma T\ , \tau_{32} = -F\frac{\partial \xi}{\partial t}$$

$$\tau_{31} = \mu\left(2\frac{\partial^2\phi}{\partial x_1 \partial x_3} - \frac{\partial^2\psi}{\partial x_3^2} + \frac{\partial^2\psi}{\partial x_1^2}\right) - F\frac{\partial \eta}{\partial t}$$

θ is the ratio of the coefficients of heat transfer to the thermal conductivity. From the boundary conditions (3), (5), (6), and (7) we get:

$$B_1 e^{ihH} - B_2 e^{-ihH} = -\overline{B}_2 e^{-i\overline{h}H}$$

$$B_1 e^{ihH} + B_2 e^{-ihH} = -\overline{B}_2 e^{i\overline{h}H}$$

$$M(B_1 e^{ihH} - B_2 e^{-ihH}) = -\overline{M}\,\overline{B}_2 e^{-i\overline{h}H} \quad (48)$$

$$M(B_1 e^{ihH} + B_2 e^{-ihH}) = -\overline{M}\,\overline{B}_2 e^{-i\overline{h}H}$$

whence:

$$B_1 = B_2 = \overline{B}_2 = 0\ , \xi = \zeta = \overline{\xi} = \overline{\zeta} = 0 \quad (49)$$

The other significant boundary conditions are responsible for the following relations:

$$(xxi)\ q_1(E_3 - F_3) + q_2(E_4 - F_4) = 0$$

$$(xxii)\ q_3(A_3 + B_3) + q_4(A_4 + B_4) + \\ +q_5(E_3 - F_3) + q_6(E_4 - F_4) = 0 \quad (50a)$$

$$(xxiii)\ q_7(A_3 - B_3) + q_8(A_4 - B_4) + \\ +q_9(E_3 - F_3) + q_{10}(E_4 - F_4) = 0$$

$$
\begin{aligned}
(xxiv)\ & iL(A_3e^{m_3H}+B_3e^{-m_3H}+A_4e^{m_4H}\\
&+B_4e^{-m_4H})\\
&-n_3(E_3e^{n_3H}+F_3e^{-n_3H})\\
&-n_4(E_4e^{n_4H}+F_4e^{-n_4H})\\
&=iL\overline{B}_3e^{-\overline{m}_3H}+iL\overline{B}_4e^{-\overline{m}_4H}\\
&+\overline{n}_3\overline{F}_3e^{-\overline{n}_3H}+\overline{n}_4\overline{F}_4e^{-\overline{n}_4H}\\
(xxv)\ & m_3(A_3e^{m_3H}-B_3e^{-m_3H})\\
&+m_4(A_4e^{m_4H}-B_4e^{-m_4H})\\
&+il(E_3e^{n_3H}-F_3e^{-n_3H}\\
&+E_4e^{n_4H}+F_4e^{-n_4H})\\
&=-\overline{m}_3\overline{B}_3e^{-\overline{m}_3H}-\overline{m}_4\overline{B}_4e^{-\overline{m}_4H}\\
&+iL\overline{F}_3e^{-\overline{n}_3H}+iL\overline{F}_4e^{-\overline{n}_4H}\\
(xxvi)\ & \Omega_3(E_3e^{n_3H}+F_3e^{-n_3H})\\
&+\Omega_4(E_4e^{n_4H}+F_4e^{-n_4H})\\
&=\overline{\Omega}_3\overline{F}_3e^{-\overline{n}_3H}+\overline{\Omega}_4\overline{F}_4e^{-\overline{n}_4H}\\
(xxvii)\ & M[q_1(E_3e^{n_3H}-F_3e^{-n_3H})\\
&+q_2(E_4e^{n_4H}+F_4e^{-n_4H})]\\
&=-\overline{M}\big(\overline{q}_1\overline{F}_3e^{-\overline{n}_3H}\\
&+\overline{q}_2\overline{F}_4e^{-\overline{n}_4H}\big)\\
(xxviii)\ & q_3(A_3e^{m_3H}+B_3e^{-m_3H})\\
&+q_4(A_4e^{m_4H}+B_4e^{-m_4H})\\
&+q_5(E_3e^{n_3H}-F_3e^{-n_3H})\\
&+q_6(E_4e^{n_4H}+F_4e^{-n_4H})\\
&=\overline{q}_3\overline{B}_3e^{-\overline{m}_3H}+\overline{q}_4\overline{B}_4e^{-\overline{m}_4H}\\
&-\overline{q}_5\overline{F}_3e^{-\overline{n}_3H}-\overline{q}_6\overline{F}_4e^{-\overline{n}_4H}\\
(xxix)\ & q_7(A_3e^{m_3H}-B_3e^{-m_3H})\\
&+q_8(A_4e^{m_4H}-B_4e^{-m_4H})\\
&+q_9(E_3e^{n_3H}-F_3e^{-n_3H})\\
&+q_{10}(E_4e^{n_4H}-F_4e^{-n_4H})\\
&=\overline{q}_7\overline{B}_3e^{-\overline{m}_3H}-\overline{q}_8\overline{B}_4e^{-\overline{m}_4H}\\
&-\overline{q}_9\overline{F}_3e^{-\overline{n}_3H}-\overline{q}_{10}\overline{F}_4e^{-\overline{n}_4H}\\
(xxx)\ & \Omega_3'(A_3e^{m_3H}+B_3e^{-m_3H})\\
&+\Omega_4'(A_4e^{m_4H}+B_4e^{-m_4H})\\
&=\overline{\Omega}_3'\,\overline{B}_3e^{-\overline{m}_3H}+\overline{\Omega}_4'\overline{B}_4e^{-\overline{m}_4H}\\
(xxxi)\ & q_{11}A_3e^{m_3H}+q_{12}B_3e^{-m_3H}+q_{13}A_4e^{m_4H}\\
&+q_{14}B_4e^{-m_4H}\\
&=\overline{q}_{12}\overline{B}_3e^{-\overline{m}_3H}+\overline{q}_{14}\overline{B}_4e^{-\overline{m}_4H}\\
(xxxii)\ & q_{11}A_3+q_{12}B_3+q_{13}A_4+q_{14}B_4=0
\end{aligned}
\tag{50b}
$$

where:

$$
\begin{aligned}
q_1&=n_3(\Omega_3+L^2-n_3^2)\ , & \overline{q}_1&\\
&=\overline{n}_3(\overline{\Omega}_3+L^2-\overline{n}_3^2)\\
q_2&=n_4(\Omega_4+L^2-n_4^2)\ , & \overline{q}_2&\\
&=\overline{n}_4(\overline{\Omega}_4+L^2-\overline{n}_4^2)\\
q_3&=(2\mu+p)\mathrm{L}^2-\rho b^2-pm_3^2\ , & \overline{q}_3&\\
&=(2\overline{\mu}+p)\mathrm{L}^2-\overline{\rho}b^2-p\overline{m}_3^2\\
q_4&=(2\mu+p)\mathrm{L}^2-\rho b^2-pm_4^2\ , & \overline{q}_4&\\
&=(2\overline{\mu}+p)\mathrm{L}^2-\overline{\rho}b^2-p\overline{m}_4^2\\
q_5&=-2iL\mu n_3\ , & \overline{q}_5&=-2iL\overline{\mu}\,\overline{n}_3\\
q_6&=-2iL\mu n_4\ , & \overline{q}_6&=-2iL\overline{\mu}\,\overline{n}_4\\
q_7&=-2iL\mu m_3\ , & \overline{q}_7&=-2iL\overline{\mu}\,\overline{m}_3\\
q_8&=-2iL\mu m_4\ , & \overline{q}_8&=-2iL\overline{\mu}\,\overline{m}_4
\end{aligned}
\tag{51a}
$$

$$
\begin{aligned}
q_9&=ibF\Omega_3-\mu L^2-\mu n_3^2\ ,\\
\overline{q}_9&=ib\overline{F}\,\overline{\Omega}_3-\overline{\mu}L^2-\overline{\mu}\,\overline{n}_3^2\\
q_{10}&=ibF\Omega_4-\mu L^2-\mu n_4^2\ ,\\
\overline{q}_{10}&=ib\overline{F}\,\overline{\Omega}_4-\overline{\mu}L^2-\overline{\mu}\,\overline{n}_4^2\\
q_{11}&=\Omega_3'(\theta+m_3)\ , & \overline{q}_{11}&=\overline{\Omega}_3'(\overline{\theta}+\overline{m}_3)\\
q_{12}&=\Omega_3'(\theta-m_3)\ , & \overline{q}_{12}&=\overline{\Omega}_3'(\overline{\theta}-\overline{m}_3)\\
q_{13}&=\Omega_4'(\theta+m_4)\ , & \overline{q}_{13}&=\overline{\Omega}_4'(\overline{\theta}+\overline{m}_4)\\
q_{14}&=\Omega_4'(\theta-m_4)\ , & \overline{q}_{14}&=\overline{\Omega}_4'(\overline{\theta}-\overline{m}_4)
\end{aligned}
\tag{51b}
$$

Elimination:

$$A_3\ ,B_3\ ,A_4\ ,B_4\ ,E_3\ ,F_3\ ,E_4\ ,F_4\ ,\overline{B}_3\ ,\overline{B}_4\ ,\overline{F}_3\ ,\overline{F}_4$$

gives the wave velocity equation in the form of:

$$\det d_{ij}=0 \tag{52}$$

where the non-vanishing entries of the twelfth-order determinant of d_{ij} are given by:

$$
\begin{aligned}
&d_{15}=q_1e^{-n_3H},\ d_{16}=-q_1e^{n_3H}\ ,\\
&d_{17}=q_2e^{-n_4H},\ d_{18}=-q_2e^{n_4H}\\
&d_{21}=q_3e^{-m_3H},\ d_{22}=q_3e^{m_3H}\ ,\\
&d_{23}=q_4e^{-m_4H},\ \ d_{24}=q_4e^{m_4H}\\
&d_{25}=q_5e^{-n_3H},\ d_{26}=-q_5e^{n_3H},\\
&d_{27}=q_6e^{-n_4H},\ \ d_{28}=-q_6e^{n_4H}\\
&d_{31}=q_7e^{-m_3H},\ d_{32}=-q_7e^{m_3H}\ ,\\
&d_{33}=q_8e^{-m_4H},\ d_{34}=-q_8e^{m_4H}\\
&d_{35}=q_9e^{-n_3H},\ d_{36}=-q_9e^{n_3H}\ ,\\
&d_{37}=q_{10}e^{-n_4H},\ d_{38}=-q_{10}e^{n_4H}\\
&d_{41}=iL\ ,\ d_{42}=iL\ ,\ \ d_{43}=iL,\ \ d_{44}=iL\\
&d_{45}=-n_3\ ,\ \ d_{46}=-n_3\ ,\ d_{47}=n_4,\ \ d_{48}=n_4\\
&d_{49}=-iL\ ,\ \ d_{410}=iL\ ,\ \ d_{411}=-\overline{n}_3\ ,\\
&\qquad d_{412}=\overline{n}_4,d_{51}=m_3\ ,\ \ \ d_{52}=-m_3\ ,\\
&d_{53}=m_4\ ,d_{54}=-m_4,d_{55}=iL\ ,\ d_{56}=iL\ ,\\
&\qquad d_{57}=iL\ ,\ \ d_{58}=iL,\ d_{59}=\overline{m}_3\ ,\\
&d_{510}=\overline{m}_4\ ,\ \ d_{511}=iL\ ,\ d_{512}=iL\\
&d_{611}=-\overline{\Omega}_3\ ,\ \ d_{612}=-\overline{\Omega}_4\ ,\ \ d_{75}=Mq_1\ ,\\
&\quad d_{76}=-Mq_1,d_{77}=Mq_2\ ,\ \ d_{78}=-Mq_2\ ,\\
&d_{711}=\overline{M}\,\overline{q}_1\ ,\ \ d_{712}=-\overline{M}\,\overline{q}_2\\
&d_{81}=q_3\ ,\ \ \ d_{82}=q_3\ ,\ \ \ d_{83}=q_4\ ,\\
&d_{84}=q_4d_{85}=q_5\ ,\ d_{86}=-q_5\ ,\ d_{87}=q_6\ ,\\
&d_{88}=-q_6,d_{89}=-\overline{q}_3\ ,\ \ d_{810}=-\overline{q}_4\ ,\\
&d_{811}=\overline{q}_5\ ,\ d_{812}=\overline{q}_6,d_{91}=q_7\ ,\\
&d_{92}=-q_7\ ,\ \ \ d_{93}=q_8\ ,\ \ \ d_{94}=-q_8\\
&d_{95}=q_9\ ,\ \ d_{96}=-q_9\ ,\ \ \ d_{97}=q_{10}\ ,\\
&d_{98}=-q_{10},d_{99}=\overline{q}_7\ ,\ \ d_{910}=\overline{q}_8\ ,\ d_{911}=\overline{q}_9\ ,\\
&\qquad d_{912}=\overline{q}_{10},d_{101}=\Omega_3'\ ,\ d_{102}=\Omega_3'\ ,\\
&\quad d_{103}=\Omega_4'\ ,\ \ \ d_{104}=\Omega_4',d_{109}=-\overline{\Omega}_3'\ ,\\
&d_{1010}=-\overline{\Omega}_4'\ ,\ \ d_{111}=q_{11}\ ,\ \ d_{112}=q_{12}\\
&\quad d_{113}=q_{13}\ ,\ d_{114}=q_{14}\ ,\ d_{119}=-\overline{q}_{12}\ ,\\
&\qquad d_{1110}=-\overline{q}_{14}
\end{aligned}
\tag{53a}
$$

$$d_{15} = q_1 e^{-n_3 H},\ d_{16} = -q_1 e^{n_3 H},$$
$$d_{17} = q_2 e^{-n_4 H},\ d_{18} = -q_2 e^{n_4 H}$$
$$d_{21} = q_3 e^{-m_3 H},\ d_{22} = q_3 e^{m_3 H},$$
$$d_{23} = q_4 e^{-m_4 H},\ d_{24} = q_4 e^{m_4 H}$$
$$d_{25} = q_5 e^{-n_3 H},\ d_{26} = -q_5 e^{n_3 H},$$
$$d_{27} = q_6 e^{-n_4 H},\ d_{28} = -q_6 e^{n_4 H}$$
$$d_{31} = q_7 e^{-m_3 H},\ d_{32} = -q_7 e^{m_3 H},$$
$$d_{33} = q_8 e^{-m_4 H},\ d_{34} = -q_8 e^{m_4 H}$$
$$d_{35} = q_9 e^{-n_3 H},\ d_{36} = -q_9 e^{n_3 H},$$
$$d_{37} = q_{10} e^{-n_4 H},\ d_{38} = -q_{10} e^{n_4 H}$$
$$d_{41} = iL,\ d_{42} = iL,\ d_{43} = iL,\ d_{44} = iL$$
$$d_{45} = -n_3,\ d_{46} = -n_3,\ d_{47} = n_4,\ d_{48} = n_4$$
$$d_{49} = -iL,\ d_{410} = iL,$$
$$d_{411} = -\overline{n}_3,\ d_{412} = \overline{n}_4$$
$$d_{51} = m_3,\ d_{52} = -m_3,$$
$$d_{53} = m_4,\ d_{54} = -m_4$$
$$d_{55} = iL,\ d_{56} = iL,\ d_{57} = iL,\ d_{58} = iL$$
$$d_{59} = \overline{m}_3,\ d_{510} = \overline{m}_4,\ d_{511} = iL,\ d_{512} = iL$$
$$d_{611} = -\overline{\Omega}_3,\ d_{612} = -\overline{\Omega}_4,$$
$$d_{75} = Mq_1,\ d_{76} = -Mq_1$$
$$d_{77} = Mq_2,\ d_{78} = -Mq_2,$$
$$d_{711} = \overline{M}\,\overline{q}_1,\ d_{712} = -\overline{M}\,\overline{q}_2$$
$$d_{81} = q_3,\ d_{82} = q_3,$$
$$d_{83} = q_4,\ d_{84} = q_4$$
$$d_{85} = q_5,\ d_{86} = -q_5,\ d_{87} = q_6,\ d_{88} = -q_6$$
$$d_{89} = -\overline{q}_3,\ d_{810} = -\overline{q}_4,\ d_{811} = \overline{q}_5,\ d_{812} = \overline{q}_6$$
$$d_{91} = q_7,\ d_{92} = -q_7,$$
$$d_{93} = q_8,\ d_{94} = -q_8$$
$$d_{95} = q_9,\ d_{96} = -q_9,$$
$$d_{97} = q_{10},\ d_{98} = -q_{10}$$
$$d_{99} = \overline{q}_7,\ d_{910} = \overline{q}_8,\ d_{911} = \overline{q}_9,\ d_{912} = \overline{q}_{10}$$
$$d_{101} = \Omega_3',\ d_{102} = \Omega_3',$$
$$d_{103} = \Omega_4',\ d_{104} = \Omega_4'$$
$$d_{109} = -\overline{\Omega}_3',\ d_{1010} = -\overline{\Omega}_4',$$
$$d_{111} = q_{11},\ d_{112} = q_{12}$$
$$d_{113} = q_{13},\ d_{114} = q_{14},\ d_{119} = -\overline{q}_{12},$$
$$d_{1110} = -\overline{q}_{14}$$
$$d_{121} = q_{11} e^{-m_3 H}, d_{122} = q_{12} e^{m_3 H},$$
$$d_{123} = q_{13} e^{-m_4 H},\ d_{124} = q_{14} e^{m_4 H}$$

(53b)

Equation (52) determines the wave velocity equation for the Rayleigh waves in a thermoelastic granular medium under initial stress.

V. Numerical Results and Discussion

The transcendental equation (52), in the determinant form, has complex roots. The real part gives the velocity of Rayleigh waves and the imaginary part gives the attenuation due to the granular nature of the medium. It is clear from (52) that the phase velocity depends on the initial stress p, the fraction F and the coupling factor ε.

Numerical results have been obtained graphically to show the effect of the initial stress on the frequency w through the wave number k of the frequency equation.

The results of the present investigation are displayed in Figures 1-16. The basic material properties are taken:

$\lambda = 7.76\text{x}10^{10}$, $\mu = 3.86\ \text{x}10^{10}$, $m_0 = 0.1$, $f_0 = 0.4$, $C_e = 383.1$,

$H = 0.9$, $\alpha_t = 1.78\text{x}10^{-5}$, $s_0 = f_0 / m_0$, $\rho_0 = 8954$, $T_0 = 293$

Harmonic vibrations have been studied using a half-interval method. The governing equations are recorded for future reference. The frequency equations have been obtained under the effect of initial stress for two cases coupled problem ($\varepsilon \neq 0$) and uncoupled problem ($\varepsilon = 0$). It is found that the frequency decreases and increases with increasing k for all cases. It should be pointed out that since the frequency equations; there are an infinite number of frequencies for each class of vibration. For a given geometry and elastic constants of the half-space, the frequency equations are essentially an implicit transcendental equations of the frequency parameter w boundary conditions. Figures 1-16 depict the variation of frequencies w along the wave number k of the half-space with different values of the initial stress P. It is seen easily from all figures that the frequencies satisfy the physical phenomena. Figures 1-4 show that when P increases the frequencies w are decreasing.

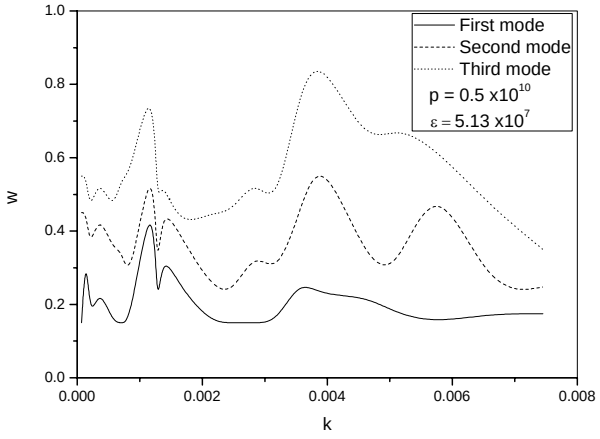

Fig. 1. Non-dimensional frequency w versus the wave number k of non-homogeneous material for $p = 0.5\text{x}10^{10}$ and $\varepsilon = 5.13\text{x}10^{7}$

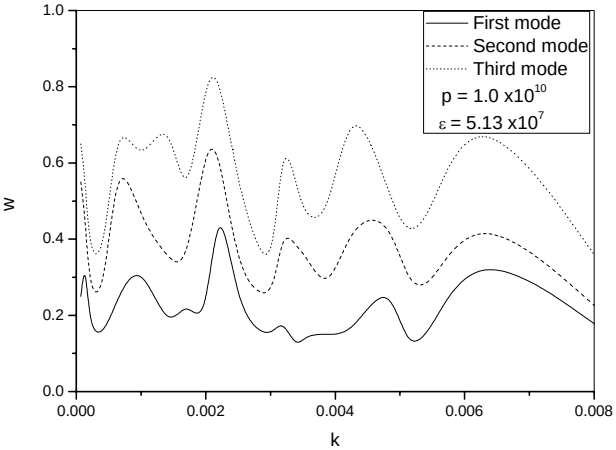

Fig. 2. Non-dimensional frequency w versus the wave number k of non-homogeneous material for $p = 1.0\text{x}10^{10}$ and $\varepsilon = 5.13\text{x}10^{7}$

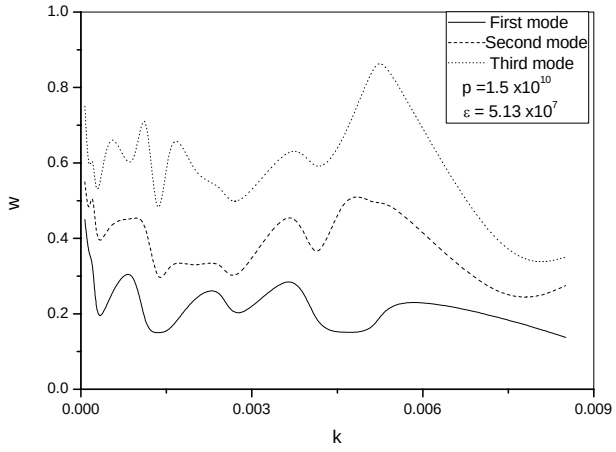

Fig. 3. Non-dimensional frequency w versus the wave number k of non-homogeneous material for $p = 1.5x10^{10}$ and $\varepsilon = 5.13x10^{7}$

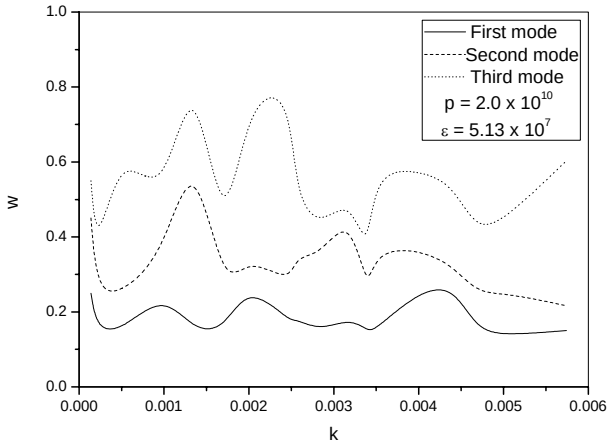

Fig. 4. Non-dimensional frequency w versus the wave number k of non-homogeneous material for $p = 2.0x10^{10}$ and $\varepsilon = 5.13x10^{7}$

Moreover, the non dimensional frequency is greatly affected by the initial stress of the half-space for the coupled problem. Figures 5-8 show that the effect of initial stress on the frequency *w*.

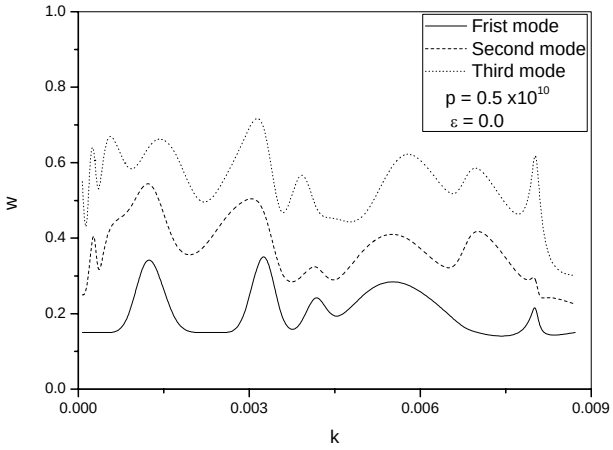

Fig. 5. Non-dimensional frequency w versus the wave number k of non-homogeneous material for $p = 0.5x10^{10}$ and $\varepsilon = 0.0$

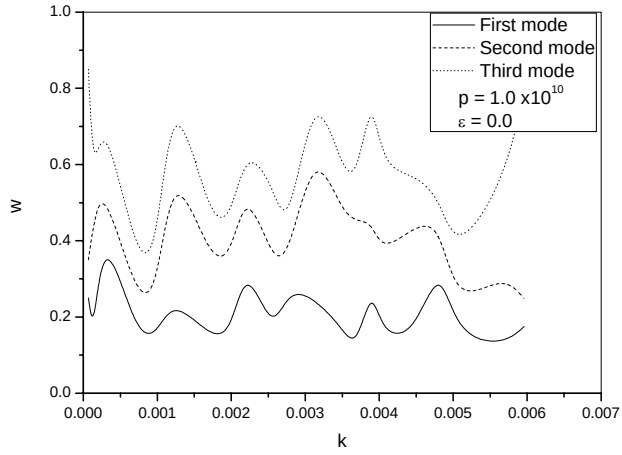

Fig. 6. Non-dimensional frequency w versus the wave number k of non-homogeneous material for $p = 1.0x10^{10}$ and $\varepsilon = 0.0$

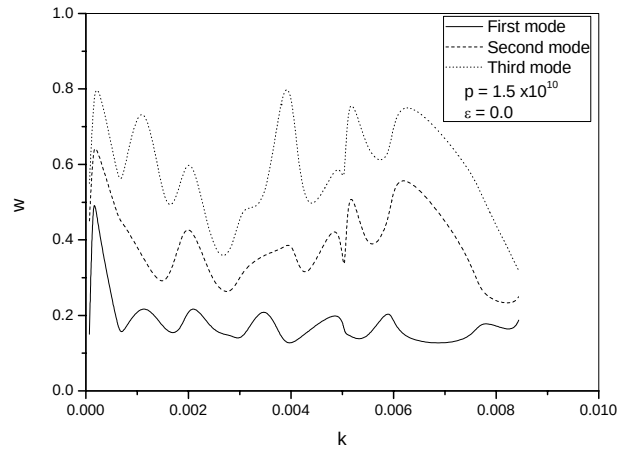

Fig. 7. Non-dimensional frequency w versus the wave number k of non-homogeneous material for $p = 1.5x10^{10}$ and $\varepsilon = 0.0$

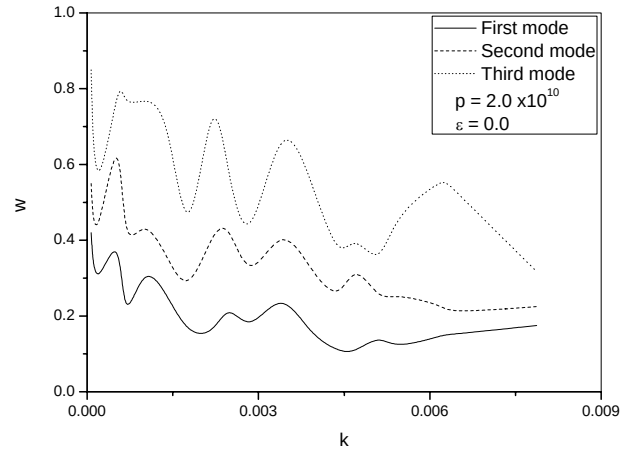

Fig. 8. Non-dimensional frequency w versus the wave number k of non-homogeneous material for $p = 2.0x10^{10}$ and $\varepsilon = 0.0$

It is seen easily from all Figures 5-8 show that the frequencies are decreasing and increasing with increasing the wave number *k*. It is also shown that the non dimensional frequencies w decreases when the initial stress increases for uncoupled problem.

Figures 9-12 show that the frequency w at $\varepsilon \neq 0$ greater than the frequency at $\varepsilon = 0$.

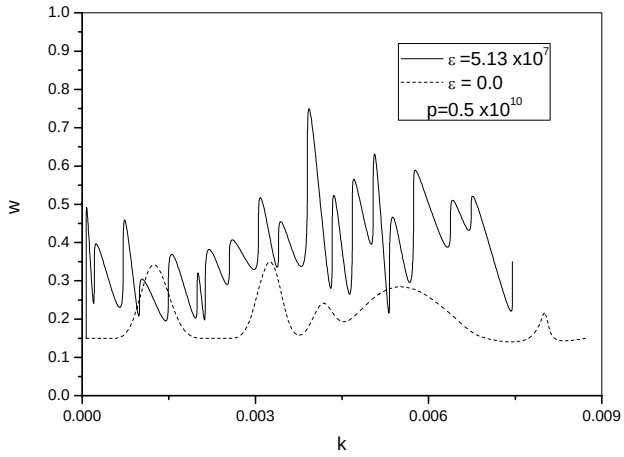

Fig. 9. Non-dimensional frequency w versus the wave number k of non-homogeneous material for $\varepsilon \neq 0.0$ and $\varepsilon = 0.0$ at $p = 0.5 \times 10^{10}$

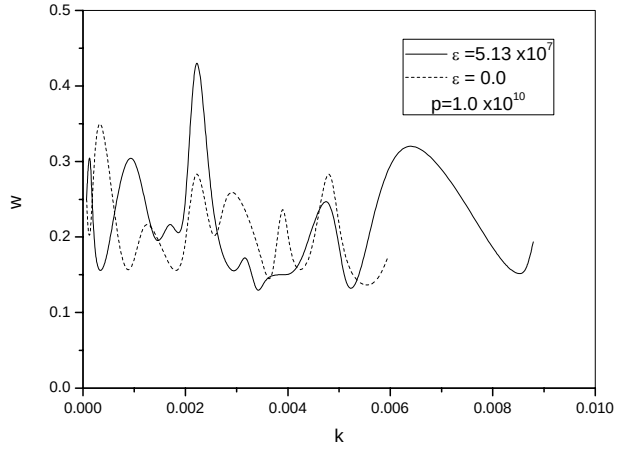

Fig. 10. Non-dimensional frequency w versus the wave number k of non-homogeneous material for $\varepsilon \neq 0.0$ and $\varepsilon = 0.0$ at $p = 1.0 \times 10^{10}$

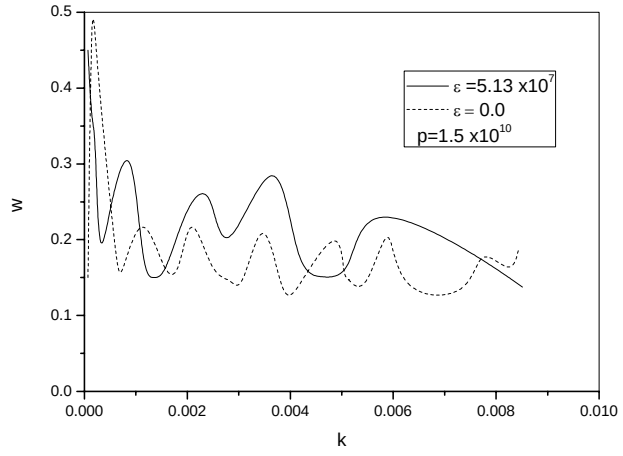

Fig. 11. Non-dimensional frequency w versus the wave number k of non-homogeneous material for $\varepsilon \neq 0.0$ and $\varepsilon = 0.0$ at $p = 1.5 \times 10^{10}$

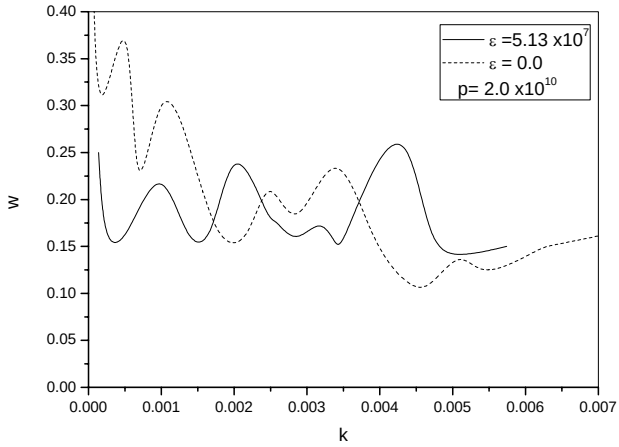

Fig. 12. Non-dimensional frequency w versus the wave number k of non-homogeneous material for $\varepsilon \neq 0.0$ and $\varepsilon = 0.0$ at $p = 2.0 \times 10^{10}$

Figures 13-16 show that the variation of the frequency w for different values of initial stress at $\varepsilon \neq 0$ and at $\varepsilon = 0$.

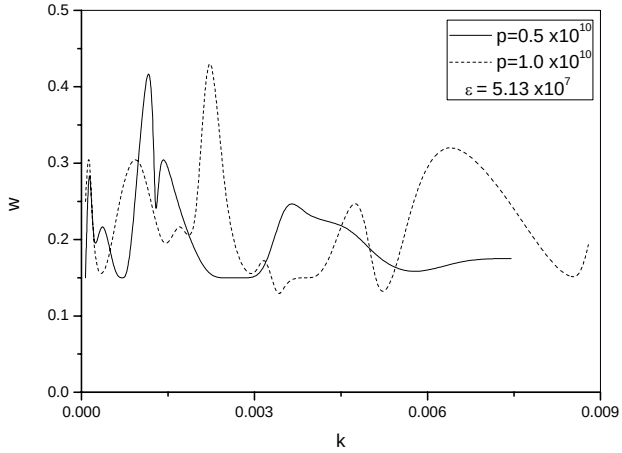

Fig. 13. Non-dimensional frequency w versus the wave number k of non-homogeneous material for $p = 0.5 \times 10^{10}$ and $p = 1.0 \times 10^{10}$ at $\varepsilon \neq 0.0$

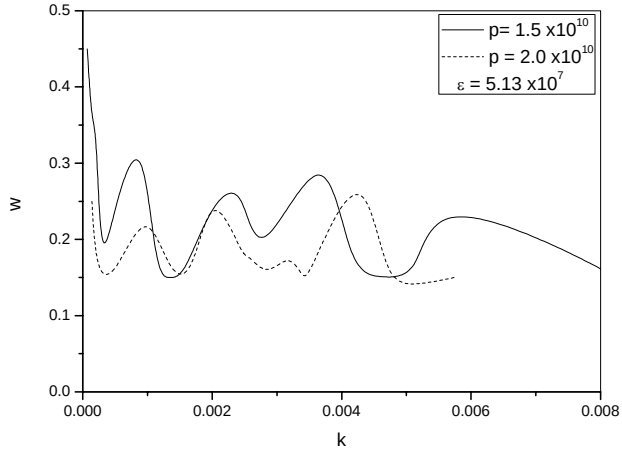

Fig. 14. Non-dimensional frequency w versus the wave number k of non-homogeneous material for $p = 1.5 \times 10^{10}$ and $p = 2.0 \times 10^{10}$ at $\varepsilon \neq 0.0$

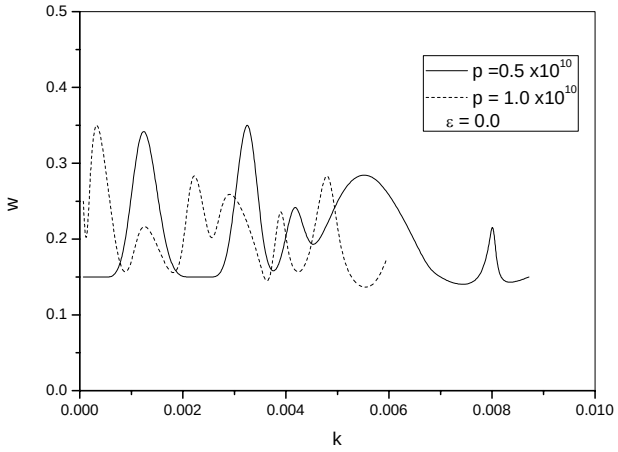

Fig. 15. Non-dimensional frequency w versus the wave number k of non-homogeneous material for p = $0.5x10^{10}$ and p =$1.0x10^{10}$ at ε = 0.0

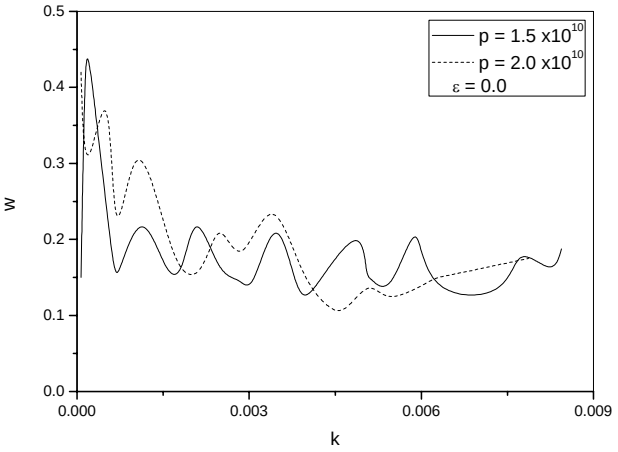

Fig. 16. Non-dimensional frequency w versus the wave number k of non-homogeneous material for p = $1.5x10^{10}$ and p =$2.0x10^{10}$ at ε = 0.0

It is seen from the results, that initial stress of the half-space have significant effects on the free vibration frequency of embedded half-space. This may be of great importance in structural design of practical engineering. Especially, in the areas that have server restrictions on the dynamics of the structures, the results of this example illustrate that new types material may provide such demanded conditions.

VI. Conclusion

The exact solution for half-space subjected to initial stress and thermal stress is obtained. Harmonic vibrations of elastic half-space have been studied using a half-interval method. The governing equations in Cartesian coordinates are recorded for future reference. The frequency equations have been obtained under the effect of initial stress, thermal stress and mechanical coupled parameter ε. Variation of the frequencies w with the wave number have been shown graphically and they are compared in the absence of initial stress. In addition, the formulation of the method is quite straightforward, and the bulk of the computational effort can be completed numerically. The results presented in this paper should prove useful for researchers in material science, designers of new materials as well as for those working on the development of theory elasticity.

References

[1] Oshima, N., (1955), A symmetrical stress tensor and its application to a granular medium, *Proceedings of the 3 rd Japan National congress for Applied Mechanics* **77**, pp.77-83.

[2] El-Naggar, A. M., (1992), On the dynamical problem of a generalized thermoelastic granular infinite cylinder under initial stress, *Astrophysics and Space Science* **190**(2), pp. 177–190.

[3] Dawan, N. C., Chakraporty, S. K., (1998), On Rayleigh waves in Green–Lindsay model of generalized thermoelastic media, *Indian Journal Pure and Applied Mathematics* **20**, pp. 276–283.

[4] Abd-Alla, A. M., Hammad, H. A. H., Abo-Dahab, S. M., (2004), Rayleigh waves in a magnetoelastic half-space of orthotropic material under influence of initial stress and gravity field, *Applied Mathematics and Computation* **154**, pp. 583–597.

[5] El-Naggar, A. M., Abd-Alla, A. M., Ahmed, S. M., (1994), Rayleigh waves in a magnetoelastic initially stressed conducting medium with the gravity field, *Bulletin of the Calcutta Mathematical Society* **86**, pp. 51–56.

[6] Ahmed, S. M., (2000), Rayleign wave s in a thermoelastic granular medium under initial stress, *International Journal of Mathematics and Mathematical Science* **23**(9), pp. 627 –637.

[7] Abd-Alla, A. M., and Ahmed, S. M., (1998), Rayleigh waves in an orthotropic thermoelastic medium under gravity and initial stress, *Earth, Moon and Planets* **75**, pp. 185–197.

[8] Abd-Alla, A. M, Mahmoud, S. R, (2010), Magneto-thermoelastic problem in rotating non-homogeneous orthotropic hollow cylinder under the hyperbolic heat conduction model, *Meccanica* **45**, pp. 451-462.

[9] Venkatesan, M., Ponnusamy, P., (2007), Wave propagation in a generalized thermoelastic solid cylinder of arbitrary cross-section immersed in a fluid, *International Journal of Mechanical Sciences* **49**, pp. 741-751.

[10] Roychoudhuri, S. K., Bandyopadhyay, N., (2003), Thermoelastic wave propagation in a rotating elastic medium without energy dissipation, *Int. J. Math& Math. Sci.* **1**, pp. 99-107.

[11] Sharma, J. N., Grrover, D., (2009), Body wave propagation in rotating thermoelastic media, *Mech. Res. Comm*, **36**, pp. 715-721.

[12] El-Naggar, A. M., Abd-Alla, A. M., Fahmy, M. A., Ahmed, S. M., (2003), Thermal stresses in a rotating non-homogeneous orthotropic hollow cylinder, *Heat and Mass transfer*, **39**, pp. 41-46.

[13] Abd-Alla, A. M., Abd-El-Salam, M. R., Hosham, H. A., (2007), Numerical solution of Magneto-thermoelastic problem Non-homogeneous isotropic material, *J. of Applied Mathematical Modelling* **31**, pp. 1662-1670.

[14] Abd-Alla, A.M., (1999), Propagation of Rayleigh waves in an elastic half-space of orthotropic material, *Applied Mathematics and Computation* **99**, pp. 61-619.

[15] Abd-Alla, A. M, Abo-Dahab, S. M, Hammad, H. A, Mahmoud, S. R., (2011), On generalized magneto-thermoelastic Rayleigh waves in a granular medium under the influence of agravity field and initial stress, *Journal of Vibration and Control* **17**(1), pp. 115–128.

[16] Nowacki, W., (1962), *Thermoelasticity*, Addison-Wesely Publishing Company, Inc. London.

Authors' information

[1]Physics Department Faculty of Science Taif University- K.S.A.

[2]Physics Department Faculty of Science in Aswan Sauth Valley University- Egypt.

Praise Worthy Prize

International Review of Physics (I.R.E.PHY.), Vol. 5, N. 6
December 2011

Magnetic Field and Relaxation Times Effects on the Propagation of Thermoelastic Waves from Isothermal or Insulated Boundaries of a Half Space

S. M. Abo-Dahab[1], R. A. Mohamed[2], A. M. Abd-Alla[3]

Abstract – *In the present paper, an estimation to study effects of the relaxation times and magnetic field on the reflection of P-wave and SV-wave on the boundary of a half-space of homogeneous, isotropic thermoelastic medium taking into our consideration the boundary is stress-free as well as insulated or isothermal.* ***GL*** *model of generalized thermoelasticity has been applied to obtain the amplitudes of the Reflection coefficients. Lame's potentials are used in the two dimensions oxz that tend to separate the governing equations into three equations that sought in harmonic travelling form. We introduce the equations of the velocity of P-wave, T-wave and SV-wave. The boundary conditions for mechanical and Maxwell's stresses and thermal insulated or isothermal are applied to determine the reflection coefficients for P-wave, T-wave and SV wave. Some new aspects are obtained of the reflection coefficients and displayed graphically and the new conclusions are presented. Effects of relaxation times and magnetic field on the reflection of generalized thermoelastic waves are noticed and depicted graphically. Finally, it is shown that, under some conditions and some modifications, the previous results are special cases from our results.*

Keywords*: Magnetic Field, Reflection, Half Space, P-Wave, T-Wave, SV-Wave, Relaxation Times, Isothermal Boundaries, Insulated Surface*

Nomenclature

$\vec{B}$	Is the magnetic induction
C_v	Is the specific heat per unit mass
$\vec{F}$	Is Lorenz's body forces
$\vec{h}$	Is the perturbed magnetic field
h_i	Are the components of heat flux tensor
H_o	Is constant magnetic field
$\vec{J}$	Is the electric current density
k	Is the wave number
K	Is the thermal coductivity
k_T	Is the isothermal
t	Is the time
T	Is the absolute temperature
T_0	Is the natural temperature of the medium, $\left\|\frac{T-T_0}{T_0}\right\| \ll 1$
u_i	Are the components of the displacement tensor
v	Is the phase speed
α_t	Is the thermal expansion
γ	$=\alpha_t(3\lambda+2\mu)$
δ_{ij}	Is Kronecker delta
λ and μ	Are Lame's parameters
μ_e	Is the magnetic permeability
σ_{ij}	Are the components of stress tensor
τ_0, τ_1	Are the thermal relaxation times
τ_{ij}	Are the Maxwell's stress tensor
ω	Is the frequency
ℓ	Is the standard length

I. Introduction

Recently, more attentions has made for the theory of thermoelasticity because of its utilitarian aspects in diverse fields, especially, Structures, Biology, Geology, Geophysics, Acoustics, Physics, Plasma, etc. Duhamel [1] and Neumann [2] introduced the theory of uncoupled thermoelasticity which contain two shortcomings. First, the fact that the mechanical state of the elastic body has no effect on the temperature, is not in accordance with true physical experiments. Second, the heat equation being parabolic predicts an infinite speed of propagation for the temperature, which is not physically admissible. The theory of elasticity with nonuniform heat which was in half-space subjected of thermal shock in this context which known as the theory of uncoupled thermoelasticity and the temperature is governed by a parabolic partial

Manuscript received and revised November 2011, accepted December 2011

differential equation in temperature term only has been discussed [3]. Biot [4] introduced the theory of classical thermoelasticity, the equation of motion is hyperbolic in nature, whereas the heat conduction equation is parabolic in nature; the theory predicts a finite speed for predominantly elastic disturbances but an infinite speed for predominantly thermal disturbances, which are coupled together. Obviously, this result is physically unrealistic, so, [5]-[11] made an experimental investigations conducted on various solids, for example, have shown that heat pulses do propagate with finite speed. These theories remove the paradox of infinite speed of heat propagation inherent in the conventional coupled dynamical theory of thermoelasticity introduced by Biot [4]. Lord and Shulman [12], have discovered the theory which determines the finite speed for the motion due to thermal field using one relaxation time. By including temperature rate, Green and Lindsay [13] violated the classical Fourier's law of heat conduction when the body under consideration has a center of symmetry. This theory also predicts a finite speed of heat propagation using two relaxation times. This implies that the thermal wave propagates with infinite speed, a physically impossible result.

During the second half of twentieth century, nonisothermal problems of the theory of elasticity became increasingly impact. This is due mainly to their many applications in widely diverse fields. First, in the nuclear field, the external high temperatures and temperature gradients originating inside nuclear reactors influence their design and operations. Secondly, the high velocities of modern aircraft give rise to aerodynamic heating, which produces intense thermal stresses, reducing the strength of the aircraft structure [14]. Nowacki [15] investigated the dynamic problems of thermoelasticity. Some problems of thermoelasticity are discussed [16]-[17]. Three different models of thermoelasticity in an alternative way have been discussed including the anisotropic case [18]. A survey article of representative theories in the range of generalized thermoelasticity is due to Hetnarski and Ignaczak [19].

In recent years, the theory of magneto-thermoelasticity which deals the interactions among strain, temperature and electromagnetic fields has drawn the attention of many researchers because of its extensive uses in diverse fields, such as Geophysics for understanding the effect of the Earth's magnetic field on seismic waves, damping of acoustic waves in a magnetic field, emission of electromagnetic radiations from nuclear devices, development of a highly sensitive superconducting magnetometer, electrical power engineering, optics, etc. Knopoff [20] and Chadwick [21] studied these types of problems in the beginning and developed by Kaliski and Petykiewicz [22].

The generalized magneto-thermoelasticity in a perfectly conducting medium is investigated [23]. Baksi et al. [24] illustrate magneto-thermoelastic problems with thermal relaxation and heat sources in a three dimensional infinite rotating elastic medium.

[25]-[27] studied the reflection of thermoelastic waves from the free surface of a solid half-space and at the interface of two semi-infinite media in welded contact, in the context of generalized thermoelasticity. Sharma et al. [28] considered the titled problem of reflection of thermoelastic waves at (i) a stress free thermally insulated/isothermal boundary (ii) a rigidly fixed thermally insulated/isothermal boundary for LS, GL and GN models for generalized thermoelasticity and calculated the coefficient ratios. The ratios of (i) reflected P-wave, SV-wave and thermal wave with incident P-wave; as also the ratios of (ii) reflected SV-wave, P-wave, and thermal wave with incident SV-wave are calculated in terms of the roots of two auxiliary equations governing the partial differential equations of the field variables. Montanaro [29] investigated an isotropic linear thermoelasticity with hydrostatic initial stress. Abd-Alla et al. [30] studied the reflection of the generalized magneto-thermo-viscoelastic plane waves. Abo-Dahab and Mohamed [31] pointed out the influence of magnetic field and hydrostatic initial stress on reflection phenomena of P and SV waves from a generalized thermoelastic solid half-space. Singh [32] investigated the reflection of P and SV waves from free surface of an elastic solid with generalized thermodiffusion. Singh et al. [33] discussed the reflection of generalized thermoelastic waves from a solid half-space under hydrostatic initial stress. Recently, Das et al. [34] investigated the reflection of generalized thermoelastic waves from isothermal and insulated boundaries of a half space; the paper has some modifications by the author of the present paper.

In this paper, we have investigated the influences of the magnetic field, thermal relaxation times on the reflection of thermoelastic waves from isothermal and insulated boundaries of a half space using **GL** model. Lame's potentials used in the (x-z) plane. We obtain the equations of the velocity of P-wave, T-wave and SV-wave. The boundary conditions for mechanical and Maxwell's stresses and thermal isothermal and insulated are applied to determine the reflection coefficients for P-wave, T-wave and SV-wave. The numerical example is used to discuss the dependence of reflection coefficients upon thermal relaxation times, magnetic field and angle of incidence for P-wave and SV-wave. Finally, the amplitudes ratios of the reflection coefficients have been calculated and displayed graphically.

II. Formulation of the Problem and Governing Equations

Consider the rectangular Cartesian coordinate system be fixed at a point on the boundary of the half-space with $z > 0$ axis directed normally inside the medium with $x-$ axis along the horizontal direction $y-$ axis is taken in the direction of the line of intersection of the plane wave front with the plane surface (as in Fig. 1). If we restrict our analysis to plane strain in the (x-z) plane, then all the field variables may be taken as functions of $x; z$ and t,

hence the displacement vector may be taken $\left(u\left(x,z,t\right),0,w\left(x,z,t\right)\right)$ and the magnetic field must be taken in a perpendicular direction on the plane motion, i.e., $\vec{H} = H_y$.

The governing equations for an isotropic, homogeneous elastic solid with generalized thermoelastic at reference temperature T_0 with the body forces are:

(i) the constitutive equation:

$$\sigma_{ij} = \left[\lambda e_{kk} - \gamma\left(1+\tau_1\frac{\partial}{\partial t}\right)T\right]\delta_{ij} + 2\mu e_{ij} \tag{1}$$

$$e_{ij} = \frac{1}{2}\left(\frac{\partial u_i}{\partial x_j} + \frac{\partial u_j}{\partial x_i}\right) \tag{2}$$

(ii) Maxwell electromagnetic stress τ_{ij} is given by:

$$\tau_{ij} = \mu_e\left[H_i h_j + H_j h_i - H_k\cdot h_k\delta_{ij}\right] \tag{3}$$

(iii) the equation of motion:

$$\sigma_{ji,j} + F_i = \rho\ddot{u}_i \tag{4}$$

which tends to:

$$\mu u_{i,jj} + \left(\lambda+\mu\right)u_{j,ij} - \gamma\left(1+\tau_1\frac{\partial}{\partial t}\right)T_{,i} + F_i = \rho\ddot{u}_i \tag{5}$$

where:

$$\vec{F} = \vec{J}\times\vec{B} \tag{6}$$

Consider that the medium is a perfect electric conductor, we take the linearized Maxwell equations governing the electromagnetic field, taking into account absence of the displacement current (**SI**) as the form [35]:

$$curl\vec{h} = \vec{J} \tag{7a}$$

$$curl\vec{E} = -\mu_e\frac{\partial\vec{h}}{\partial t} \tag{7b}$$

$$div\vec{h} = 0 \tag{7c}$$

$$div\vec{E} = 0 \tag{7d}$$

where:

$$\vec{h} = curl\left(\vec{u}\times\vec{H}_o\right) \tag{8}$$

where we have used:

$$\vec{H} = \vec{H}_o + \vec{h}$$

the constant primary magnetic field $\vec{H}_o$ acting on y direction:

(iv) the equation of heat conduction:

$$K\vec{\nabla}^2 T = \rho C_v\left(1+\tau_0\frac{\partial}{\partial t}\right)\dot{T} + \gamma T_o\vec{\nabla}\cdot\left(1+\tau_0\delta_{ij}\frac{\partial}{\partial t}\right)\dot{\vec{u}} \tag{9}$$

which tends to:

$$KT_{,kk} = \rho C_v\left(1+\tau_0\frac{\partial}{\partial t}\right)\dot{T} + \gamma T_o\vec{\nabla}\cdot\left(1+\tau_0\delta\frac{\partial}{\partial t}\right)\dot{e}_{kk} \tag{10}$$

For **GL** model, the relaxation times τ_o and τ_1 satisfy the inequality $\tau_0 \geqslant \tau_1 > 0$, $\delta = 0$.

For two-dimensional motion in (x-z) plane, the equations (5) and (10) can be written as:

$$\left(\lambda+2\mu+\mu_e H_o^2\right)u_{1,11} + \left(\lambda+\mu+\mu_e H_o^2\right)u_{3,13} + \mu u_{1,33} - \gamma\left(1+\tau_1\frac{\partial}{\partial t}\right)T_{,1} = \rho\ddot{u}_1 \tag{11}$$

$$\left(\lambda+2\mu+\mu_e H_o^2\right)u_{3,33} + \left(\lambda+\mu+\mu_e H_o^2\right)u_{1,31} + \mu u_{3,11} - \gamma\left(1+\tau_1\frac{\partial}{\partial t}\right)T_{,3} = \rho\ddot{u}_3 \tag{12}$$

$$K\left(\frac{\partial^2 T}{\partial x^2} + \frac{\partial^2 T}{\partial z^2}\right) = \rho C_v\left(1+\tau_0\frac{\partial}{\partial t}\right)\frac{\partial T}{\partial t} + \gamma T_0\frac{\partial}{\partial t}\left(\frac{\partial u}{\partial x} + \frac{\partial w}{\partial z}\right) \tag{13}$$

To transform the equations (11)-(13) into non-dimensional form, we take the following dimensionless form:

$$T' = \frac{T}{T_0},\quad \tau_0' = \frac{v}{\ell}\tau,\quad \tau_1' = \frac{v}{\ell}\tau_1,\quad t' = \frac{v}{\ell}t,\quad u' = \frac{\left(\lambda+2\mu+\mu_e H_o^2\right)u}{\ell\gamma T_0} \tag{14a}$$

$$x' = \frac{x}{\ell}, \quad z' = \frac{z}{\ell}, w' =, \frac{\left(\lambda + 2\mu + \mu_e H_o^2\right) w}{\ell \gamma T_0}$$
$$\sigma'_{ij} = \frac{\sigma_{ij}}{\gamma T_0}, \qquad \tau'_{ij} = \frac{\tau_{ij}}{\gamma T_0} \tag{14b}$$

Substituting from equations (14) into equations (11)-(13) and suppressing the primes, we obtain:

$$C_2^2 \nabla^2 \vec{u} + \left(C_1^2 - C_2^2\right) \vec{\nabla}\left(\vec{\nabla} \cdot \vec{u}\right) + \\ -C_1^2 \left(1 + \tau_1 \frac{\partial}{\partial t}\right) \vec{\nabla} T = \frac{\partial^2 \vec{u}}{\partial t^2} \tag{15}$$

$$C_3^2 \nabla^2 T - \left(1 + \tau_0 \frac{\partial}{\partial t}\right) \dot{T} - \in \vec{\nabla} \cdot \ddot{\vec{u}} = 0 \tag{16}$$

$$\sigma_{ij} = \left[\left(1 - 2\frac{C_2^2}{C_1^2}\right) \vec{\nabla} \cdot \vec{u} - \left(1 + \tau_1 \frac{\partial}{\partial t}\right) T\right] \delta_{ij} + 2\frac{C_2^2}{C_1^2} e_{ij} \tag{17}$$

where:

$$C_1^2 = \frac{\lambda + 2\mu + \mu_e H_o^2}{\rho \upsilon^2}, \quad C_2^2 = \frac{\mu}{\rho \upsilon^2}, \\ C_3^2 = \frac{K}{\rho C_v \upsilon^2}, \quad \in = \frac{\gamma^2 T_0}{\lambda + 2\mu + \mu_e H_o^2} \tag{18}$$

The displacement components u_1 and u_3 may be written in terms of scaler and vector potential functions ϕ and ψ respectively as follow:

$$\vec{u} = \vec{\nabla} \phi + \vec{\nabla} \times \vec{\psi} \tag{19}$$

which take the form:

$$u_1 = \frac{\partial \phi}{\partial x} - \frac{\partial \psi}{\partial z}, \qquad u_3 = \frac{\partial \phi}{\partial z} + \frac{\partial \psi}{\partial x} \tag{20}$$

Substituting from equations (20) into equations (15)-(17), we get:

$$\nabla^2 \phi - \left(1 + \tau_1 \frac{\partial}{\partial t}\right) \dot{T} - \frac{\ddot{\phi}}{C_1^2} = 0 \tag{21}$$

$$\nabla^2 \vec{\psi} = \frac{\ddot{\vec{\psi}}}{C_2^2} \tag{22}$$

$$C_3^2 \nabla^2 T - \left(1 + \tau_0 \frac{\partial}{\partial t}\right) \dot{T} - \in \nabla^2 \dot{\phi} = 0 \tag{23}$$

From equations (21)-(23) we see that SV-wave does not affect by the thermal and magnetic fields but P-wave has been affectd. The solution of equation (22) corresponds to the propagation of SV-wave with velocity C_3.

For plane P-wave,T-wave and SV-wave, respectively, in x-z plane (as shown in Fig. 1) of a linear isotropic homogeneous thermoelastic solid with influence of magnetic field we have.

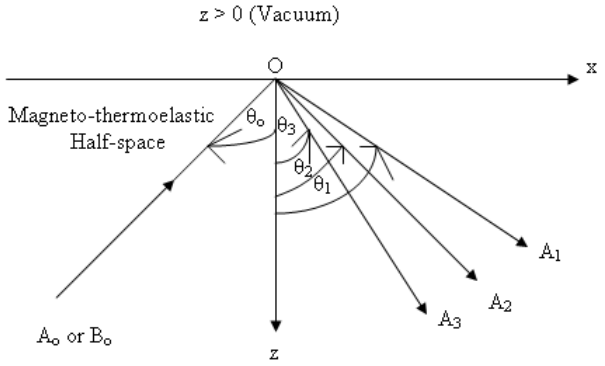

Fig. 1. Schematic of the problem

Eliminating the temperature from equations (21) and (23), one may obtain:

$$C_1^2 C_3^2 \nabla^4 \phi - \left[\begin{array}{l} C_1^2 \left(1 + \tau_0 \frac{\partial}{\partial t}\right) + \\ + \in \left(1 + \tau_1 \frac{\partial}{\partial t}\right) + C_3^2 \end{array}\right] \cdot \\ \cdot \nabla^2 \dot{\phi} + \left(1 + \tau_0 \frac{\partial}{\partial t}\right) \ddot{\phi} = 0 \tag{24}$$

choosing $\vec{\psi} = (0, \psi, 0)$, then equation (22) tends to:

$$\nabla^2 \psi = \frac{\ddot{\psi}}{C_2^2} \tag{25}$$

For analytical solution of equation (24) in the form of the harmonic travelling wave, we suppose that the solution takes the form:

$$\phi = A e^{i\left[k(x \sin\theta - z \cos\theta) - \omega t\right]} \tag{26}$$

where, A is arbitrary constant and $(\sin\theta, \cos\theta)$ denotes the projection of the wave normal onto xz-plane.

Substitute equation (26) into equation (24), one obtain:

$$C_1^2 C_3^2 k^4 - \left[C_1^2 \tau_0 + \in \tau_1' + C_3^2\right] \omega k^2 + \tau_0 \omega^3 = 0 \tag{27}$$

where:

$$\tau_0' = 1 - i\omega\tau_0, \qquad \tau_1' = 1 - i\omega\tau_1$$

Solving equation (27), one may obtain the roots k_1^2 and k_2^2 as follow:

$$k_1^2 = p^2\omega \quad \text{and } k_2^2 = q^2\omega \tag{28}$$

where:

$$p^2, q^2 = \frac{1}{2C_1^2C_3^2}\left[\left\{\left(\tau_0^{'} + \in \tau_1^{'}\right)C_1^2 + C_3^2 \pm \sqrt{M}\right\}\right] \tag{29}$$

$$M = \left\{\left(\tau_0^{'} + \in \tau_1^{'}\right)C_1^2 + C_3^2\right\}^2 - 4\tau_0^{'}C_1^2C_3^2\omega \tag{30}$$

where, k_1^2 and k_2^2 indicate to modified longitudinal $P-$wave and a thermal $T-$wave respectively.

The solution of equation (25) takes the form:

$$\psi = Be^{ik_3\left[\left(x\sin\theta - z\cos\theta\right) - \omega t\right]} \tag{31}$$

where:

$$k_3^2 = \frac{\omega^2}{C_2^2} \tag{32}$$

III. Case I: Plane P-Wave Incident Upon a Plane Surface

Due to the existing of three waves reflected from incident P-wave or SV-wave as shown in Fig. 1, we take into our consideration, if the wave normal of the incident wave makes angle θ_o with the negative direction of z-axis, and those of reflected P, T and SV-waves make $\theta_1, \theta_2, \theta_3$, also with $z-$axis, the displacement potentials ϕ and ψ and temperature T take the following forms:

$$\begin{aligned}\phi = {} & A_o\, exp\left[ik_1\left(x\sin\theta_o - z\cos\theta_o\right) - i\omega t\right] + \\ & + A_1\, exp\left[ik_1\left(x\sin\theta_1 + z\cos\theta_1\right) - i\omega t\right] + \\ & + A_2\, exp\left[ik_2\left(x\sin\theta_2 + z\cos\theta_2\right) - i\omega t\right]\end{aligned} \tag{33}$$

$$\begin{aligned}T = {} & \xi_o A_o\, exp\left[ik_o\left(x\sin\theta_o - z\cos\theta_o\right) - i\omega t\right] + \\ & + \xi_1 A_1\, exp\left[ik_1\left(x\sin\theta_1 + z\cos\theta_1\right) - i\omega t\right] + \\ & + \xi_2 A_2\, exp\left[ik_2\left(x\sin\theta_2 + z\cos\theta_2\right) - i\omega t\right]\end{aligned} \tag{34}$$

$$\psi = B_1\, exp\left[ik_3\left(x\sin\theta_3 + z\cos\theta_3\right) - i\omega t\right] \tag{35}$$

where:

$$\begin{aligned}\xi_o &= \frac{1}{\tau_1^{'}}\left(\frac{\omega^2}{C_1^2} - k_2^2\right) = \frac{k_2^2}{\tau_1^{'}}\left(\frac{1}{C_1^2q^2} - 1\right), \\ \xi_1 = \xi_2 &= \frac{1}{\tau_1^{'}}\left(\frac{\omega^2}{C_1^2} - k_1^2\right) = \frac{k_1^2}{\tau_1^{'}}\left(\frac{1}{C_1^2p^2} - 1\right)\end{aligned} \tag{36}$$

A_o is the amplitudes of incident P-waves and A_1, A_2 and B_1 are the amplitudes of reflected P, T and SV-waves, respectively.

The boundary conditions at the free surface (i.e., $z = 0$) take the form:

$$\begin{aligned}&\sigma_{zz} + \tau_{zz} = 0, \quad \sigma_{xz} + \tau_{xz} = 0, \quad \frac{\partial T}{\partial z} + hT = 0 \\ &at \quad z = 0\end{aligned} \tag{37}$$

For the reflected waves, the wave numbers and the angles of incidence and reflected may be written as:

$$k_1\sin\theta_o = k_1\sin\theta_1 = k_2\sin\theta_2 = k_3\sin\theta_3 \tag{38}$$

which takes the equivalent form:

$$\sin\theta_o = \sin\theta_1 = \frac{q}{p}\sin\theta_2 = \frac{1}{C_2p}\sin\theta_3 \tag{39}$$

III.1. Incident of P-Wave at a Stress-Free Thermally Insulated Boundary $(h \to 0)$

From equations (1)-(3) and (33)-(35) into the boundary conditions in equation (37), we obtain a system of three algebraic equations take the forms:

$$\sum A_{ij}X_j = D_i, \quad (i, j = 1, 2, 3) \tag{40}$$

where:

$$\begin{aligned}A_{11} &= \frac{q^2}{p^2}\left[2\delta^2\sin^2\theta_2 - 1 + \tau_1^{'}\left(1 - \frac{1}{C_1^2q^2}\right)\right], \\ A_{12} &= 2\delta^2\sin^2\theta_1 - 1 + \tau_1^{'}\left(1 - \frac{1}{C_1^2p^2}\right)\end{aligned} \tag{41a}$$

$$\begin{aligned}A_{13} &= -\frac{\delta^2}{C_2^2p^2}\sin 2\theta_3, \\ A_{21} &= \frac{q^2}{p^2}\sin 2\theta_2, \\ A_{22} &= \sin 2\theta_1, \quad A_{23} = \frac{-1}{C_2^2p^2}\cos 2\theta_3\end{aligned} \tag{41b}$$

$$A_{31} = \frac{q^3}{p^3}\left(\frac{1}{C_1^2 q^2} - 1\right)\cos\theta_2,$$
$$A_{32} = \left(\frac{1}{C_1^2 p^2} - 1\right)\cos\theta_1, \qquad A_{31} = 0 \tag{41c}$$

X_j and B_j for incident P-wave may be written as:

$$D_1 = -A_{12}, \qquad D_2 = A_{22}, \qquad D_3 = A_{32} \tag{42}$$

$$X_1 = \frac{A_1}{A_o}, \quad X_2 = \frac{A_2}{A_o}, \quad X_3 = \frac{B_1}{A_o} \tag{43}$$

Solving the equation (40), we obtain:

$$X_1 = \frac{2}{\Delta}\left[\begin{array}{l}\left(2\delta^2 \sin^2\theta_1 - 1 + \tau_1'\left(1 - \frac{1}{C_1^2 p^2}\right)\right)\cdot \\ \cdot\left(1 - \frac{1}{C_1^2 p^2}\right)\frac{\cos\theta_1 \cos 2\theta_3}{C_2^2 p^2}\end{array}\right]$$

$$X_2 = 1 - \frac{2}{\Delta}\left[\begin{array}{l}\left(\frac{q}{p}\right)^3\left(\frac{1}{C_1^2 q^2} - 1\right)\cdot \\ \cdot\left(\begin{array}{l}2\delta^2 \sin^2\theta_1 - 1 + \\ + \tau_1'\left(1 - \frac{1}{C_1^2 p^2}\right)\end{array}\right)\frac{\cos\theta_2 \cos 2\theta_3}{C_2^2 p^2}\end{array}\right]$$

$$X_3 = \frac{2}{\Delta}\left[\left(2\delta^2 \sin^2\theta_1 - 1 + \tau_1'\left(1 - \frac{1}{C_1^2 p^2}\right)\right)\right]\cdot$$
$$\cdot\left[\begin{array}{l}\left(\frac{q}{p}\right)^3\left(\frac{1}{C_1^2 q^2} - 1\right)\times\cos\theta_2 \sin 2\theta_1 + \\ -\left(\frac{q}{p}\right)^2\cdot\left(\frac{1}{C_1^2 p^2} - 1\right)\sin 2\theta_2 \cos\theta_1\end{array}\right]$$

where:

$$\Delta = \left(\frac{q}{p}\right)^3\left(\frac{1}{C_1^2 q^2} - 1\right)\cos\theta_2 \cdot$$
$$\cdot\left[-\frac{\cos 2\theta_3}{C_2^2 p^2}\left(\begin{array}{l}2\delta^2 \sin^2\theta_1 - 1 + \\ + \tau_1'\left(1 - \frac{1}{C_1^2 p^2}\right)\end{array}\right) + \frac{\delta^2 \sin 2\theta_1 \sin 2\theta_3}{C_2^2 p^2}\right] + \tag{44}$$
$$+\left(\frac{q}{p}\right)^2\left(\frac{1}{C_1^2 p^2} - 1\right)\cos\theta_1 \cdot$$
$$\cdot\left[-\frac{\sin 2\theta_2 \sin 2\theta_3}{C_1^2 p^2} + \left(\begin{array}{l}2\delta^2 \sin^2\theta_2 - 1 + \\ + \tau_1'\left(1 - \frac{1}{C_1^2 q^2}\right)\end{array}\right)\frac{\cos 2\theta_3}{C_2^2 p^2}\right]$$

III.2. Incident of P-Wave at a Stress-Free Isothermal Boundary $(h \to \infty)$

The solution of equation (40), the amplitudes ratios can be written as:

$$X_1 = \frac{2}{\Delta}\left[\begin{array}{l}\left(2\delta^2 \sin^2\theta_1 - 1 + \tau_1'\left(1 - \frac{1}{C_1^2 p^2}\right)\right) \\ \left(\frac{1 - C_1^2 p^2}{1 - C_1^2 q^2}\right)\cos 2\theta_3\end{array}\right],$$

$$X_2 = 1 + \frac{1}{\Delta}\left[\left(2\delta^2 \sin^2\theta_1 - 1 + \tau_1'\left(1 - \frac{1}{C_1^2 p^2}\right)\right)\cos 2\theta_3\right],$$

$$X_3 = \frac{2C_2^2 p^2}{\Delta}\left[\left(2\delta^2 \sin^2\theta_1 - 1 + \tau_1'\left(1 - \frac{1}{C_1^2 p^2}\right)\right)\right]\cdot$$
$$\cdot\left[\sin 2\theta_1 - \left(\frac{q}{p}\right)^2\left(\frac{1 - C_1^2 p^2}{1 - C_1^2 q^2}\right)\sin 2\theta_2\right],$$

$$\Delta = \left[\begin{array}{l}-\cos 2\theta_3\left(2\delta^2 \sin^2\theta_1 - 1 + \tau_1'\left(1 - \frac{1}{C_1^2 p^2}\right)\right) + \\ + \delta^2 \sin 2\theta_1 \sin 2\theta_3\end{array}\right] +$$
$$-\left(\frac{1 - C_1^2 p^2}{1 - C_1^2 q^2}\right)\left[\frac{\delta^2 q^2}{p^2}\sin 2\theta_2 \sin 2\theta_3 + \right. \tag{45}$$
$$\left. -\left(\frac{q}{p}\right)^2 \cos 2\theta_3\left(2\delta^2 \sin^2\theta_1 - 1 + \tau_1'\left(1 - \frac{1}{C_1^2 p^2}\right)\right)\right]$$

IV. Case II: Plane SV-Wave Incident Upon a Plane Surface

For incident SV-wave as shown in Fig. 1, the displacement potentials ϕ and ψ and temperature T take the following forms:

$$\phi = A_1 \exp\left[ik_1\left(x\sin\theta_1 + z\cos\theta_1\right) - i\omega t\right] + \\ + A_2 \exp\left[ik_2\left(x\sin\theta_2 + z\cos\theta_2\right) - i\omega t\right] \tag{46}$$

$$T = \xi_1 A_1 \exp\left[ik_1\left(x\sin\theta_1 + z\cos\theta_1\right) - i\omega t\right] + \\ + \xi_2 A_2 \exp\left[ik_2\left(x\sin\theta_2 + z\cos\theta_2\right) - i\omega t\right] \tag{47}$$

$$\psi = B_o \exp\left[ik_1\left(x\sin\theta_o - z\cos\theta_o\right) - i\omega t\right] + \\ + B_1 \exp\left[ik_3\left(x\sin\theta_3 + z\cos\theta_3\right) - i\omega t\right] \tag{48}$$

B_o is the amplitudes of incident SV-waves and A_1, A_2 and B_1 are the amplitudes of reflected P, T and $SV-$ waves, respectively.

For the reflected waves, the wave numbers and the angles of incidence and reflected may be written as:

$$k_3 \sin\theta_o = k_1 \sin\theta_1 = k_2 \sin\theta_2 = k_3 \sin\theta_3 \qquad (49)$$

which takes the equivalent form:

$$\sin\theta_o = \frac{p}{C_2}\sin\theta_1 = \frac{q}{C_2}\sin\theta_2 = \sin\theta_3 \qquad (50)$$

IV.1. Incident of SV-Wave at a Stress-Free Thermally Insulated Boundary $(h \to 0)$

Solving the equation (40), we obtain:

$$X_1 = \frac{A_1}{B_o} = \frac{1}{\Delta}\left[\frac{p^3}{C_1^2 C_2^2}\left(\frac{1}{C_1^2 p^2}-1\right)\sin 4\theta_1 \cos\theta_2\right]$$

$$X_2 = \frac{A_2}{B_o} = -\frac{1}{\Delta}\left[\frac{q^3}{C_1^2 C_2^2}\left(\frac{1}{C_1^2 q^2}-1\right)\sin 4\theta_1 \cos\theta_3\right]$$

$$X_3 = \frac{B_1}{B_o} = -1 + \frac{2}{\Delta}\left[\frac{\sin 2\theta_1}{C_1^2}\left\{\begin{array}{l} p^3 q^2\left(\frac{1}{C_1^2 p^2}-1\right)\sin 2\theta_3 \cos\theta_2 + \\ -p^2 q^3\left(\frac{1}{C_1^2 q^2}-1\right)\sin 2\theta_2 \cos\theta_3 \end{array}\right\}\right]$$

$$\Delta = q^3\left(\frac{1}{C_1^2 q^2}-1\right)\cos\theta_3 \cdot \left[\frac{p^2}{C_2^2}\left\{\begin{array}{l} 2\delta^2 \sin^2\theta_2 - 1 + \\ +\tau_1'\left(1-\frac{1}{C_1^2 p^2}\right)\cos 2\theta_1 \end{array}\right\}\right] + p^3\left(\frac{1}{C_1^2 p^2}-1\right)\cos\theta_2\left[\frac{q^2}{C_1^2}\sin 2\theta_1 \sin 2\theta_3 + \right.$$
$$\left. -\frac{q^2}{C_2^2}\left\{\begin{array}{l} 2\delta^2 \sin^2\theta_3 - 1 + \\ +\tau_1'\left(1-\frac{1}{C_1^2 q^2}\right) \end{array}\right\}\cos 2\theta_1\right] \qquad (51)$$

IV.2. Incident of SV-Wave at a Stress-Free Isothermal Boundary $(h \to \infty)$

The solution of equation (40), the amplitudes ratios can be written as:

$$X_1 = \frac{1}{\Delta}\left[\frac{1}{C_1^2 C_2^2}\left(\frac{1-C_1^2 p^2}{1-C_1^2 q^2}\right)\sin 2\theta_1 \cos 2\theta_1\right]$$

$$X_2 = \frac{-2}{\Delta}\left[\frac{1}{C_1^2 C_2^2}\sin 2\theta_1 \cos 2\theta_1\right]$$

$$X_3 = -1 + \frac{2}{\Delta}\left[\begin{array}{l} \left(\frac{q}{C_1}\right)^2 \sin 2\theta_1 \sin 2\theta_3 \\ \left(\frac{1-C_1^2 p^2}{1-C_1^2 q^2}\right) - \left(\frac{p}{C_1}\right)^2 \sin 2\theta_1 \sin 2\theta_2 \end{array}\right]$$

$$\Delta = \left[\begin{array}{l} \left(\frac{p}{C_2}\right)^2 \cos 2\theta_1 \left(\begin{array}{l} 2\delta^2 \sin^2\theta_2 - 1 + \tau_1' \cdot \\ \cdot\left(1-\frac{1}{C_1^2 p^2}\right) \end{array}\right) + \\ -\left(\frac{p}{C_1}\right)^2 \sin 2\theta_1 \sin 2\theta_2 \end{array}\right] + \qquad (52)$$
$$-\left(\frac{1-C_1^2 p^2}{1-C_1^2 q^2}\right)\left[\begin{array}{l} \frac{q^2}{C_2^2}\left(2\delta^2 \sin^2\theta_3 - 1 + \tau_1'\left(1-\frac{1}{C_1^2 q^2}\right)\right)\cdot \\ \cdot \cos 2\theta_1 - \left(\frac{q}{C_1}\right)^2 \sin 2\theta_1 \sin 2\theta_3 \end{array}\right]$$

If one neglects influence of the magnetic field, thermal relaxation times, the results obtained are deduced the results obtained by Das et al., [34] with some modifications and slight change in symbols.

Also, in the absence of the thermal field, magnetic field, relaxation times, the results obtained are deduced to the results obtained in Achenbach [36].

V. Numerical Results and Discussions

For computational work, the following material constants at $T_0 = 300^{\circ}\mathrm{C}$ are considered a copper material for an elastic solid with generalized thermoelastic solid:

$$\lambda = 8.2\times10^{10}\ \mathrm{N/m^2}, \quad \mu = 4.2\times10^{10}\ \mathrm{N/m^2},$$
$$\rho = 8.95\times10^{3}\ \mathrm{kg/m^2}$$

$$c_v = 3.845\times10^{2}\ \mathrm{m^2 K^{-1} s^{-2}}$$
$$\alpha_t = 1.67\times10^{-5}/K, \quad \omega = 10^2$$

Figs. 2-5 and Fig. 6-9 display the effects of magnetic field and thermal relaxation times on incident P-wave and SV-wave respectively; at a stress-free thermally insulated boundary $(h \to 0)$ and at a stress-free isothermal boundary $(h \to \infty)$, on the reflection coefficients A_1/A_o, A_2/A_o, B_1/A_o and A_1/B_o, A_2/B_o, B_1/B_o respectively.

For the incident P-wave: at a stress-free thermally insulated boundary $(h \to 0)$, Fig. 2 shows the influence of magnetic field H_o on reflection coefficients respect with the angle of incidence θ if the relaxation times give a constant value. It is obvious that the absolute values of A_1/A_o and A_2/A_o increase with an increasing of the magnetic field but the absolute values of B_1/A_o decreases with an increasing of H_o. Fig. 3 displays the effect of relaxation times on reflection coefficients for incidence P-wave with respect to the angle of incidence θ, it is seen that the magnitude values of reflection coefficient A_1/A_o, A_2/A_o and B_1/A_o increase with an increasing of the relaxation times. At a stress-free isothermal boundary $(h \to \infty)$, Fig. (4), (5) show the influence of magnetic field H_o and thermal relaxation times on reflection coefficients respect with the angle of incidence θ. It is seen that the absolute values of A_1/A_o, A_2/A_o and B_1/A_o increase with an increasing of the magnetic field and relaxation times.

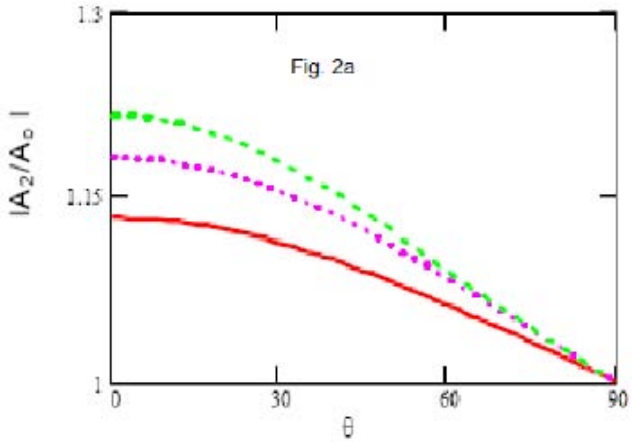

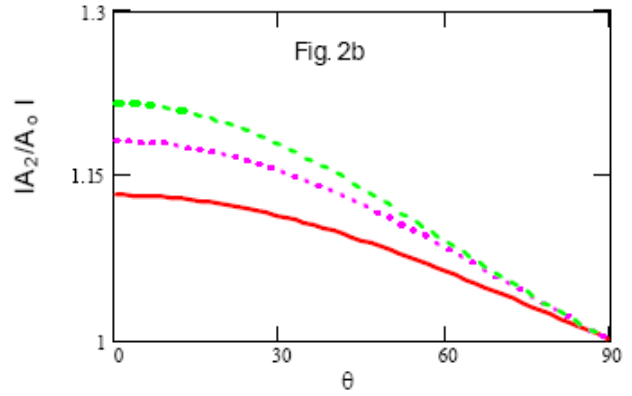

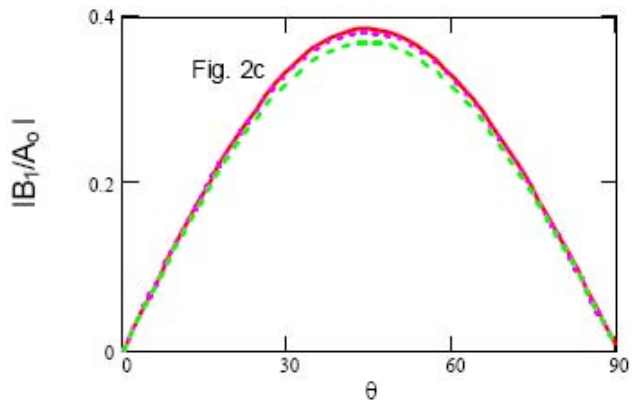

Atastress – free thermally insulated boundary $(h \to 0)$

Figs. 2. Effect of the magnetic field on reflection coefficients for the incidence P - wave, when $\tau_0 = 2\tau_1 = 0.2, H_o = 10^5$ ____ ,$H_o = 3\times10^5$....., $H_o = 5\times10^5$ – –

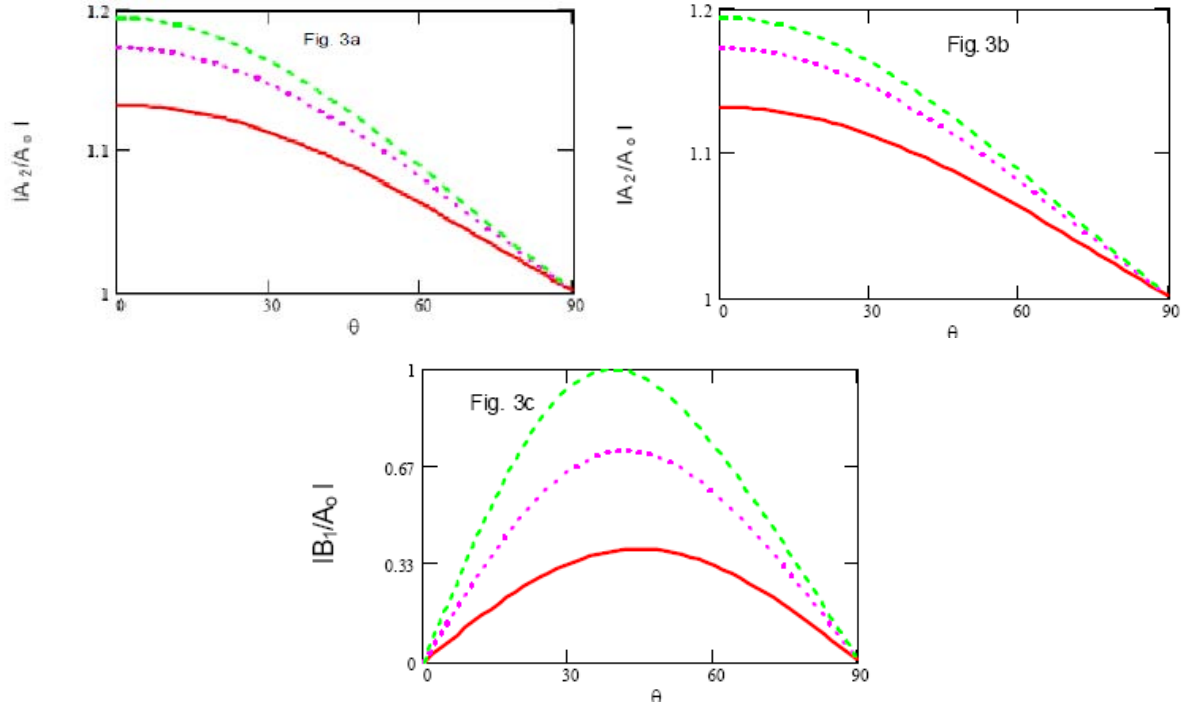

Atastress – free thermally insulated boundary $(h \to 0)$

Figs. 3. Effect of the relaxation times on reflection coefficients for the incidence P - wave,where

$H_o = 10^5, \tau_0 = 2\tau_1, \tau_1 = 0.1$ ____ , $\tau_1 = 0.2$....., $\tau_1 = 0.3$ – –

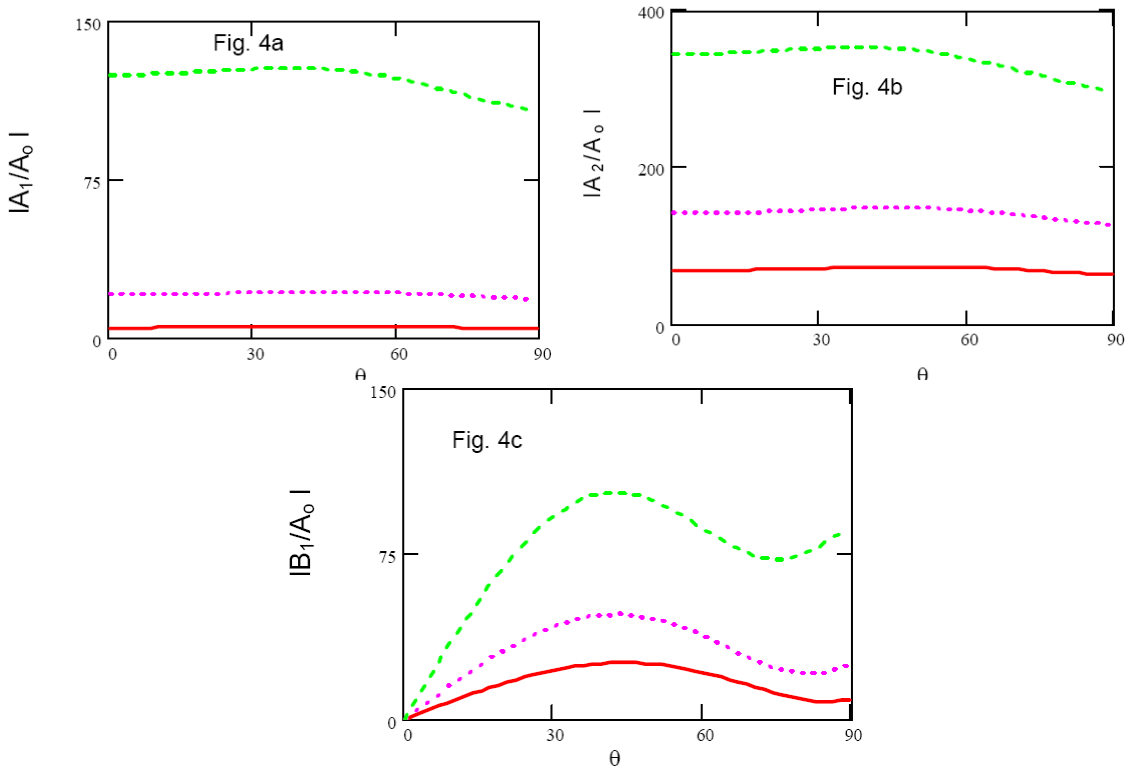

At astress - free isothermal boundary $(h \to \infty)$

Figs. 4. Effect of the magnetic field on reflection on coefficients fot the incidence P - wave, when

$\tau_o = 2\tau_1 = 0.2, H_o = 10^5$ ____ , $H_o = 3\times10^5$....., $H_o = 5\times10^5$ – –

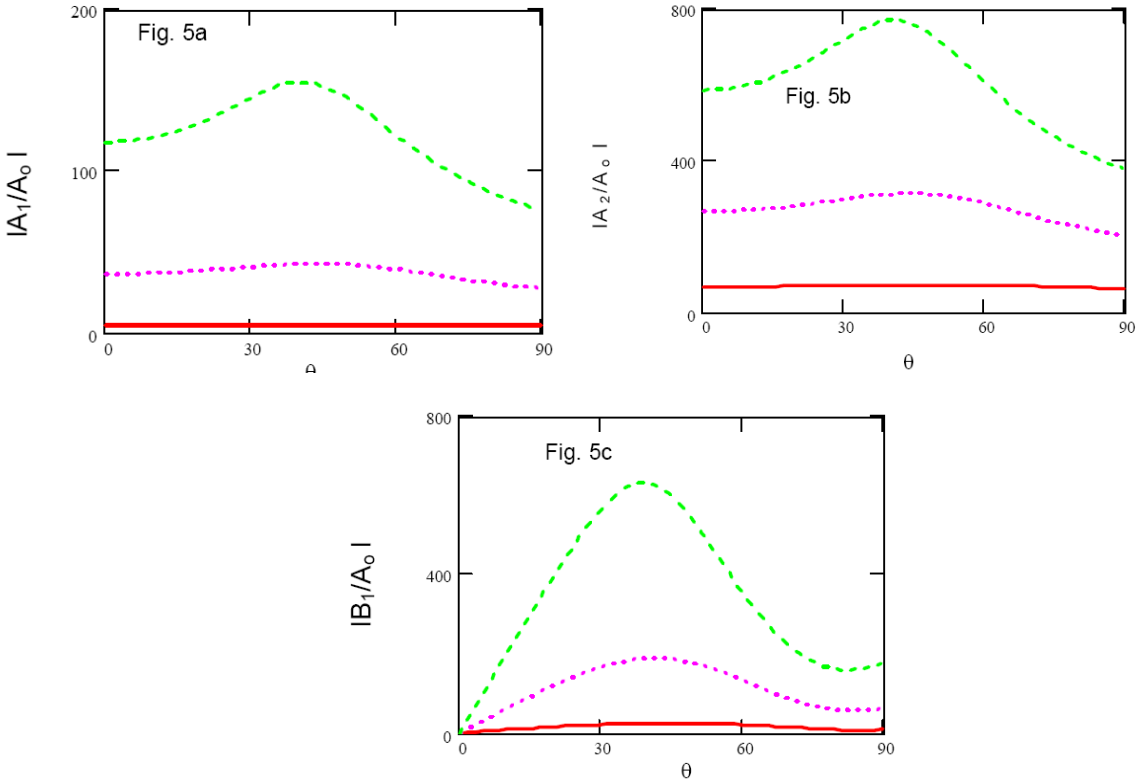

At astress - free isothermal boundary $(h \to \infty)$

Figs. 5. Effect of the relaxation on time sorce flection coefficients for the incidence P - wave, when

$H_o = 10^5, \tau_o = 2\tau_1, \tau_1 = 0.1$ ____ $, \tau_1 = 0.2 ..... , \tau_1 = 0.3$ – –

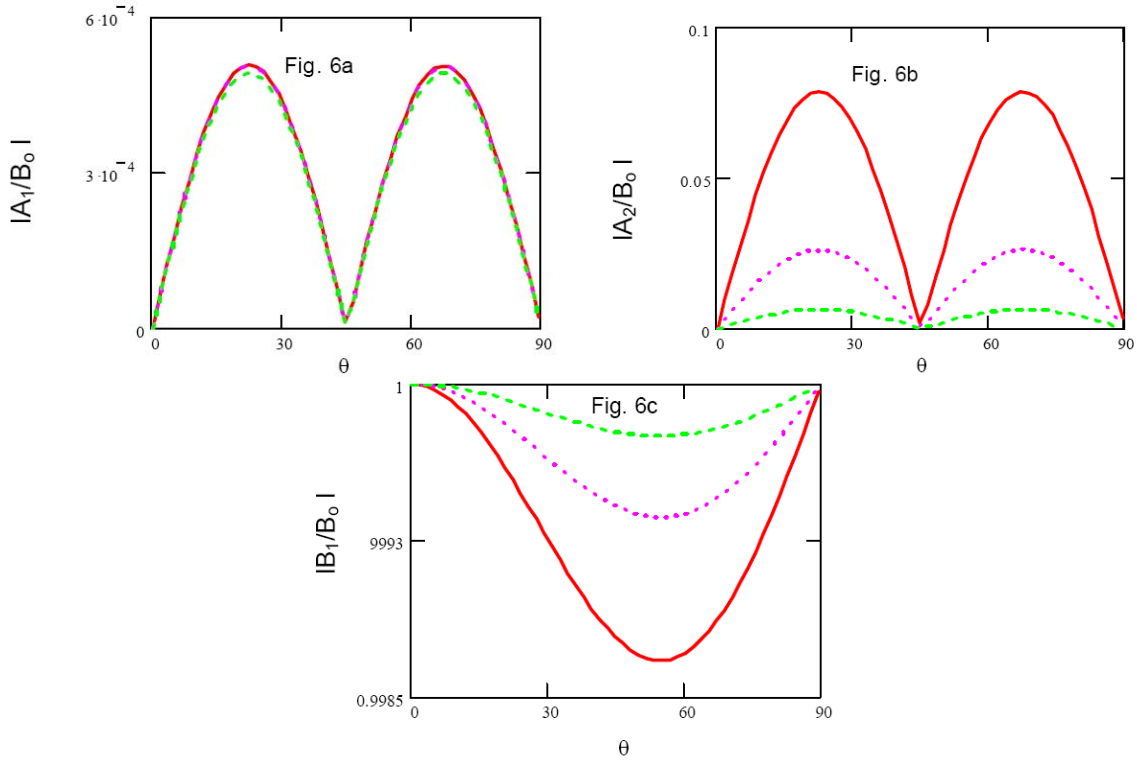

At a stress - free thermally insulated boundary $(h \to 0)$

Figs. 6. Effect of the magnetic field on reflection coefficients for the incidence *SV* - wave, when

$\tau_o = 2\tau_1 = 0.2, H_o = 10^5$ ____ $, H_o = 3 \times 10^5 ..... , H_o = 5 \times 10^5$ – –

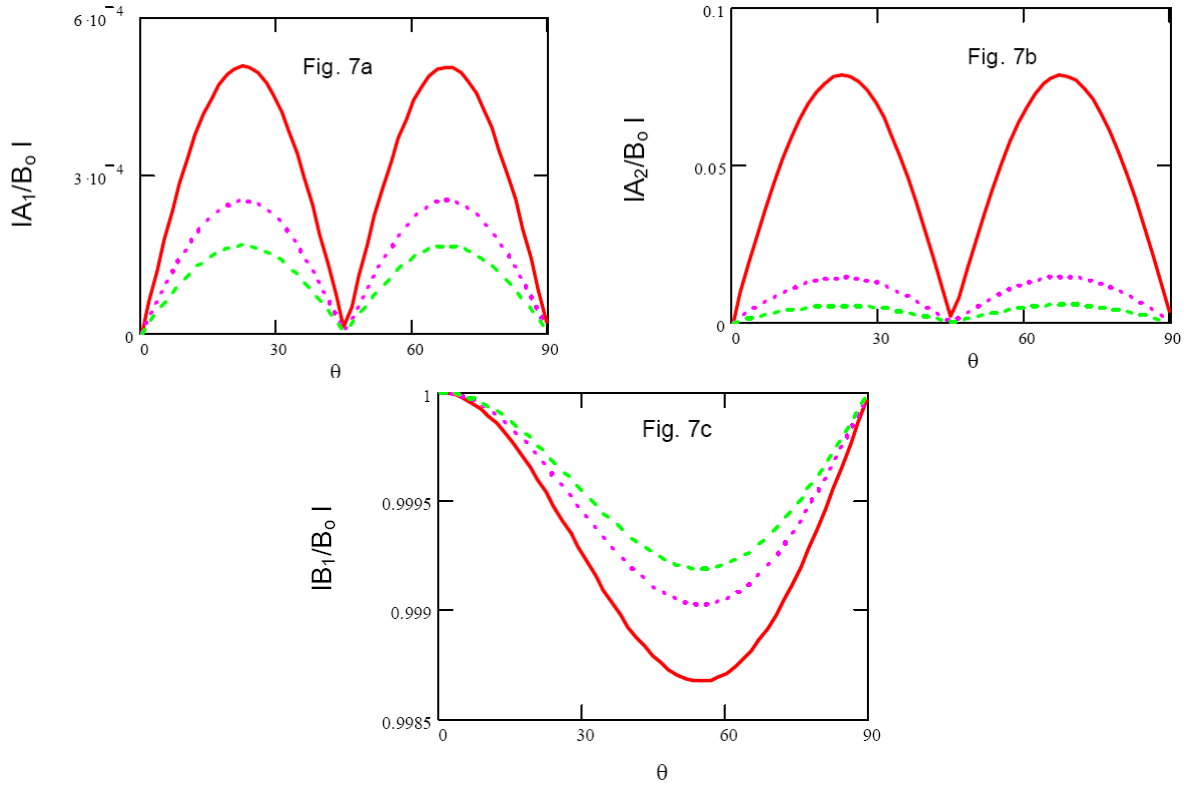

At a stress - free thermally insulated boundary $(h \to 0)$

Figs. 7. Effect of the relaxation times on reflection coefficients for the incidence SV - wave, when

$H_o = 10^5, \tau_o = 2\tau_1, \tau_1 = 0.1$ ____ , $\tau_1 = 0.2$....., $\tau_1 = 0.3$ – –

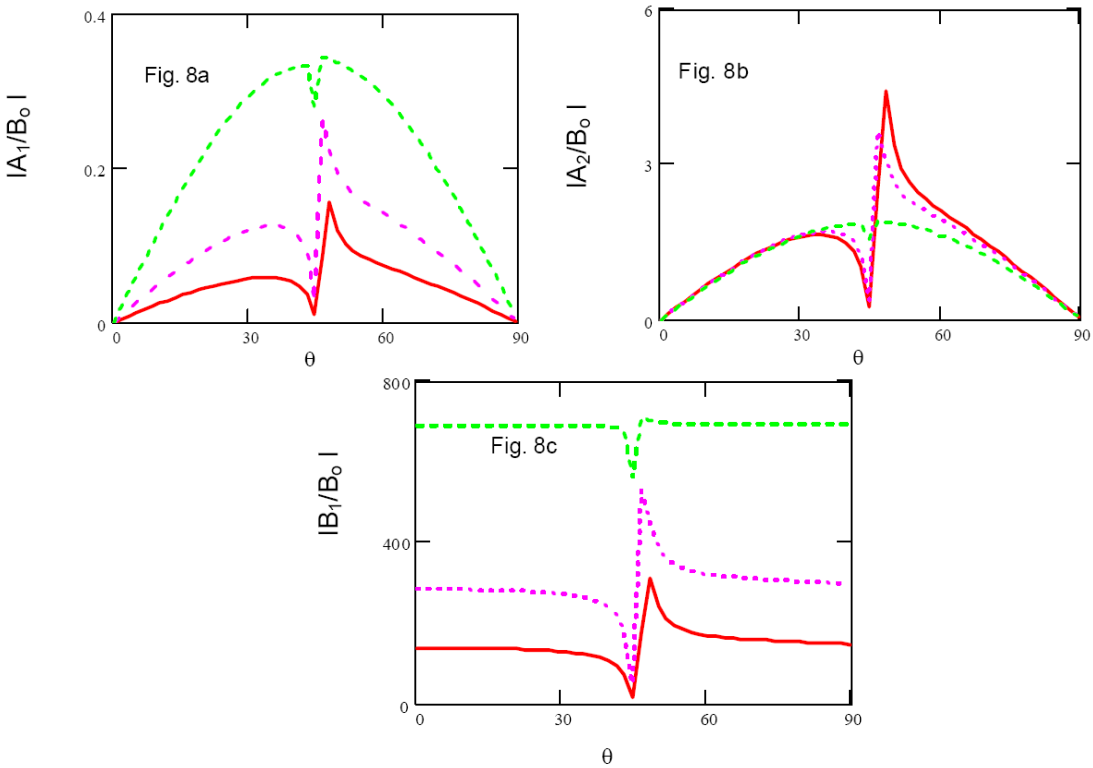

At astress – freeisothermalboundary $(h \to \infty)$

Figs. 8. Effect og the magnetic field on reflection coefficients for the incidence SV - wave, when

$\tau_o = 2\tau_1 = 0.2, H_o = 10^5$ ____ , $H_o = 3\times10^5$....., $H_o = 5\times10^5$ – –

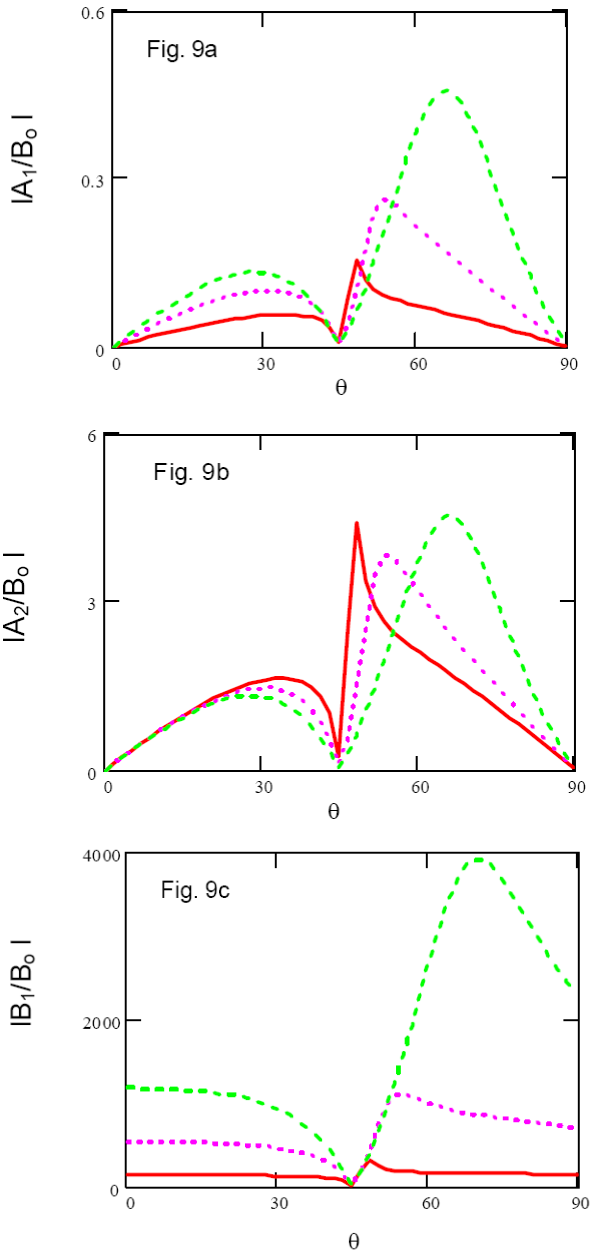

At astress – freeisothermalboundary $(h \to \infty)$

Figs. 9. Effect of the relaxation on time sonreflection on coefficients for the incidence SV - wave, when

$H_o = 10^5, \tau_o = 2\tau_1, \tau_1 = 0.1$ ___ , $\tau_1 = 0.2$ ..... , $\tau_1 = 0.3$ – –

It is clear that , from Figs. 2, 3 that $|A_1/A_o|$ and $|A_2/A_o|$ start from its primary value at at $\theta = 0^o$ and then tend to zero at $\theta = 90^o$ but $|B_1/A_o|$ starts and tends to zero at $\theta = 0^o$. From Figs. 4, 5, it appear that $|B_1/A_o|$ starts from zero at $\theta = 0^o$.

For the incident SV-wave: at a stress-free thermally insulated boundary $(h \to 0)$, Fig. 6 shows the influence of magnetic field H_o on reflection coefficients respect with the angle of incidence θ if the relaxation times are constant. It is shown that the absolute values of A_1/B_o are decreased slight with an increasing of magnetic field, $|A_2/B_o|$ decreases with an increasing of the magnetic field but the absolute values of B_1/B_o increases with an increasing of H_o. Fig. 7 displays the effect of relaxation times on reflection coefficients for incidence SV-wave with respect to the angle of incidence θ, it is seen that the magnitude values of reflection coefficient A_1/B_o and A_2/B_o decrease with an increasing of the relaxation times but $|B_1/B_o|$ increases. At a stress-free isothermal boundary $(h \to \infty)$, Figs. 8, 9 show the influence of magnetic field H_o and thermal relaxation times on reflection coefficients respect with the angle of incidence θ. It is seen that the absolute values of A_1/A_o , and B_1/B_o increase with an increasing of the magnetic field and relaxation times but $|A_2/B_o|$ increases and then at a critical value decreases with an increasing of the magnetic field, also, it is appear that $|A_2/A_o|$ assume decreases and then increases with an increasing of the thermal relaxation times.

It is clear that from Fig. 6, 7 that $|A_1/B_o|$ and $|A_2/B_o|$ start and tend to zero at $\theta = \{0^o, 90^o\}$ but $|B_1/B_o|$ starts and tends to the unity at $\theta = \{0^o, 90^o\}$. From Figs. 8, 9, it is clear that $|A_1/B_o|$ and $|A_2/B_o|$ start and tend to zero at $\theta = \{0^o, 90^o\}$.

Finally, it is shown that $|A_1/B_o|$, $|A_2/B_o|$ and $|B_1/B_o|$ have a critical value for the angle of incidence θ and change their paths with an increasing of θ.

VI. Conclusion

The main conclusions due to the influences of the magnetic field and thermal relaxation times on the reflection of P and SV-waves, can be summarized as follow:

The reflection coefficients are affected strongly by the angle of incidence θ, magnetic field and thermal relaxation times. The magnetic field affected strongly on the absolute values of all reflection coefficients unless $|B_1/A_o|$ for P-wave and $|A_1/B_o|$ for SV-wave at a stress-free thermally insulated boundary $(h \to 0)$ there is a slight affect. The thermal relaxation times affected strongly on all values of the reflection coefficients. Finally, it is seen that the angle of incidence θ affects very strong on all values of the reflection coefficients and $\theta = 45^o$ displays a critical value for the reflection coefficients in SV-wave At a stress-free isothermal boundary $(h \to \infty)$. Finally, it is too clear that all operators are affected on the amplitude ratios, which have

a good influence on Seismic waves, Earthquakes, Geophysics, Volcanos, Plasma, Geometrical Geology, Nuclear fields, Geology and etc.

References

[1] J. Duhamel, Some memoire sur les phenomenes thermo-mechanique, *J. de L Ecole Polytechnique* **15,** 1-31 (1837)

[2] F. Neumann, *Vorlesungen Uber die Theorie der Elasticitat*, Meyer: Brestau 1885

[3] V. Danilovskaya, Thermal stresses in an elastic half-space due to sudden heating of its boundary, *Prikl Mat. Mekh.* **14,** 316-324 **(**1950)

[4] M. A. Biot, *Mechanics of Incremental Deformation*, Wiley, New York 1965

[5] C. C. Ackerman, W.C. Overton Jr., Second sound in solid helium-3, *Phys. Rev. Lett.* **22,** 764-766 (1969)

[6] R. J. Von-Gutfeld, A. H. Nethercot Jr., Temperature dependence of heat-pulse propagation in sapphire, *Phys. Rev. Lett.* **17,** 868-871 (1966)

[7] R. A. Guyer, J.A. Krumhansi, Thermal conductivity, second sound and phonon hydrodynamic phenomena in non-metallic crystals, *Phys. Rev. Lett.* **148,** 778-788 (1966)

[8] B. Taylor, H. J. Marris, C. Flbaum, Phonon focusing in solids, *Phys. Rev. Lett.* **23,** 416-419 (1969)

[9] S. J. Rogers, Transport of heat and approach to second sound in some isotropically pure alkali-halide crystals, *Phys. Rev. Lett.* **3,** 1440-1457 (1971)

[10] H. E. Jackson, C. T. Walker, Thermal conductivity second sound and phonon interactions in NQF, *Phys. Rev.* **B-3,** 1428-1439 (1971)

[11] V. Narayanamurti, R.C. Dynes, Observation of second sound in Bismuth, *Phys. Rev. Lett.* **28,** 1461-1465 (1972)

[12] H. Lord, Y. Shulman, A generalized dynamical theory of thermoelasticity, *J. Mech. Phys. Solids* **15,** 299-309 (1967)

[13] E. Green, K. A. Lindsay, Thermoelasticity, *J. Elasticity* **2,** 1-7 (1972)

[14] W. Nowinski, *Theory of Thermoelasticity with Applications*, Sijthoff and Noordhoof Int., Netherlands 1978

[15] W. Nowacki, Dynamic Problems of Thermoelasticity, in *P. H. Francis and R. B. Hetnarski (eds.), Noordhoff Leyden* **43,** 269-282 (1975)

[16] E. Green, P. M. Naghdi, On Undamped Heat Waves in an Elastic Solid, *J. Thermal Stresses* **15,** 253-264 (1992)

[17] H. H. Sherief, *On Generalized Thermoelasticity*, Ph. D. Thesis, University of Calgary, Canada (1980)

[18] R. S. Dhaliwal, H. H. Sherief, Generalized thermoelasticity for anisotropic media, *Quart. Appl. Math.* **33,** 1-8 (1980)

[19] R. B. Hetnarski, J. Ignaczak, Generalized Thermoelasticity, *J. Thermal Stresses* **22,** 451-476 (1999)

[20] L. Knopoff, The interaction between elastic wave motions and a magnetic field in electrical conductors, *J. Geophys. Res.* **60,** 441-456 (1955)

[21] P. Chadwick, Elastic waves propagation in a magnetic field, *Proceeding of the International Congress of Applied Mechanics, Brusseles, Belgium*, 143-153 (1957)

[22] S. Kaliski, J. Petykiewicz, Equation of motion coupled with the field of temperature in a magnetic field involving mechanical and electrical relaxation for anisotropic bodies, *Proc. Vibr. Probl.* **4,** 1 (1959)

[23] M. A. Ezzat, H. M. Youssef, Generalized magneto-thermoelasticity in a perfectly conducting medium, *Int. J. of Solids and Structures* **42,** 6319--6334 (2005)

[24] Baksi, R. K. Bera, L. Debnath, A study of magneto-thermoelastic problems with thermal relaxation and heat sources in a three dimensional infinite rotating elastic medium, *Int. J. Eng. Sci.* **43,** 1419--1434 (2005)

[25] N. Sinha, S. B. Sinha, Reflection of thermoelastic waves at a solid half-space with thermal relaxation, *J. Phys. Earth* **22,** 237-244 (1974)

[26] S. B. Sinha, K. A. Elsibai, Reflection of thermoelastic waves at a solid half-space with two thermal relaxation times, *J. Thermal Stresses* **19,** 763-777 (1996)

[27] S. B. Sinha, K. A. Elsibai, Reflection and refraction of thermoelastic waves at an interface of two semi-infinite media with two thermal relaxation times, *J. Thermal Stresses* **20,** 129-146 (1997)

[28] J. N. Sharma, V. Kumar, Dayal Chand, Reflection of generalized thermoelastic waves from the boundary of half space, *J. Thermal Stresses* **26,** 925- 942 (2003)

[29] Montanaro, On singular surface in isotropic linear thermoelasticity, *J. Acoust. Soc. Am.* **106,** 1586-1588 (1999)

[30] N. Abd-Alla, A.A. Yahia, S.M. Abo-Dahab, On reflection of the generalized magneto-thermo-viscoelastic plane waves, *Chaos, Solitons & Fractals* **16,** 211--231 (2003)

[31] S. M. Abo-Dahab, R. A. Mohamed, Influence of magnetic field and hydrostatic initial stress on reflection phenomena of P and SV waves from a generalized thermoelastic solid half-space, *J. Vibration & Control* **16,** 685-699 (2010)

[32] Singh, Reflection of P and SV waves from free surface of an elastic solid with generalized thermodiffusion, *J. Earth Syst. Sci.* **114**(2), 1-10 (2005)

[33] Singh, A. Kumar, J. Singh, Reflection of generalized thermoelastic waves from a solid half-space under hydrostatic initial stress, *Appl. Math. & Comp.* **177,** 170--177 (2006)

[34] N. C. Das, A. Lahiri, S. Sarkar, S. Basu, Reflection of generalized thermoelastic waves from isothermal and insulated boundaries of a half space, *Computers and Mathematics with Applications* **56,** 2795-2805 (2008)

[35] S. K. Roychoudhuri, S. Mukhopadhyay, Magneto-thermoelastic interactions in an infinite viscoelastic cylinder of temperature-rate dependent material subjected to a periodic loading, *Int. J. Eng. Sci.* **36**(5/6), 635-643 (1998)

[36] J. D. Achenbach, *Wave Propagation in Elastic Solids*, North Holland Pub. Co., Amsterdam, 1975

Authors' information

[1]Math. Dept., Faculty of Science, SVU, Qena 83523, Egypt- Math. Dept., Faculty of Science, Taif University, Saudi Arabia
E-mail: sdahb@yahoo.com

[2] Math. Dept., Faculty of Science, SVU, Qena 83523, Egypt
E-mail: rabdalla_1953@yahoo.com

[3] Math. Dept., Faculty of Science, Taif University, Saudi Arabia
E-mail: mohmrr@yahoo.com

Praise Worthy Prize

International Review of Physics (I.R.E.PHY.), Vol. 5, N. 6
December 2011

Influence of Initial Stress as a Convective Boundary Condition on Natural Frequencies of a Poroelastic Hollow Cylinder

A. M. El-Naggar[1], Ibrahim A. Abbas[2], S. M. Abo-Dahab[3], M. Elsagheer[4]

Abstract – *In this paper, we study the radial vibrations of a poroelastic hollow cylinder with convective boundary conditions. Biot's theory is employed for wave propagation in a porous solid, the frequency equation for radial vibration of a poroelastic cylinder is obtained includes initial stress as a convective boundary condition. The frequency equation has been derived in the form of a determinant form involving Bessel functions. The root of the frequency frequency equation determines the circular frequency. Special case from this study is investigated if the initial stress is neglected. The numerical computations of the frequency equations for the radial vibrations of a poroelastic cylinder is obtained and are illustrated graphically. It is found the frequency equation of the waves has been affected by the poroelasticity and the initial stress which indicated that their very pronounced on the natural frequency.*

Keywords*: Natural Frequencies, Poroelastic Hollow Cylinder, Initial Stress, Convective*

Nomenclature

$\alpha = 1 - \delta K$	Is the elastic coefficient
β	Is the porosity
γ	Is the coefficient of fluid content
δ	Is the unjacketed compressibility
$\in$	Is the unjacketed compressibility
λ and μ	Are the Lame's parameters
α_{11}, α_{12} and α_{22}	Define the elastic properties of the material
$\beta_{11}\beta_{11}$ and β_{11}	Define its dynamic properties
ρ	Is the mass per unit volume of the fluid-solid aggregate
ρ_f	Is the density of the solid material
ρ_s	Is the density of the fluid material
$\rho_{11} + \rho_{12} = (1-\beta)\rho_s$	Is the mass per unit volume of the fluid
$\rho_{11} + \rho_{12} = \beta\rho_f$	Is the mass per unit volume of the solid
ρ_{12}	Is a mass coupling parameter between the fluid and the solid
τ_{ij}	Is the components of stress tensor
Ω	Is the dimensionless parameter of frequency
$A = \lambda + M(\alpha - \beta)^2$	Is the material coefficients are related to the solid
e	Is the expansion of the solid phase
$K = \left(\lambda + \frac{2}{3}u\right)$	Is the jacketedin compressibility
$M = \left(\gamma + \delta - \delta^2 K\right)^{-1}$	Is the elastic coefficient
P_o	Is the pressure initial stress
$Q = \beta(\alpha - \beta)M$ and $R = \beta^2 M$	Are the material coefficients are related to the fluid
S	Is the excess fluid pressure
$\vec{u} = (u_r\, u_\theta, u_z)$	Is the displacement vector in the solid
$\vec{v} = (v_r, v_\theta, v_z)$	Is the displacement vector in the fluid

I. Introduction

Theory of propagation of elastic waves in a system composed of a porous elastic solid saturated by a viscous fluid, it is assumed that the fluid is compressible and may flow relative to the solid causing friction to arise and the relative motion of the fluid in the pores is of the Poiseuille type. As already pointed out by Kirchhoff this is valid only below a certain frequency which we denote by f_t, and which depends on the kinematic viscosity of the fluid and the size of the pores. We have in mind particularly the application to cases where the fluid is a liquid, and we have therefore disregarded the thermoelastic effect. We include only materials such that the walls of the main pores are impervious and for which the pore size is concentrated around its average value. Extension to more general materials will be considered along with the

Manuscript received and revised November 2011, accepted December 2011

thermoelastic effect in a later and more complete theory.A theory is developed for the propagation of stress waves in a porous elastic solid containing a compressible viscous fluid. The emphasis of the present treatment is on materials where fluid and solid are of comparable densities as for instance in the case of water-saturated rock. It is restricted to the lower frequency range where the assumption of Poiseuille flow is valid. It is found that the material may be described by four nondimensional parameters and a characteristic frequency. There are two dilatational waves and one rotational wave. The physical interpretation of the result is clarified by treating first the case where the fluid is frictionless. The case of a material containing a viscous fluid is then developed and discussed numerically. Phase velocity dispersion curves and attenuation coefficients for the three types of waves are plotted as a function of the frequency for various combinations of the characteristic parameters.Biot's theory of poroelasticity is a solution of the problem of elastic wave propagation in fluid-saturated porous media. It can be used to compute seismic and sonic responses of fluid-saturated reservoirs through numerical modeling.

In this work, Biot's equations are used for modeling wave propagation in 2D heterogeneous poroelastic media through a second-order accurate time, fourth-order accurate space, staggered-grid finite-difference scheme. For implementing the numerical scheme, Biot's equations are reformulated into a first-order system of four equations of motion and four constitutive equations, expressed explicitly in particle-velocity components, stresses and pore-fluid pressure. Results for a homogeneous medium illustrate the effect of some physical parameters on the slow wave propagation.

In general, the porosity influences the velocity, and the viscosity to permeability ratio influences the attenuation of the slow wave. Besides, simulations in heterogeneous media, from poroelastic and an equivalent elastic modeling, are performed and compared, both in seismic and sonic ranges of frequencies.

The results illustrate the effect of Biot's poroelasticity. Although the poroelastic effect is not apparent at seismic frequency, it is relevant at sonic frequency, and the use of this wave propagation theory may provide valuable results in sonic log inversion.

Biot [4] was introduced the general theory of three-dimensional consolidation, and discussed theory of elasticity and consolidation for a porous an isotropic solid [7]. Biot [5] investigated general solutions of the equations of elasticity and consolidation for porous material. Biot [8],[9] introduced theory of propagation of elastic waves in a fluid-saturated porous solid part I: Low frequency range and part II Higher frequency range. Jones [18] studies Rayleigh waves in a porous elastic and saturated solid. Biot [6] explained generalized theory of acoustic propagation in porous dissipative media. Deresiewice [13] explained the effect of boundaries on wave propagation in a liquid-fluid porous solid and on surface waves in a half-space. Biot [10] studied nonlinear and semilinear rheology of porous solids. Paul [21] studied the displacements produced in a porous elastic half-space by an impulsive line load (nondissipative case) and [22] studied the disturbance produced in a semi-infinite poroelastic medium by a surface a load. Rice and Cleary [25] studied some basic stress-diffusion solutions for fluid-saturated elastic porous media with compressible constituents.Yew and Jogi [33] iterduced study of wave motions in fluid-saturated porous rocks. Bowen [11] discussed compressible porous media models by use of the theory of mixtures. Sharma and Gogna [29] studied seismic wave propagation in a viscoelastic porous solid saturated by viscous liquid.

Philippacopoulos [23] studied Lamb's problem for fluid-saturated and porous media and [24] investigated wave in partially saturated medium due to surface loads. Seyed [27] studied model impedances for a spherical source in a fluid-fluid spherical cavity embedded within a fluid-infiltrated elastic porous medium.

Yang and Sato [32] studied dynamic response of saturated layered half-space with different hydraulic interface conditions. Yang [31] studied importance of flow condition on seismic waves at a saturated porous solid boundary. Schanz and Cheng [26] discussed transient wave propagation in a one-dimensional poroelastic column.

Wang [30] investigated theory of linear poroelasticity with applications to geomechanics and hydrogeology. Ciarletta [12] illustrated the reflection of plane waves by the free boundary of a porous elastic half space.

Hassanien and etc [16] investigated variable viscosity and thermal conductivity effects on combined heat and mass transfer in mixed convection over of the case uniform heat flux (UHF) and uniform mass flux (UMF) wedge in porous media the entire regime. James and etc. [17]investigated transient reflection and transmission of ultrasonic wave in cancellous bone. Kaishin Liu and Ying Liua [19] discussed propagation characteristic of Rayleigh waves in orthotropic fluid saturated porous media. Abousleiman and Ekbote [2] solutions for the inclined borehole in a porothermoelastic transversely isotropic medium. Ying Liu and etc [34] isllated characteristic analysis of wave propagation in anisotropic fluid-saturated porous media. Abbas [1] referred to the natural frequencies of a poroelastic hollow cylinder which is considered a special case of this study. Pallavika and etc [20] introduced finite difference modeling of SH-wave propagation in multilayered porous crust.

Sharma [28] discussed wave propagation in thermoelastic saturated porous medium. Bai [3] investigated consolidation solutions of a saturated porothermoelastic hollow cylinder with infinite length.

Gaur and Sonia Rani [14] studied surface wave propagation in non-dissipative porous medium. Gupta and etc [14] discussed the effect of initial stress on propagation of love waves in an anisotropic porous layer. In this paper, an attempt is made to investigate the radial vibrations of a poroelastic hollow cylinder with convective boundary conditions. Biot's theory [8] is employed for wave propagation in a porous solid, the

frequency equation for radial vibration of a poroelastic cylinder is obtained includes initial stress as convective boundary condition. The frequency equation has been derived in the form of a determinant form involving Bessel functions. The root of the frequency frequency equation determines the circular frequency. The special case if the initial stress is neglected is discussed from this study. The numerical computations of the frequency equations for the radial vibrations of a poroelastic cylinder is obtained and are illustrated graphically.

II. Basic Equations

Let us consider an infinite circular cylindrical bar of poroelastic material saturated in a fluid with longitudinal axis coinciding with the $z-axis$ of the cylindrical coordinate system (r,θ,z). Inner and outer radii are a and b, respectively. The stress tensor is separated into two parts [8]. The first acting on the solid part and the second acting on the fluid part there are denoted as the following tensor:

$$\begin{Bmatrix} \sigma_{rr} & \tau_{r\theta} & \tau_{rz} \\ \tau_{r\theta} & \sigma_{\theta\theta} & \tau_{\theta z} \\ \tau_{rz} & \tau_{\theta z} & \sigma_{zz} \end{Bmatrix}, \qquad \begin{Bmatrix} S & 0 & 0 \\ 0 & S & 0 \\ 0 & 0 & S \end{Bmatrix} \tag{1}$$

We denote the strain tensor in the solid by:

$$\begin{Bmatrix} e_{rr} & \frac{1}{2}\gamma_{r\theta} & \frac{1}{2}\gamma_{rz} \\ \frac{1}{2}\gamma_{r\theta} & e_{\theta\theta} & \frac{1}{2}\gamma_{\theta z} \\ \frac{1}{2}\gamma_{rz} & \frac{1}{2}\gamma_{\theta z} & e_{zz} \end{Bmatrix} \tag{2}$$

where the strain-mechanical displacement relations in cylindrical coordinates take the form:

$$\begin{aligned} e_{rr} &= \frac{\partial u_r}{\partial r}, & \gamma_{r\theta} &= \frac{1}{r}\frac{\partial u_r}{\partial \theta} + \frac{\partial u_\theta}{\partial r} - \frac{u_\theta}{r}, \\ e_{\theta\theta} &= \frac{1}{r}\frac{\partial u_\theta}{\partial \theta} + \frac{u_r}{r}, & \gamma_{rz} &= \frac{\partial u_r}{\partial z} + \frac{\partial u_z}{\partial r}, \\ e_{zz} &= \frac{\partial u_z}{\partial z}, & \gamma_{\theta z} &= \frac{1}{r}\frac{\partial u_z}{\partial \theta} + \frac{\partial u_\theta}{\partial z} \end{aligned} \tag{3}$$

and we denote the strain in the fluid by:

$$\varepsilon_{rr} = \frac{\partial v_r}{\partial r}, \quad \varepsilon_{\theta\theta} = \frac{1}{r}\frac{\partial v_\theta}{\partial \theta} + \frac{v_r}{r}, \quad \varepsilon_{zz} = \frac{\partial v_z}{\partial z} \tag{4}$$

where we can write:

$$e = div\vec{u}, \qquad \varepsilon = div\vec{v} \tag{5}$$

The stress relations for an isotropic poroelastic body in cylindrical coordinates take the form:

$$\begin{aligned} &\sigma_{rr} = 2Ne_{rr} + Ae + Q\varepsilon, \quad \tau_{r\theta} = Ne_{r\theta}, \\ &\sigma_{\theta\theta} = 2Ne_{\theta\theta} + Ae + Q\varepsilon, \quad \tau_{rz} = Ne_{rz}, \\ &\sigma_{zz} = 2Ne_{zz} + Ae + Q\varepsilon, \quad \tau_{\theta z} = Ne_{\theta z}, \\ &S = Qe + R\varepsilon \end{aligned} \tag{6}$$

where:

$$\begin{aligned} &N = \mu \qquad A = \lambda + M(\alpha - \beta)^2, \\ &Q = \beta(\alpha - \beta)M, \quad R = \beta^2 M \end{aligned} \tag{7}$$

and:

$$\alpha = 1 - \delta K, \qquad M = \left(\gamma + \delta - \delta^2 K\right)^{-1} \tag{8}$$

$$\rho_{11} + \rho_{12} = (1-\beta)\rho_s, \quad \rho_{11} + \rho_{12} = \beta\rho_f \tag{9}$$

$$e = e_{rr} + e_{\theta\theta} + e_{zz}, \qquad \varepsilon = \varepsilon_{rr} + \varepsilon_{\theta\theta} + \varepsilon_{zz} \tag{10}$$

The dynamic equations in cylindrical coordinates takes the form:

$$\begin{aligned} &\frac{\partial \sigma_{rr}}{\partial r} + \frac{1}{r}\frac{\partial \tau_{r\theta}}{\partial \theta} + \frac{\partial \tau_{rz}}{\partial z} + \frac{\sigma_{rr} - \sigma_{\theta\theta}}{r} = \\ &= \frac{\partial^2}{\partial t^2}(\rho_{11}u_r + \rho_{12}v_r), \\ &\frac{\partial \tau_{r\theta}}{\partial r} + \frac{1}{r}\frac{\partial \sigma_{\theta\theta}}{\partial \theta} + \frac{\partial \tau_{\theta z}}{\partial z} + \frac{2\tau_{r\theta}}{r} = \\ &= \frac{\partial^2}{\partial t^2}(\rho_{11}u_\theta + \rho_{12}v_\theta), \\ &\frac{\partial \tau_{rz}}{\partial r} + \frac{1}{r}\frac{\partial \tau_{\theta z}}{\partial \theta} + \frac{\partial \sigma_{zz}}{\partial z} + \frac{\tau_{rz}}{r} = \\ &= \frac{\partial^2}{\partial t^2}(\rho_{11}u_z + \rho_{12}v_z) \end{aligned} \tag{11}$$

$$\begin{aligned} &\frac{\partial S}{\partial r} = \frac{\partial^2}{\partial t^2}(\rho_{12}u_r + \rho_{22}v_r), \\ &\frac{\partial S}{\partial \theta} = r\frac{\partial^2}{\partial t^2}(\rho_{12}u_\theta + \rho_{22}v_\theta), \\ &\frac{\partial S}{\partial z} = \frac{\partial^2}{\partial t^2}(\rho_{12}u_z + \rho_{22}v_z) \end{aligned} \tag{12}$$

III. Solutions of the Problem

The equations which are govern the wave propagation in a fluid-saturated porous body according to [8] are:

$$\begin{aligned}&(A+2N)\vec{\nabla}e - N\,\vec{\nabla}\times\vec{\nabla}\times\vec{u} + Q\,\vec{\nabla}\varepsilon = \\ &= \left(\rho_{11}\ddot{\vec{u}} + \rho_{12}\ddot{\vec{v}}\right), \\ &\vec{\nabla}(Qe + R\varepsilon) = \left(\rho_{12}\ddot{\vec{u}} + \rho_{22}\ddot{\vec{v}}\right)\end{aligned} \tag{13}$$

Considering radial vibrations of the medium, the displacement vectors u and v has its only non-vanishing components u_r and v_r which are independent of θ and z, while the other components are zero which take the form:

$$u_r = u(r,t), \qquad v_r = v(r,t) \tag{14}$$

so that the constitutive equations of the medium in thier axially symmetric form are:

$$\begin{aligned}\sigma_{rr} &= 2N\frac{\partial u}{\partial r} + Ae + Q\varepsilon, \\ \sigma_{\theta\theta} &= 2N\frac{u}{r} + Ae + Q\varepsilon, \\ S &= Qe + R\varepsilon,\end{aligned} \tag{15}$$

with:

$$e = \frac{\partial u}{\partial r} + \frac{u}{r}, \qquad \varepsilon = \frac{\partial v}{\partial r} + \frac{v}{r} \tag{16}$$

Thrtefore, from the above equations we get:

$$\begin{aligned}&(A+2N)\frac{\partial e}{\partial r} + Q\frac{\partial \varepsilon}{\partial r} = (\rho_{11}\ddot{u} + \rho_{12}\ddot{v}), \\ &Q\frac{\partial e}{\partial r} + R\frac{\partial \varepsilon}{\partial r} = (\rho_{12}\ddot{u} + \rho_{22}\ddot{v})\end{aligned} \tag{17}$$

let:

$$\begin{aligned}&P = A + 2N\,, \quad H = P + R + 2Q\,, \\ &\rho = \rho_{11} + 2\rho_{12} + \rho_{22}\end{aligned} \tag{18}$$

From Eq. (14) it is defined the velocity of radial wave $\upsilon_c^2 = \dfrac{H}{\rho}$ in the aggregate under the condition that $e = \varepsilon$, i.e., if the relative between fluid and solid were completely prevented in some way.

We chose the following nondimenisonal:

$$\alpha_{11} = \frac{P}{H}, \qquad \alpha_{12} = \frac{R}{H}, \qquad \alpha_{22} = \frac{Q}{H} \tag{19}$$

$$\beta_{11} = \frac{\rho_{11}}{\rho}, \quad \beta_{12} = \frac{\rho_{12}}{\rho}, \qquad \beta_{22} = \frac{\rho_{22}}{\rho} \tag{20}$$

Then with the parameters, Eqs. (17) get:

$$\begin{aligned}&\alpha_{11}\frac{\partial e}{\partial r} + \alpha_{12}\frac{\partial \varepsilon}{\partial r} = \frac{1}{\upsilon_c^2}\frac{\partial^2}{\partial t^2}(\beta_{11}u + \beta_{12}v), \\ &\alpha_{12}\frac{\partial e}{\partial r} + \alpha_{22}\frac{\partial \varepsilon}{\partial r} = \frac{1}{\upsilon_c^2}\frac{\partial^2}{\partial t^2}(\beta_{12}u + \beta_{22}v)\end{aligned} \tag{21}$$

Substituting from Eqs. (7) and (8) into Eqs. (12) we obtain:

$$\begin{aligned}&\alpha_{11}\left[\frac{\partial^2 u}{\partial r^2} + \frac{1}{r}\frac{\partial u}{\partial r} - \frac{u}{r^2}\right] + \alpha_{12}\left[\frac{\partial^2 v}{\partial r^2} + \frac{1}{r}\frac{\partial v}{\partial r} - \frac{v}{r^2}\right] = \\ &= \frac{1}{\upsilon_c^2}\frac{\partial^2}{\partial t^2}(\beta_{11}u + \beta_{12}v), \\ &\alpha_{12}\left[\frac{\partial^2 u}{\partial r^2} + \frac{1}{r}\frac{\partial u}{\partial r} - \frac{u}{r^2}\right] + \alpha_{22}\left[\frac{\partial^2 v}{\partial r^2} + \frac{1}{r}\frac{\partial v}{\partial r} - \frac{v}{r^2}\right] = \\ &= \frac{1}{\upsilon_c^2}\frac{\partial^2}{\partial t^2}(\beta_{12}u + \beta_{22}v)\end{aligned} \tag{22}$$

For harmonic radial vibrations with frequency ω the Eqs. (22) are one solutions of the above equations in the following form:

$$u_r = u(r)e^{i\omega t}\,, \qquad v_r = v(r)e^{i\omega t} \tag{23}$$

Therefore Eqs. (22) get:

$$\begin{aligned}&\alpha_{11}\left[\frac{d^2 u}{dr^2} + \frac{1}{r}\frac{du}{\partial r} - \frac{u}{r^2}\right] + \alpha_{12}\left[\frac{d^2 v}{\partial r^2} + \frac{1}{r}\frac{dv}{dr} - \frac{v}{r^2}\right] = \\ &= -k^2(\beta_{11}u + \beta_{12}v), \\ &\alpha_{12}\left[\frac{d^2 u}{dr^2} + \frac{1}{r}\frac{du}{dr} - \frac{u}{r^2}\right] + \alpha_{22}\left[\frac{d^2 v}{dr^2} + \frac{1}{r}\frac{dv}{dr} - \frac{v}{r^2}\right] = \\ &= -k^2(\beta_{12}u + \beta_{22}v)\end{aligned} \tag{24}$$

where $k^2 = \omega^2/\upsilon_c^2$ is a wave number.

Solving Eqs. (24a) and (24b) we get:

$$\begin{aligned}&\frac{d^2 u}{dr^2} + \frac{1}{r}\frac{du}{\partial r} + \left(a_1 - \frac{1}{r^2}\right)u + a_2 v = 0, \\ &\frac{d^2 v}{dr^2} + \frac{1}{r}\frac{dv}{\partial r} + \left(a_3 - \frac{1}{r^2}\right)v + a_4 u = 0\end{aligned} \tag{25}$$

where (eq. (26)):

$$a_1 = \frac{k^2(\alpha_{22}\,\beta_{11} - \alpha_{12}\,\beta_{12})}{(\alpha_{22}\,\alpha_{11} - \alpha_{12}^2)}, a_2 = \frac{k^2(\alpha_{22}\,\beta_{12} - \alpha_{12}\,\beta_{22})}{(\alpha_{22}\,\alpha_{11} - \alpha_{12}^2)}$$

$$a_3 = \frac{k^2(\alpha_{11}\,\beta_{22} - \alpha_{12}\,\beta_{12})}{(\alpha_{22}\,\alpha_{11} - \alpha_{12}^2)}, a_4 = \frac{k^2(\alpha_{11}\,\beta_{12} - \alpha_{12}\,\beta_{11})}{(\alpha_{22}\,\alpha_{11} - \alpha_{12}^2)}$$

Eqs. (25) are decupled using simple manipulation to yield:

$$\left[\frac{d^2}{dr^2}+\frac{1}{r}\frac{d}{dr}-\frac{1}{r^2}+s_1^2\right]\left[\frac{d^2}{dr^2}+\frac{1}{r}\frac{d}{dr}-\frac{1}{r^2}+s_2^2\right]u=0 \quad (27)$$

where s_1^2 , s_2^2 are the roots of the following algebraic equation:

$$s^4-(a_1+a_3)s^2+a_1a_3-a_2a_4=0 \quad (28)$$

The general solutions of Eq. (15) may be expressed as:

$$u=A_1J_1(s_1r)+B_1Y_1(s_1r)+A_2J_1(s_2r)+B_2Y_1(s_2r) \quad (29)$$

$$v=C_1J_1(s_1r)+D_1Y_1(s_1r)+C_2J_1(s_2r)+D_2Y_1(s_2r) \quad (30)$$

where $A_1, A_2, B_1, B_2, C_1, C_2, D_1,$ and D_2 are arbitrary constants and J_1 and Y_1 are Bessel functions of the first and second kind of order one.

The constant C and D are related with A and B as follow:

$$[C_i, D_i]=\frac{s_i^2-a_1}{a_2}[A_i, B_i] \qquad i=1,2 \quad (31)$$

The boundary conditions are the follows:

$$\sigma_{rr}=P_0 \quad \text{and} \quad S=-P_o \quad at \quad r=a \quad \text{and} \quad r=b \quad (32)$$

From Eq. (32):

$$\begin{pmatrix} X_{11} & X_{12} & X_{13} & X_{14} \\ X_{21} & X_{22} & X_{23} & X_{24} \\ X_{31} & X_{32} & X_{33} & X_{34} \\ X_{41} & X_{42} & X_{43} & X_{44} \end{pmatrix}\begin{pmatrix} A_1 \\ B_1 \\ A_2 \\ B_2 \end{pmatrix}=P_0e^{-i\omega t}\begin{pmatrix} 1 \\ 1 \\ -1 \\ -1 \end{pmatrix} \quad (33)$$

where:

$$X_{11}=\left(2N+A+Q\frac{s_1^2-a_1}{a_2}\right)s_1J_0(s_1a)-\frac{2N}{a}J_1(s_1a)$$

$$X_{12}=\left(2N+A+Q\frac{s_1^2-a_1}{a_2}\right)s_1Y_0(s_1a)-\frac{2N}{a}Y_1(s_1a)$$

$$X_{13}=\left(2N+A+Q\frac{s_2^2-a_1}{a_2}\right)s_2J_0(s_2a)-\frac{2N}{a}J_1(s_2a)$$

$$X_{14}=\left(2N+A+Q\frac{s_2^2-a_1}{a_2}\right)s_2Y_0(s_2a)-\frac{2N}{a}Y_1(s_2a)$$

$$X_{21}=\left(2N+A+Q\frac{s_1^2-a_1}{a_2}\right)s_1J_0(s_1b)-\frac{2N}{b}J_1(s_1b)$$

$$X_{22}=\left(2N+A+Q\frac{s_1^2-a_1}{a_2}\right)s_1Y_0(s_1b)-\frac{2N}{b}Y_1(s_1b)$$

$$X_{23}=\left(2N+A+Q\frac{s_2^2-a_1}{a_2}\right)s_2J_0(s_2b)-\frac{2N}{b}J_1(s_2b)$$

$$X_{24}=\left(2N+A+Q\frac{s_2^2-a_1}{a_2}\right)s_2Y_0(s_2b)-\frac{2N}{b}Y_1(s_2b)$$

$$X_{31}=\left(Q+R\frac{s_1^2-a_1}{a_2}\right)s_1J_0(s_1a)$$

$$X_{32}=\left(Q+R\frac{s_1^2-a_1}{a_2}\right)s_1Y_0(s_1a)$$

$$X_{33}=\left(Q+R\frac{s_2^2-a_1}{a_2}\right)s_2J_0(s_2a)$$

$$X_{34}=\left(Q+R\frac{s_2^2-a_1}{a_2}\right)s_2Y_0(s_2a)$$

$$X_{41}=\left(Q+R\frac{s_1^2-a_1}{a_2}\right)s_1J_0(s_1b)$$

$$X_{42}=\left(Q+R\frac{s_1^2-a_1}{a_2}\right)s_1Y_0(s_1b)$$

$$X_{43}=\left(Q+R\frac{s_2^2-a_1}{a_2}\right)s_2J_0(s_2b)$$

$$X_{44}=\left(Q+R\frac{s_2^2-a_1}{a_2}\right)s_2Y_0(s_2b)$$

IV. Numerical Results and Discussions

It is obvious that equation (24) involves the dimensions a and b of the cylinder, the wave number k . To simplify the calculation of this equation we confine our attention to make these quantities dimensionless, therefore we introduce the following transformations:

$$h=\frac{a}{b}, \quad \Omega=\frac{w}{w_i}, \quad w_i=\frac{\upsilon_c\pi}{b(1-h)}$$

$$k=\frac{\omega}{\upsilon_c}=\frac{\pi}{b(1-h)}\Omega, \qquad k_1=ak=\frac{h\pi}{1-h}\Omega$$

The equation (24) gets:

$$\begin{pmatrix} X_{11} & X_{12} & X_{13} & X_{14} \\ X_{21} & X_{22} & X_{23} & X_{24} \\ X_{31} & X_{32} & X_{33} & X_{34} \\ X_{41} & X_{42} & X_{43} & X_{44} \end{pmatrix}\begin{pmatrix} A_1 \\ B_1 \\ A_2 \\ B_2 \end{pmatrix}=\frac{P_0}{H}e^{-i\omega t}\begin{pmatrix} a \\ a \\ -1 \\ -1 \end{pmatrix} \quad (34)$$

where:

$$X_{11}=\left(\alpha_{11}+\alpha_{12}\frac{s_1^2-a_1}{a_2}\right)s_1aJ_0(s_1a)-\frac{2N}{H}J_1(s_1a),\quad X_{31}=\left(\alpha_{12}+\alpha_{22}\frac{s_1^2-a_1}{a_2}\right)s_1J_0(s_1a)$$

$$X_{12}=\left(\alpha_{11}+\alpha_{12}\frac{s_1^2-a_1}{a_2}\right)s_1aY_0(s_1a)-\frac{2N}{H}Y_1(s_1a),\quad X_{32}=\left(\alpha_{12}+\alpha_{22}\frac{s_1^2-a_1}{a_2}\right)s_1Y_0(s_1a)$$

$$X_{13}=\left(\alpha_{11}+\alpha_{12}\frac{s_2^2-a_1}{a_2}\right)s_2aJ_0(s_2a)-\frac{2N}{H}J_1(s_2a),\quad X_{33}=\left(\alpha_{12}+\alpha_{22}\frac{s_2^2-a_1}{a_2}\right)s_2J_0(s_2a)$$

$$X_{14}=\left(\alpha_{11}+\alpha_{12}\frac{s_2^2-a_1}{a_2}\right)s_2aY_0(s_2a)-\frac{2N}{H}Y_1(s_2a),\quad X_{34}=\left(\alpha_{12}+\alpha_{22}\frac{s_2^2-a_1}{a_2}\right)s_2Y_0(s_2a)$$

$$X_{21}=\left(\alpha_{11}+\alpha_{12}\frac{s_1^2-a_1}{a_2}\right)s_1aJ_0(s_1b)-\frac{2N}{H}hJ_1(s_1b),\quad X_{41}=\left(\alpha_{12}+\alpha_{22}\frac{s_1^2-a_1}{a_2}\right)s_1J_0(s_1b)$$

$$X_{22}=\left(\alpha_{11}+\alpha_{12}\frac{s_1^2-a_1}{a_2}\right)s_1aY_0(s_1b)-\frac{2N}{H}hY_1(s_1b),\quad X_{42}=\left(\alpha_{12}+\alpha_{22}\frac{s_1^2-a_1}{a_2}\right)s_1Y_0(s_1b)$$

$$X_{23}=\left(\alpha_{11}+\alpha_{12}\frac{s_2^2-a_1}{a_2}\right)s_2aJ_0(s_2b)-\frac{2N}{H}hJ_1(s_2b),\quad X_{43}=\left(\alpha_{12}+\alpha_{22}\frac{s_2^2-a_1}{a_2}\right)s_2J_0(s_2b)$$

$$X_{24}=\left(\alpha_{11}+\alpha_{12}\frac{s_2^2-a_1}{a_2}\right)s_2aY_0(s_2b)-\frac{2N}{H}hY_1(s_2b),\quad X_{44}=\left(\alpha_{12}+\alpha_{22}\frac{s_2^2-a_1}{a_2}\right)s_2Y_0(s_2b)$$

$$\begin{pmatrix}A_1\\B_1\\A_2\\B_2\end{pmatrix}=\frac{1}{\Delta}\begin{pmatrix}X_{11}&-X_{21}&X_{31}\\-X_{12}&X_{22}&-X_{32}\\X_{13}&-X_{23}&X_{33}\end{pmatrix}\begin{pmatrix}C_1\\C_2\\C_3\end{pmatrix}\qquad(35)$$

For computational work, the following poroelastic material with the parameters [29], [33]:

$$\lambda = 0.3032\times10^{11}\text{dynes /cm}^2$$
$$\mu = 0.922\times10^{11}\text{dynes /cm}^2$$
$$\rho_s = 2.66\ \text{gm/cm}^3$$

$$\rho_f = 1\ \text{gm/cm}^3$$
$$\delta = 0.7378\times10^{-11}\left(\text{dynes/cm}^2\right)^{-1}$$
$$\gamma = 0.889\times10^{-11}\left(\text{dynes/cm}^2\right)^{-1}$$

Figs. 1-3 display the variations of the velocities u and v, S and σ under influences of the ρ_{12}, β and Ω resspetively, respect to the radius r

From Fig. 1, it is appear that the horizontal velocity u and the stress σ are decreased with an increasing of the radius r arrives to zero for the high values, its obvious that it decrease with an increasing of the mass coupling parameter ρ_{12} and it is seem that σ match with the the large values of r for varies values of ρ_{12}.

Also, it is obvious that the vertical velocity v and the flud porosity S are increased with the increased values of r, there is a slight increase in v with an increasing of ρ_{12} but S increased with an increaing of ρ_{12} for the small values of r and then decreases with increasing of the radius r.

From Fig. 2, it is seen that u and σ are decreased with the increased values of the radius r and the porosity β but the velocity v and S are increasing with the increasing of the radius r and the porosity β.

It is shown that from Fig. 3, that horizontal velocity u and the stress σ are decreased clearly with an increasing of the radius r, its obvious that it decrease with an increasing of the dimensionless parameter of frequency Ω and it is seem that σ match with the the large values of r for varies values of Ω.

Also, it is obvious thatthe vertical velocity v and the flud porosity S are increased with the increased values of r, there is a an increase in v with an increasing of β but S increased with an increaing of β for the small values of r and then decreases with increasing of the radius r.

V. Special Case

If the initial stress is neglected, Eq. (33) takes the form:

$$\begin{vmatrix}X_{11}&X_{12}&X_{13}&X_{14}\\X_{21}&X_{22}&X_{23}&X_{24}\\X_{31}&X_{32}&X_{33}&X_{34}\\X_{41}&X_{42}&X_{43}&X_{44}\end{vmatrix}=0\qquad(36)$$

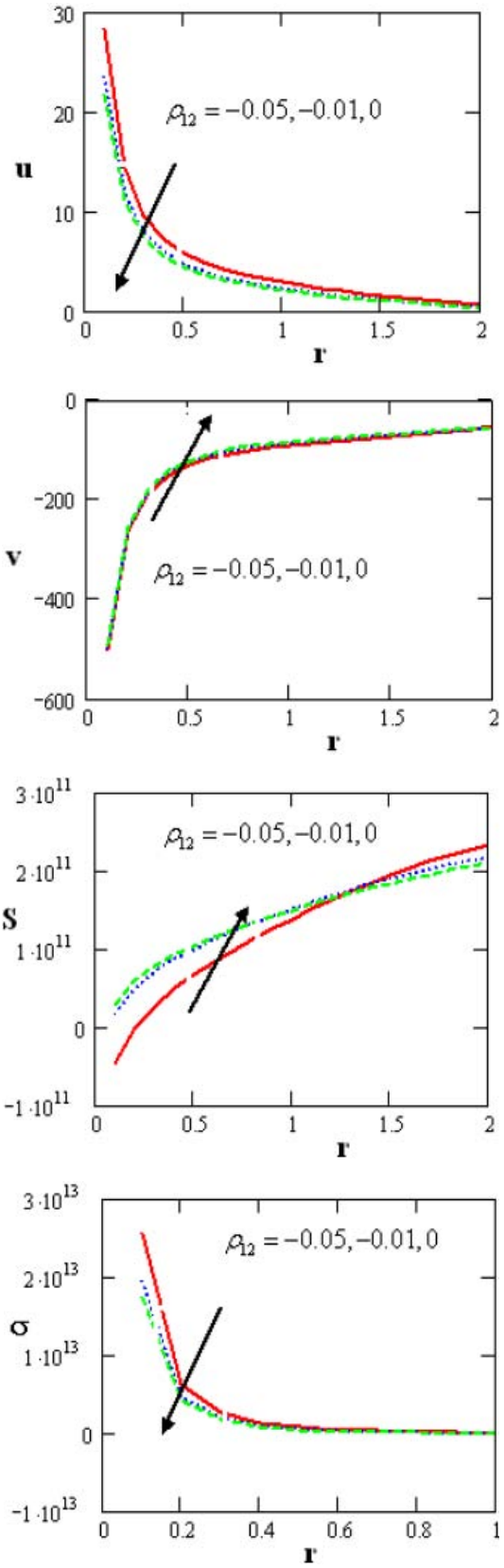

Fig. 1. Variations of the displacements component u and v, excess fluid pressure S and the stress in the solid σ respect to the radius r with varies values of mass parameter coupling ρ_{12}

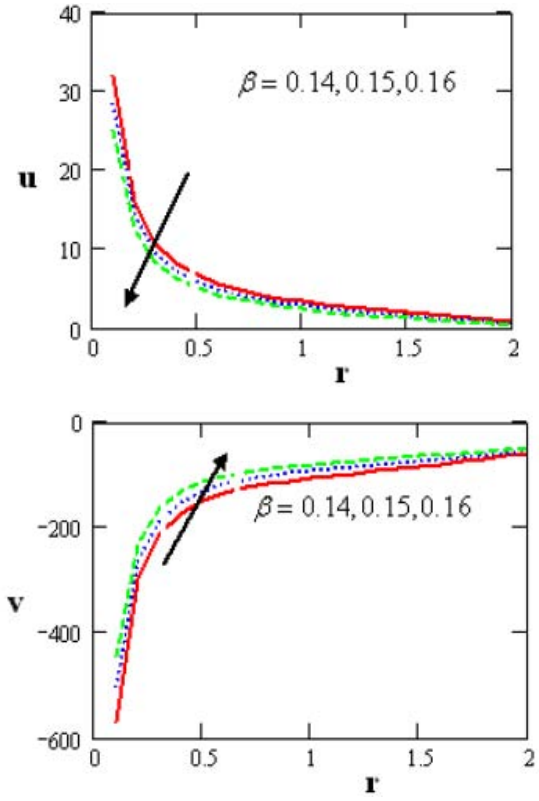

Fig. 2. Variations of the displacements components u and v, excess fluid pressure S and the stress in the solid σ respect to the radius r with varies values of the porosity β

In (36):

$$X_{11} = \left(2N + A + Q\frac{s_1^2 - a_1}{a_2}\right)s_1 J_0(s_1 a) - \frac{2N}{a}J_1(s_1 a)$$

$$X_{12} = \left(2N + A + Q\frac{s_1^2 - a_1}{a_2}\right)s_1 Y_0(s_1 a) - \frac{2N}{a}Y_1(s_1 a)$$

$$X_{13} = \left(2N + A + Q\frac{s_2^2 - a_1}{a_2}\right)s_2 J_0(s_2 a) - \frac{2N}{a}J_1(s_2 a)$$

$$X_{14} = \left(2N + A + Q\frac{s_2^2 - a_1}{a_2}\right)s_2 Y_0(s_2 a) - \frac{2N}{a}Y_1(s_2 a)$$

$$X_{21} = \left(2N + A + Q\frac{s_1^2 - a_1}{a_2}\right)s_1 J_0(s_1 b) - \frac{2N}{b}J_1(s_1 b)$$

$$X_{22} = \left(2N + A + Q\frac{s_1^2 - a_1}{a_2}\right)s_1 Y_0(s_1 b) - \frac{2N}{b}Y_1(s_1 b)$$

$$X_{23} = \left(2N + A + Q\frac{s_2^2 - a_1}{a_2}\right)s_2 J_0(s_2 b) - \frac{2N}{b}J_1(s_2 b)$$

$$X_{24} = \left(2N + A + Q\frac{s_2^2 - a_1}{a_2}\right)s_2 Y_0(s_2 b) - \frac{2N}{b}Y_1(s_2 b)$$

$$X_{31}=\left(Q+R\frac{s_1^2-a_1}{a_2}\right)s_1J_0(s_1a)$$

$$X_{32}=\left(Q+R\frac{s_1^2-a_1}{a_2}\right)s_1Y_0(s_1a)$$

$$X_{33}=\left(Q+R\frac{s_2^2-a_1}{a_2}\right)s_2J_0(s_2a)$$

$$X_{34}=\left(Q+R\frac{s_2^2-a_1}{a_2}\right)s_2Y_0(s_2a)$$

$$X_{41}=\left(Q+R\frac{s_1^2-a_1}{a_2}\right)s_1J_0(s_1b)$$

$$X_{42}=\left(Q+R\frac{s_1^2-a_1}{a_2}\right)s_1Y_0(s_1b)$$

$$X_{43}=\left(Q+R\frac{s_2^2-a_1}{a_2}\right)s_2J_0(s_2b)$$

$$X_{44}=\left(Q+R\frac{s_2^2-a_1}{a_2}\right)s_2Y_0(s_2b)$$

The root of Eq. (36) determines the circular frequency Ω which displays grphically in Fig. 4 and the varies values of the determinant (36) computed numerically and displayes graphically with the varies values of ρ_{12}, Ω and β in Figs. 5 and 6.

From Fig. 4, it is clear that the circular frequency Ω decrease with an increasing of the thichness h but increase with an increasing of the mass parameter coupling ρ_{12} and the porosity β.

Figs. 5 and 6 display the varies values of the determinant Δ with the varies values of the mass parameter coupling ρ_{12}, the porosity β and circular velocity Ω respect to the thichness h. It is obvious that Δ increase with an increasing of h and the circular frequency Ω, also, it is shown that Δ decrease with the mass parameter coupling ρ_{12} and the porosity β for the small values of h and then increase with the high values of the thichness.

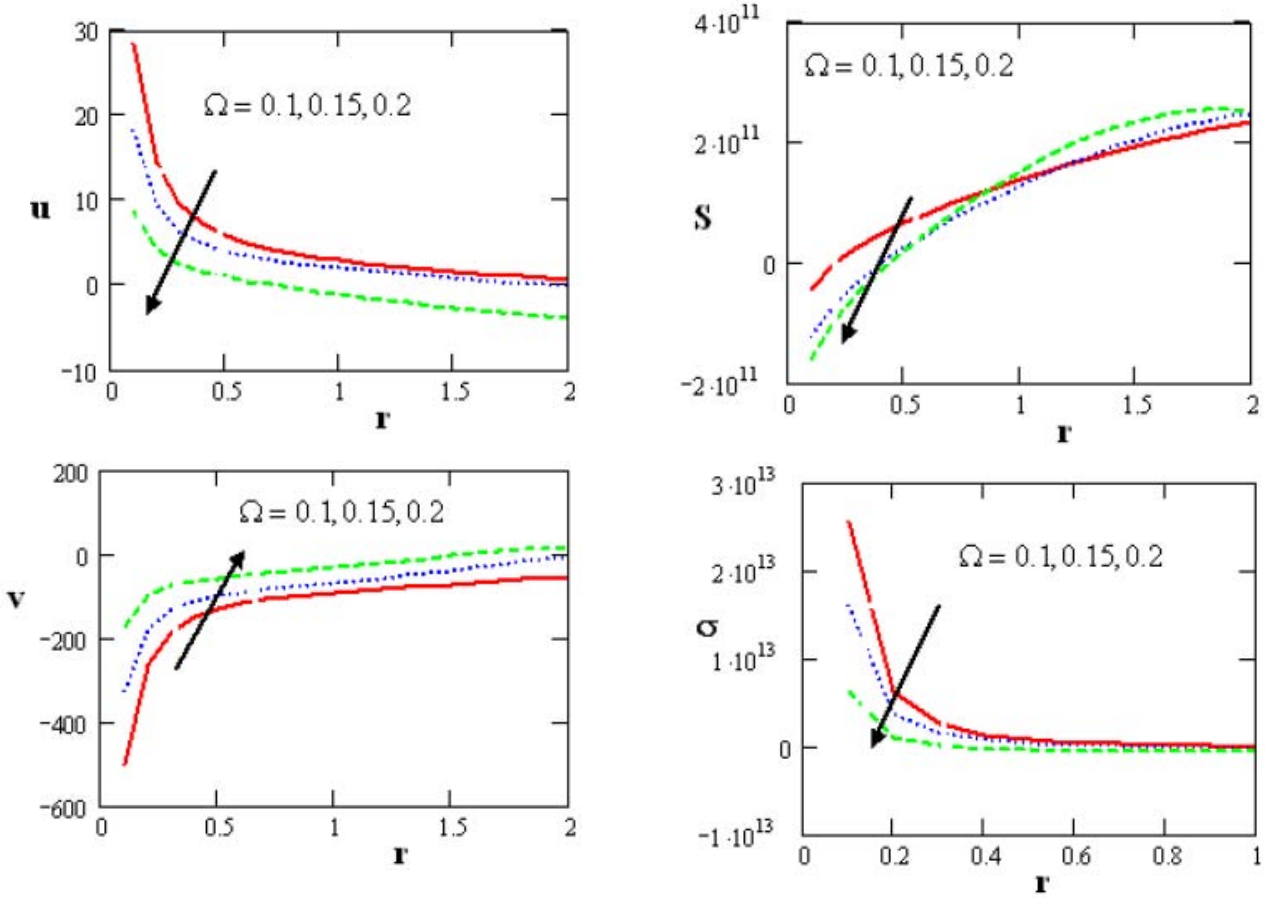

Fig. 3. Variation of the displacements components u and v, excess fluid pressure S and the stress in the solid σ respect to the other radius r with varies values of the circular frequency Ω

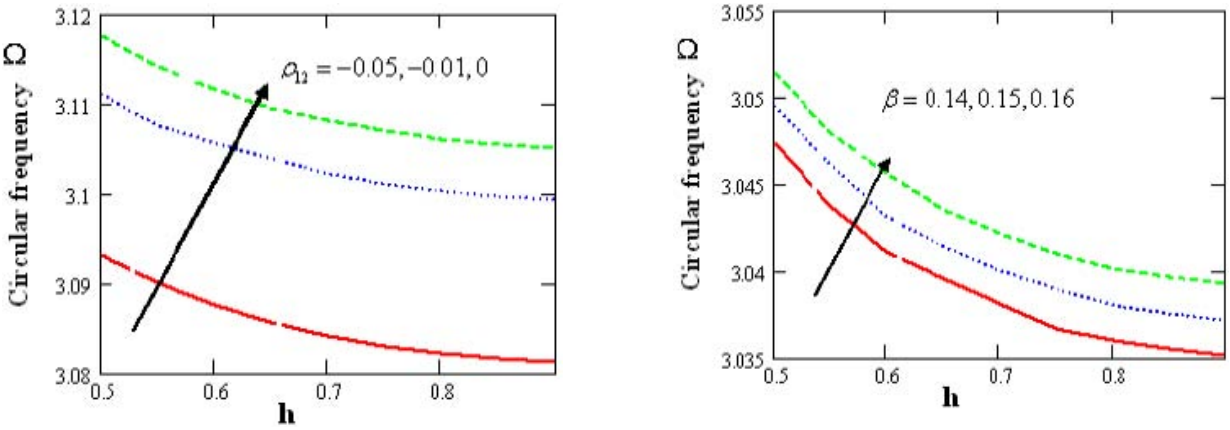

Fig. 4. Variations of the circular frequency Ω respect to thickness h with varies values of ρ_{12} and β

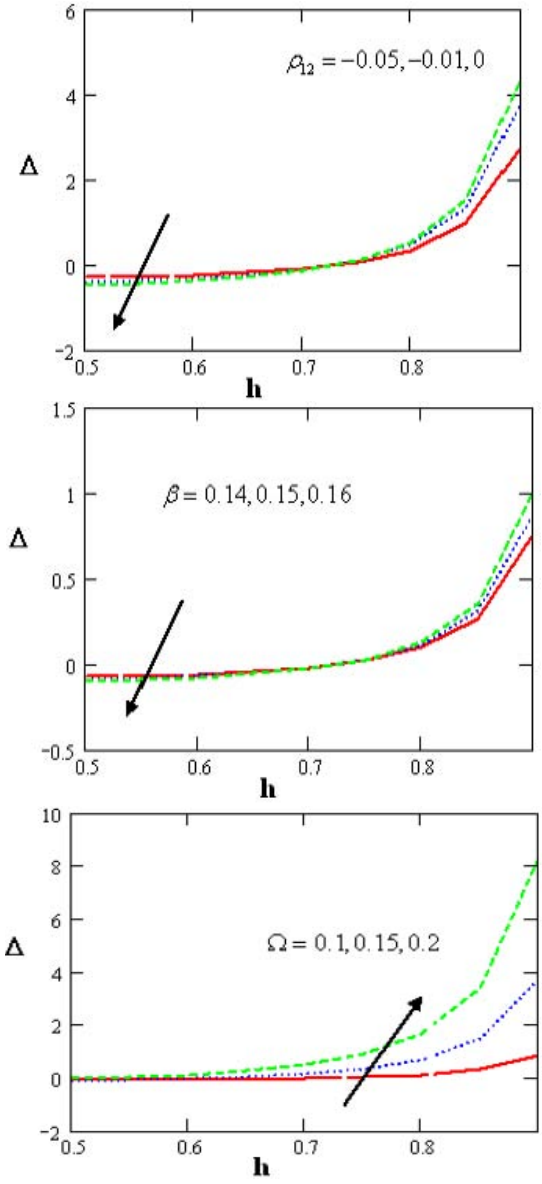

Fig. 5. Variations of the determinant Δ respect the thickness h with varies values of ρ_{12}, β and Ω

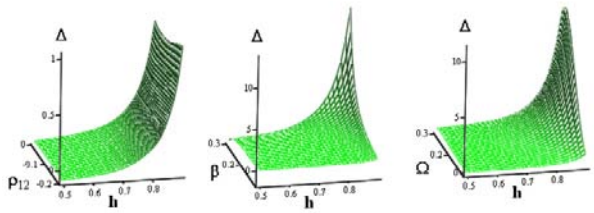

Fig. 6. Variations of the determinant Δ respect to $(h, \rho_{12}), (h, \beta)$ and (h, Ω)

References

[1] Abbas. I. A., Natural frequencies of a poroelastic hollow cylinder. *Acta Mech*. **186,** 229-237 (2006).

[2] Abousleiman Y., Ekbote, S. Solutions for the inclined borehole in a porothermoelastic transversely isotropic medium. *In Journal of Applied Mechanics*. **72**, 102-114 (2005).

[3] Bai, B. Consolidation solutions of a saturated porothermoelastic hollow cylinder with infinite length. Engineering. **2,** 37-45 (2010).

[4] Biot, M. A. General theory of three-dimensional consolidation. *Journal of Applied Physics*. **12**, 155-164 (1941).

[5] Biot, M. A. General solutions of the equations of elasticity and consolidation for a porous material. *Journal of Applied Mechanic Trans.* **23**, 91-96 (1956).

[6] Biot, M. A. Generalized theory of acoustic propagation in porous dissipative media. *Journal of the Acoustical Society of America*. **34**, 1254-1264 (1962).

[7] Biot ,M. A. Theory of elasticity and consolidation for a porous an isotropic solid. *Journal of Applied Physics*. **26**, 182-185 (1955).

[8] Biot, M. A., Theory of propagation of elastic waves in a fluid-saturated porous solid, part I: Low frequency range. *Journal of the Acoustical Society of America*. **28**, 168-178 (1956).

[9] Biot, M. A. Theory of propagation of elastic waves in a fluid-saturated porous solid, part II: Higher frequency range. *J. Acoust. Soc. Am*. **28**, 179-191 (1956).

[10] Biot, M. A. Nonlinear and semilinear rheology of porous solids. *J. Geophy*.**78**, 4924-4937 (1973).

[11] Bowen, R. M., Compressible porous media models by use of the theory of mixtures. *Int. J. Eng. Sci*. **20**, 697-735 (1982).

[12] Ciarletta, M., Sumbalyan M. A., Reflection of plane waves by the free boundary of a porous elastic half space. *Journal of Sound and Vibration*. **259**(2), 253--264(2003).

[13] Deresiewice, H., The effect of boundaries on wave propagation in aliquid-fluid porous solid, IV. Surface waves in a half-space. *Bull. Seismol. Soc. Am.* **52**, 179-191 (1962).

[14] Gaur, V. K., Sonia, Rani., Surface wave propagation in non-dissipative porous medium, *International Journal of Educational Administration.* **2,** 443-454 (2010).

[15] Gupta, S., Chattopadhyay, A. and Majhi, D. K. Effect of initial stress on propagation of love waves in an anisotropic porous layer. *Journal of Solid Mechanics*. **2**, 50-62 (2010).
[16] Hassanien, I. A., Essawy, A. H. and N. M. Moursy, N. M. Variable viscosity and thermal conductivity effects on combined heat and mass transfer in mixed convection over a UHF/UMF wedge in porous media the entire regime. *Applied Mathematics and Computation*. **145,** 667--682 (2003).
[17] James, L. uchanan and etc. Transient reflection and transmission of ultrasonic wave in cancellous bone. *Applied Mathematics and Computation*. **142**, 561--573 (2003) .
[18] Jones, J., Rayleigh waves in a porous, elastic, satuarated solid. Journal of the Acoustical Society of America. **33**, 959-962 (1961).
[19] Kaishin, Liu, Ying, Liua. Propagation characteristic of Rayleigh waves in orthotropic fluid saturated porous media. *Journal of Sound and Vibration*. **271**, 1--13 (2004).
[20] Pallavika and etc. Finite difference modeling of SH-wave propagation in multilayered porous crust. *J. Ind. Geophys. Union*.**12**, 165-172 (2008).
[21] Paul, S. On the displacements produced in a porous elastic half-space by an impulsive line load (nondissipative case). *Pure Appl. Geophys.* **114**, 604-614 (1976).
[22] Paul, S., On the disturbance produced in a semi- infinite poroelastic medium by a surface a load. *Pure Appl. Geophys*. **114**, 615-627 (1976).
[23] Philippacopoulos, A. Lamb's problem for fluid-saturated, porous media. *Bull. Seismol. Soc. Am*. **78**, 908-923 (1998).
[24] Philippacopoulos, A. Wave in partially saturated medium due to surface loads. *J. Engng. Mech. Div. Proc. ASCE* **114**, 1740-1759 (1998).
[25] Rice, J. R., Cleary, M. P. Some basic stress-diffusion solutions for fluid-saturated elastic porous media with compressible constituents, *Reviews of zeophysics and Space Physics*. **14**, 227-241 (1976).
[26] Schanz, M., Cheng, A. H. D. Transient wave propagation in a one-dimensional poroelastic column. *Acta Mech*. **145,** 1-18 (2000).
[27] Seyed, M. Hasheminejad, Model impedances for a spherical source in a fluid-fluid spherical cavity embedded within a fluid-infiltrated elastic porous medium, *Int. J. Solids Structures*. **35**, 129-148 (1998).
[28] Sharma, M. D. Wave propagation in thermoelastic saturated porous medium. *J. Earth Syst. Sci*. **117**(6), 951--958 (2008).
[29] Sharma, M. D., Gogna, M. L., Seismic wave propagation in a viscoelastic porous solid saturated by viscous liquid. *Pageoph* **135,** 383-400 (1991).
[30] Wang, H. F., Theory of Linear Poroelasticity with Applications to Geomechanics and Hydrogeology, Princeton Univ. Press, (2000).
[31] Yang, J., Importance of flow condition on seismic waves at a saturated porous solid boundary. *Journal of Sound and Vibration*. **221** 391-413 (1999).
[32] Yang, J. and Sato, T, Dynamic response of saturated layered half-space with different hydraulic interface conditions. *Archive of Applied Mechanics*. **68**, 677 -- 688 (1998) .
[33] Yew, C. H., Jogi, P. N. Study of wave motions in fluid-saturated porous rocks. *Journal of the Acoustical Society of America*. **60,** 2-8 (1976).
[34] Ying, Liu and etc. Characteristic analysis of wave propagation in anisotropic fluid-saturated porous media. *Journal of Sound and Vibration*. **282**, 863--88 (2005).

Authors' information

[1]Math. Dept., Faculty of Science, Benha University, Egypt.

[2]Math. Dept., Faculty of Science, Sohag University, Egypt.
E-mail: ibrabbas7@yahoo.com

[3]Math. Dept., Faculty of Science, Taif University, Saudi Arabia
Math. Dept., Faculty of Science, SVU, Qena, Egypt.
E-mail: sdahb@yahoo.com

[4]Math. Dept., Faculty of Science, Northern Borders University, Arar, Saudi Arabia. Math. Dept., Faculty of Science, Sohag University, Egypt.
E-mail: elsagheer_mohamed@yahoo.com

1971-6796(201112)5:6;1-C